WNT1-inducible signaling pathway protein-1 (WISP1), a novel critical protein in hepatotoxic liver injury

DISSERTATION

ZUR ERLANGUNG DES AKADEMISCHEN GRADES DES DOKTORS

DER NATURWISSENSCHAFTEN (DR. RER.NAT)

DER CHEMISCHEN FAKULTÄT DER TECHNISCHEN UNIVERSITÄT DORTMUND

VORGELEGT VON

LARISSA PÜTTER, M. SC.

DORTMUND 2017

1. GUTACHTER: PROF. DR. JAN G. HENGSTLER
2. GUTACHTER: PROF. DR. FRANK WEHNER

Für meine Mutter und meinen viel zu früh verstorbenen Vater

Eidesstattliche Versicherung (Affidavit)

Name, Vorname
(Surname, first name)

Matrikel-Nr.
(Enrolment number)

Belehrung:

Wer vorsätzlich gegen eine die Täuschung über Prüfungsleistungen betreffende Regelung einer Hochschulprüfungsordnung verstößt, handelt ordnungswidrig. Die Ordnungswidrigkeit kann mit einer Geldbuße von bis zu 50.000,00 € geahndet werden. Zuständige Verwaltungsbehörde für die Verfolgung und Ahndung von Ordnungswidrigkeiten ist der Kanzler/die Kanzlerin der Technischen Universität Dortmund. Im Falle eines mehrfachen oder sonstigen schwerwiegenden Täuschungsversuches kann der Prüfling zudem exmatrikuliert werden, § 63 Abs. 5 Hochschulgesetz NRW.

Die Abgabe einer falschen Versicherung an Eides statt ist strafbar.

Wer vorsätzlich eine falsche Versicherung an Eides statt abgibt, kann mit einer Freiheitsstrafe bis zu drei Jahren oder mit Geldstrafe bestraft werden, § 156 StGB. Die fahrlässige Abgabe einer falschen Versicherung an Eides statt kann mit einer Freiheitsstrafe bis zu einem Jahr oder Geldstrafe bestraft werden, § 161 StGB.

Die oben stehende Belehrung habe ich zur Kenntnis genommen:

Official notification:

Any person who intentionally breaches any regulation of university examination regulations relating to deception in examination performance is acting improperly. This offence can be punished with a fine of up to EUR 50,000.00. The competent administrative authority for the pursuit and prosecution of offences of this type is the chancellor of the TU Dortmund University. In the case of multiple or other serious attempts at deception, the candidate can also be unenrolled, Section 63, paragraph 5 of the Universities Act of North Rhine-Westphalia.

The submission of a false affidavit is punishable.

Any person who intentionally submits a false affidavit can be punished with a prison sentence of up to three years or a fine, Section 156 of the Criminal Code. The negligent submission of a false affidavit can be punished with a prison sentence of up to one year or a fine, Section 161 of the Criminal Code.

I have taken note of the above official notification.

Ort, Datum
(Place, date)

Unterschrift
(Signature)

Titel der Dissertation:
(Title of the thesis):

Ich versichere hiermit an Eides statt, dass ich die vorliegende Dissertation mit dem Titel selbstständig und ohne unzulässige fremde Hilfe angefertigt habe. Ich habe keine anderen als die angegebenen Quellen und Hilfsmittel benutzt sowie wörtliche und sinngemäße Zitate kenntlich gemacht.
Die Arbeit hat in gegenwärtiger oder in einer anderen Fassung weder der TU Dortmund noch einer anderen Hochschule im Zusammenhang mit einer staatlichen oder akademischen Prüfung vorgelegen.

I hereby swear that I have completed the present dissertation independently and without inadmissible external support. I have not used any sources or tools other than those indicated and have identified literal and analogous quotations.

The thesis in its current version or another version has not been presented to the TU Dortmund University or another university in connection with a state or academic examination.*

*Please be aware that solely the German version of the affidavit ("Eidesstattliche Versicherung") for the PhD thesis is the official and legally binding version.

Ort, Datum
(Place, date)

Unterschrift
(Signature)

TABLE OF CONTENTS

SUMMARY

Human chronic liver diseases continue to be a global burden in the European population, since approximately 29 million people still suffer from chronic liver diseases. In the past, a major progress has been made regarding the knowledge and management of liver diseases. The progression from early hepatic fibrosis to a chronic liver disease can probably result in the development of cirrhosis or hepatocellular carcinoma. Characteristic biological features of these disorders include inflammation, cell death, matrix deposition or angiogenesis and can lead to the progression of liver fibrosis. Some of these biological features also contribute to drug-induced liver injury (DILI), which is still the most common reason for drug withdrawal from the market. In the past, hepatotoxic effects were mostly associated with alterations in metabolism or redox state. Nowadays, it is well-known that complex signaling and transcriptional mechanisms are involved in the progression of hepatic injury as well as during the regenerative response.

Based on gene array analysis, WISP1 was identified as the strongest up-regulated member of the CCN family with regard to acute liver damage. Time-resolved analysis using qRT-PCR, confirmed the up-regulation of WISP1 expression in liver homogenates. Furthermore, the analysis of different cell populations revealed hepatocytes as the main source of WISP1 RNA upon CCl_4 administration. Moreover, WISP1 was detected in human liver disease samples. Additionally, organ specific expression of WISP1 in mice, revealed the lung, brain and spleen as organs with the highest WISP1 RNA levels.

To assess the contribution of WISP1 to drug-induced liver injury, mice containing a genetic deletion of WISP1, as well as their corresponding wild type counterparts were used. This genetically modified mouse model was used in combination with two well-known models for hepatotoxicity, namely CCl_4 and APAP. Surprisingly, time-resolved analysis of CCl_4-induced liver damage revealed not only an enhanced susceptibility of WISP1 knockout mice, but also a time-shift in induction of liver damage in comparison to wild type mice. Moreover, APAP-induced liver damage also unveiled an enhanced susceptibility of WISP1 knockout mice. This suggests that the protective effect of WISP1 is not a unique effect, but rather a general key mediator in response to hepatic injury. These pro-survival effects were neither mediated by alterations in cytochrome P450 metabolism, nor by alterations in redox state. Subsequently, qRT-PCR detected an up-regulation of WISP1 expression upon CCl_4- and APAP-induced liver injury which peaked at 12h in wild type mice. Moreover, high levels of WISP1 protein were detected in the plasma samples of wild type mice, whereas among the same population protein levels in the liver tissue were found to be rather low.

Further analysis of signal transduction revealed alterations in MAPK-associated signaling pathways, such as early (2h) activation of stress-associated signaling (JNK) in WISP1 knockout mice upon CCl_4 administration, as well as enhanced inflammation associated signaling (STAT3). However, no alterations were observed for signal transduction after APAP

administration, suggesting that the protective phenotype is mediated through different pathways.

The enhanced liver damage of WISP1 knockout mice was associated with an increased inflammatory response, confirmed by increased pro-inflammatory cytokine and chemokine expression as well as by an enhanced amount of infiltrating immune cells. Moreover, *in vitro* stimulation of hepatocytes, using pro-inflammatory cytokines, resulted in a concentration-dependent increased susceptibility to cell death of WISP1 knockout hepatocytes. A similar effect was observed, when stimulating hepatocytes *in vitro* by using APAP.

Liver regeneration was investigated by histological analysis, qRT-PCR and western blot after CCl_4 administration in a time-resolved manner up to D4. The capacity to recover from liver injury was comparable among both WISP1 knockout and wild type mice. However, liver damage of WISP1 knockout mice was not fully recovered at D4 which was associated with prolonged activation of proliferation markers and cell cycle dependent genes, such as PCNA and CycD1. These results suggest that WISP1 does not play a major role in liver regeneration after CCl_4 administration.

Finally, a time-resolved gene array analysis of WISP1 knockout and wild type mice was performed in which both groups were treated with CCl_4. Compared to wild type mice, genes associated with metabolism were down-regulated and genes associated with lipid metabolism showed an up-regulation in WISP1 knockout mice. Quantitative RT-PCR confirmed an up-regulation of cytochrome P450 enzymes, including Cyp4a10 and Cyp4A14, which were reported to be involved in ω-hydroxylation of saturated and unsaturated fatty acids. Moreover, two serine protease inhibitors showed a decreased expression in WISP1 knockout mice at all time points. Additionally, CIDEC, which was reported to promote the development of alcoholic steatohepatitis, was stronger induced on D1 in mice lacking WISP1.

In conclusion, my study identified for the first time that mice lacking WISP1 show an enhanced susceptibility to CCl_4- as well as to APAP-induced liver damage. These findings suggest that WISP1 might have a pro-survival and protective role with regard to acute liver injury. Time-resolved analysis detected alterations in signal transduction as well as changes in the inflammatory response. Furthermore, gene array data revealed changes regarding lipid metabolism in WISP1 knockout mice. Taken together, WISP1 seems to be an important protective mediator during acute liver injury and may be involved in the regulation of lipid metabolism as related to liver damage. The identification of a novel mediator during acute liver injury may also help to gain a deeper insight into the precise signal transduction and mechanisms in the progression of acute liver injury. Moreover, WISP1 seems to be an attractive potential target for therapeutic interventions, since human liver disease samples also showed an up-regulation of WISP1 expression.

ZUSAMMENFASSUNG

Chronische Lebererkrankungen des Menschen sind eine globale Belastung in der europäischen Bevölkerung, da schätzungsweise immer noch 29 Millionen Patienten davon betroffen sind. In der Vergangenheit gab es einen großen Fortschritt in Bezug auf das Wissen und den Umgang mit Leberkrankheiten. Der Verlauf einer frühen Leberfibrose hin zu einer chronischen Lebererkrankung kann unter anderem zu der Entwicklung einer Zirrhose oder eines hepatozellulärem Karzinoms führen. Entzündung, Zelltod, Ablagerung der Matrix oder Gefäßneubildungen sind charakteristische biologische Merkmale und können zur Entwicklung einer Leberfibrose beitragen. Einige dieser charakteristischen Merkmale sind auch bei einer Medikamenten-induzierten Lebertoxizität zu beobachten, welche immer noch eine der häufigsten Ursachen für den Rückzug eines Medikaments vom Markt ist. Früher wurden hepatotoxische Effekte meistens mit einer Veränderung des Metabolismus oder des Redoxzustandes assoziert. Allerdings ist es heutzutage bekannt, dass komplexe Signalübertragungen und transkriptionelle Mechanismen sowohl an der Entwicklung eines Leberschadens als auch bei der anschließenden Regeneration beteiligt sind.

Basierend auf Gene Array Analysen wurde WISP1 als das am stärksten hochregulierte Mitglied der CCN Familie bei einer Leberschädigung identifiziert. Zeitaufgelöste Genexpressionsanalysen mittels qRT-PCR bestätigten die Induktion von WISP1 in Leberhomogenaten. Weitere Analysen verschiedener Leberzellpopulationen zeigten, dass Hepatozyten die Hauptquelle der WISP1 RNA während einer CCl_4 Intoxikation sind. Zudem wurde eine Expression von WISP1 in humanem Gewebe, welches verschiedene Leberkrankheiten aufwies, detektiert. Zusätzlich konnte eine organspezifische Analyse in Mäusen zeigen, dass Organe wie die Lunge, das Gehirn und die Milz eine hohe WISP1 Expression aufweisen.

Um die Beteiligung von WISP1 an einer medikamenten-induzierten Leberschädigung zu untersuchen, wurden Mäuse mit einer genetischen Deletion des WISP1 Gens verwendet. Dieses genetisch veränderte Mausmodell wurde mit den gängigen Lebertoxizitätsmodellen Tetrachlorkohlenstoff (CCl_4) und Paracetamol (APAP) kombiniert. In einer zeitaufgelösten Analysen einer CCl_4-induzierten Leberschädigung konnte gezeigt werden, dass WISP1 knockout Mäuse nicht nur eine höhere Sensitivität aufweisen als die Wildtyp-Mäuse, sondern auch eine Zeitverschiebung in der Entstehung des Leberschadens zeigen. Diese erhöhte Empfindlichkeit konnte auch bei einem Paracetamol-induziertem Leberschaden gezeigt werden. Dies deutet daraufhin, dass der schützende Effekt von WISP1 nicht spezifisch ist, sondern WISP1 als ein allgemeiner Schüsselfaktor in der Antwort auf eine Leberschädigung gesehen werden kann. Dieser protektive Effekt von WISP1 konnte nicht auf eine Veränderung der Cytochrom P450 Enzyme oder des Redoxzustandes zugeführt werden. Die Genexpression von WISP1 war während eines CCl_4- und eines APAP-induzierten Leberschadens stark hoch reguliert, mit einem maximalen Wert nach 12h in den Wildtyp-

Mäusen. Während WISP1 auf der Proteinebene in großen Mengen auch im Plasma nachgewiesen werden konnte, waren die Werte im Lebergewebe eher gering.

Analysen der Signalübermittlung zeigten Änderungen im MAP-Kinase-Weg, wie zum Beispiel eine frühe Aktivierung der c-Jun N-terminale Kinasen (JNK) in CCl_4 behandelten WISP1 knockout Mäusen. Weiterhin konnte eine Aktivierung des JAK-STAT-Signalweges festgestellt werden, die mit einer erhöhten Entzündungsreaktion verbunden ist. Jedoch wurden keine Veränderungen in der Signalübermittlung nach Verabreichung von Paracetamol detektiert. Dies weist daraufhin, dass der protektive Phänotyp vermutlich durch andere Signalwege vermittelt wird.

Der vergrößerte Leberschaden in den WISP1 knockout Mäusen ist mit einer gesteigerten Immunantwort verbunden, welche durch eine erhöhte Expression an entzündungsfördernden Chemokinen und Zytokinen, sowie einer erhöhten Anzahl an infiltrierenden Immunzellen bestätigt werden konnte. *In vitro* Stimulationen von WISP1 knockout Hepatozyten, mit entzündungsfördernden Zytokinen, wiesen einen konzentrationsabhängigen Anstieg der Empfindlichkeit in Hinblick auf den Zelltod auf. Ein ähnlicher Effekt konnte unter Stimulation der Hepatozyten mit Paracetamol gezeigt werden.

Die Leberregeneration wurde nach Behandlung mit Tetrachlorkohlenstoff zeitabhängig bis Tag vier, mithilfe von histologischen Analysen, qRT-PCR und Western blot Analysen, untersucht. Hierbei war die Fähigkeit zur Regeneration nach einem Leberschaden in Wildtyp und WISP1 knockout Mäusen vergleichbar. Jedoch war der Leberschaden in WISP1 knockout Mäusen an Tag vier nicht vollständig regeneriert, was sich unter anderem in einer verlängerten Aktivierung von Proliferationsmarkern und zellzyklusabhängigen Genen, wie zum Beispiel PCNA und CycD1, zeigte. Dies deutet daraufhin, dass WISP1 in der Leberregeneration, nach einer CCl_4 Intoxikation, eine untergeordnete Rolle spielt.

Schließlich wurde eine zeitabhängige Gene Array Analyse von CCl_4 behandelten Wildtyp und WISP1 knockout Mäusen durchgeführt. Verglichen mit den Wildtyp Mäusen, waren Gene in den WISP1 knockout Mäusen, welche mit dem Metabolismus assoziiert sind herunter reguliert, während Gene, die mit dem Lipidmetabolismus verbunden sind, induziert waren. Mithilfe einer quantitativen Echtzeit-PCR wurde bestätigt, dass Cytochrome P450 Enzyme, wie Cyp4a10 und Cyp4a14, verstärkt exprimiert sind. Diese Enzyme sind an der ω-Hydroxylierung von gesättigten und ungesättigten Fettsäuren beteiligt. Außerdem zeigten zwei Serin Protease Inhibitoren eine verminderte Expression in den WISP1 knockout Mäusen zu allen Zeitpunkten. Zusätzlich ist CIDEC, welches die Entwicklung einer alkoholischen Steatohepatitis fördern soll, an Tag eins in den WISP1 knockout Mäusen stärker induziert.

Abschließend kann festgestellt werden, dass meine Arbeit erstmalig zeigt, dass Mäuse die kein WISP1 besitzen, eine erhöhte Empfindlichkeit gegenüber einer Tetrachlorkohlenstoff- und einer Paracetamol-induzierter Leberschädigung aufweisen. Diese Ergebnisse zeigen, dass WISP1 einen schützenden und positiven Einfluss auf das Überleben der Leberzellen nach einer akuten Schädigung hat. Zeitaufgelöste Analysen haben Veränderungen in der Signalübermittlung, sowie in der Entzündungsreaktion ergeben.

Weiterhin zeigten Gene Array Daten, dass WISP1 knockout Mäuse Veränderungen in Hinblick auf den Lipid Metabolismus aufweisen. Zusammenfassend kann festgehalten werden, dass WISP1 ein wichtiger und protektiver Vermittler während einer akuten Leberschädigung zu sein scheint. Zudem könnte WISP1 in die Regulation des Lipidmetabolismus involviert sein. Die Identifizierung neuer Vermittler könnte helfen, ein tieferes Verständnis für die Signalübermittlung und die Mechanismen während einer akuten Lebertoxizität zu bekommen. Da auch menschliche Proben eine Induktion der Expression von WISP1 zeigten, scheint WISP1 außerdem ein attraktives Target für potentielle therapeutische Interventionen zu sein.

ABBREVIATIONS

%	Percent
°C	Celsius degree
µg	Microgram
µl	Microliter
µm	Micrometer
ActD	Actinomycin D
AIF	Apoptosis-inducing factor
ALF	Acute liver failure
ALT	Alanine aminotransferase
Ap-1	Activator protein-1
Apaf-1	Apoptotic protease activating factor-1
APAP	N-acetyl-p-aminophenol, Acetaminophen, paracetamol
APC	Adenomatous polyposis coli
APS	Ammonium persulphate
ASK1	Apoptosis signal-related kinase
AST	Aspartate aminotransferase
ATF	Activating transcription factor
ATP	Adenosine triphosphate
Axin	Axis inhibitor
Bax	Bcl-2-associated X protein
BCA	Bicinchoninic acid
Bcl-2	B-cell lymphoma-2
BcL-XL	B-cell lymphoma-extra large
Bid	BH3 interacting death domain
Bik	BCL-2 interacting killer
Bim	BCL-2-like-11
BIP	Binding immunoglobulin protein
BKL	Biobase Knowledge Library
bp	Base pair
BP	Biological process
BSA	Bovine Albumin Fraction V
Ca	Calcium
$CaCl_2$	Calcium chloride
CC	Cellular component
CCC	Cholangiocellular carcinoma
CCl	C-C motif chemokine
CCl_3*	Trichloromethyl free radical
CCl_3COO*	Trichloromethylperoxy radical
CCl_4	Carbon tetrachloride
CD	Cluster of differentiation
cDNA	Complementary DNA
cFLIP	Cellular fas-associated death domain-like interleukin-1-β-converting enzyme-inhibitory protein
cFLIPL	Full-length or long form of c-FLIP
CHOP	C/EBP homologous protein
CHX	Cycloheximide
cIAP1/2	Cellular inhibitor of apoptosis-1/2
CIDEC	Cell death inducing DFFA like effector c

CK1	Casein kinase 1
CM	Collagen monolayer
cm^2	Square centimeter
CO_2	Carbon dioxide
CRD	Cysteine-rich domain
CS	Collagen sandwich
CT	Cysteine knot
CTGF, CCN2	Connective tissue growth factor
ctrl	Control
CXC	C-X-C chemokine
CXCL	Chemokine (C-X-C motif) ligand 1
CXCR	C-X-C chemokine receptor
Cyc	Cyclin
Cyp1a2	Cytochrome P450 enzyme 1a2
Cyp2B1	Cytochrome P450 enzyme 2b1
Cyp2E1	Cytochrome P450 enzyme 2e1
Cyr61, CCN1	Cysteine-rich 61
D	Day
DAB	3, 3 -diaminobenzidine
DAMP	Damage-associated molecular pattern
Ddit3	DNA-damage inducible transcript 3
DEG	Differentially expressed gene
DEPC	Diethylpyrocarbonate
D-Gal	D-galactosamine
DILI	Drug-induced liver injury
DISC	Death-inducing signaling complex
DMEM	Dulbecco's Modified Eagle Medium
DNA	Deoxyribonucleic acid
dNTP	Deoxynucleotide triphosphate
DTT	DL-Dithiothreitol
DVL	Dishevelled
ECL	Enhanced Chemiluminescence
ECM	Extracellular matrix
EDTA	Ethylenediaminetetraacetic acid
EGF	Epidermal growth-factor
EGTA	Ethylene glycol tetraacetic acid
eIF-2α	Eukaryotic translation Initiation Factor 2-α
ELISA	Enzyme-linked immunosorbent assay
EndoG	Endonuclease G
ER	Endoplasmic reticulum
ERAD	ER-associated degradation
ERK	Extracellular signal-regulated protein kinases 1 and 2
Ero1l	Endoplasmic oxidoreductin-1-like protein
FADD	Fas-associated death domain
FBS	Fetal bovine serum
FDR	False discovery rate
FGF2	Fibroblast growth factor 2
fz	Frizzled
g	Gram
GADD34	Growth arrest and DNA damage-inducible protein-34

Gadd45β	Growth arrest and DNA damage-inducible 45 beta
GAPDH	Glyceraldehyde 3-phosphate dehydrogenase
GO	Gene ontology
GOI	Gene of interest
gp	Glycoprotein
GPCR	G-protein coupled receptors
GRG	Groucho-related gene
GRP94	Glucose related protein 94
GS	Glutamine synthetase
GSH	Glutathione
GSK3β	Glycogen synthase kinase-3β
h	Hour
H&E	Hematoxylin and eosin staining
H2O	Water
H2O2	Hydrogen peroxide
HCC	Hepatocellular carcinoma
HCl	Hydrogen chloride
HEPES	4-(2-hydroxyethyl)-1-piperazineethanesulfonic acid
HGF	Hepatocyte growth-factor
HKG	House keeper gene
HMGB1	High mobility group box 1 protein
HRP	Horseradish peroxidase
HSC	Hepatic stellate cells
Hsd3b5	Hydroxyl-delta-5-steroid dehydrogenase, 3 beta- and steroid delta-isomerase 5
HSGP	Heparin sulfate proteoglycan
Hsp	Heat shock protein
i.p.	Intraperitoneal
ICAM	Intercellular Adhesion Molecule
Ier3	Immediate early response 3
IFNγ	Interferon-γ
IGFBP	Insulin-like growth factor binding protein
IKK	Inhibitor of κB kinase
IL	Interleukin
IRE1α	Inositol-requiring enzyme 1α
ITCH	Itchy homolog
IκBα	Nuclear factor of kappa light polypeptide gene enhancer in B-cells inhibitor, alpha
JAK	Janus kinase
JNK	Jun NH2-terminal kinases
KCl	Potassium Chloride
kDa	Kilodalton
KEGG	Kyoto Encyclopedia of Genes and Genome
kg	Kilogram
KH_2PO_4	Potassium dihydrogen phosphate
L	Liter
Lcn2	Lipocalin 2
LEF	Lymphocyte enhancer-binding factor
LGS	Legless
LRP	Low-density lipoprotein receptor-related protein
LRP5/6	Low-density-lipoprotein-receptor-related protein 5/6
LSEC	Liver sinusoidal endothelial cells

mA	Milliampere
MAP2K, MEK or MKK	MAPK kinase
MAPK	Mitogen-activated protein kinase
MAPKKK, MAP3K	MAPK kinase kinase kinase
MF	Molecular function
mg	Milligram
$MgSO_4$	Magnesium sulfate
min	Minutes
ml	Milliliter
mM	Millimolar
MPT	Mitochondrial membrane permeability transition
mRNA	Messenger RNA
Mt	Metallothionein
mTNFα	Membrane-bound TNFα
mTOR2	Mechanistic target of rapamycin
Na_2HPO_4	Di-Sodium Hydrogen Phosphat anhydrous
NaCl	Sodium chloride
NAPQI	N-acetyl-p-benzoquinone imine
NEM	N-Ethylmaleimide
NF-κB	Nuclear factor kappa-light-chain-enhancer of activated B cells
ng	Nanogram
nm	Nanometer
Nov, CCN3	Nephroblastoma overexpressed
NP-40	Nonidet P-40
NPC	Non-parenchymal cell
PAGE	Polyacrylamide gel electrophoresis
PAMP	Pathogen-associated molecular patterns
PBS	Phosphate buffered saline solution
PCA	Principal component analyses
PCNA	Proliferating cell nuclear antigen
PCR	Polymerase chain reaction
PDGF	Platelet-derived growth factor
PDK1	Phosphoinositide-dependent protein kinase 1
PERK	PKR-like ER kinase
PFA	Paraformaldehyde
pg	Picogram
PI3,4,5-P3	Phosphatidylinositol-3,4,5-triphosphate
PI3K	Phosphatidylinositol 3-kinase
PI-4,5-P2	Phosphorylates phosphatidylinositol-4,5-bisphosphate
PKB	Protein kinase B
pmol	Picomole
PP1c	Protein phosphatase 1
PPAR	Peroxisome proliferator-activated receptors
PTEN	Phosphatase and tensin homolog
PVDF	Polyvinylidene fluoride
PYGO	Pygopus
qRT-PCR	Real-time quantitative PCR
RGD	Arg-Gly-Asp
RIP1	Receptor-interacting protein-1
RIP3	Receptor interacting protein kinase 3

RNA	Ribonucleic acid
RNase	Ribonuclease
ROS	Reactive oxygen species
rpm	Revolutions per minute
RSK	Ribosomal S6 kinase
RT	Reverse transcriptase
RTK	Receptor tyrosine kinase
S.E.	Standard error
S1P	Site 1 protease
S2P	Site 2 protease
SAPK	Stress-activated protein kinase
SDS	Sodium dodecyl sulfate
sec	Second
Ser	Serine
siRNA	Small interfering RNA
STAT3	Signal transducer and activator of transcription 3
sTNFα	Soluble TNFα
Sult2a8	Sulfotransferase family 2A, dehydroepiandrosterone (DHEA) – preferring, member 8
TAK1	Transforming growth factor-β-activated kinase-1
TBE	Tris/Borate/EDTA
tBID	Truncated BID
TBS-T	Tris Buffered Saline with Tween 20
TCF1	T-cell factor1
TEMED	Tetramethylethylenediamine
TGF-β	Transforming growth factor-β
TGFβR	TGF-β receptors
Thr	Threonine
TLR	Toll-like receptors
TNFR	TNF receptor
Tnfrsf12a	Tumor necrosis factor receptor superfamily, member 12a
TNFα	Tumor necrosis factor alpha
TRADD	TNFR1-associated death domain protein
TRAF2	TNF receptor-associated factor-2
TRIS	Tris(hydroxymethyl)aminomethane
TSP-1	Thrombospondin type-1
TUNEL	Terminal transferase uridyl nick end labelling
Tyr	Tyrosine
UNG	Uracil-DNA glycosylase
UPR	Unfolded Protein Response
V	Volt
VCAM-1	Vascular cell adhesion molecule 1
VSMC	Vascular smooth muscle cell
VWC	Von Willebrand factor type C
WISP1, CCN4	Wnt-inducible signaling pathway protein-1
XBP1	X-box binding protein 1
XIAP	X-linked inhibitor of apoptosis protein
α-KG	α-ketoglutarate

1 INTRODUCTION

1.1 The global burden of liver disease

The past 30 years revealed a major progress in the knowledge and management of liver diseases, however, there are still approximately 29 million individuals who suffer from chronic liver disease in Europe. Cirrhosis of the liver and primary liver cancer are significant indicators in terms of liver transplantation in Europe (5,500 per year) and represent the end-stage of liver pathology, thereby reflecting the associated mortality rate. Liver cancer is responsible for about 47,000 deaths per year in the EU, estimated by the World Health Organization (WHO). Furthermore, liver cirrhosis accounts for 1.8 % of all deaths in Europe (170,000 deaths per year). Harmful alcohol consumption, viral hepatitis B and C as well as metabolic syndromes related to obesity and being overweight are the four leading causes of chronic liver diseases. Each of these four causes is amenable to prevention and treatment, thereby leading to a potential reduction of liver diseases among the general population [1, 2].

The progression from chronic liver injury to cirrhosis often causes inflammatory damage, parenchymal cell death, matrix deposition and angiogenesis, all of which may lead to progressive fibrosis. Early hepatic fibrosis, the wound healing response of the liver, can be resolved if the underlying cause is eliminated. However, in the case of cirrhosis only regression but without resolution can be expected as an improved clinical outcome. Epigenetic marks, cofactors such as obesity and alcohol, as well as genetic polymorphisms can enhance the risk of fibrosis progression [3, 4]. Taken together, there is a strong need for prevention programs, novel treatments and early stage diagnosis to help preventing the progression to further clinical stages and complications [1, 2].

Moreover, another cause for liver disease in Europe is drug-induced liver injury (DILI). This is one of the most critical problems leading to the failure of many drugs during preclinical and clinical studies [5] and occurs in an incidence of 10 to 15 in 10,000 to 100,000 in the United States [6]. Additionally, hepatotoxicity is the leading cause of drug withdrawal from the market [7]. DILI is multi-factorial and can mimic all forms of acute and chronic liver disease such as hepatitis or cholestasis, which shows the complexity of clinical scenarios [6]. Moreover, similar to chronic liver disease, there are various factors which can influence DILI, such as the adaptive immune system, infections, environment factors and genetics. Therefore, many drugs pass the animal toxicity tests, because they are performed in healthy animals [7].

Taken together, this highlights the need for a deeper understanding and further investigations into biological processes, for example, inflammation and cell death during acute and chronic liver injury, as a means of tackling the burden and problem of liver disease.

1.2 Liver

The liver is situated in the upper right area of the abdominal cavity, close to the diaphragm (Figure 1). It serves a central role in metabolic homeostasis and detoxification of the body. The liver is responsible for synthesis, storage, metabolism and redistribution of vitamins, fats, carbohydrates and nutrients. Moreover, production of albumin, acute-phase proteins and cofactors are important functions of the liver [8, 9]. Approximately 80 % of the blood supply comes from the portal vein, containing nutrient-rich blood from stomach and intestine. The remaining 20 % of blood supply comes from the hepatic artery, which provides oxygenated blood from the aorta [10, 11]. The blood exits the liver through the hepatic vein, which drains into the inferior vena cava.

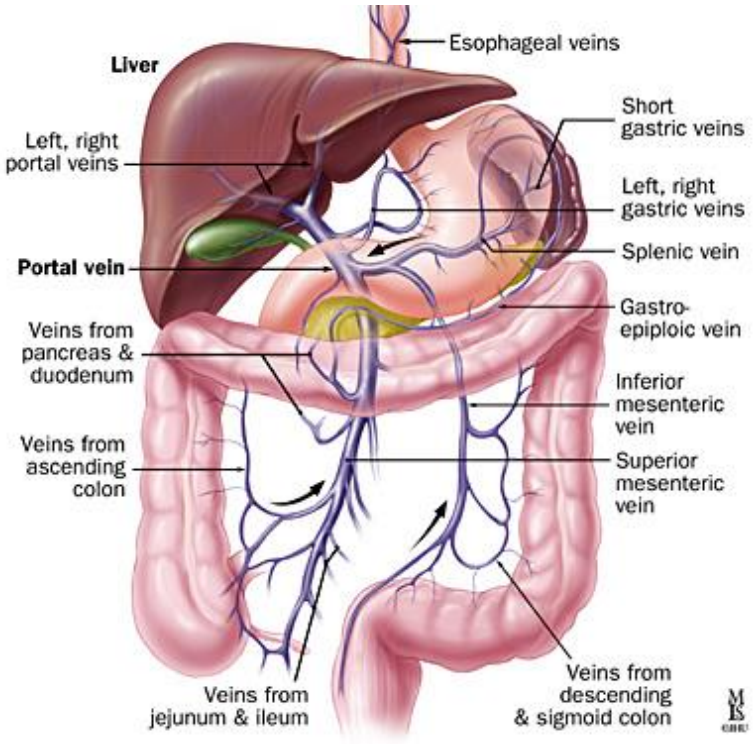

Figure 1: **Liver enterohepatic circulation.** Approximately 80 % of liver blood supply comes from the portal vein and 20 % from the hepatic artery. Blood derived from the portal vein is rich in nutrients and pathogen-derived molecules, since it is derived by the capillaries from gastrointestinal tract, pancreas and spleen. Therefore, xenobiotics will pass the liver through the portal vein for metabolization [12]. (Figure from http://www.Hopkins-gi.org)

1.3 Structure (basic anatomy)

The classical structural unit of the liver is called hepatic lobule. It has a hexagonal shape and the central vein is localized in the middle of the hepatic lobule (Figure 2). At the edges of the lobule there are the portal triads, which are constituted by the portal vein, bile duct and the hepatic artery. Plates of hepatocytes (cords) radiate from the central vein to the borders of the lobule. The hepatic sinusoids, which separate the hepatic plates from one

another, are lined by liver sinusoidal endothelial cells. The blood flows through the sinusoids from the portal triad via the central vein and drains into the hepatic vein, which then leaves the liver and enters into the inferior vena cava [13, 14]. The plates of hepatocytes are joined by tight junctions, adherens junctions and the desmosomal belt. The apical pole is represented by the bile canaliculi, which are formed in the interface of the hepatocytes. The bile flows (as opposed to the blood flow) from the bile canaliculi into the bile ducts, which are localized at the portal triads. The basolateral site of hepatocytes are in contact with blood capillaries or sinusoids, where the secretion of various components and the uptake of recycled bile salts occur. To increase the surface for the exchange of substances, the hepatocytes have microvilli which extend in the space of Disse [15].

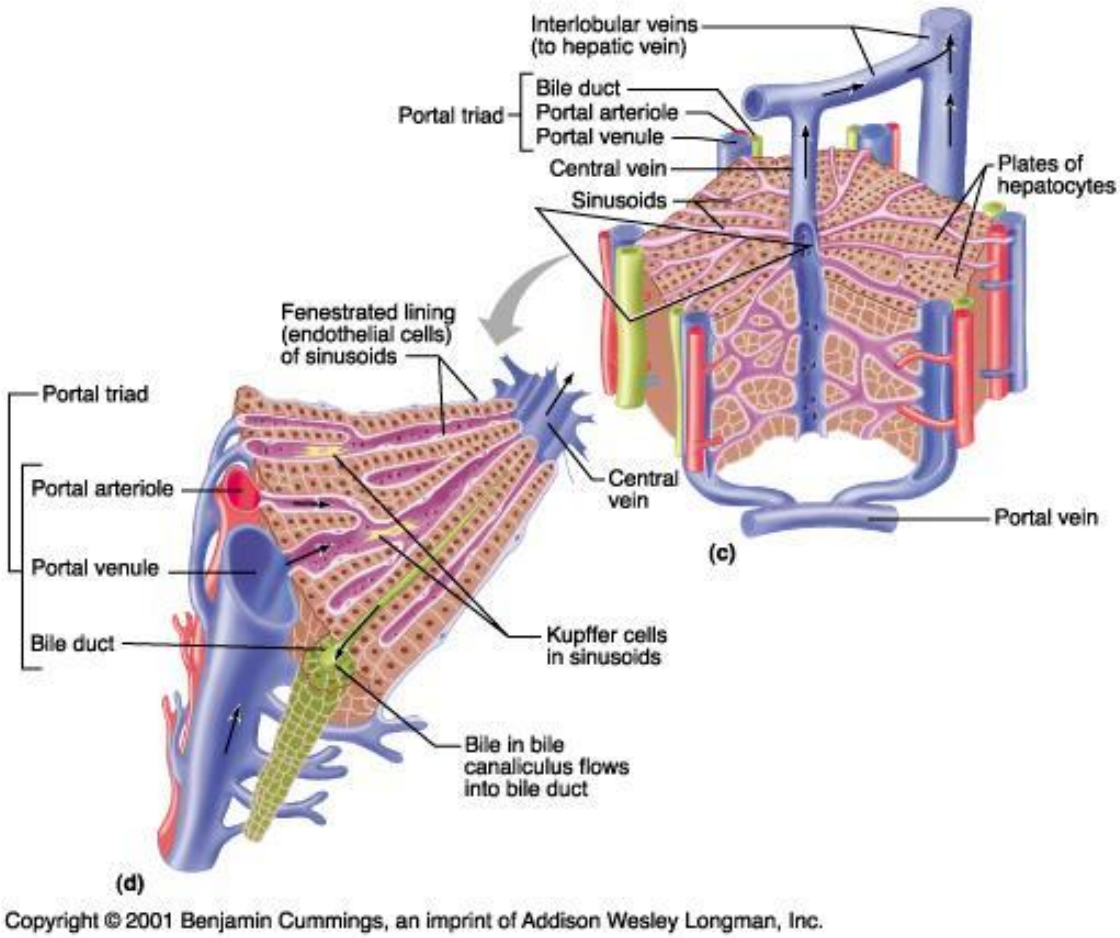

Figure 2: Basic structure of a hepatic lobule. The diagram shows the classical structure unit of the liver: the hepatic lobule. At the edges, the portal triads are placed, consisting of the hepatic artery, the bile duct and the portal vein. From the central vein, plates of hepatocytes (cords) radiate to the perimeter of the lobule. The blood flows through hepatic sinusoids from the portal triad to the central vein (Figure from http://www.easynotecards.com).

1.4 Liver zonation

The liver acinus is the smallest functional unit of the liver and is characterized by the regional compartmentalization of metabolic capacities and can be divided into three zones: a periportal zone (1), a transitional zone (2) and a pericentral zone (3) (Figure 3). Within these zones, different metabolic pathways are described, which are regulated by chemical gradients of oxygen, hormones, growth factors and metabolites. There are two types of metabolic zonation in the liver: the gradient (dynamic) and the compartment (stable) zonation. The gradient-type zonation works dynamically in response to sinusoidal blood-flow derived gradients. All hepatocytes in this zonation express the gene, but in a gradient-dependent manner. One example is the gluconeogenesis process, which exhibits a periportal to pericentral gradient of activity. In the compartment-like zonation, gene-products are expressed only in a restricted region, independent of the metabolic state of the liver. The best examples of compartment-like zonation are ammonia metabolism and glutamine synthetase (GS) [11, 16, 17].

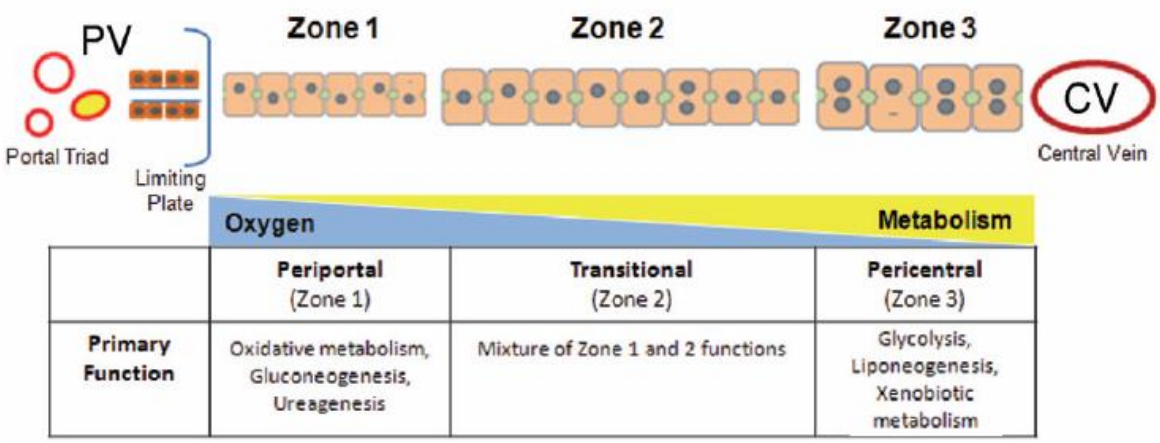

	Periportal (Zone 1)	Transitional (Zone 2)	Pericentral (Zone 3)
Primary Function	Oxidative metabolism, Gluconeogenesis, Ureagenesis	Mixture of Zone 1 and 2 functions	Glycolysis, Liponeogenesis, Xenobiotic metabolism

Figure 3: Structural and functional zonation of the liver. Discrete zones of the liver between the portal vein (PV) and the central vein (CV). The figure illustrates the difference in cell size, phenotype and gradients in the oxygen tension and metabolism. Figure adapted and modified from [15].

1.5 Liver cell types and function

Hepatocytes, also known as the parenchymal cells, account for about 80 % of liver mass. The remaining 20 % is comprised of non-parenchymal cells including Kupffer cells, stellate cells, liver sinusoidal endothelial cells, cholangiocytes, neutrophils and lymphocytes [8, 18].

The space of Disse is the perisinusoidal space between the basolateral surface of the hepatocytes and the anti-luminal side of sinusoidal endothelial cells (Figure 4). The hepatic stellate cells are localized in the space of Disse. The Kupffer cells are localized on the luminal side of the endothelial cells [18, 19].

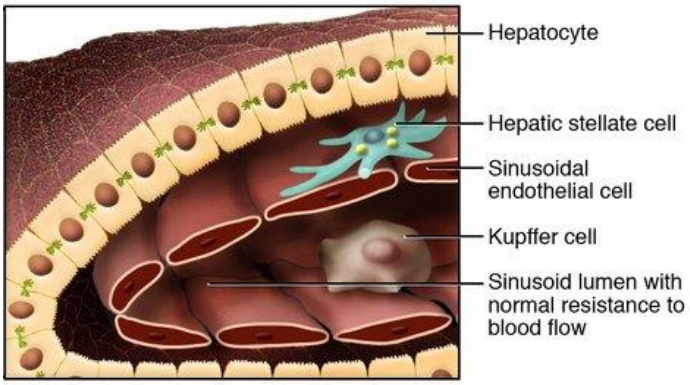

Figure 4: Major cell types in the liver. Several diverse cell types are located in the liver: hepatocytes, liver sinusoidal endothelial cells, Kupffer cells, hepatic stellate cells, cholangiocytes, hepatic progenitor cells, lymphocytes and neutrophils. Kupffer cells are localized in the hepatic sinusoids, which separate hepatic cords from one another. Hepatic stellate cells are localized in the space of Disse. Figure adapted and modified from [20].

1.5.1 Hepatocytes

Hepatocytes are highly differentiated epithelial cells that have primary roles in metabolism, protein production and biotransformation of xenobiotics. They make up about 60 % of the total cell population in the liver and have an average diameter of about 25-30 µm [21]. Hepatocytes have a cuboidal shape and possess one or more nuclei. They are rich in various cell organelles: mitochondria (about 1700 per cell on average), peroxisomes (about 370 per cell), lysosomes (about 250 per cell), Golgi complexes (about 50 per cell) and rough and smooth endoplasmic reticulum (about 15% of cell volume) [22, 23].

1.5.2 Liver sinusoidal endothelial cells (LSEC)

Liver sinusoidal endothelial cells (LSEC) comprise about 15-20 % of the liver cell population and about 50 % of the non-parenchymal cells in the liver [12, 23]. LSEC are elongated thin cells, which possess a large number of pinocytotic vesicles, representing a significant endocytotic activity. Moreover, a prominent feature of LSEC are multiple fenestrae throughout the cell, each with a diameter of 100 nm, which allow free diffusion of many substances between the blood and the hepatocyte basolateral surface. Additionally, they play an important role in hepatic immunity since they function as antigen-presenting cells and actively secrete cytokines, nitric oxide and some extracellular matrix (ECM) components [15, 21].

1.5.3 Kupffer cells

The Kupffer cells are liver-resident macrophages, which comprise about 8-12 % of the liver cell population and about 35 % of the non-parenchymal cells in the liver [21, 23]. They reside in the lumen of the liver sinusoids, adherent to the endothelial cells and thus they are

directly exposed to the contents of blood. Kupffer cells are known to have the endocytic and phagocytic capacity of efficiently extracting cellular debris, soluble bacterial products and endotoxins from the blood via endosomal and lysosomal pathways. Upon activation, e.g. during chemical-induced liver injury, Kupffer cells are able to produce cytokines in order to induce the expression of acute phase proteins to stimulate liver regeneration [12, 15, 24].

1.5.4 Hepatic stellate cells (HSC)

The hepatic stellate cells (HSC), also known as Ito cells, are located in the space of Disse. They are in close contact with both the sinusoidal endothelial cells and the hepatocytes. Making up about 3-8 % of the total number of liver cells, they present long extend dendrite-like processes that wrap around the sinusoids. During resting conditions hepatic stellate cells store vitamin A and lipids. However, upon chronic liver damage, they transdifferentiate to a fibrogenic, ECM-producing and proliferating cell phenotype. Moreover, HSC are considered to produce growth factors and cytokines, which play an important role in the regulation of hepatocyte growth and the development of inflammatory response [21, 23, 25].

1.5.5 Cholangiocytes

Cholangiocytes, also identified as intrahepatic bile duct cells, are biliary epithelial cells that line the bile ducts. They make up about 5 % of the total liver cell population and play an important role in regulating liver immune response through secretion of cytokines and mediators influencing the immune cell activity [15, 26].

1.6 Drug metabolism and hepatotoxicity

The liver is the main detoxifying organ of the human body. Drug and xenobiotics are taken up by the liver and converted into a water-soluble product, which can be easily excreted. These reactions are comprised of two steps: First Phase I, in which highly reactive functional groups are created by oxidation, reduction or hydrolysis; second Phase II, in which reactive products of phase I are conjugated into a highly polar (soluble) and inactive derivate that can be excreted [27].

Most of phase I reactions are catalyzed by cytochrome P450 enzymes. These enzymes belong to the superfamily of heme enzymes, and about one quarter of the 57 cytochromes P450s are considered to be involved in the metabolism of xenobiotics [28, 29]. Moreover, the metabolism of drugs and xenobiotics by cytochrome P450 enzymes exhibit a well-defined zonation occurring mostly in the pericentral region [30]. For example, Cyp2E1 is known to be involved in the metabolism of ethanol, carbon tetrachloride (CCl_4) and acetaminophen (APAP), and its expression is restricted to the pericentral zone [31-33].

Conjugation reactions in phase II are catalyzed by glutathione S-transferase, N-acetyltransferases, UDP- glucuronosyltransferase or sulfotransferases [34]. In the pericentral zone, glucuronidation takes place, whereas sulfation occurs predominantly in the periportal zone [11].

1.7 Animal models of hepatotoxicity

Acute liver failure, due to drug-induced hepatotoxicity, is the leading cause of acute liver failure in both the North American and European countries. Acetaminophen (APAP) accounts for nearly 50 % of all cases of acute liver injury. Additionally, 10 % of all cases are due to acute liver failure because of hepatitis A and B infections and nearly 5 % of all cases are associated to auto-immune hepatitis. Therefore, the availability of experimental models is needed to provide a better understanding of acute liver injury as well as to identify novel drug targets and assess the mechanisms of toxicity [33, 35]. One of the most popular models for investigating hepatotoxic effects in the liver, is APAP. However, models involving carbon tetrachloride (CCl_4), ethanol, thioacetamide and endotoxin are also commonly used [36].

1.7.1 Carbon tetrachloride

Carbon tetrachloride (CCl_4) is a well-known toxicant, which is widely used to induce liver injury in mice [37-39]. It has also been used as an organic solvent in industrial processes like spray painting, degreasing or metal processing [40]. CCl_4 becomes activated through Cyp2e1 enzymes and to a minor extend by Cyp2B1. Biotransformation of CCl_4 leads to the production of highly reactive and hepatotoxic trichloromethyl free radical (CCl_3*), which can covalently bind to lipids, proteins or DNA (Figure 5). CCl_3* can further react with oxygen, leading to the conversion into an even more reactive trichloromethylperoxy radical (CCl_3COO*). This free radical can cause hepatotoxic damage by lipid peroxidation reactions on the cell membranes. Finally, CCl_4-metabolites cause covalent binding and lipid peroxidation, which influences the cellular homeostasis leading to the induction of oxidative stress and cellular damage [41, 42].

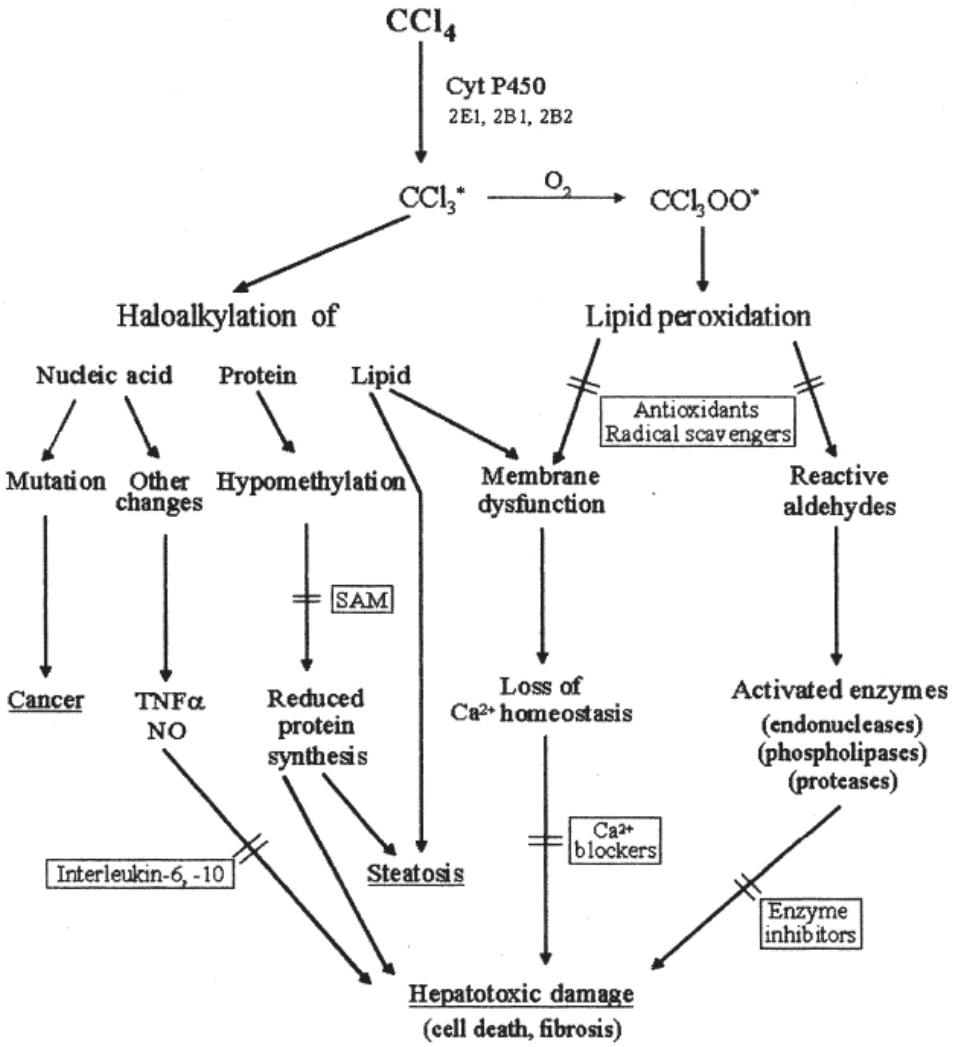

Figure 5: Biotransformation and cell toxicity of CCl_4. For the metabolic activation of CCl_4, cytochrome P450 enzymes (Cyp2E1) are necessary. Biotransformation generates highly reactive trichloromethyl free radical (CCl_3*), which can react with various biological substances. Furthermore, CCl_3* can react with oxygen, forming a more reactive metabolite trichloromethylperoxy radical (CCl_3OO*). As a consequence, covalent binding and lipid peroxidation affects liver cell homeostasis leading to the induction of oxidative stress and severe cell damage. Figure adapted and modified from [41].

1.7.2 Acetaminophen (APAP)

Acetaminophen (APAP, paracetamol, N-acetyl-*p*-aminophenol) is an analgesic and antipyretic drug which is currently being used worldwide. Moreover, in therapeutic doses it is well accepted as an effective and safe drug [43, 44]. However, an overdose of acetaminophen can cause centrilobular hepatic necrosis and even acute liver failure (ALF) in humans and experimental animals [45]. Similar to CCl_4, the toxicity of APAP is strongly dependent on the metabolism by cytochrome P450 enzymes, such as Cyp2E1 [46, 47]. Once APAP is metabolized by Cyp2E1, reactive intermediate N-acetyl-p-benzoquinone imine (NAPQI) is generated, which is rapidly conjugated to glutathione (GSH) for detoxification (Figure 6). However, toxic doses cause cellular and mitochondrial GSH depletion, which leads to excessive reactive metabolite formation that causes protein adduct formation.

Modification of mitochondrial proteins causes mitochondrial damage, ATP depletion and oxidative stress, which leads to the activation of JNK pathway. Activated JNK translocates to the mitochondria and further increases reactive oxygen species (ROS) formation, leading to mitochondrial membrane permeability transition (MPT). Lysis and matrix swelling of the outer mitochondrial membrane lead to the release of endonucleases apoptosis-inducing factor (AIF) and endonuclease G (EndoG) from the mitochondria. Endonucleases translocate to the nucleus and cause nuclear DNA fragmentation, finally leading to oncotic necrosis [7, 48-51].

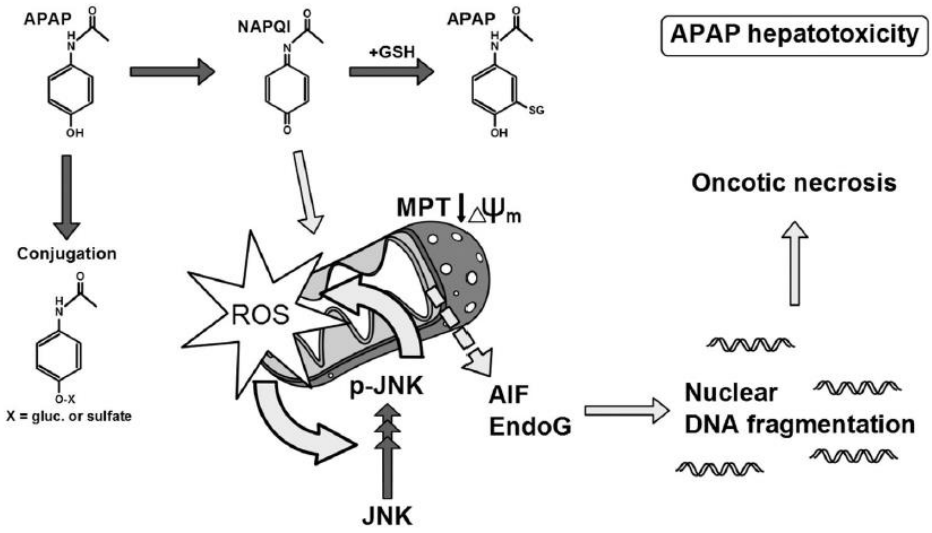

Figure 6: Mechanism of acetaminophen toxicity. Under therapeutic conditions, acetaminophen (APAP) is conjugated and excreted. A small amount is converted into the reactive metabolite N-acetyl-p-benzoquinone (NAPQI). Small amounts of NAPQI can be detoxified by glutathione (GSH), however, an overdose of NAPQI leads to covalent binding to proteins which in turn lead to mitochondrial protein alkylation and the induction of oxidative stress. Therefore, JNK pathway is activated and p-JNK translocate to the mitochondria and further increases the oxidative stress. Mitochondrial membrane permeability transition (MPT) occurs, resulting in the release of endonucleases apoptosis-inducing factor (AIF) and endonuclease G (EndoG) from the intermembrane space. Endonucleases translocate to the nucleus and lead to nuclear DNA fragmentation. Figure adapted and modified from [48, 49].

1.8 Sterile inflammation during acute liver injury

Hepatic inflammation is a common feature of various liver diseases, such as alcohol steatohepatitis, nonalcoholic steatohepatitis, ischemia/reperfusion and drug-induced liver injury. This sterile inflammatory response occurs without involvement of pathogens and is required for wound repair and restoration of homeostasis. However, dysregulated sterile inflammation can lead to various acute and chronic inflammatory diseases [52, 53].

Figure 7 represents the mechanism of drug-induced sterile inflammation, which is well described for APAP and CCl_4 toxicity [25, 54-56]. Drugs or chemicals can be metabolized by hepatocytes, leading to the formation of reactive metabolites. Such metabolites can cause cell injury and necrosis. Thereby, cellular components such as DNA, RNA and proteins

are released. These cellular components are also called damage-associated molecular patterns (DAMPs) and are known to trigger inflammation via binding to toll-like receptors (TLR) on macrophages and neutrophils. DAMPs, such as DNA, bind to TLR9 whereas HMGB1 acts through TLR4 [53, 56-60]. Engagement of TLR on Kupffer cells activates NF-κB pathway, resulting in the production of pro-inflammatory cytokines (TNF-α, IL-6, TGF-β, IL-10, IL-1), chemokines (CXCL2, CXCL8) and reactive nitrogen and oxygen species. Elevated levels of TNF-α mainly cause activation of death receptor signaling in hepatocytes, leading to an amplification of hepatocyte cell death [61-63]. However, IL-6 is known to activate STAT3 signaling in hepatocytes leading to the transcription of anti-apoptotic and anti-oxidative genes [55]. Secretion of IL-1β and chemokines by Kupffer cells trigger neutrophil extravasation through expression of adhesion molecules, such as ICAM-1 or VCAM-1, on endothelial cells [25, 64]. However, accumulation of neutrophils cause release of ROS and proteases, evoking further hepatocyte necrosis [61], as well as phagocytosis of cell debris for contribution to wound healing [65, 66].

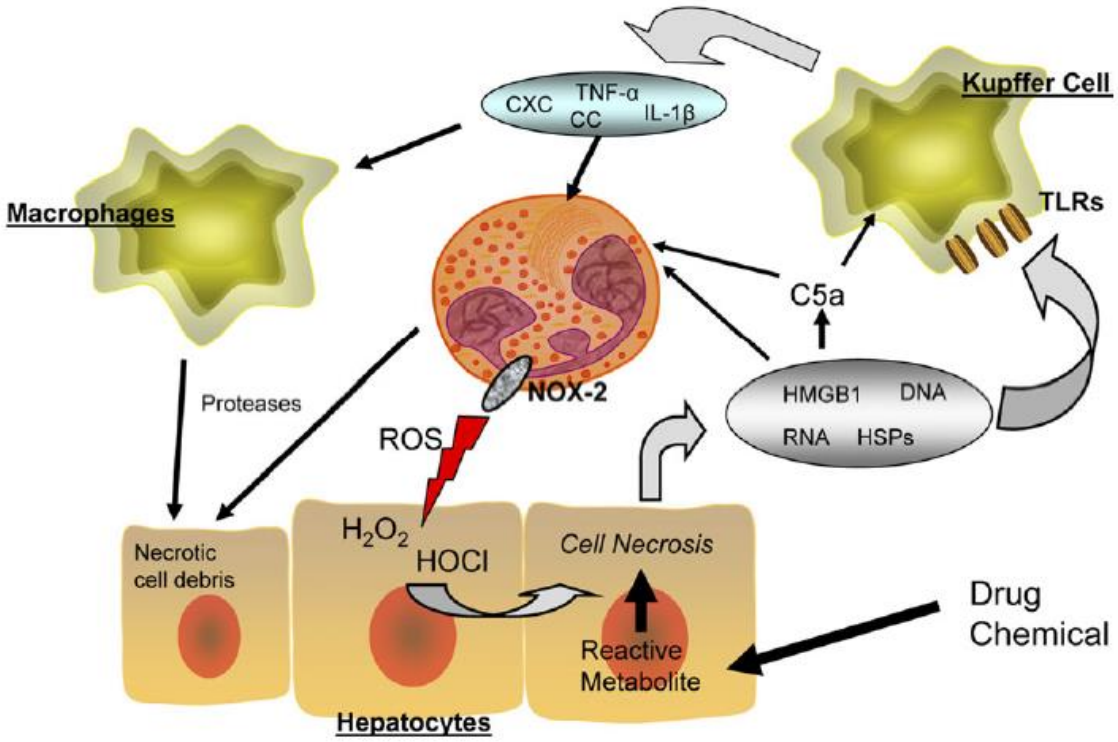

Figure 7: Mechanism of drug-induced sterile inflammation. Drugs or chemicals can induce cell necrosis and injury via reactive metabolites, resulting in the release of cellular components like DNA, RNA and proteins (HMGB1, HSPs). These damage-associated molecular patterns (DAMPs) bind to toll-like receptors on macrophages and neutrophils, triggering cytokine and chemokine secretion. Thereby, monocytes and neutrophils in the blood can be activated and recruited to the liver. Subsequently, they extravasate into the parenchyma and adhere to the target cells. By generating reactive oxygen species (ROS), neutrophils can trigger cell toxicity. However, both neutrophils and macrophages can phagocytose cell debris. Figure adapted and modified from [64].

Various studies showed that there are still controversies concerning the contribution of inflammation to acute liver injury. For example, Liu et al [67] investigated the role of neutrophils in the progression of APAP toxicity. In this case, neutrophils were depleted using anti-Gr-1 antibody before the administration of APAP, resulting in reduced APAP-induced toxicity. However, Jaeschke et al [68] suggested that the protective effect of depleting neutrophils is mediated through the induction of metallothionein 1 (MT-1) and MT-2, which were reported to protect the organism against liver injury [69]. Furthermore, antagonism of TLR or inhibition of DAMP receptors were shown to protect against hepatic ischemia-reperfusion injury [70, 71] and deletion of interferon-γ (IFNγ) reduced liver injury upon APAP overdose in mice [72]. Taken together, these studies suggest a pro-damaging influence of inflammation upon liver injury. In contrast, several studies showed a pro-regenerative contribution of inflammation. For example, depletion of Kupffer cells ($CD68^+$) using clodronate liposomes resulted in an enhanced hepatic injury combined with an increase of TNF levels in serum [73, 74]. Moreover, genetic deletion of STAT3 in myeloid cells reduced liver damage upon administration of CCl_4, which was found to be associated with enhanced immune cell infiltration, cytokine and chemokine formation and elevated hepatic STAT3 activation [55].

In conclusion, these studies highlight the complexity of inflammation during acute liver injury. There is a strong need for further investigations regarding the impact of inflammation, in particular homeostatic processes versus pathological processes.

1.9 Signaling pathways involved during hepatotoxicity/regeneration

1.9.1 Canonical Wnt/β-catenin pathway

Currently, the Wnt/β-catenin pathway is the best understood pathway controlling liver zonation. Drug metabolism is strongly dependent on Wnt pathway, since the expression of two major cytochrome P450 enzymes (Cyp2e1, Cyp1a2) is controlled by Wnt signaling [30]. Sekine et al showed that mice with a specific deletion of β-catenin were insensitive to CCl_4 administration [75]. Out of 19 Wnt factors identified in mice, 11 are known to be expressed in the liver [76, 77]. Moreover, WISP1 was reported to be a Wnt/β-catenin-induced protein [78].

Periportal hepatocytes are rich in APC (adenomatous polyposis coli), the inhibitor of β-catenin, allowing accumulation of active unphosphorylated β-catenin in perivenous hepatocytes (Figure 8). Deletion of APC leads to a perivenous-like liver, whereas deletion of β-catenin leads to a periportal-like liver [30].

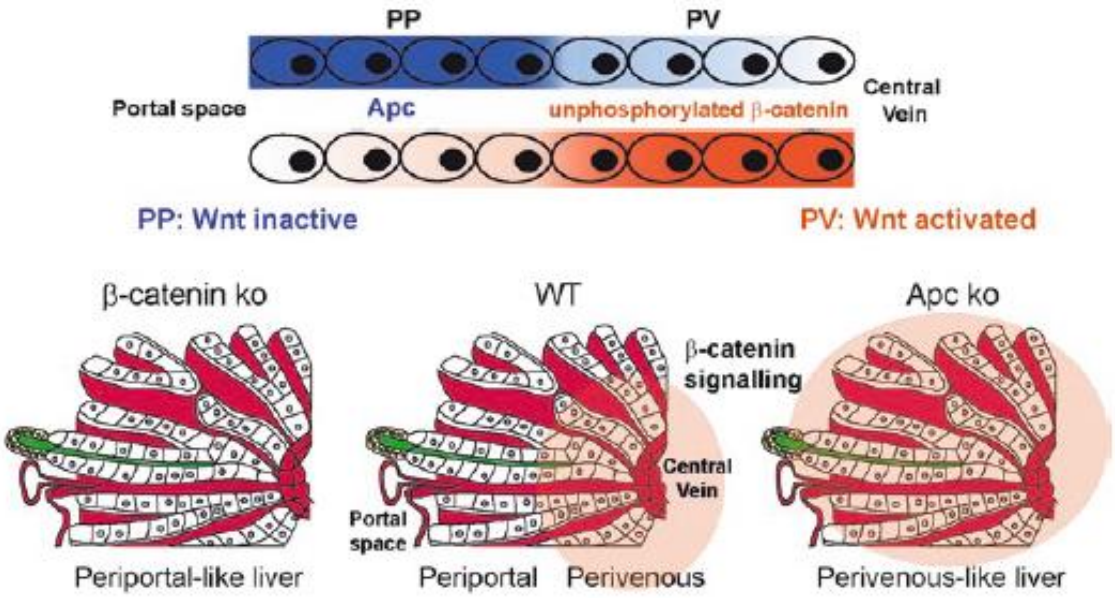

Figure 8: Wnt/β-catenin pathway in liver zonation. APC is enriched in periportal hepatocytes, leading to the accumulation of unphosphorylated β-catenin in the perivenous region. Deletion of β-catenin in mice leads to a periportal-like liver, whereas an APC knockout leads to a perivenous-like liver. Adapted from Colnot et al. Figure adapted and modified from [30].

In the absence of Wnt, β-catenin is kept at low levels by association to a degradation complex. This complex is formed by the active serine-threonine kinase glycogen synthase kinase-3β (GSK3β), two tumor suppressor proteins called APC (Adenomatous Polyposis coli) and Axin (Axis inhibitor) as well as the serine/threonine kinases CK1 (casein kinase 1) (Figure 9a). Whereby, GSK3β and CK1 phosphorylate β-catenin, which results in the ubiquitination of β-catenin by β-TRCP. This leads further to the proteasomal degradation of β-catenin. TCF1 (T-cell factor)/LEF (lymphocyte enhancer-binding factor) is bound to the nucleus and inactivated by repressors belonging to members of the GRG (groucho-related gene) family. Activation of Wnt signaling starts by binding of Wnt to its receptor Frizzled (fz) through the cysteine-rich domain (CRD), together with its co-receptor low-density-lipoprotein-receptor-related protein 5/6 (LRP5/6) (Figure 9b). Binding of Wnt to its receptor leads to the inactivation of GSK3β by dishevelled (DVL; the mammalian homologue of the Drosophila melanogaster protein DSH) resulting in the dissociation of β-catenin degradation complex. Therefore, unphosphorylated β-catenin translocates to the nucleus and associated with TCF1 leading to the activation of transcription of target genes. The transcription activity depends on pygopus homologue (PYGO) and legless homologue (LGS), two nuclear proteins [30, 79, 80].

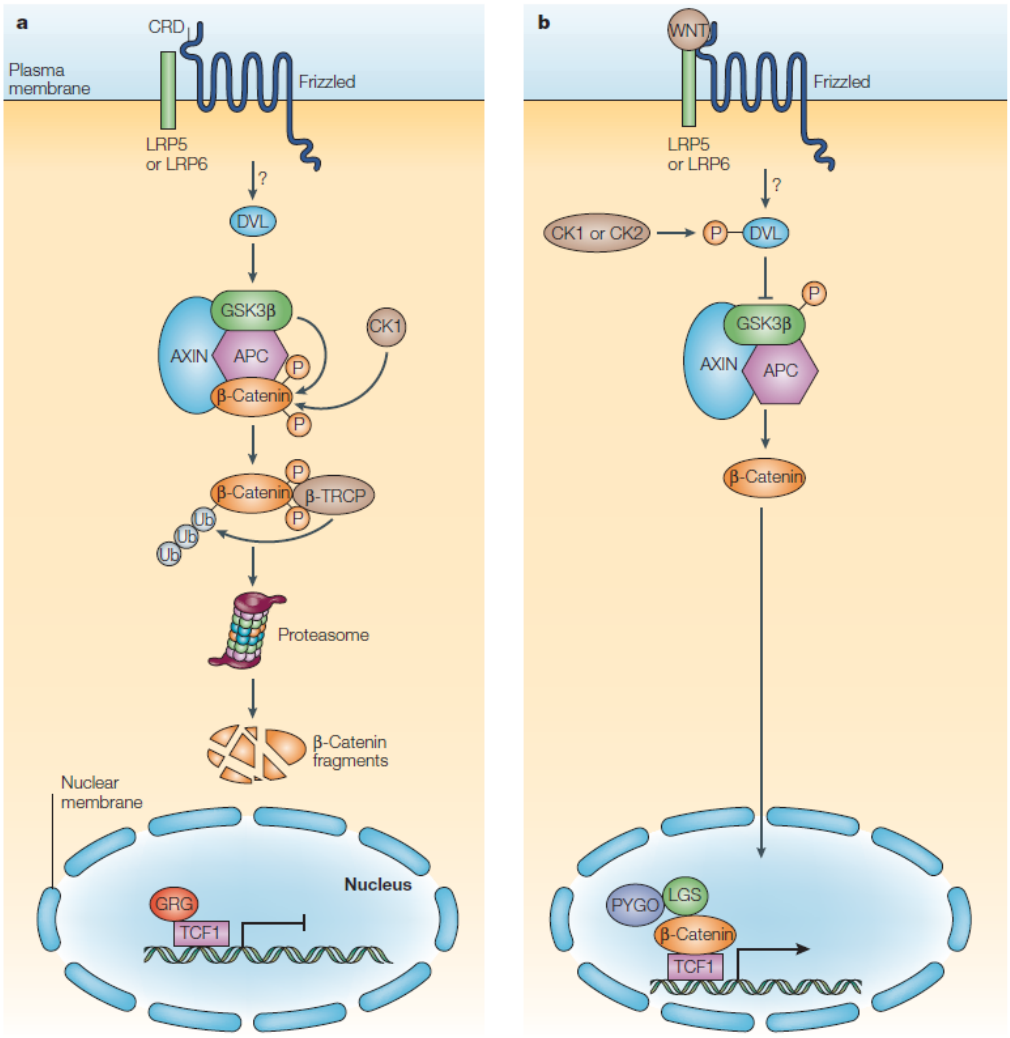

Figure 9: Wnt/β-catenin pathway. a) Non-activated Wnt signaling. In the absence of Wnt, β-catenin is kept at low levels in the cytoplasma through phosphorylation of CK1 and GSK3β, within the degradation complex. Phosphorylated β-catenin is ubiquitinylated by β-TRCP, resulting in the degradation by the proteasome. **b) Activated Wnt signaling.** Wnt binding to its receptor Frizzled (fz), together with the co-receptor LRP5 or LRP6, causes dissociation of the degradation complex. Unphosphorylated β-catenin translocates to the nucleus and binds to TCF, which leads to the transcription of target genes. Figure adapted and modified from [79]**.**

1.9.2 Janus kinase (JAK) - signal transducer and activator of transcription (STAT) pathway

As described above, inflammation is a major feature of drug-induced liver injury. Thereby, activated Kupffer cells produce pro-inflammatory cytokines, such as TNFα or IL-6, which influence further immune cell infiltration during the progress of liver injury. One of the best known signaling pathways, induced during liver inflammation and regeneration, is the JAK-STAT-pathway. Hepatoprotective cytokine IL-6 can bind to its receptor gp80 located on hepatocytes, leading to the dimerization of gp130 signal chain (Figure 10). The JAK kinase is associated with gp130 chains where it undergoes dimerization and autophosphorylation. Subsequently, activated JAK phosphorylates gp130, which further activates STAT3 monomers. Once STAT3 is phosphorylated, it forms dimers and translocates to the nucleus,

inducing the expression of various genes including anti-oxidative and anti-apoptotic genes, thereby protecting the hepatocytes from damage [8, 21, 55, 81, 82].

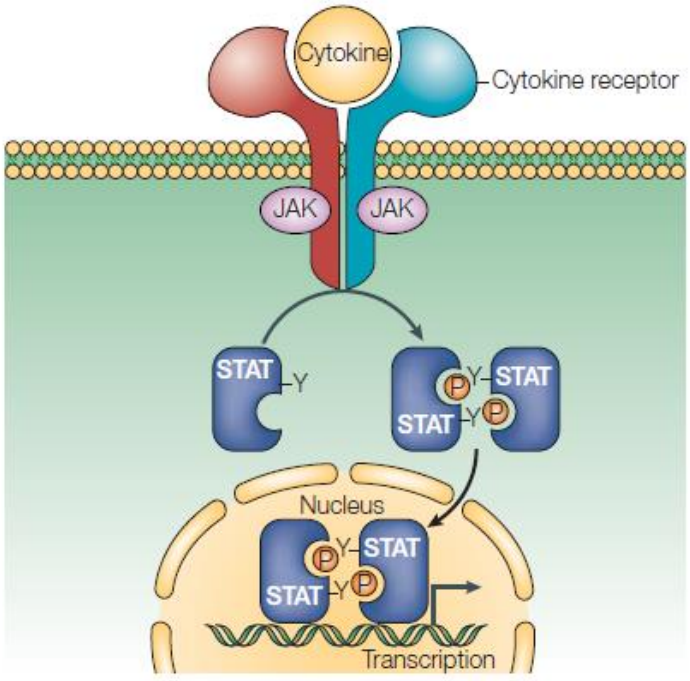

Figure 10: Schematic representation of JAK-STAT-pathway. Binding of cytokines to the receptor results in the dimerization of the receptor. Subsequently, activated JAK tyrosine kinases lead to the phosphorylation of cytoplasmic transcription factors STAT. Phosphorylation allows dimerization of STATs leading to the translocation into the nucleus, which results in the activation of transcription of various target genes. Figure adapted and modified from [83].

1.9.3 Mitogen-activated protein kinase (MAPK)

Several studies of downstream targets of MAPK signaling revealed an important contribution to drug-induced liver injury such as JNK. Already a decade ago, Gunawan et al reported that JNK is critical for APAP toxicity since JNK inhibitor (SP600125) was shown to reduce APAP-induced liver injury in mice. This was demonstrated in reduced serum transaminases values and smaller dead cell areas. However, a protective effect was not observed when using ERK (PD98059) or p38 (SB203589) inhibitors. In the same study, the usage of JNK inhibitor did not protect against liver injury upon CCl_4 intoxication [84]. Recently, Cubero et al demostrated that combined activity of JNK1 and JNK2 protects against APAP-induced liver injury by controlling the oxidative stress response. Moreover, deletion of JNK 1 and 2 in hepatocytes ($JNK^{\Delta hepa}$) led to a sustained JNK1 activation of infiltrating cells and NPCs upon APAP administration, which correlates with increased transaminases and enlarged dead cell areas [85]. Furthermore, activation of ERK1/2 was associated with DNA replication of hepatocytes *in vivo* and proliferation of hepatocytes *in vitro* [82]. On the top of that, Bhushan et al showed a dose-dependent increase of phosphorylated ERK as well as p38 after APAP intoxication [86]. Preclinical studies, which investigated p38 inhibitors, showed a

reduced inflammatory response in animal models suggesting a pivotal role in the regulation of inflammation [87-89].

Mitogen-activated protein kinase (MAPK) signal transduction pathway is a highly conserved eukaryotic mechanism of cells known to regulate important cellular functions, such as proliferation, differentiation or apoptosis [88]. Upon activation through hormones, growth factors, cytokines, DAMPs, PAMPs or environmental stress, a kinase cascade consisting of various MAPKs is activated (Figure 11). First, MAPK kinase kinase (MAP3K or MAPKKK) phosphorylates and thereby activates MAPK kinase (MAP2K; MAPKK; MKK or MEK), leading to the activation of one or more MAPKs. Specific MAP2K are known to activate their downstream MEKs, for example, MEK1/2 activates the MAPK ERK1/2, whereas MKK4/7 lead to the activation of MAPK JNK1/2/3 and MKK3/6 activates p38 isoforms respectively. Those MAPK can further phosphorylate various targets such as transcription factors, membrane transporters, nuclear pore proteins or other kinases [88, 90]. More importantly, there is dynamic balance among the three MAPKs ERK1/2, JNK1/2/3 and p38, which is fundamental for the fate of the cell [91].

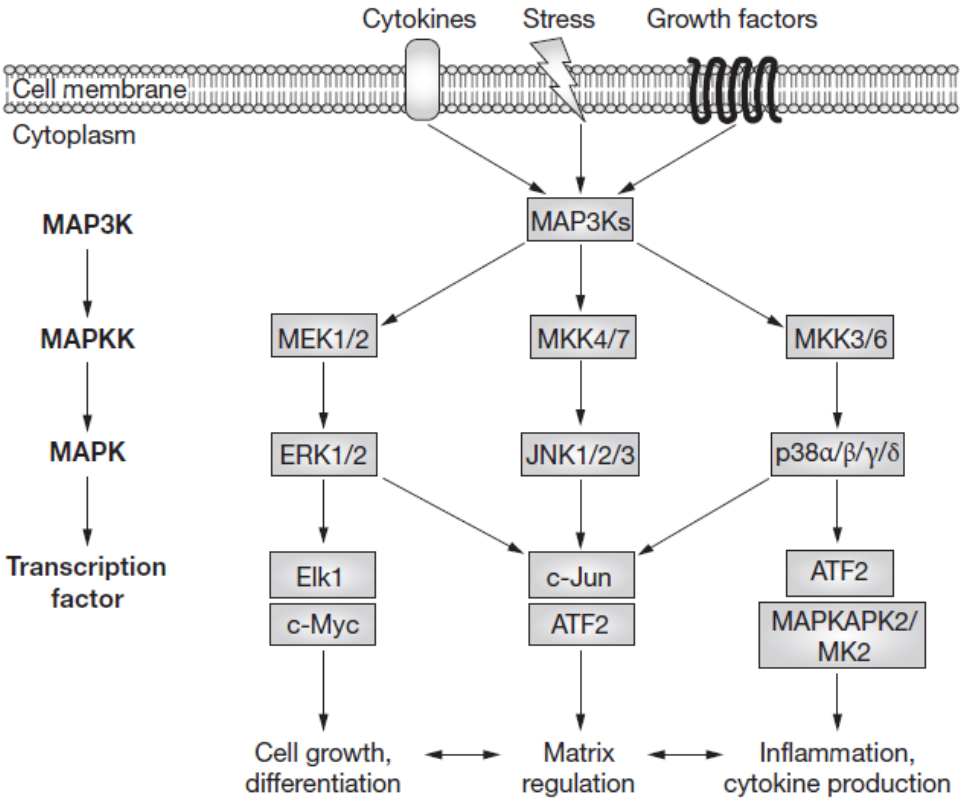

Figure 11: The MAPK signaling cascade. Extracellular stimuli can activate a kinase cascade, which starts with the MAPK kinase kinase (MAP3K or MAPKKK). MAP3K phosphorylates MAPK kinase (MAP2K, MAPKK or MEK), which in turn phosphorylates one or more MAPKs (ERK, JNK, p38). These three MAPKs can further phosphorylate various targets, such as transcription factors or other kinases (MAPKAPK2 or MK2). Downstream targets of the transcription factors can further influence cell growth, differentiation, matrix regulation and inflammation or cytokine production. There is a dynamic balance among ERK, JNK and p38. Furthermore, the responses are overlapping, which is important to determine the fate of the cell. Figure adapted and modified from [87].

Jun NH2-terminal kinases (JNKs), also known as stress-activated protein kinases or SAPKs, can be activated by various environmental stresses (heat shock, oxidants, ionizing radiation), genotoxins, inflammatory cytokines such as TNFα or IL-1β, ischemic reperfusion injury or DAMPs/PAMPs [88, 92]. MEK4 and MEK7 catalyze the dual phosphorylation of Thr183 and Thr185 leading to the activation of JNK1-3, whereas JNK3 is exclusively expressed in the central nervous system, testis and heart. In contrast to JNK3, JNK1 and 2 are expressed in hepatocytes [85, 88]. Activated JNK phosphorylates c-Jun at serine residues Ser63 and Ser73 in the NH_2-terminal region of c-Jun leading to the activation of activator protein-1 (Ap-1), as well as various transcription factors, such as ATF-2, Elk1 and JunD [88] leading to the regulation of apoptosis and inflammation [91, 93].

The extracellular signal-regulated kinases (ERK1 and ERK2) can be activated by growth factors, such as TGFβ or HGF, as well as pro-inflammatory cytokines including TNFα [82]. Dual phosphorylation of tyrosine and threonine (Tyr185, Thr187) by MEK1 and MEK2 is required to activate ERK1/2. This leads to the phosphorylation of numerous substrates, such as transcription factor c-Myc and protein kinases, such as ribosomal S6 kinase (RSK) [93]. The transcription factor c-Myc is known to be an early transcription factor associated to hepatocyte proliferation, cell growth and loss of differentiation [94-96]. Moreover, overexpression of c-Myc was associated with promoting progressive of liver fibrosis by the activation of HSC [97].

The four isoforms of p38 α, β, γ, δ are activated by environmental stress, inflammatory cytokines, such as IL-1 and TNF, as well as DAMPs and PAMPs. Similarly to JNK and ERK, p38 requires dual phosphorylation of Thr180 and Tyr182 by MEK3 and MEK6 to be activated. Phosphorylated p38 in turn activates transcription factors such as ATF2, MAPKAPK2, Elk1 and CHOP. P38 was associated with cytokine production and inflammation, since blockage of p38 decreases synovial inflammation, cartilage damage and bone destruction in animal models of arthritis [87, 88]. Moreover, similar to JNK, p38 was associated with the induction of apoptosis [91].

1.9.4 The Unfolded Protein Response (UPR)

The endoplasmic reticulum (ER) is responsible for protein folding, biosynthesis, translocation and post-translational modifications [98]. However, the biotransformation of CCl_4 leads to the production of highly reactive metabolites, which can bind to lipids, proteins or DNA [41]. These alterations of macromolecules can cause membrane dysfunction, including loss of Ca^{2+} from the ER membrane. This process leads to the accumulation of unfolded proteins in the ER lumen (ER stress) triggering an unfolded protein response (UPR) [98-100]. The UPR is sensed by three transmembrane ER stress sensors: inositol-requiring enzyme 1α (IRE1α; also known as ERN1), PKR-like ER kinase (PERK; also known as EIF2AK3), and activating transcription factor 6α (ATF6α) (Figure 12). However, prolonged or enhanced ER stress can induce apoptosis by the activation of transcription factor C/EBP homologous protein (CHOP) [101, 102]. CHOP was reported to induce the expression of pro-apoptotic

genes, including BCL-2-like-11 (Bim) as well as endoplasmic oxidoreductin-1-like protein (Ero1l) and the repression of anti-apoptotic genes like B-cell lymphoma-2 (Bcl-2) [99]. Moreover, CHOP knockout mice were reported to show reduced liver necrosis and increased survival upon APAP intoxication [103].

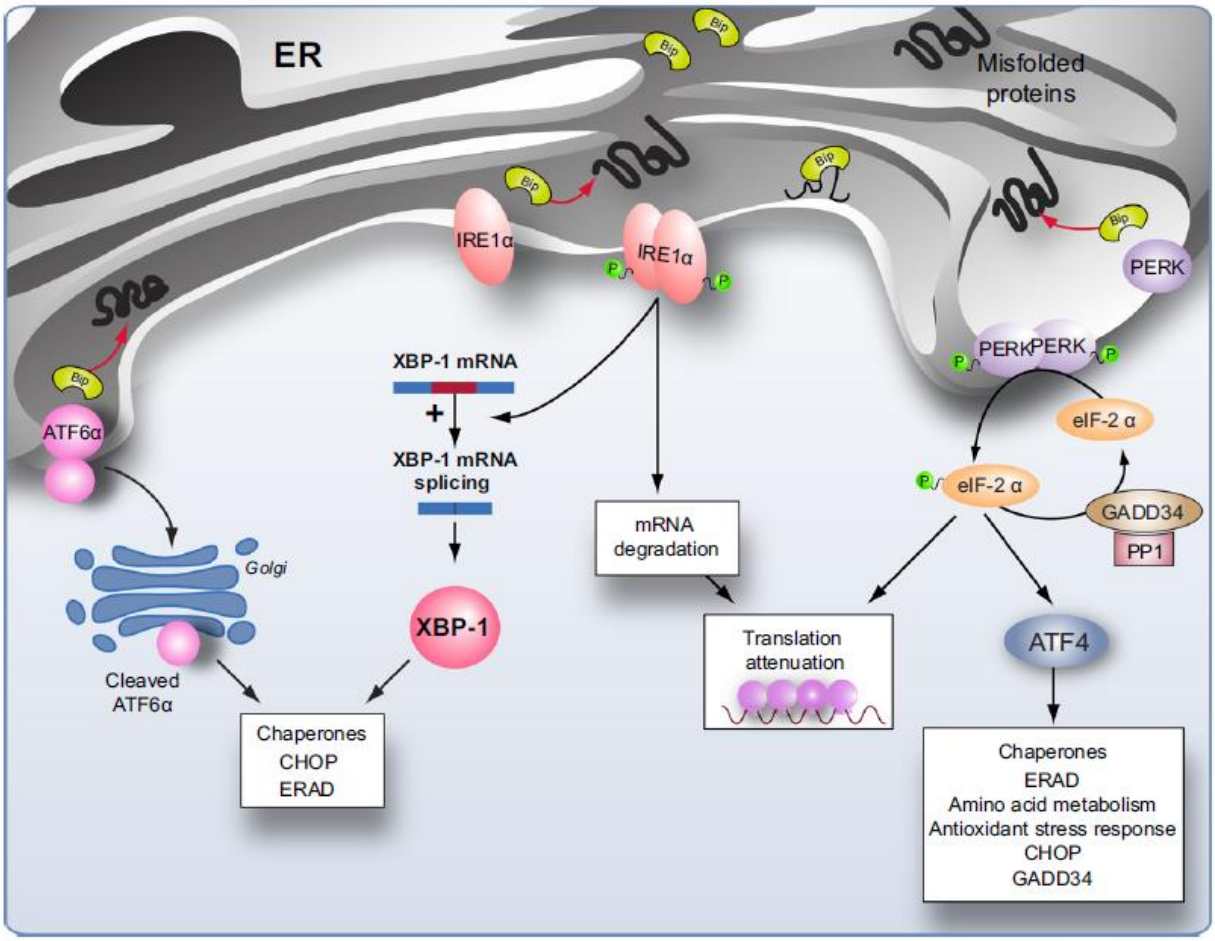

Figure 12: The unfolded protein response sensors. The three ER stress sensors ATF6α, IRE1α and PERK can mediate the ER stress response. Accumulation of misfolded proteins leads to the dissociation of chaperone protein BIP from the sensors, resulting in their activation. UPR activation results in the activation of pathways to restore homeostasis by translation attenuation to reduce the number of proteins entering the ER. Furthermore, UPR induces the transcription of proteins, which increases the folding capacity. Figure adapted and modified from [101].

IRE1α possess two enzymatic activities: a serine/threonine kinase domain and an endoribonuclease (RNase) domain. Once binding immunoglobulin protein (BIP) is dissociated, IRE1α is activated by dimerization and transautophosphorylation, leading to the activation of the endoribonuclease. RNase activity initiates splicing of X-box binding protein 1 (XBP1), thus producing a translational frameshift that results in an enhanced translation of Xbp1 protein. The spliced form of Xbp1 (Xbp1s) translocates to the nucleus, leading to the transcription of protein-folding enzymes. Chaperons, such as ER-associated degradation (ERAD) components and CHOP lead to an increased ER function and size [100, 101].

Similar to IRE1α, PERK dimerizes and autophosphorylates by the dissociation of BIP from the ER luminal domain. Activated PERK phosphorylates eukaryotic translation initiation factor 2-α (eIF-2α) leading to a transiently global translation attenuation [100, 104]. However, translation of some species of mRNA is selectively enhanced upon activation of eIF-2α, such as activating transcription factor 4 (ATF4). This leads to the transcription of genes associated with oxidative stress resistance, amino acid metabolism and apoptosis including expression of the transcription factor CHOP. Expression of growth arrest and DNA damage-inducible protein-34 (GADD34) is induced by CHOP and ATF4 leading to the formation of a complex with the protein phosphatase 1 (PP1c) to target dephosphorylation of eIF-2α. This negative feedback loop results in restoration of mRNA translation [100, 101, 104].

The third ER-stress sensor, ATF6α, is activated as well via the dissociation of BIP. Upon its activation, ATF6 translocates to the Golgi compartment, following a proteolytic cleavage by Golgi enzymes site 1 protease (S1P) and S2P leading to the production of a cytosolic fragment that migrates to the nucleus. Finally, the fragment induces the transcription of certain ER chaperone genes such as BIP, GRP94 (glucose related protein 94), Xbp1 and ERAD together with the transcription factor CHOP [100-102, 104].

1.9.5 Phosphatidylinositol 3-kinase (PI3K)/Akt signaling cascade

The phosphatidylinositol 3-kinase (PI3K)/Akt signaling cascade is known to play an important role during cell cycle progression, differentiation, apoptosis, transcription and metabolism [21, 105]. Moreover, Akt is activated during APAP-induced liver injury [86] and it was shown to take on a protective role by decreasing p53 mediated apoptosis [106].

Activation of receptor tyrosine kinases (RTKs), Ras or G-protein coupled receptors (GPCRs) through binding of various signaling molecules, such as epidermal growth-factor (EGF), TNF-α, IL-6, platelet-derived growth factor (PDGF) or hepatocyte growth-factor (HGF) [81, 105, 106] results in autophosphorylation of tyrosine residues. Subsequently, phosphatidyl-inositol-3-kinases (PI3Ks) is recruited to the membrane and phosphorylates phosphatidylinositol-4,5-bisphosphate (PI-4,5-P2) to generate second messenger phosphatidylinositol-3,4,5-triphosphate (PI3,4,5-P3). PI3K phosphorylation capacity can be reversed by phosphatase and tensin homolog (PTEN), which degrade PI3,4,5-P3 to PI-4,5-P2. PI3,4,5-P3 provides phospholipid binding sites for phosphoinositide-dependent protein kinase 1 (PDK1) and Akt/protein kinase B (PKB), which leads them to be recruited to the plasma membrane. Once Akt is recruited to the plasma membrane, phosphorylation on threonine residue (Thr308) takes place by means PDK1. Phosphorylation of serine residue (Ser473) in the Akt COOH-terminus, requires mTor complex 2 (mTOR2). Although phosphorylation of Thr308 is sufficient for the activation of Akt, full activation requires phosphorylation of both residues. Activated Akt migrates through the cytosol leading to the translocation into the nucleus followed by modulation of cell survival and cell cycle progression [81, 105-107].

1.9.6 Death receptor signaling via TNFa or TGFβ

Tumor necrosis factor alpha (TNFα) is a pro-inflammatory cytokine, which is a key mediator in a variety of diseases including ischemia/reperfusion injuries, as well as upon drug-induced liver injury (DILI) [6, 7, 108]. Activated Kupffer cells, along with leukocytes, release TNFα which can bind to its receptors TNF receptor 1 (TNFR1) and TNF receptor 2 (TNFR2) [109]. However, with regard to liver physiology, TNFR1 has a predominant role [63]. Upon binding of TNFα to its receptor, either hepatocyte death or survival pathways may be activated. Moreover, TNFα is commonly used in combination with D-galactosamine (D-Gal) as an experimental model *in vivo* of induced hepatitis. Thereby, D-Gal blocks transcription specifically in hepatocytes leading to the inhibition of mRNA synthesis of anti-apoptotic genes, ultimately resulting in the activation of caspase cascade and DNA fragmentation [35, 110]. *In vitro*, the same effect can be provoked by adding the transcription inhibitor actinomycin D (ActD) or the translation inhibitor cycloheximide (CHX) in combination with TNFα [24].

Soluble TNFα (sTNFα) and membrane-bound TNFα (mTNFα) can bind to its receptor TNFR1 and TNFR2. However, only TNFR1 is involved in the apoptotic signaling since TNFR2 lacks a functional death domain. After binding of TNFα to its receptor, trimerization of the receptor occurs (Figure 13). TNFR1-associated death domain protein (TRADD) binds to the trimeric death domain, further recruiting receptor-interacting protein-1 (RIP1), cellular inhibitor of apoptosis-1/2 (cIAP1/2) and TNF receptor-associated factor-2 (TRAF2) leading to the formation of complex I. This complex induces the activation of the inhibitor of κB kinase (IKK) complex, which includes IKKα, IKKβ, and IKKγ/NEMO. The IKK complex further induces phosphorylation and proteasomal degradation of the NF-κB regulatory subunit IκBα leading to the activation of NF-κB. Translocation of NF-κB to the nucleus leads to the activation of transcription of anti-apoptotic genes such as $cFLIP_L$, TRAF1/2, cIAP-1/2, XIAP and Gadd45β to regulate cell survival and proliferation [108, 111].

Additionally, complex I can also lead to the activation of MAPK cascade including JNK, p38 and ERK. Oligomerization of TRAF2/5 results in the binding of transforming growth factor-β-activated kinase-1 (TAK1) to TRAF2/5. TAK1 itself is a MAPKKK, which further phosphorylates MAPKK, such as MEK4/7, leading to the activation of MAPK including JNK. Moreover, apoptosis signal-related kinase (ASK1) was reported to activate JNK leading to the transcription of pro-apoptotic and proliferation-dependent genes [108, 109]. Upon normal conditions transient JNK activation promotes proliferation and is rapidly inactivated by phosphatases. However, upon prolonged and sustained activation of JNK, ubiquitin ligase ITCH is phosphorylated and cFLIP is targeted for degradation resulting in the activation of caspase cascade, thus leading to the induction of apoptosis. Therefore, JNK antagonizes NF-κB during TNFα mediated signal transduction [108, 112].

Finally, internalization of complex I leads to the degradation of cIAP1/2 and the dissociation of TRAF2, TRADD and RIP1 from complex. Association with FADD and caspase 8 and 10 results in the formation of complex 2 or so called death-inducing signaling complex

(DISC). Initiator caspases 8/10 are further activated by an autoproteolytic process leading to the activation of effector caspase 3/6/7. Apoptosis can be triggered by two different pathways: either caspase 8 directly cleaves caspase 3, thereby promoting apoptosis; or caspase 8 initiates signal amplification to induce mitochondrial death pathway. In the latter case, cytosolic Bid is cleaved by caspase 8 resulting in the active form tBID, which translocates to the mitochondrial membrane and contributes to mitochondrial permeability (mitochondrial permeability transition, MPT). Subsequently, cytochrome C is released from the mitochondria, triggering the formation of the apoptosome; a complex consisting of cytochrome C, Apaf-1 and caspase 9. The apoptosome processes and activates effector caspase 3 resulting in apoptosis-induced cell death through the cleavage of cytoplasmic and nuclear substrates [108, 109, 113].

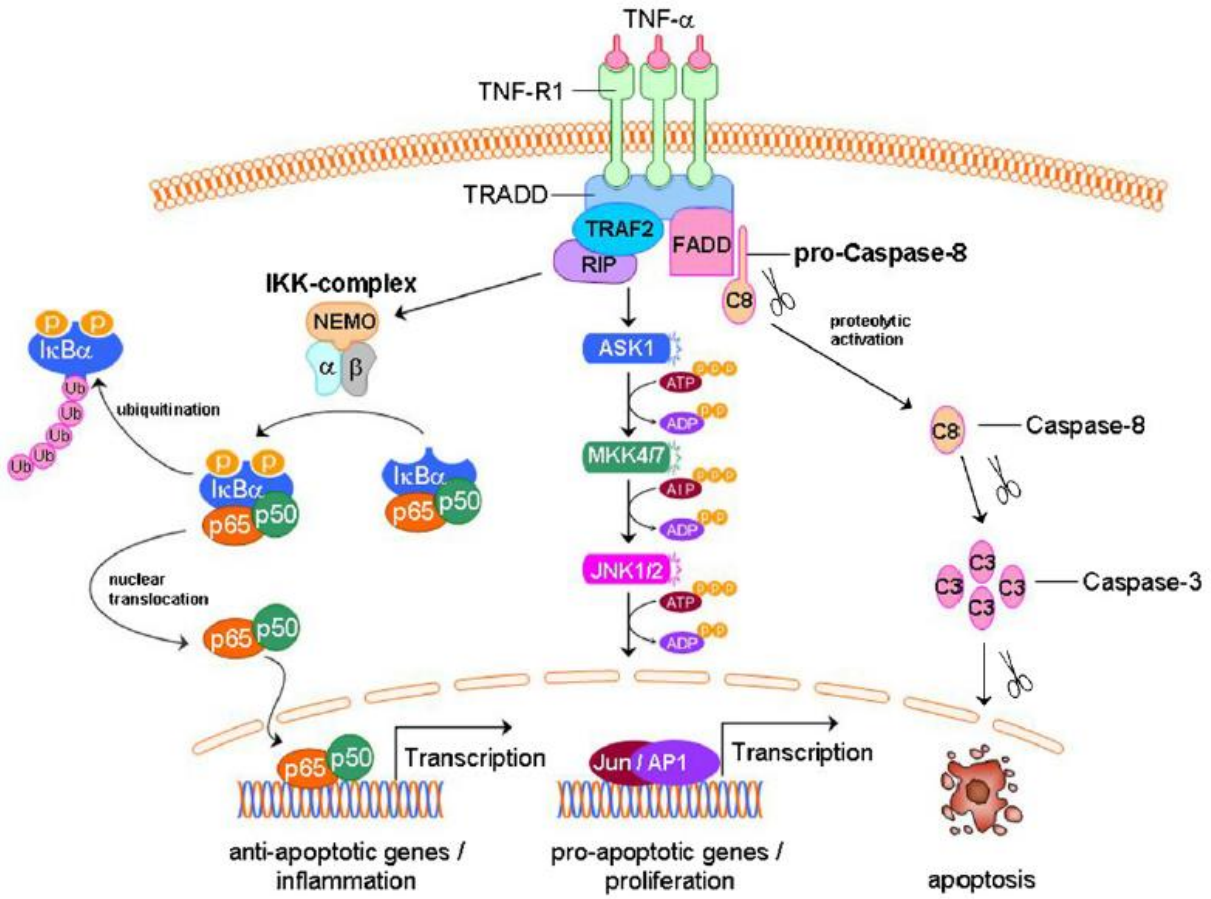

Figure 13: TNFα signaling. Upon binding of TNFα to its receptor TNFR1, receptor trimerization occurs and NF-κB pathway is activated through IKK complex. Nuclear translocation of NF-κB activates transcription of pro-inflammatory and anti-apoptotic genes. Additionally, TNFα induces pro-apoptotic pathway via association of TRADD and FADD leading to the activation of caspase-dependent apoptosis through initiator caspase 8 and effector caspase 3. Finally, TNFα can induce MAPK-associated pathways, such as JNK, leading to the transcription of pro-apoptotic and proliferation-dependent genes. However, upon sustained activation of JNK, c-FLIP is degraded resulting in the induction of caspase cascade. Figure adapted and modified from [109].

Transforming growth factor-β (TGFβ) is a pleiotropic cytokine, which has various functions including cell cycle control, regulation of early development, differentiation, hematopoiesis, angiogenesis, chemotaxis and immune functions [114]. However, its pivotal role in the liver and other organs, such as lung and kidney, is the development of fibrosis [115]. TGFβ expression is markedly enhanced in patients with chronic liver disease and in animal models of liver fibrosis as well as after partial hepatectomy and CCl_4/APAP-induced liver injury [24, 116]. Overexpression of TGFβ is associated with increased matrix deposition. Furthermore, neutralization of the activity results in attenuation of liver fibrosis. Upon stimulation, TGFβ can be released by hepatocytes, Kupffer cells and hepatic stellate cells (HSC). This leads to the activation of HSC and the production of extracellular matrix proteins, resulting in the resolution of inflammation and wound closure [20, 24]. However, TGFβ was also associated to apoptosis *in vitro* via Smad proteins and AP-1 [117] or by GADD45β through p38 activation [118, 119]. Furthermore, *in vivo* studies also revealed an apoptosis induction in transgenic mice that overexpress TGFβ [120, 121].

TGFβ acts through its membrane-bound receptors type I and type II (TGFβRI and TGFβRII) leading to the formation of a heterotetrameric complex. Thereby, TGFβRI is phosphorylated by TGFβRII and subsequently the receptor activated Smad proteins, Smad2 and Smad3, are activated. Phosphorylation of Smad2 and Smad3 leads to the formation of a heteromeric complex including Smad4 (co-Smad). This complex translocates to the nucleus to regulate gene transcription, including pro- and anti-apoptotic genes, such as p53, Bax, BcL-2, BcL-X_L or Bik [114, 118, 122] . Furthermore, TGFβ can act through the TGFβ activated kinase 1 (TAK1), which was reported to belong to the MAP kinase family. TAK1 kinase is reported to activate p38 mitogen-activated protein kinase (p38 MAPK), as well as c-Jun N-terminal kinase (JNK), which were associated with stress and inflammation as well as to apoptosis [122, 123]. Moreover, TGFβ can induce apoptosis through pro-apoptotic events, such as oxidative stress, down-regulation of Bcl-2 family members, up-regulation of pro-apoptotic factor Bax and the initiation of caspase cascades [118].

1.10 The CCN family

The CCN family was already first described more than a quarter of a century ago [124-126]. Thereby, the first three members were cysteine-rich 61 (Cyr61; CCN1), connective tissue growth factor (CTGF; CCN2) and nephroblastoma overexpressed (Nov, CCN3), which provide the acronym for the CCN family [127]. A few years later, Pennica et al identified three additional members: WNT1-inducible signaling pathway protein-1 (WISP1 or CCN4), WISP2 (CCN5) and WISP3 (CCN6), which were reported as Wnt-inducible secreted proteins [128]. This group of six highly conserved secreted proteins share a modular structure containing an N-terminal secretory peptide followed by four different domains (Figure 14): an insulin-like growth factor binding protein-like domain (IGFBP; module I), a von Willebrand factor type C repeat module (VWC), a thrombospondin type-1 repeat module (TSP-1) and a cysteine knot-containing module (CT) (Figure 14). Moreover, module II and III are connected

by a hinge region, which is susceptible for proteolytic cleavage [129-132]. Besides CCN5, which lacks the cysteine knot, all modules are encoded by a separate conserved exon, suggesting that the CCN genes are evolved through exon shuffling [133]. CCN proteins contain 349 up to 381 amino acids with the exception of CCN5 [134].

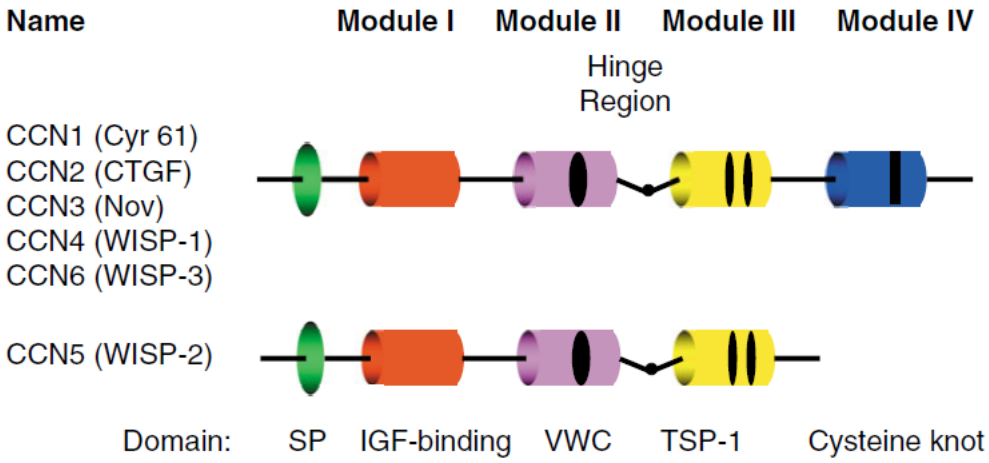

Figure 14: Structure of the CCN family members. The CCN family consists of 6 members: CCN1 (Cyr61), CCN2 (CTGF), CCN3 (Nov) and CCN 4-6 (WISP-1 – 3). They share a similar structure containing a secretory signal peptide (SP), an IGF-binding domain (Module I), a von Willebrand type C domain (VWC, Module II), a thrombospondin-1 domain (TSP-1, Module III) and a cysteine knot (Module IV) domain. Only CCN5 is lacking the cysteine knot at the end. The domains are linked by a hinge region, which is susceptible to protease cleavage. Figure adapted and modified from [129].

This family of secreted extracellular matrix (ECM)-associated proteins belong to the group of matricellular proteins, including thrombospondin-1 (TSP1), SPARC (secreted protein, acidic and rich in cysteine), hevin, osteopontin and tenascin C and X. Matricellular proteins are known to be dynamically expressed rather than serving structural roles in the matrix [131, 135].

CCN proteins are expressed in many organs during embryonic development and their biological relevance was shown via embryonic or perinatal lethality of knockout mice regarding CCN1, CCN2 and CCN5 [136-141]. The expression of CCN proteins is downregulated during adulthood in various tissues. However, the transcription of genes encoding CCN proteins can be upregulated by various mitogenic signals and environmental disorders, such as exposure of growth factors (PDGF, FGF2), inflammatory cytokines (TNF, IL-1β, TGFβ), oxygen deprivation, steroid hormones, ultraviolet radiation and mechanical forces. Therefore, it is not surprising that CCN proteins are involved in various important functional pathways including mitogenesis, migration, adhesion, cell survival, differentiation, angiogenesis, tumorigenesis, inflammation and wound healing, as reviewed in [130, 132]. These biological processes are mediated mainly through binding of CCN proteins to integrin receptors, including co-factors in some contexts. CCN proteins do not contain the canonical RGD sequence. Therefore, they interact with integrins through their non-canonical binding

sites, which are shown in figure 15. Up to now, eight integrin receptors have been identified to mediate interactions with CCN1-3 proteins as well as co-receptors, such as heparin sulfate proteoglycans (HSGPs) and low-density lipoprotein receptor-related proteins (LRPs) [131, 132, 142].

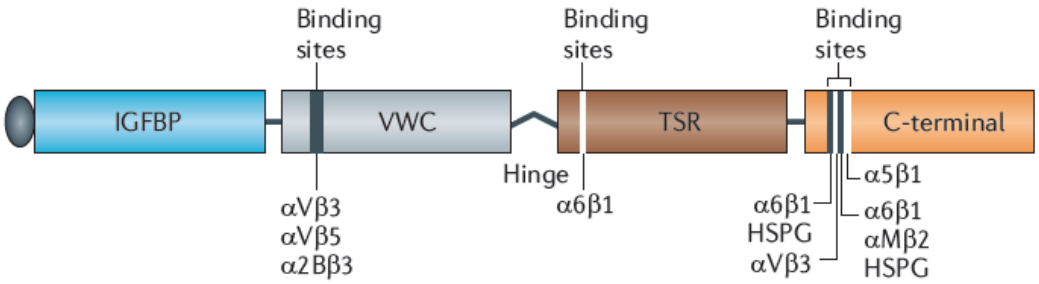

Figure 15: CCN protein structure and the localization of integrin-binding sites. Eight integrins were reported to bind CCN proteins, as well as co-receptors such as HSPGs and LRPs. CCN proteins do not contain the canonical RGD sequence. Therefore, non-canonical binding sites are essential for interaction of CCN proteins with integrins. Figure adapted and modified from [132].

Although the CCN proteins share a similar structure, they were reported to play divergent roles in liver pathophysiology. For example, CCN1 was shown to be induced upon hepatic injury in mouse models. Furthermore, it was shown to act as a key regulator of liver fibrosis through triggering cellular senescence in hepatic stellate cells and portal fibroblasts leading to limited fibrogenesis and the regression of liver fibrosis [143, 144]. Moreover, CCN1 was reported to mediate opposing biological activities just by interacting with different integrins on various cell types, as reviewed in [145]. Furthermore, Chen et al unveiled an apoptotic synergistic effect of CCN1 and TNFα. In cases of liver injury, TNFα is one of the most prominent pro-inflammatory cytokines leading to the expression of anti-apoptotic proteins [111]. The binding of CCN1 and TNFα to their receptors, results in the production of reactive oxygen species by CCN1 and leads to the sustained activation of JNK and a blockage of NF-κB. Thus, cytotoxicity effect of TNFα is induced and activation of caspase cascade proceeds, leading to apoptosis in the affected cells [144-146]. In contrast to CCN1, CCN2 was shown to act synergistically with TGFβ1 in order to promote matrix deposition and fibrogenesis [147]. Moreover, knockdown of CCN2 by usage of small interfering RNA (siRNA) or oligonucleotides reduced CCl4-induced liver fibrosis [148, 149], suggesting that CCN2 acted as a pro-fibrotic regulator [132, 134].

A recent study by Perbal revealed an increasing interest in CCN proteins, since the number of publications raised from 18 between 1996-1998 up to 3,335 in 2015-2016 [150]. Moreover, CCN proteins have been taken to account for potential therapeutic approaches since they are secreted proteins, which could be tackled by humanized monoclonal antibodies to block their activity. For example, FG-3019, a humanized antibody against CCN2, was shown to be safe and well tolerated in patients with idiopathic pulmonary fibrosis [151-153]. Another Phase II study using the same antibody revealed efficiency to reverse

liver fibrosis in patients, which was caused by chronic hepatitis B infection (ClinicalTrials.gov identifier: NCT01217632). However, up to now clinical trials were only planned for the investigation of efficacy to target CCN2. Taken together, this highlights the impact of CCN proteins to a broad spectrum of diseases making this protein family even more important and attractive for further investigations [132].

1.10.1 WNT1-inducible signaling pathway protein-1 (WISP1)

WNT1-inducible signaling pathway protein-1 (WISP1), a member of the CCN family, was first identified as a target of β-catenin Wnt-transformed cells and in colon cancer cells. Additionally, it was shown to induce dedifferentiation and tumorigenic features in fibroblasts [128, 154]. The murine WISP1 is located on chromosome 15 and the human WISP1 gene is located on chromosome 8q24.1–q24.3 [128, 134]. The murine cDNA length is about 1,766 and the human is about 2,830 bp. Furthermore, WISP1 is expressed as a protein of 367 amino acids and it can be glycosylated at several residues resulting in an apparent molecular weight of 60 kDa. WISP1 gene expression can be mainly detected in adult lung, heart, kidney, pancreas, ovary, placenta, spleen and small intestine. However, the expression levels in brain, liver, skeletal muscle, thymus, colon and peripheral blood leukocytes are either low or absent [128].

Most of the studies regarding the potential effect of WISP1 are associated with proliferation, migration and survival. For example, WISP1 was reported to attenuate p53 mediated apoptosis by the activation of antiapoptotic Akt pathway leading to inhibition of cytochrome C release and up-regulation of antiapoptotic Bcl-X_L [106]. In line with this, Venkatachalam et al showed that WISP1 antagonizes TNF-α mediated cardiomyocyte death, suggesting that WISP1 act in a pro-mitogenic and pro-survival manner in myocardial constituent cells [155]. Overexpression of WISP1 in vascular smooth muscle cells (VSMCs) led to enhanced migration and proliferation through the activation of Akt signaling [156]. In opposition to claims pertaining to the pro-survival role of WISP1, Tong et al reported that WISP1 expression was enhanced 6h after ischemia-reperfusion. The usage of anti-WISP1 led to decreased ALT and AST values as well as to decreased pro-inflammatory cytokine levels [157].

Moreover, WISP1 was reported to be induced upon various cytokines, for example, Dooley et al showed in a gene array study that WISP1 is induced in primary mouse hepatocytes stimulated with TGFβ, which is a profibrogenic cytokine. Furthermore, several studies suggested that WISP1 is induced by various cytokines such as IL-1β, TNFα in cardiac myocytes or TGFβ in osteoblasts [158-161].

Since most of the studies in the past were focused on investigating effects of CCN1-3, there are only 114 research articles published to date regarding WISP1 [150]. Moreover, there is no known publication, which describes the precise role of WISP1 in liver pathophysiology. Just recently, Murahovschi showed that WISP1 can induce cytokine and

chemokine expression as well as secretion in human monocyte-derived macrophages [162]. This suggests that WISP1 is a potent regulator during immune response with a yet undefined role in terms of acute liver injury.

1.11. Aim of this work

The aim of this study was to investigate the potential influence of WNT1-inducible signaling pathway protein-1 (WISP1, CCN4) during acute liver injury. For this purpose, a WISP1 knockout mouse line was established and confirmed for the absence of WISP1 by immunohistochemical staining as well as by qRT-PCR in different organs.

In order to study the potential influence of WISP1 during acute liver injury, two well-known liver toxicant models were applied *in vivo*, including CCl_4 and paracetamol. Potential effects were studied in a dose and time-dependent manner. Therefore, I used histological as well as molecular biology techniques, such as western blot and qRT-PCR analysis. The results revealed a significant enhanced liver injury in WISP1 knockout mice, which was associated with an increase inflammatory response as well as stronger induced stress signaling. Since first results revealed differences regarding inflammation, I further implemented *in vitro* studies to investigate the effects on wild type and WISP1 knockout hepatocytes to inflammatory cytokines as well as paracetamol. These analyses also revealed an enhanced susceptibility of WISP1 knockout hepatocytes to cell death. Finally, a time resolved global gene expression profile of wild type and WISP1 knockout mice was carried out using Affymetrix microarrays. To identify mechanisms responsible for transcriptional alterations, I used a combination of gene array analysis, bioinformatics and knowledge-based interpretation of the identified deregulated genes. Finally, I validated the identified biological motifs by using qRT-PCR.

2 MATERIALS AND METHODS

2.1 Materials

2.1.1 Technical equipment

Table 1: Equipment

Equipment	Company
Autoclave	5075 ELV, Tuttenauer
Balance	EW, Kern
Benches	HERA-Safe, Heraeus
Bright Field Microscope	Primo Vert, Zeiss, Software ZEN from Zeiss
Bunsen Burner	IBS Fireboy Plus, Integra Bioscences
Centrifuge	Megafuge 1.0R, Thermo Scientific
Centrifuge	Centrifuge 5415 R, Eppendorf
Centrifuge with cooling function	5424R, Eppendorf
EC 350 – Modular tissue embedding center	Microm, Walldorf, Germany
Electrophoresis Chamber	Sub-Cell® Model 192 Cell, BioRad
Electrophoresis Chamber (western blot)	Mini-PROTEAN® Tetra Cell Systems, BioRad
HM 450 Sliding Microtome	Microm, Walldorf, Germany
Ice machine	AF 100, Scotsman
Image acquisition system	E-BOX CX5, Vilber Lourmat
Image acquisition system	Fusion Fx7, Vilber Lourmat
Incubators	CO_2 Incubator C150 R Hinge 230, Binder
Infinite M200 Pro Plate reader	Tecan
Laminar Flow Hood	Electronics FAZ 2, Waldner
Magnetic stirrer	IKAMAG RCT, IKA
Mercury Lamp	Nikon Insilight C-HGFI
Microcentrifuge	Mini Spin Plus, Eppendorf
Microscope	Olympus BX61 microscope
Microscope CCD-Camera	AxioCam ICm 1
Minicentrifuge	FVL-2400N Combi-Spin, Biosan
Minishaker	MS 2, IKA
pH meter	CG 842, Schott
Pipetteboy	Integra
Pipettes	Research and Reference, Eppendorf
Power Supplies	Standard Power Pack 25, Biometra
	Power Pack 300, BIO RAD
Precision balance	EW 150-3M, Kern
Real Time PCR System	7500 Real-Time PCR System, Applied Biosystems
Shaker	KS 260 basic, IKA
Software	Olympus Fluoview Ver. 4.O
Sonicator	Bandelin, SONOPLUS
Spectrometer	NanoDrop 2000, Thermo Scientific
Spin Tissue Processor STP 120	Microm, Walldorf, Germany
Sub-Cell	Model 192, BIO RAD
TaqMan 7500 Real-Time PCR	Applied Biosystems
Thermocycler	TGRADIENT, Biometra
Thermoshaker	HTM 130, HLC
	PHMT Grant-bio, Keison
Transfer chamber	Trans-Blot® SD Semi-Dry Transfer Cell, BioRad
UV/Vis Spectrometer	V-530, Jasco
Vacuum pump	Diaphragm Vacuum Pump, Vacuumbrand

Vortex	Vortex-Genie 2, Bender&Hobein
Water purification system	Maxima Ultra-Pure Water, ELGA
Waterbath	GFL 1083, Gesellschaft für Labortechnik

2.1.2 Consumables

Table 2: Consumables

Consumable	Company	Catalog No
Biosphere Filtered Tip, 1000uL	Sarstedt, Numbrecht, Germany	70.762.211
Biosphere Filtered Tip, 100uL	Sarstedt, Numbrecht, Germany	70.760.212
Biosphere Filtered Tip, 200uL	Sarstedt, Numbrecht, Germany	70.760.211
Biosphere Filtered Tip, 20uL	Sarstedt, Numbrecht, Germany	70.1116.210
Blotting Paper Grade 703, 46x57cm	VWR international, Darmstadt, Germany	732-0591
Cell culture microtiter plate, 96 well	Greiner bio-one	655986
Cell Scraper, 25cm	Sarstedt, Numbrecht, Germany	83.183
Corning™ 96-Well Clear Bottom Black or White Polystyrene Microplates	Costar 3610, Thermo Scientific, Braunschweig, Germany	07-200-566
Cover glass, 24 x 32 mm	VWR International (Argos Technologies)	631-0711
Falcon tube, 15mL	Sarstedt, Numbrecht, Germany	62.554.512
Falcon tube, 50mL	Sarstedt, Numbrecht, Germany	62.547.254
Gentle Skin Classic Laboratory Gloves	Meditrade, Kiefersfelden, Germany	1221R
Hypodermic Needle, 26G x 5/8	BD Bioscience, San Jose, USA	304300
Inject F, 1ml	B Braun, Germany	9166017V
Kimtech Science Delicate Task Wipes	Kimberly-Clark Professionals, Roswell, USA	7216
MicroAmp Optical 96-well Reaction Plate	Applied Biosystems, California, USA	N801-0560
MicroAmp Optical Adhesion Film	Applied Biosystems, California, USA	4311971
Parafilm Wrap	Cole-Parmer, Kehl/Rhein, Germany	PM-992
PCR SingleCap 8er-SoftStrips 0.2ml	Biozym Scientific GmbH, Germany	710988
Pestle & microtube 1,5 ml	VWR International (Argos Technologies)	431-0098
Pipette Tips, 1000uL	Sarstedt, Numbrecht, Germany	70.762
Pipette Tips, 200uL	Sarstedt, Numbrecht, Germany	70.760.002
Pipette Tips, 20uL	Sarstedt, Numbrecht, Germany	70.1116
Polyscreen PVDF Transfer Membrane	Perkin-Elmer, Massachusetts, USA	NEF1002001PK
RNase-free Microfuge Tubes 1.5 mL	Ambion, Thermo Fischer Scientific, Waltham, USA	AM12400
RNaseZap® RNase Decontamination Solution	Ambion, Thermo Fischer Scientific, Waltham, USA	AM9780/AM9782
SafeSeal 0.5mL microtube	Sarstedt, Numbrecht, Germany	72.699
SafeSeal 1.5mL micotube	Sarstedt, Numbrecht, Germany	72.706
SafeSeal 2.0mL microtube	Sarstedt, Numbrecht, Germany	72.695.500
Serological Pipette, 10mL	Sarstedt, Numbrecht, Germany	86.1254.001
Serological Pipette, 25mL	Sarstedt, Numbrecht, Germany	86.1685.001
Serological Pipette, 5mL	Sarstedt, Numbrecht, Germany	86.1253.001
Sterile filter, Filtrapur S0.2	Sarstedt, Numbrecht, Germany	83.1826.001
SuperFrost Plus® microscopic slides	Thermo Scientific, Braunschweig, Germany	J1800AMNZ
Surgipath Paraplast	Leica, Germany	39601006
Tissue Culture Plate Flat-Bottom 6-Well Plate	Sarstedt, Numbrecht, Germany	83.1839
Tissue-Loc™ HistoScreen™ Cassette	Thermo Scientific, Braunschweig, Germany	C-1000
Vacuum Filtration Unit, 0.22um, 250mL	Sarstedt, Numbrecht, Germany	83.1822.001
WypAll L30 wipes	Kimberly-Clark Professionals, Roswell, USA	7301

2.1.3 Chemicals and kits

Table 3: Chemicals and kits

Chemical	Company	Catalog No
2-propanol	Carl Roth, Karlsruhe, Germany	AE73.1
Acetic acid	Carl Roth, Karlsruhe, Germany	3738.5
Actinomycin D, from *Streptomyces* species	Sigma-Aldrich Corp., St. Louis, MO, USA	A9415
Agarose	Biozym Scientific GmbH, Hessisch Oldendorf, Germany	840004
Alanine Aminotransferase Activity Assay Kit	Sigma-Aldrich Corp., St. Louis, MO, USA	MAK052
Amino acid solution (Costumer formulation)	PAN Biotech GmbH, Aidenbach, Germany	SO-33100
APS	Sigma-Aldrich Corp., St. Louis, MO, USA	3678-25g
Aspartate Aminotransferase (AST) Activity Assay Kit	Sigma-Aldrich Corp., St. Louis, MO, USA	MAK055
Avidin/Biotin Blocking Kit	Vector Laboratories, Lörrach, Germany	SP-2001
Boric acid	Carl Roth, Karlsruhe, Germany	5935.1
Bovine Albumin Fraction V (BSA)	Carl Roth, Karlsruhe, Germany	8076.4
Bromophenol Blue	Merck, Darmstadt, Germany	108122
Buffer concentrate A	Carl Roth, Karlsruhe, Germany	L510.1
Buffer concentrate K	Carl Roth, Karlsruhe, Germany	L511.1
Calcium chloride ($CaCl_2$)	Sigma-Aldrich Corp., St. Louis, MO, USA	5239.1
CCl_4	Sigma-Aldrich Corp., St. Louis, MO, USA	7345.1
Cell Lysis Buffer 2	R&D Systems, Minneapolis, USA	#895347
Cell Titer Blue Assay	Promega, Wisconsin, USA	G8081
Chloroform	Carl Roth, Karlsruhe, Germany	7331.2
Citric acid monohydrate	Carl Roth, Karlsruhe, Germany	3958.2
Collagenase from Clostridium hystolyticum	Sigma-Aldrich Corp., St. Louis, MO, USA	C2674
Complete feed for Rats&Mice - Maintenance	Ssniff Spezialdiaeten, Soest, Germany	V1534-000
D-(+)- Glucose monohydrate	Sigma-Aldrich Corp., St. Louis, MO, USA	49159
DAB Peroxidase substrate kit	Vector Laboratories, Lörrach, Germany	SK 4100
Dako Pen	Dako, Hamburg, Germany	REF S2002
DeadEnd™ Colorimetric TUNEL System	Promega, Wisconsin, USA	G7130
DEPC Treated Water	Invitrogen GmbH, Darmstadt, Germany	750024
di-Sodium Hydrogen Phosphate anhydrous (Na_2HPO_4)	Carl Roth, Karlsruhe, Germany	P030.2
DMSO	Sigma-Aldrich Corp., St. Louis, MO, USA	34869
DNA ladder, 100 bp	Invitrogen GmbH, Darmstadt, Germany	15628-050
DTT (DL-Dithiothreitol)	Sigma-Aldrich Corp., St. Louis, MO, USA	D9779
EDTA	Carl Roth, Karlsruhe, Germany	8040.3
EGTA	Carl Roth, Karlsruhe, Germany	3054.2
Eosin Y disodium salt	Sigma-Aldrich Corp., St. Louis, MO, USA	E4382
Ethanol	Merk, Darmstadt, Germany	100983
Ethanol, 70%	Walter CMP, Kiel, Germany	WAL10506
Ethidium Bromide	Invitrogen GmbH, Darmstadt, Germany	15585-011
Ficoll	Sigma-Aldrich Corp., St. Louis, MO, USA	F4375
FluorPreserve™ Reagent	Calbiochem, Darmstadt, Germany.	345787
Glycerin	Carl Roth, Karlsruhe, Germany	3783.2
Glycine	Carl Roth, Karlsruhe, Germany	HN07.3
HEPES	Carl Roth, Karlsruhe, Germany	9105.4
High Capacity cDNA Reverse Transcription Kit	Applied Biosystems, Karlsruhe, Germany	4368813
Hydrochloric Acid, 32%	Carl Roth, Karlsruhe, Germany	P074.4
Hydrogen peroxide 30% (H_2O_2)	Sigma-Aldrich Corp., St. Louis, MO, USA	H1009
Isopropyl	Carl Roth, Karlsruhe, Germany	6752.2

Ketamin-ratiopharm® 50 mg O.K. Injection Solution	Ratio pharm, Ulm, Germany	N64477.04
L- Glutamine	Sigma-Aldrich Corp., St. Louis, MO, USA	G3126
Luminol	Sigma-Aldrich Corp., St. Louis, MO, USA	A8511
Magic Mark XP Western Protein Standard	Invitrogen GmbH, Darmstadt, Germany	LC5602
Magnesium sulfate ($MgSO_4$)	Carl Roth, Karlsruhe, Germany	P027.2
Mayer´s Hemalum solution	Merck, Darmstadt, Germany	1.09249.0500
Methanol	Sigma-Aldrich Corp., St. Louis, MO, USA	322415
Microscopy Entellan	Merck, Darmstadt, Germany	1.07960.0500
Mouse/Rat WISP-1/CCN4 Quantikine ELISA Kit	R&D Systems, Minneapolis, USA	MWSP10
Nonidet P-40 (NP-40)	Roche Diagnostics GmbH, Manheim	11754599001
Olive oil	Sigma-Aldrich Corp., St. Louis, MO, USA	75343-1L
Paracetamol (4-Acetamidophenol 98 %)	Sigma-Aldrich Corp., St. Louis, MO, USA	A 7302
Paraffin Histowax Surgipath paraplast	Leica Microsystems, Wetzlar, Germany	3901006
p-Coumaric acid	Sigma-Aldrich Corp., St. Louis, MO, USA	C9008
Phire Animal Tissue Direct PCR Kit	Thermo Scientific, Braunschweig, Germany	F-140WH
Phosphatase Inhibitor Cocktail II	Sigma-Aldrich Corp., St. Louis, MO, USA	P5726
Phosphatase Inhibitor Cocktail III	Sigma-Aldrich Corp., St. Louis, MO, USA	P0044
Pierce BCA Protein Assay Kit	Thermo Scientific, Braunschweig, Germany	23225
Ponseau S	Carl Roth, Karlsruhe, Germany	5938.1
Potassium Chloride (KCl)	Carl Roth, Karlsruhe, Germany	6781 .1
Potassium dihydrogen phosphate (KH_2PO_4)	Carl Roth, Karlsruhe, Germany	3904.1
Precision Plus Protein standard	Bio-Rad Laboratories, Munich, Germany	161-0374
Propidium Iodide	Sigma-Aldrich Corp., St. Louis, MO, USA	P4170
Protease Inhibitor Cocktail	Sigma-Aldrich Corp., St. Louis, MO, USA	P8340
Qiazol Lysis Reagent	Qiagen, Hilden, Germany	79306
Recombinant Human TGF-beta 1 Protein (TGFβ)	R&D Systems, Minneapolis, USA	240-B
Recombinant Human TNF-alpha Protein (TNFα)	R&D Systems, Minneapolis, USA	210-TA
Rompun 2%	Bayer Health Care, Leverkusen, Germany	-
Roti Histofix 4%	Carl Roth, Karlsruhe, Germany	P087.5
Roti-Histol	Carl Roth, Karlsruhe, Germany	6640.1
Rotiphorese® Gel 30 (37,5:1)	Carl Roth, Karlsruhe, Germany	3029.1
SDS pellets	Carl Roth, Karlsruhe, Germany	CN30.1
Sera Plus (Special Processed FBS)	PAN Biotech GmbH, Aidenbach, Germany	3702-P103009
Sodium chloride (NaCl)	Carl Roth, Karlsruhe, Germany	3957.2
Sodium deoxycholate	Sigma-Aldrich Corp., St. Louis, MO, USA	D6750
Sodium hydroxide pellets	Merck, Darmstadt, Germany	1.06482
Taq DNA Polymerase kit	5-Prime, Hamburg, Germany	2900169
TaqMan® Universal Master Mix II, with UNG	Applied Biosystems, Karlsruhe, Germany	4440038
TEMED	Carl Roth, Karlsruhe, Germany	2367.1
Trichloroacetic Acid	Carl Roth, Karlsruhe, Germany	8789.2
Trichloromethane/Chloroform	Carl Roth, Karlsruhe, Germany	7331.2
TRIS	Carl Roth, Karlsruhe, Germany	4855.2
Tris-HCl	Sigma-Aldrich Corp., St. Louis, MO, USA	T3253
Triton X-100	Carl Roth, Karlsruhe, Germany	3051
Trizma base	Sigma-Aldrich Corp., St. Louis, MO, USA	33742
Trypan Blue	Sigma-Aldrich Corp., St. Louis, MO, USA	T6146
Tween 20	Sigma-Aldrich Corp., St. Louis, MO, USA	P7949
Tween 80	Sigma-Aldrich Corp., St. Louis, MO, USA	P8074
VECTASTAIN Elite ABC Kit (Rat IgG)	Vector Laboratories, Lörrach, Germany	PK-4004
Whatman paper	VWR, Langenfeld, Germany	28298
Xylol AnalaR Norampur	VWR, Langenfeld, Germany	UN1307

2.1.4 Buffers for liver perfusion and in vivo collection

Table 4: Buffers for liver perfusion and in vivo collection

Buffer	Chemical	Amount
Collagenase buffer	Amino acid solution	30 ml
	$CaCl_2$ solution (19 g/L $CaCl_2$* 2 H_2O)	10 ml
	Collagenase Type 1	100 mg
	Glucose solution (9 g/L)	155 ml
	Glutamine (7 g/ml)	2.5 ml
	HEPES (60 g/L) (pH 8.5)	25 ml
	KH buffer	25 ml
EGTA buffer	Amino acid solution	60 ml
	EGTA solution (47.5 g/L)	1.6 ml
	Glucose solution (9 g/L)	248 ml
	Glutamine (7 g/L)	4 ml
	KH buffer	30 ml
	HEPES (60 g/L) (pH 8.5)	30 ml
KH buffer	Potassium chloride (KCl)	1.75 g
	Potassium dihydrogen phosphate (KH_2PO_4)	1.6 g
	Sodium chloride (NaCl)	60 g
	filled to 1 L with H_2O, set pH to 7.4	
PBS (10x)	Potassium chloride (KCl)	10 g
	Potassium dihydrogen phosphate (KH_2PO_4)	10 g
	Sodium chloride (NaCl)	400 g
	di-Sodium Hydrogen Phosphat anhydrous (Na_2HPO_4)	46 g
	set pH to 7.4, filled up to 5 L with distilled water	
Suspensions buffer	Albumin Fraction V	400 mg
	Amino acid solution	30 ml
	$CaCl_2$ solution (19 g/L $CaCl_2$* 2 H_2O)	1.6 ml
	Glucose solution (9 g/L)	124 ml
	Glutamine (7 g/ml)	2 ml
	HEPES (60 g/L) (pH 7.6)	20 ml
	KH buffer	20 ml
	$MgSO_4$ solution (24,6 g/L $MgSO_4$ * $7H_2O$)	0.8 ml

2.1.5 Cell culture

2.1.5.1 Cell culture chemicals

Table 5: Cell culture chemicals

Other Chemicals	Company	Catalog No
Acetic acid glacial	Carl Roth, Karlsruhe, Germany	3738.5
Rat tail collagen	Roche Diagnostics GmbH, Manheim,	11171179001
DMEM low glucose 1.0 g/L 10x	BioConcept, Allschwil, Switzerland	1-25K03-I
Gentamycin	PAN Biotech GmbH, Aidenbach, Germany	P06-13001
Insulin (ITS) 100x	Sigma-Aldrich Corp., St. Louis, MO, USA	I3146
Penicillin/Streptomycin	PAN Biotech GmbH, Aidenbach, Germany	P06-07100
Sera Plus (Special Processed FBS)	PAN Biotech GmbH, Aidenbach, Germany	3702-P103009
Stable L- Glutamine	PAN Biotech GmbH, Aidenbach, Germany	P04-82100
William's Medium E	PAN Biotech GmbH, Aidenbach, Germany	P04-29510

2.1.5.2 Cell culture medium

Table 6: Cell culture medium

Additives for cell culture medium	Final Concentration	For 500 ml Medium	Company	Catalog No
William's Medium E	-	-	PAN Biotech GmbH, Aidenbach, Germany	P04-29510
Dexamethasone	100 nM	20 µl from 2.5 mM stock in EtOH	Sigma-Aldrich Corp., St. Louis, MO, USA	D4902-25MG
Gentamycin	10 µg/ml	500uL	PAN Biotech GmbH, Aidenbach, Germany	P06-13001
Insulin (ITS) 100x	2 ng/ml	5 µl	Sigma-Aldrich Corp., St. Louis, MO, USA	I3146
Penicillin/Streptomycin	100 U/ml Pen; 100 U/ml Strep	5 ml	PAN Biotech GmbH, Aidenbach, Germany	P06-07100
Stable L- Glutamine	2 mM	5 ml	PAN Biotech GmbH, Aidenbach, Germany	P04-82100
Sera Plus (Special Processed FBS)	10 % (Full Media only)		PAN Biotech GmbH, Aidenbach, Germany	3702-P103009

2.1.6 Protein lysate buffer

Table 7: RIPA buffer for western blot

RIPA buffer	
50 mM Tris-Cl (pH 7,5)	
150 mM NaCl	
1 % Nonidet P-40 (NP-40)	
0,5 % sodium deoxycholate	
0,1 % SDS	
Added prior to use:	
Protease inhibitor	1:100
Phosphatase inhibitor 2	1:100
Phosphatase inhibitor 3	1:100

2.1.7 Buffers for SDS electrophoresis and western blot

Table 8: Buffers for SDS electrophoresis and western blot

Buffer	Chemical and amount
10 % APS (Ammonium persulphate):	0.5 g APS in 5 ml dist. water
10 % SDS (Sodium dodecyl sulphate):	0.5 g SDS in 5 ml dist. water
5 % BSA solution:	5 g Albumin in 100 ml TBS-T
Anode buffer:	Buffer concentrate A (Roth) 40 ml Methanol 80 ml Dist. water 280 ml
Cathode buffer:	Buffer concentrate K (Roth) 40 ml Methanol 80 ml Dist. water 280 ml
Loading buffer (5 x):	Bromophenol blue 5 mg DTT 1 M 2.5 ml Glycerol 5 ml SDS 10 % 0.5 g Tris-HCl 1 M 2.25 ml
Ponseau S:	1 g Ponseau S in 500 ml 3 % trichloride acetic acid
Running buffer (10 x):	Glycine 144.0 g SDS 10.0 g Tris base 30.3 g
Separation buffer: (3 M Tris-HCl)	Tris 36.34 g in 100 ml dist. water pH set to 8.8
Stacking buffer: (0.47 M Tris-HCl)	Tris 5.69 g in 100 ml dist. water pH set to 6.7
Stripping buffer:	Glycine 15 g SDS 1 g Tween 20 10 ml pH set to 2.2 1 L total volume (dist. water)
TBS (10 x)	NaCl 265 g TRIS 60 g filled up to 5 L with distilled water set pH to 7.4
TBS-T:	TBS 250 ml Tween-20 2.5 ml Dist. water 250 ml filled up to 2.5 L with distilled water

2.1.8 List of primary antibodies

Table 9: Primary antibodies for western blot analyses

Antigen	Origin	Company	Catalog No	Dilution
p-STAT3 XP®	Rabbit	Cell Signaling New England Biolabs GmbH, Frankfurt am Main, Germany	9145	1:1000 (WB)
STAT3 XP®	Rabbit	Cell Signaling New England Biolabs GmbH, Frankfurt am Main, Germany	8768	1:1000 (WB)
pAkt XP®	Rabbit	Cell Signaling New England Biolabs GmbH, Frankfurt am Main, Germany	4060	1:2000 (WB)
Akt	Rabbit	Cell Signaling New England Biolabs GmbH, Frankfurt am Main, Germany	4691	1:1000 (WB)
PCNA XP®	Rabbit	Cell Signaling New England Biolabs GmbH, Frankfurt am Main, Germany	13110	1:2000 (WB)
p-p44/42 (p-ERK1/2)	Rabbit	Cell Signaling New England Biolabs GmbH, Frankfurt am Main, Germany	9101	1:1000 (WB)
p-SAPK/JNK	Rabbit	Cell Signaling New England Biolabs GmbH, Frankfurt am Main, Germany	4668	1:1000 (WB)
p-p38 XP®	Rabbit	Cell Signaling New England Biolabs GmbH, Frankfurt am Main, Germany	4511	1:1000 (WB)
p38 XP®	Rabbit	Cell Signaling New England Biolabs GmbH, Frankfurt am Main, Germany	8690	1:1000 (WB)
SAPK/JNK	Rabbit	Cell Signaling New England Biolabs GmbH, Frankfurt am Main, Germany	9252	1:1000 (WB)
RIP3	Rabbit	Cell Signaling New England Biolabs GmbH, Frankfurt am Main, Germany	14401	1:1000 (WB)
CYP2E1	Rabbit	LSBio, LifeSpan BioSciences Inc., Seattle, Washington, USA	LS-C313045	1:1000 (WB)
Cleaved Caspase 3	Rabbit	Cell Signaling New England Biolabs GmbH, Frankfurt am Main, Germany	9664	1:1000 (WB)

2.1.9 List of secondary antibodies

Table 10: Secondary antibodies for western blot analyses

Antigen	Origin	Company	Catalog No	Dilution
GAPDH	Rabbit	Cell Signaling New England Biolabs GmbH, Frankfurt am Main, Germany	2118	1:1000 (WB)
β-actin	Mouse	Sigma-Aldrich Corp., St. Louis, MO, USA	A5316	1:10000

2.1.10 ECL solution

Table 11: ECL solution

Chemical	Amount
Luminol (250 mM in DMSO)	2.5 ml
p-coumaric acid (90 mM in DMSO)	0.55 ml
Fill it up with 0.1 M TRIS to 250 ml, protect from light, store at 4°C	
Mix 5 ml ECL solution with 3 µl H_2O_2 prior to use	

2.1.11 Buffers for PCR

Table 12: TBE-buffer

Buffer	Amount
TBE-buffer (10 x)	Boric acid 55 g TRIS 108 g 40 ml EDTA (0.5 M pH 8) Fill up to 2 L with distilled water

Table 13: Ficoll loading buffer

Buffer	Amount
Ficoll loading buffer	Bromophenol blue 125 mg Ficoll 7.5 g Add 50 ml dist. water

2.1.11.1 Primers for PCR

All primers were purchased from Eurofins, Ebersberg, Germany.

Table 14: Primers for genotyping

Primer		Sequence 5´→ 3´
alt Puro3a	forward	AATTGCATCGCATTGTCTGAGTAGG
Wisp-alt6	forward	TACGCAATAGGAGTGTGTGCACG
Wisp-alt9	reverse	GGCAGTGTCTCCATATCATTTGATAGG

Table 15: PCR primers

Primer		Sequence 5´→ 3´
XBP1	forward	GAACCAGGAGTTAAGAACACG
XBP1	reverse	AGGCAACAGTGTCAGAGTCC

2.1.12 Taqman assay

Table 16: Taqman assays (Thermo Scientific, Braunschweig, Germany)

Target gene	Gene name	Assay Catalog No.
Atf3	activating transcription factor 3	Mm00476032_m1
Ccl2	chemokine (C-C motif) ligand 2	Mm00441242_m1
Ccl3	chemokine (C-C motif) ligand 3	Mm00441259_g1
Ccl4	chemokine (C-C motif) ligand 4	Mm00443111_m1
Ccl5	chemokine (C-C motif) ligand 5	Mm01302427_m1
CCnd1	cyclin D1	Mm00432359_m1
CCne2	cyclin E2	Mm00438077_m1
CHOP	DNA-damage inducible transcript 3 (Ddit3)	Mm01135937_g1
Cidec	cell death-inducing DFFA-like effector c	Mm00617672_m1
Ctgf	connective tissue growth factor	Mm01192933_g1
Cxcl1	chemokine (C-X-C motif) ligand 1	Mm04207460_m1

Cxcl2	chemokine (C-X-C motif) ligand 2	Mm00436450_m1
Cxcl5	chemokine (C-X-C motif) ligand 5	Mm00436451_g1
Cyca2	cyclin A2	Mm00438063_m1
Cycg2	cyclin G2	Mm00432394_m1
Cyp2e1	cytochrome P450, family 2, subfamily e, polypeptide 1	Mm00491127_m1
Cyp4a10	cytochrome P450, family 4, subfamily a, polypeptide 10	Mm02601690_gH
Cyp4a14	cytochrome P450, family 4, subfamily a, polypeptide 14	Mm00484135_m1
Cyr61	cysteine rich protein 61	Mm00487499_g1
Gadd45ß	growth arrest and DNA-damage-inducible 45 beta	Mm00435121_g1
GAPDH	Glyceraldehyde-3-phosphate dehydrogenase	4352932E
Ifng	interferon gamma	Mm01168134_m1
Il6	interleukin 6	Mm00446190_m1
Lcn2	lipocalin 2	Mm01324470_m1
Myc	myelocytomatosis oncogene	Mm00487804_m1
Nov	nephroblastoma overexpressed gene	Mm00456855_m1
Pcna	proliferating cell nuclear antigen	Mm00448100_g1
PCNA	proliferating cell nuclear antigen	Mm00448100_g1
Serpina12	serine (or cysteine) peptidase inhibitor, clade A (alpha-1 antiproteinase, antitrypsin), member 12	Mm01337213_m1
Sperina1d	serine (or cysteine) peptidase inhibitor, clade A, member 1D	Mm00842094_mH
TNF	tumor necrosis factor	Mm00443260_g1
WISP1	WNT1 inducible signaling pathway protein 1	Mm00457574_m1

2.2 Methods

2.2.1 Animal models

All experiments involving animals were carried out in accordance with the European Union Community Council guidelines. Experiments were either performed with C57BL/6NRj (Janvier Labs, France) or WISP1 knockout and wild type mice. Mice were fed *ad libitum* with Ssniff R/M-H, 10 mm standard diet (Ssniff, Soest, Germany). Experiments were approved by the German authorities.

2.2.1.1 WISP1 knockout mice

Heterozygous WISP1 mice (B6;129S5-Wisp1tm1Lex/Orl) were purchased from Lexikon Pharmaceuticals (Lexko-1174). Heterozygous mice were bred in our animal facility to obtain homozygous WISP1 knockout and wild type mice. The gene knock down is accomplished by replacing Exon 2 of WISP1 by a construct containing a puromycin resistance cassette for clone selection, and a stop codon at its 3' end to inhibit transcription of WISP1 (Figure 16). The company reported no differences in bone marrow or blood leucocyte content in the WISP1 knockout mice. Therefore, the WISP1 knockout model can be used to assess the role of WISP1 in acute liver injury.

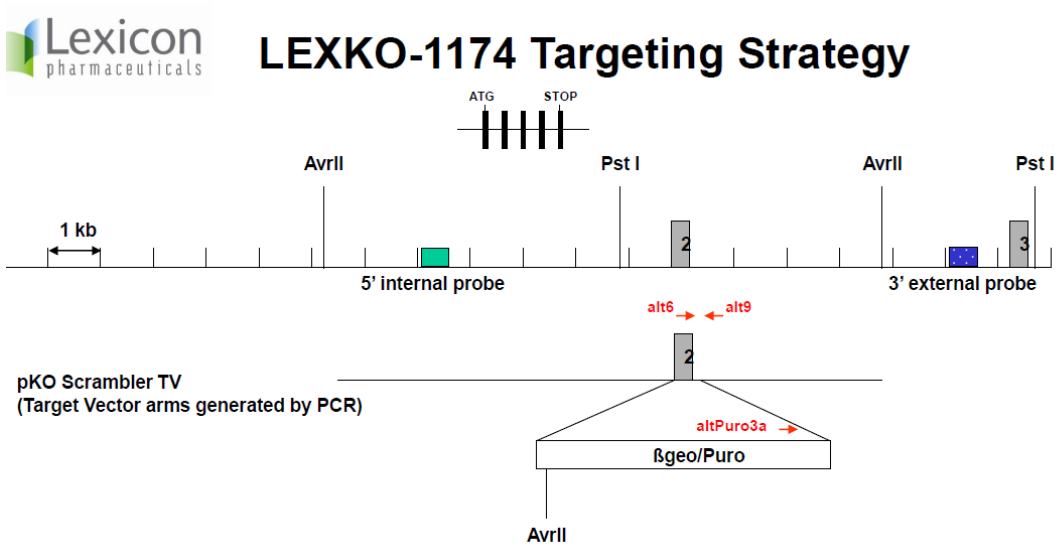

Figure 16: Generation of WISP1 knockout mice. Exon 2 of WISP1 was replaced by a construct containing a puromycin resistant cassette and a stop codon at its 3` end region resulting in the inhibition of the transcription of WISP1.

2.2.1.2 Genotyping of WISP1 mice

For the genotyping of WISP1 mice, Phire Animal Tissue Direct PCR Kit (Thermo Scientific) was used. Ear punch tissue from mice was collected in a microtube containing

25 µl Dilution buffer. To release the DNA from the tissue, 1.5 µl of DNARelease Additive were added and microtube was shortly flicked to ensure proper mixing. Afterwards, the samples were heated in a thermo shaker to 98°C for 25 min with gentle agitation followed by a short centrifugation step. To verify that the DNA release was successful, the DNA concentration was assessed using a spectrometer (NanoDrop2000). The reaction mixture for one PCR reaction is listed in table 17, and the PCR primers are specified in table 14. For the wild type mice, the PCR primers Alt6 and Alt9 were used; whereas, for the mutant samples Alt9 and Puro3A primer pairs were used at a concentration of 10 pmol/µl (Table 18). Finally, 1 µl of DNA was added to each wild type and mutant PCR. The reaction steps for PCR reaction are listed in table 19.

Table 17: Master mix conditions for PCR reaction

Phire Animal Tissue Direct PCR Kit	Volume per reaction [µl]
Phire Animal Tissue PCR Buffer	10
Primer forward	5
Primer reverse	5
Phire Hot Start II DNA Polymerase	0.4
Final volume	**20.4 + 1 µl of DNA**

Table 18: PCR primer set up for WT and mutant PCR reaction

	Wild type PCR	Mutant PCR
Primers	Alt6 + Alt9	Alt Puro3A + Alt9
PCR product	363 bp	459 bp

Table 19: Thermocycler program for PCR reaction (genotyping)

Step	Temperature [°C]	Time [min]	Note
1	94	3	
2	94	0.5	
3	58	1	
4	72	1	Go to step 2, repeat 39 cycles
5	72	10	
6	Pause at 4		

Thereafter, the PCR product was mixed with 5 µl of Gel loading dye and shortly centrifuged before loading onto a 1.5 % Agarose gels (250 ml) containing 18 µl ethidium bromide. Gel electrophoresis was performed at 150 V for approximately 2h in 1 x TBE buffer (Table 12) using the BioRad Sub-Cell Model 192 system (BioRad). The PCR product in the agarose gel was detected using E-BOX C5 (Vilber Lourmat, Germany).

2.2.2 CCl_4-induced acute liver damage

To study the possible influence of WISP1 in acute liver damage, the model compound CCl_4 was used. CCl_4 was dissolved according to table 20 with olive oil and injected

intraperitoneally (i.p.) as described previously [14]. To induce different degrees of liver damage, various concentrations from a mild dose to a maximum dose of CCl_4 were chosen. The control group received olive oil only as the vehicle control. All solutions were freshly prepared and mixed before injections.

Table 20: Overview for preparation of different CCl_4 solutions

Dose [mg/kg]	CCl_4 [µl]	Olive oil [µl]
0	0	4000
76	47.5	3952.5
132.4	82.75	3917.25
460	287.5	3712.5
920	575	3425
1600	1000	3000

2.2.3 Paracetamol

For the second model of acute liver damage, the hepatotoxic compound paracetamol was selected. Mice were starved overnight and a single dose of 300 mg/kg paracetamol, dissolved in sterile PBS, was administered intraperitoneally. Therefore, a solution containing 14.9 g/L paracetamol was first heated in a water bath at 60°C for 5-10 min to ensure solubilization. Thereafter, the solution was cooled to room temperature and sterile filtered. The final volume injected into the mice was 20.12 µl/g. The control mice were injected with sterile PBS as the vehicle control [49]. All solutions were prepared freshly before the injection.

2.2.4 Collection of liver tissue and blood sampling

At the indicated time points, mice were anesthetized using a mixture of sedative Rompun 2 % (20 mg/kg) and anesthetic Ketamine (120 mg/kg) that was administered via i.p. The abdominal wall was opened carefully after checking that all reflexes were lost. Therefore, mice were fixed in a dorsal position on a grid.

2.2.4.1 Blood sampling and plasma separation

To analyze the activity of liver enzymes, immunoassays for ALT and ELISA were performed using approximately 400 µl of blood that was collected by heart puncture with a 26G cannula containing 25 µl EDTA (32 mg/ml). The blood was carefully transferred into a precooled sterile 1.5 ml tube and centrifuged for 10 min at 4°C and 13,000 rpm. Thereafter, the supernatant (about 200 µl plasma), was separated into two precooled and sterile 0.5 ml tubes. Plasma was stored at -80°C for further analyses.

2.2.4.1.1 Alanine Aminotransferase (ALT) Activity Assay Kit

Alanine transferase (ALT), also known as serum glutamic-pyruvic transaminase (SGPT) was measured colorimetrically using the Alanine Aminotransferase Activity Assay Kit (Sigma). The transfer of an amino group from alanine to α-ketoglutarate (α-KG) results in the generation of pyruvate, leading to a colorimetric product, which is proportional to the ALT enzymatic activity. One unit of ALT is defined as the amount of enzyme that generates 1.0 µmole of pyruvate per min at 37°C. The assay was performed as described by manufacturer's instructions. Plasma samples from the control mice were measured without dilution prior to assay. Samples with expected high values of ALT were diluted prior to performing the assay (1:100, 1:200, 1:400).

2.2.4.1.2 ELISA

To determine the concentration of WISP1 in blood plasma and liver tissue samples, Quantikine® ELISA Mouse/Rat WISP-1/CCN4 immunoassay was used. Therefore, all plasma samples were diluted 1:10 with Calibrator Diluent RD6-31 (1:2) prior to measurement. Liver tissue samples were prepared from snap frozen tissue. First, the samples were transferred into a new 1.5 ml microtube to measure the weight of liver piece followed by homogenizing in 150 µl sterile PBS with a pestle. An equal volume of Cell lysis Buffer 2 was added and samples were shortly mixed to obtain a homogenous lysate. Afterwards, the samples were lysed at room temperature for 30 min with gentle agitation in a thermo shaker followed by a centrifugation step at 13.000 rpm at 4°C for 10 min. Supernatants were transferred into a new microtube and stored at -80°C for analysis. The assay was performed according to the manufacturer`s protocol. The concentration of WISP1 was calculated according to the standard curve and the dilution of the sample. For liver tissue samples the concentration was calculated for pg/mg of liver tissue.

2.2.4.2 Collection of liver tissue samples

Directly after blood collection, the whole liver was carefully excised without destroying the liver capsule and briefly rinsed with sterile PBS. The left liver lobe was divided into two halves. One half was collected in Tissue-Loc™ HistoScreen™ Cassettes for paraffin embedding and the other half was cut into small pieces (0.5 cm^2) and snap-frozen in liquid nitrogen (Figure 17). Snap frozen samples were stored at -80°C for further analyses. The right segment of median liver lobe was also collected for paraffin embedding. All other lobules were cut into smaller pieces and transferred into a 1.5 ml tube and snap-frozen.

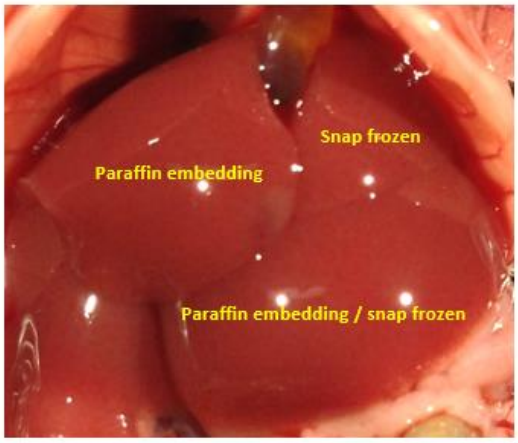

Figure 17: Collection of liver tissue samples. The left liver lobe was divided into two halves. One half was collected for paraffin embedding and the other half was cut into pieces and snap frozen in liquid nitrogen. The median lobe was collected also for paraffin embedding.

2.2.4 2.1 GSH measurement

For GSH measurement, about 20 mg of snap frozen tissue was weighed out directly in 100 µl NEM buffer. The tissue was homogenized with a pestle and the resulting lysate was snap frozen in liquid nitrogen. Further analyses were done as previously described [163].

2.2.4.3 Paraffin embedding of mouse liver tissue

For paraffin embedding, tissue samples were fixed in 4 % PFA for 2 days at 4°C. Afterwards, the samples were washed with sterile PBS for 2 days at 4°C followed by embedding in paraffin using Microm STP120 embedding automate (Microm, Walldorf, Germany). The program for embedding is listed in table 21. Thereafter, the tissue samples were submerged in paraffin using EC 350 – Modular tissue embedding center.

Table 21: Embedding program for mouse liver tissue

Step	Treatment	Time [min]
1	70 % ethanol	30
2	70 % ethanol	60
3	90 % ethanol	30
4	90 % ethanol	30
5	99 % ethanol	30
6	99 % ethanol	35
7	99 % ethanol	60
8	xylol	30
9	xylol	35
10	xylol	60
11	Paraffin Histowax	80
12	Paraffin Histowax	105

2.2.5 Liver slices for histological analyses

For histological analyses, the liver tissue was sliced in 5 µm sections using the HM 450 Sliding Microtome followed by a fixation on glass microscopy slides at 60°C for 20 min. All tissue slides were stored at 4°C until further usage.

2.2.5.1 Hematoxylin and eosin staining

For the first step, the tissue slides were incubated three times in Roti-Histol for tissue deparaffinization. Afterwards, the tissue on the slides were rehydrated in an ethanol gradient (95 %, 90 %, 80 %, 70 %) for 5 min each, followed by washing in distilled water for 5 min. After rehydration, the tissue slides were incubated in Mayer´s Hemalum solution (1:5 diluted with distilled water, filtered before use) for 5 min. Subsequently, the slides were washed for 15 min under running tap water followed by an incubation in 1 % Eosin solution for 3 min (1 % Eosin Y with 1 drop of acetic acid, filtered before use). Thereafter, the slides were washed in distilled water for 10 s and dehydrated in ethanol gradient for 5 s each (70 %, 80 %, 90 %). Finally, the sections were incubated two times for 5 min in 100 % ethanol followed by 3 min incubation in Roti-Histol. Subsequently, the stained tissue was preserved with Entellan, allowed to dry overnight, and analyzed the next day using bright-field microscopy to quantify the dead cell areas.

2.2.5.1.1 Quantification of dead cell areas

In order to quantify the dead cell areas of the H&E stained liver sections, 5 or 10 images per mice (biological replicate) were acquired using Cell^M software. First, to precisely quantify the necrotic lesions, the entire area of the image was quantified. Then, the areas showing no hepatocyte nuclei were determined as dead cell areas (Figure 18). The % of the dead cell area was calculated according to the formula shown below.

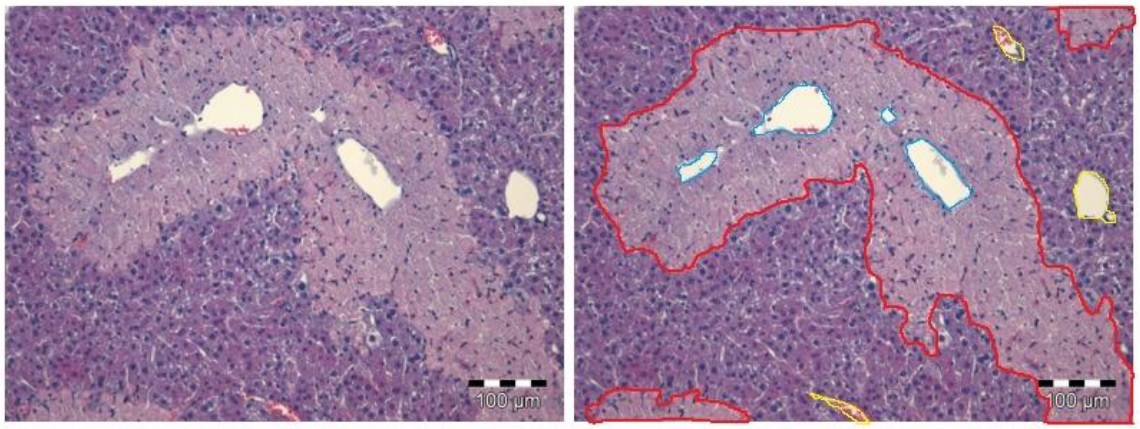

$$\textbf{Dead cell area } (\%) = \frac{\textbf{area of lesion} - \textbf{central vein}}{\textbf{total image area} - \textbf{portal vein}} \textbf{ x 100}$$

Figure 18: Quantification of H&E staining. The dead cell areas were defined as areas where no hepatocyte nuclei are visible (red area). To precisely determine the dead cell areas, empty areas of the central veins (blue) and portal veins (yellow) were subtracted from the total area. 10 images from each biological replicate were quantified and calculated for the % of dead cell area as shown in the formula above. Scale bar 100 µm.

2.2.5.2 Immunohistochemistry (Cyp2e1, Ly6G, CD45, F4/80)

For immunohistochemical staining, paraffin slides of 5 µm thickness were used. For deparaffinization, the slides were incubated four times in Roti-Histol for 5 min each. Afterwards, rehydration was performed using a descending ethanol gradient (100 %, 95 %, 90 %, 80 %, 70 %) for 5 min each followed by an incubation in distilled water for 5 min. For antigen retrieval, the slides were boiled with citrate buffer (2.1 g/L in distilled water, pH 6.0) for 15 min followed by a cool down with fresh citrate buffer for 30 min. Afterwards, the slides were washed in distilled water for 5 min and blocked for endogenous peroxidase activity in 3 % H_2O_2 for 10 min at room temperature followed by another washing step in PBS for 3 min (three times). Thereafter, unspecific binding sites were blocked by incubation in 3 % BSA/1 % Tween80 in PBS for 1 hour at room temperature in a humidified chamber. Moreover, endogenous avidin and biotin were blocked using Avidin/Biotin blocking kit (Vector Laboratories) each for 15 min at room temperature. Next, the slides were incubated overnight with primary antibodies in 0.3 % BSA/ 1 % Tween80 according to table 22 in a humid chamber at 4°C.

Table 22: Conditions for primary antibodies

Antigen	Origin	Dilution	DAB substrate	Company	Catalog No.
Ly6G	rat	1:250	4 min	R&D Systems	MAB1037
CD45	rat	1:100	5 min	BD Pharmingen	550539
F4/80	rat	1:50	15 min	BioRad	MCA497
Cyp2E1	rabbit	1:50	4 min	LSBio	LS-C313045

After overnight incubation with the primary antibody, the slides were washed three times in PBS for 3 min followed by incubation with the secondary antibody as listed in table 23. Antibody solution contained 30 µl serum and 15 µl secondary antibody in 2 ml PBS. After 30 min incubation at room temperature, the slides were washed three times in PBS for 3 min each. In the next step, tissues were incubated in a mixture of 40 µl of reagent A and 40 µl of reagent B in 2 ml PBS for another 30 min incubation at room temperature. Afterwards, the slides were washed again as previously described and incubated in the dark with the DAB substrate (2 drops buffer stock solution, 2 drops hydrogen peroxidase, 4 drops DAB substrate in 5 ml PBS). DAB substrate incubation times are listed in table 22. Next, the slides were shortly washed under running tap water followed by incubation with Mayer´s Hemalum solution (1:5 diluted with distilled water, filtered before use) for 2 min. Subsequently, the slides were washed with running tap water for 6 min and rehydrated in an ethanol gradient for 1 min each (30 %, 50 %, 70 %, 80 %, 90 %, 95 %, 100 %), followed by an incubation in Roti-Histol for 3 min. Finally, the slides were fixed with Entellan and covered with a glass slide.

Table 23: Kits for secondary antibodies

Antibody	Kit	Enzyme	Company	Catalog No.
Anti-Rat	Vectastain	ABC - HRP	Vector	PK4004
Anti-Rabbit	Vectastain	ABC - HRP	Vector	PK6101

2.2.5.3 Immunohistochemistry (WISP1)

For immunohistochemical staining, paraffin embedded liver sections of 5 µm thickness were used. After deparaffinization, for four times 5 min each using Roti-Histol, slides were rehydrated using a descending ethanol gradient (100 %, 95 %, 90 %, 80 %, 70 %, 50 %, 30 %) for 5 min each. Afterwards, the slides were washed for 5 min in distilled water, followed by antigen retrieval with citrate buffer (2.1 g/L, pH 6.0) for 15 min. Subsequently, the slides were cooled down for 30 min using fresh citrate buffer. Thereafter, the slides were washed two times for 5 min in PBS, followed by H_2O_2 (3 %) blocking for 15 min at room temperature. Next, the slides were washed three times for 5 min each in PBS, followed by blocking of unspecific binding sites using 3 % BSA/ 0.1 % Tween20 for 2h. Moreover, endogenous avidin and biotin were blocked using Avidin/Biotin blocking kit (Vector Laboratories) each for 15 min at room temperature. Afterwards, the slides were incubated overnight with a primary antibody diluted in 0.3 % BSA/ 0.1 % Tween20 (Table 24). On the next day, the slides were washed in PBS three times for 5 min each, followed by the incubation step with the secondary antibody as listed in table 25. The antibody solution contained 30 µl serum and 15 µl secondary antibody in 2 ml PBS. After 1h incubation at room temperature, the slides were washed three times in PBS for 5 min each. In the next step, 40 µl of reagent A and 40 µl of reagent B were mixed in 2 ml PBS and used for another

30 min incubation at room temperature. Afterwards, the slides were washed again as previously described and incubated in the dark with DAB substrate (2 drops buffer stock solution, 2 drops hydrogen peroxidase, 4 drops DAB substrate in 5 ml PBS). DAB substrate incubation times are listed in table 24. Subsequently, the slides were washed using running tap water for 10 min, followed by incubation with Mayer´s Hemalum solution (1:5 diluted with distilled water, filtered before use) for 90 sec. The slides were then washed using running tap water for 10 min, followed by rehydration in an ethanol gradient (70 %, 90 %, 95 %, 100 %) for 5 min each. Finally, the slides were incubated in Roti-Histol for 3 min and fixed with Entellan and covered with a glass slide.

Table 24: Conditions for primary antibody

Organ	DAB substrate	Dilution	Antigen	origin	Company	Catalog No.
Brain	1 min	1:100	WISP1/ CCN4	sheep	R&D Systems	AF1680
Kidney	1 min	1:100	WISP1/ CCN4	sheep	R&D Systems	AF1680
Spleen	1 min	1:100	WISP1/ CCN4	sheep	R&D Systems	AF1680
Lung	1 min	1:100	WISP1/ CCN4	sheep	R&D Systems	AF1680
Heart	2 min	1:100	WISP1/ CCN4	sheep	R&D Systems	AF1680
Intestine	1 min	1:100	WISP1/ CCN4	sheep	R&D Systems	AF1680
Muscle	2 min	1:100	WISP1/ CCN4	sheep	R&D Systems	AF1680
Liver	1 min	1:100	WISP1/ CCN4	sheep	R&D Systems	AF1680

Table 25: Kits for secondary antibody

Antibody	Kit	Enzym	Company	Catalog No.
Anti-Sheep	Vectastain	ABC - HRP	Vector	PK4006

2.2.5.4 TUNEL staining

TUNEL staining was performed using the DeadEnd™ Colorimetric TUNEL System (Promega). The assay was conducted following the manufacturer's instructions with the exception of using 3 % H_2O_2 instead of 0.3 %. After DAB incubation, the slides were rinsed several times with water followed by an incubation with Mayer´s Hemalum solution (1:5 diluted with distilled water, filtered before use) for 90 sec. Afterwards, the slides were washed under running tap water for 10 min and rehydrated in ethanol gradient for 1 min each (30 %, 50 %, 70 %, 80 %, 90 %, 100 %). Finally, the slides were incubated in Roti-Histol for 5 min and mounted with Entellan.

2.2.5.5 High mobility group box 1 protein staining (HMGB1)

High mobility group box 1 protein staining was performed at the university hospital Jena (Prof. Dr. Uta Dahmen, University hospital Jena).

2.2.6 RNA isolation from liver tissue and primary mouse hepatocytes

RNA was isolated from mouse liver tissue, primary mouse hepatocytes and NPCs using QIAzol Lysis Reagent and phenol/chloroform method according to the manufacturer´s description.

a) **Snap frozen liver tissue:** Sections of about 0.5 cm^2 were homogenized with a plastic pestle in a 1.5 ml tube using 1 ml of QIAzol while kept on ice.
b) **Freshly isolated hepatocytes/ NPCs:** Volume needed for 1 million cells was calculated, transferred into a new 1.5 ml tube and centrifuged at 13,000 rpm for 10 min at 4°C. Subsequently, the supernatant was removed and cells were lysed using 1ml QIAzol.

After the homogenization step, the samples were sonicated on ice for 30 sec (5 sec pulse, 2 sec break). Thereafter, 200 µl of chloroform was added and samples were strongly shaken for 15 sec. After 2-3 min incubation at room temperature, a first phase separation was seen. After the first centrifugation step at 4°C for 15 min at 12,000 rpm, the upper aqueous phase was transferred into a new RNase free 1.5 ml tube and RNA was precipitated using 500 µl of isopropanol. Samples were incubated at room temperature for 10 min, followed by a centrifugation step at 4°C for 15 min at 12,000 rpm. Afterwards, the supernatant was removed and RNA pellet was resuspended in 1 ml of 100 % ethanol and centrifuged at 7,500 rpm at 4°C for 5 min. The supernatant was discarded and RNA pellet was resuspended with 1 ml of 75 % ethanol and centrifuged for 5min at 4°C and 7,500 rpm. Thereafter, the supernatant was removed and RNA pellet was air-dried under fume hood for 30 min. Finally, the RNA pellet was dissolved in RNase-free water depending on the pellet size (liver tissue: 100-150 µl, hepatocytes: 10-30 µl). RNA concentration and integrity was determined spectrophotometrically using the NanoDrop 2000. Extracted RNA was stored at -80°C until further usage.

2.2.6.1 cDNA synthesis

For complementary cDNA synthesis, 2 µg of RNA were transcribed using High Capacity cDNA reverse transcription kit. The reaction mixture for cDNA synthesis is listed in table 26.

Table 26: Composition of master mix for cDNA synthesis

Compound	Volume per reaction
10x RT-Buffer	2 µl
25x dNTP	0.8 µl
Random primer	2 µl
Reverse transcriptase	1 µl
H2O	4.2 µl
Total volume 1	**10 µl**
RNA	2 µg

DEPC water up to	10 µl
Total volume 2	**10 µl**
Final total volume	**20 µl**

PCR conditions were programmed as follows:

Table 27: Program for RT-PCR

Step	Temperature	Time
Incubation	25°C	10 min
Reverse Transcription	37°C	120 min
Inactivation	85°C	5 sec
	4°C	hold

The resulting cDNA was dissolved to a final concentration of 10 ng/µl with DEPC treated water and stored at -20°C.

2.2.6.2 Quantitative Real Time PCR (qRT-PCR)

The quantitative real time PCR was performed by using Taq-Man-PCR technology with a 7500 Real-Time PCR System using TaqMan® Universal Master Mix II, with UNG. Reagents were purchased from Applied Biosystems and Taqman probes are listed in table 16. The composition of master mix reaction for qRT-PCR is shown in table 28.

Table 28: Master mix composition for qRT-PCR

Compound	Volume per sample
Universal PCR Master Mix	10 µl
DEPC treated H2O	6.5 µl
Taqman probe	1 µl
25 ng cDNA	2.5 µl
Final volume	**20 µl**

Samples were measured in technical duplicates. For negative control, DEPC water instead of cDNA was used. The conditions for qRT-PCR are shown in table 29.

Table 29: Conditions for qRT-PCR

Stage	Temperature	Time	Repetitions
1	50 °C	2 min	1
2	95 °C	10 min	1
3	94 °C	15 sec	40
	60 °C	30 sec	
	72 °C	35 sec	
4	95 °C	15 sec	1
	60 °C	20 sec	
	95 °C	15 sec	
	60 °C	15 sec	

PCR products were analyzed using the 7500 Real-Time PCR System software. Glyceraldehyde-3-phosphate dehydrogenase (GAPDH) expression was used as the endogenous control for each sample. The expression levels in treated mouse liver were normalized to mouse control liver tissue. For calculation the comparative threshold method (ΔΔCt method) was used [164]. The relative expression was calculated according to the following steps.

1. ΔCt1 = Ct Gene of interest (GOI) – Ct House keeper gene (HKG)
2. ΔCt2 = Ct GOI of control samples – Ct HKG of control samples
3. ΔΔCt = ΔCt1 – ΔCt2
4. Calculation of $2^{-\Delta\Delta Ct}$

2.2.7 Analysis of Xbp1 splicing by PCR

Taq DNA Polymerase kit of 5-Prime (Hamburg, Germany) with primers from Eurofins (Ebersberg, Germany) were used to perform PCR reaction in a T-gradient thermocycler from Biometra. The reaction was conducted as depicted in the table 30 below. The final PCR product was mixed with 5 µl Ficoll loading buffer (Table 13), shortly spun down and loaded onto a 1.5 % Agarose gel. Gel electrophoresis was performed at 150 V for approximately 2h in 1 x TBE buffer (Table 12). The electrophoresis results were detected using E-BOX CX5 (Vilber Lourmat, Eberhardzell, Germany).

Table 30: Thermocycler program for Xbp1 PCR reaction

Step	Temperature	Time	Go back to step	Number of cycle repetitions
1	94	2 min		
2	94	30 s		
3	58	1 min		
4	72	1 min		
5	72	10 min	2	39
6	4		-	

2.2.8 Affymetrix gene array analysis

Whole genome gene array analysis from WISP1 knockout and wild type mice was performed using Affymetrix GenChip® Mouse Genome 430 2.0 arrays. The following time points from 460 mg/kg CCl_4 treated WISP1 knockout and wild type mice were chosen: control (olive oil), 8h, 12h, D1 and D3. RNA from 5 mice per condition was isolated as described above. RNA concentration and integrity were determined spectrophotometrically using Nanodrop 2000.

To analyze the RNA expression, 5 µg of RNA were transcribed into cDNA by oligo dT primers, and reverse transcribed to biotinylated cRNA with the GeneChip 3' IVT Express Kit. IVT product was cleaned up using CHROMA SPIN-100 columns and quantified spectrophometrically. Subsequently, cRNA was fragmented using Affymetrix's protocol.

Labeled and fragmented cRNA was hybridized to Mouse Genome 430 2.0 Affymetrix GeneChips for 16h at 45°C according to the manufacturer's instructions. Afterwards, the microarrays were washed using an Affymetrix fluidics station 450 and stained initially with streptavidin-phycoerytherin. For each sample, the signal was further enhanced by incubation with biotinylated goat anti-streptavidin followed by a second incubation with streptavidin-phycoerytherin, and a second round of intensities were measured. Microarrays were scanned using Affymetrix Gene-Chip Scanner-3000-7G controlled by GCOS software.

2.2.8.1 Microarray processing and statistical analysis

Biostatistical analysis was performed at Leibniz Institute for Natural Product Research and Infection Biology Hans-Knöll-Institute (HKI) in Jena, Germany. Affymetrix gene array data were pre-processed using 'affyPLM' packages [165] of the Bioconductor Software [166]. To obtain genes with the most evidence of differential expression, the pre-processed dataset was analyzed using linear models with least squares regression and empirical Bayes moderated t-statistics of the LIMMA (Linear Models for Microarray Data) package [167] of Bioconductor software [166]. Benjamini Hochberg false discovery rate correction (FDR) was used to adjust the obtain p-values for multiple comparisons [168]. Data obtained from healthy control liver tissue were used as a reference. The custom chip definition file from Brainarray [169] based on Unigene ID's was used to annotate the microarrays. Two selection criteria were chosen as significance level to detect differentially expressed genes (DEGs): first was p-value < 0.05 and second was an absolute fold change > 2. Processing and visualization (Principal Component Analysis) of data were performed using MATLAB tools (The MathWorks Inc., Natick, MA).

2.2.8.2 Fuzzy clustering of gene expression profiles

The time-profiles of differentially expressed genes in wild type and WISP1 knockout mice were scaled between their respective absolute temporal extreme values to focus on subsequent cluster analysis on the qualitative behavior of the expression profiles. The time series were clustered using fuzzy c-means [170] (fuzzy exponent = 1.5; maximum number of iteration = 200; minimum cost function improvement = 10-10). The optimum number N of cluster was estimated by repeated calculation (number of iterations = 100) of the fuzzy cluster index 'Separation Index'.

2.2.8.3 Gene ontology (GO) and KEGG Pathway analyses

Genes which show change ratios greater (or less) than 2-fold in the triplicate arrays at any one of the timepoints have been considered as up or down-regulated and subjected to gene ontology (GO) and pathway analysis. Differentially regulated genes were categorized

using the manually curated Gene Ontology of the Biobase Knowledge Library (BKL) of the ExPlain™ webservice (BioBase GmbH, Wolfenbüttel, Germany).

2.2.9 Protein extraction and western blot analyses

2.2.9.1 Protein isolation from liver tissue and cell culture

Protein extraction was performed as follows:

a) **Snap frozen liver tissue:** Sections of about 0.5 cm^2 were homogenized with a plastic pestle in a 1.5 ml tube using 0.5 ml of ice cold RIPA while kept on ice.
b) **Primary hepatocytes *in vitro* culture:** Culture plate was placed on ice and culture medium was removed. Subsequently, the cells were lysed with 250 µl of RIPA buffer using a cell scraper and transferred into a pre-cooled 1.5 ml tube.

Thereafter, the samples were sonicated for 30 sec (5 sec pulse, 2 sec break) while kept on ice. The homogenates were incubated for 20 min on ice at 4°C and centrifuged for 10 min at 13,000 rpm at 4°C. Solubilized proteins in the supernatant were transferred into a pre-cooled 1.5 ml tube and stored at -80°C for further analyses.

2.2.9.2 Protein quantification (BCA)

For protein quantification, bicinchoninic acid (BCA) assay was used. Depending on the estimated protein concentration 2.5 µl up to 10 µl of the sample were used together with appropriate amount of reagents recommended by the manufacturer`s protocol. The samples were heated to 60°C for 30 min and afterwards measured to determine the absorbance. The mean value of three independent measurements was used to determine the protein concentration related to protein standard curve and used dilution of the samples.

2.2.9.3 SDS-page and western blot

For SDS-PAGE, 30 to 50 µg of protein lysate were adjusted to the volume of 30 µl with distilled water including 6 µl of loading buffer (5x). The Samples were denatured at 95°C for 5 min and shortly centrifuged at 13,000 rpm. 10 % SDS-PAGE gel with 1.5 mm x 10 wells or 1.5 mm x 15 wells were used. All components for a 10 % SDS-PAGE gel are listed in table 31. In the first two lanes, Precision Plus protein standard (4 µl) and MagicMark TM XP Western Protein Standard (2 µl) were loaded onto the gel to estimate the molecular weight of separated proteins in the samples. After loading of the samples, the gel was run using the Bio-Rad Mini PROTEAN Tetra System. Biometra Standard Power Pack P25 was used to perform the gel electrophoresis for 3h at constant voltage of 25 mA.

Table 31: Components of 10 % SDS gel

Separation gel (10 %)		Stacking gel	
1 Gel		**1 Gel**	
H2O	3.2 ml	**H2O**	2.4 ml
Acrylamide	2.64 ml	**Acrylamide**	0.5 ml
Separation buffer	2 ml	**Stacking buffer**	0.4 ml
10 % SDS	80 µl	**10 % SDS**	32.5 µl
TEMED	3.2 µl	**TEMED**	2.5 µl
10 % APS	80 µl	**10 % APS**	50 µl

2.2.9.4 Semi-dry blotting

For semi-dry protein transfer, Fastblot B44 blotting system with a 5 x 8 cm size gel-membrane sandwich was used. The PVDF membrane was activated in methanol, 4 Whatman paper were saturated with cathode buffer and 12 Whatman papers were saturated with anode buffer. The correct buildup can be seen in table 32. Semi-dry blotting was performed for 40 min at a constant current of 250 mA/gel- membrane sandwich. Thereafter, the membranes were washed with distilled water and stained with Ponseau S for a few seconds to verify that the transfer was successful. Finally, Ponseau S was removed by washing the membranes in TBS-T solution for 5 min.

Table 32: Western blot set up for semi-dry blotting

Top: cathode
4 Whatman papers
Gel
PVDF membrane
12 Whatman papers
Bottom: anode

2.2.9.5 Protein immunodetection and chemiluminescence

For immunodetection of proteins, membranes were blocked with 5 % BSA or 5 % milk in TBS-T buffer for 1h at room temperature, followed by an overnight incubation at 4°C with primary antibody (Table 9) diluted either in 5 % BSA or 5 % milk solution. The next day, the membranes were washed three times for 10 min in TBS-T at room temperature. Afterwards, horseradish peroxidase-labeled secondary antibody was added in a 5 % TBS-T or 5 % milk solution for appropriate time and concentration at room temperature as listed in table 9. Thereafter, the membranes are washed again in TBS-T three times for 10 min at room temperature. Protein detection was performed by chemiluminescence using 5 ml ECL solution (Table 11) in a Fusion-FX7 imager (Vilber Lourmat) equipped with a CCD camera. Next, the membranes were incubated for 30 min with stripping buffer at room temperature to remove the probed antibodies off the membrane followed by a washing step with TBS-T for 5 min. For detection of further proteins, membranes were blocked again for 30 min with 5 % BSA or 5 % milk in TBS-T at room temperature, followed by incubation with a second

primary antibody or loading control as described in table 10. Quantification was performed using the Bio-1D (Vilber Lourmat, Germany) software.

2.2.10 Isolation of primary mouse hepatocytes and culturing method

To obtain primary mouse hepatocytes, a two-step perfusion from WISP1 knockout and wild type mice (8-12 weeks old) was performed as previously described [24]. For anesthesia, the mice received i.p. injection containing 2 % Rompun (20 mg/kg) and Ketamine (120 mg/kg). The abdominal wall was opened carefully after checking that all reflexes were lost. Therefore, mice were fixed in a dorsal position on a grid under a heating lamp. The inferior vena cava was carefully exposed followed by inserting a 24G cannula for perfusion with EDTA buffer at 37°C for 15 min with a rate flow of 15 ml/min. At this step, the liver colour immediately became pale, blood volume and Ca^{2+}-dependent adhesion factors were removed. Afterwards, the perfusion was continued with collagenase buffer, warmed up to 37°C, for an additional 15 min at the same rate flow. During this step of perfusion, the extracellular matrix is digested and depending on the collagenase activity this step can last 5-15 min. Thereafter, the liver was excised completely and transferred onto a petri dish containing suspension buffer. The liver capsule was carefully opened under a sterile hood using a forceps to release the liver cells in the suspension buffer. The cell suspension was filtered through a 100 µm cell strainer and centrifuged for 5 min at 4°C and 50 rpm. The supernatant contained the non-parenchymal cells and the pellet contained the larger and heavier hepatocytes. The pellet was resuspended with 10 ml of suspension buffer. An aliquot of the cell suspension was diluted 1:5 with suspension buffer and further mixed with 0.4 % trypan blue solution at a ratio of 1:1 for cell counting in a Neubauer chamber hemocytometer. Dead cells, which stained blue were counted together with unstained living cells in all four corner squares. The average of viable cells was multiplied by $1x10^5$ to achieve the cell number per milliliter of cell suspension. The viability varied from 90-95 % with total cell yield of 5-7 x 10^6 cells per ml.

For collection of fresh NPCs, the supernatant was transferred to a new 50 ml falcon tube. After centrifugation at 400 rpm for 10 min at 4°C, the supernatant was discarded and cells were washed using 25 ml of suspension buffer. After a second centrifugation step at 400 rpm for 10 min at 4°C, cells were resuspended using 1 ml suspension buffer and counted to assess the viability as described above.

2.2.11 *In vitro* culture of hepatocytes

Primary mouse hepatocytes were cultured in 6-well pates from Sarstedt. During all experiments, cells were maintained at 37°C and 5% CO_2.

2.2.11.1 Collagen monolayer confluent (CM)

For the cultivation of primary mouse hepatocytes on collagen monolayer, 10 mg of rat-tail collagen was dissolved in 40 ml of 0.2 % acetic acid resulting in a stock solution of 250 µg/ml. The 6-well plates were coated with the stock solution and allowed to dry overnight under the sterile bench. On the next day, the plates were shortly washed twice with sterile PBS, and Williams E medium with 10 % Sera Plus was added to the wells (Table 6). Thereafter, the appropriate cell number (Table 33) was seeded and plates were incubated for 3h in the incubator. The plates were then washed for three times with medium to remove unattached cells followed by the addition of a final volume of 2 ml Williams E medium.

Table 33: Conditions for collagen monolayer and collagen sandwich culture system

Culture system	Amount of cells [x10^6]	Medium [ml/well]
Collagen monolayer (CM)	1	2
Collagen sandwich (CS)	0.85	2

2.2.11.2 Collagen sandwich (CS)

For cultivation of primary mouse hepatocytes in collagen sandwich system, 10 mg of rat-tail collagen was dissolved in 9 ml of 0.2 % acetic acid for at least 3h to obtain a final concentration of 1.1 mg/ml. Afterwards, the collagen was mixed with 10x DMEM (ratio 9:1) resulting in a yellow solution (pH indicator): By slowly adding 1 M NaOH on ice, the solution was neutralized until the colour changed from yellow to fuchsia. Finally, 350 µl of collagen solution was added to each well and properly distributed to obtain an even first layer followed by an incubation for 45 min at 37°C to allow polymerization. Next, full media (Table 6) was added to wells and an appropriate cell amount was seeded (Table 33). Cells were allowed to attach for 3h in an incubator. Subsequently, the unattached cells were removed by washing the plates three times with cell culture media and the second collagen layer was added to the cells, as described above. After 45 min polymerization, Williams E medium with all additives (Table 6) was added.

2.2.11.3 Stimulation of primary hepatocytes with TNFα or TGFβ

Stimulation of primary WISP1 knockout and wild type hepatoyctes was performed on D1 in culture using collagen monolayer (CM) configuration. Recombinant human TNFα protein (10 µg) was reconstituted in sterile PBS containing 0.1 % bovine serum albumin to a final concentration of 10 ng/µl. Recombinant human TGFβ protein (2 µg) was reconstituted in sterile 4 mM HCl containing 0.1 % bovine serum albumin to a final concentration of 10 ng/µl. Reconstituted proteins were stored in 20-50 µl aliquots at -20°C. On the day of stimulation, a stock solution (10 ng/ml) in Williams E medium plus additives (Table 6) was prepared for each cytokine containing 0.1 µg/ml Actinomycin D. The stock solution was used

to prepare further dilutions of 1 ng/ml, 2.5 ng/ml, 5 ng/ml and 7.5 ng/ml of the cytokines. Williams E medium was used as the control condition. Before stimulation, cells were washed with Williams E medium three times to remove dead cells followed by adding 2 ml per well of prepared cytokine solutions. TNFα stimulated cells were incubated for 8h and TGFβ stimulated hepatocytes were incubated for 24h at 37°C. Subsequently, representative images were taken from each condition and protein samples were collected as described previously (Chapter 2.2.9.1). In order to study time resolved effects, the highest TNFα concentration (10 ng/ml) was chosen to stimulate primary hepatocytes for 30 min, 1h, 2h, 4h, 6h, 8h, 10h and 24h. At the indicated time points, representative images were taken and protein samples were collected as described above.

2.2.11.3.1 Quantification of apoptotic hepatocytes

To quantify apoptotic hepatocytes after cytokine stimulation, images were taken using a 20x magnification with bright field microscope. Five images per condition were counted for apoptotic and vital hepatocytes using ImageJ *Cell Counter* (Figure 19).

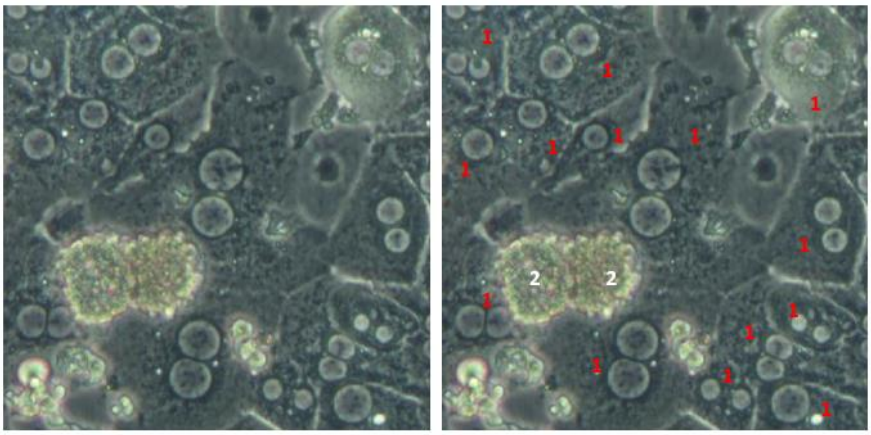

Figure 19: Example for counting vital and apoptotic primary hepatocytes in collagen monolayer configuration. On the left side, representative picture of cytokine-stimulated primary hepatocytes is shown. Vital hepatocytes were clearly distinguished from apoptotic cells by showing typical cuboidal morphology and multiple nuclei. Apoptotic cells a showed different morphology caused by blebbing and no nuclei were visible. On the right side, marker 1 in red depicted all vital hepatocytes and marker 2 in white identified cells, which were counted as apoptotic hepatocytes.

The % of apoptotic cells was calculated as shown below:

$$\%\ \textbf{of apoptotic cells} = \frac{\textbf{number of apoptotic cells}}{\textbf{total amount of cells}}\ \textbf{x 100}$$

2.2.11.4 Stimulation of primary hepatocytes with paracetamol

The first step was to prepare a stock solution of 10 mM paracetamol dissolved in Williams E medium (Table 6). The solution was incubated for approximately 15 min in a water bath to ensure proper solubilization. Afterwards, the stock solution was sterile filtered and used to prepare further solutions containing 7.5 mM, 5 mM, 2.5 mM and 1 mM paracetamol in Williams E medium. For stimulation with paracetamol, the collagen sandwich (CS) configuration was used. For the first approach, hepatocytes were stimulated after 3h of attachment and incubated for 24h. For the second approach, hepatocytes were stimulated at D1 in culture and incubated for 24h.

2.2.11.4.1 Propidium idodide staining

In order to quantify dead cells after paracetamol treatment, propidium iodide staining was performed. The propidium iodide was diluted 1:500 in Williams E medium directly before usage. Medium was removed and 2 ml of propidium iodide solution was added to the cells in the dark. After incubation for 15 min at 37°C, cells were washed three times with sterile PBS followed by adding Williams E medium. Finally images were acquired using Nikon Eclipse TS100 microscope.

2.2.11.4.2 Quantification of propidium iodide staining

To quantify the propidium iodide staining, 10 images were taken per condition. Propidium iodide stained cells were counted as dead and cells without a fluorescence signal as living cells (Figure 20) using ImageJ *Cell Counter*.

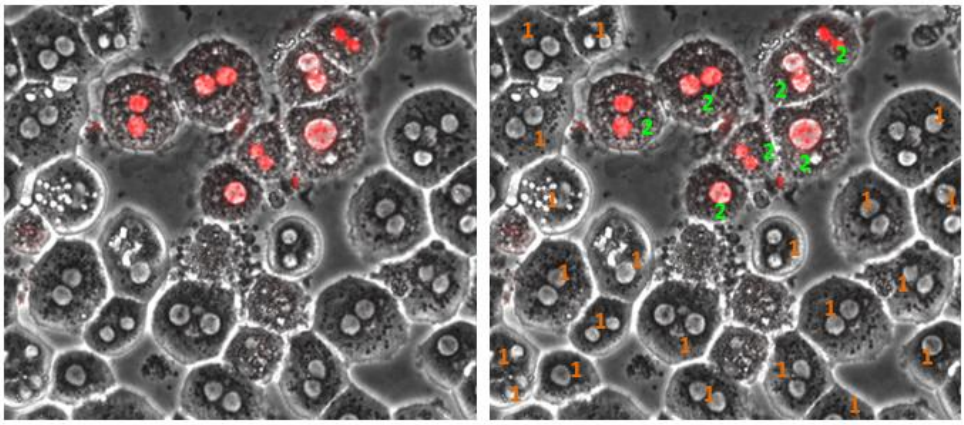

Figure 20: Example for counting dead cells after paracetamol stimulation using collagen sandwich configuration. On the left side, representative image of hepatocytes stained with propidium iodide is shown. Dead cells showed red stained nuclei and can be clearly distinguished from living cells. On the right side, orange marker number 1 shows counted cells as alive and green marker number 2 exhibits counted cells as dead.

The % of dead cells was calculated as shown below:

$$\% \textbf{ of dead cells} = \frac{\textbf{Number of dead cells}}{\textbf{Total amount of cells}} \textbf{ x 100}$$

3 RESULTS

3.1 WISP1 expression increases after induction of liver damage in C57Bl/6N mice

In a previous transcriptomic study of acute liver injury with CCl_4 in C57Bl/6N mice [171], we observed an induction of Wnt-induced secreted protein-1 (WISP1) expression during the first 24h after CCl_4 administration. To validate this result and to obtain a more precise overview of the time course of WISP1 induction, levels of WISP1 RNA were quantified by qRT-PCR. Therefore, livers from 3 independent C57Bl/6N mice treated with 1.6 g/kg CCl_4 intraperitoneally for 8h, 12h, D1, D2 and D4 were used. The results confirmed gene array data showing an increase in WISP1 expression after 8h, which was further increased until D1 and returned back to control levels again at D2 (Figure 21).

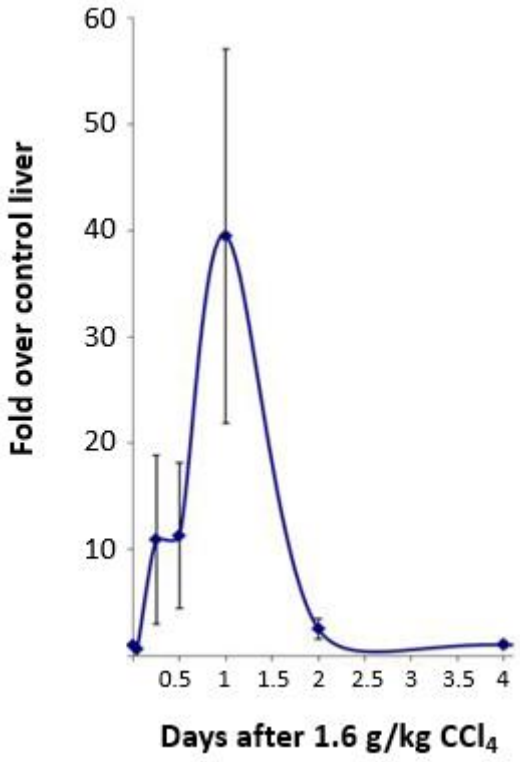

Figure 21: Real time qPCR analysis of WISP1 mRNA in mouse liver tissue at the indicated time points after 1.6 g/kg CCl_4 administration intraperitoneal. The results show an increase of WISP1 expression with a maximum of about 40-fold at D1 after CCl_4 administration. WISP1 RNA turned back to control levels at D2. Data represent mean values and standard deviations of three independent biological replicates per time point.

3.2 WISP1 expression in control (healthy liver tissue) is mainly derived by non-parenchymal cells

The previous qRT-PCR result showed an increase in WISP1 expression after administration of CCl_4 in liver tissue homogenates. To determine the cellular source of WISP1 expression (i.e. hepatocytes or non-parenchymal cells (NPCs)) in a normal liver, C57Bl/6N mice were treated intraperitoneally with oil as the control vehicle (healthy liver tissue). After 24h, the livers were perfused and RNA from freshly isolated hepatocytes and non-parenchymal cells was isolated. WISP1 expression levels were determined in each cell population using healthy liver tissue extracts as the reference. Quantitative RT-PCR analysis revealed low WISP1 expression in primary hepatocytes, whereas WISP1 expression was approximately 20-fold higher in NPCs compared to liver homogenates (Figure 22).

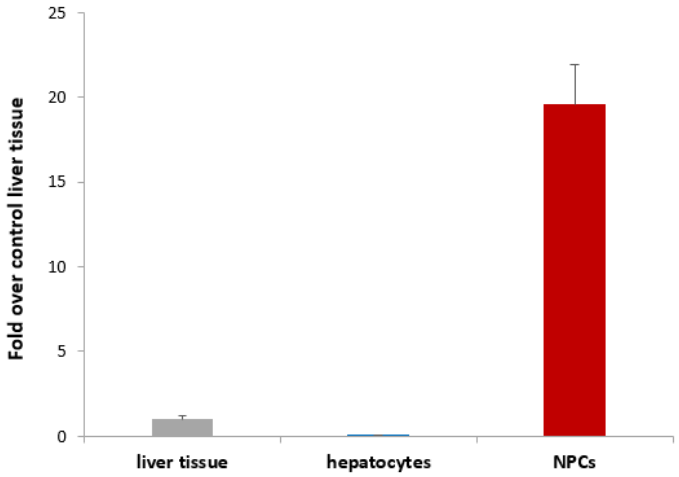

Figure 22: Quantitative RT-PCR of WISP1 expression show highest levels in non-parenchymal cells. WISP1 expression is higher in NPCs (20-fold) compared to hepatocytes (0.05-fold) in healthy livers. Liver homogenates (vehicle control) were used as the reference. Data represent mean of three biological replicates ± S.E.

The results revealed that under control conditions, WISP1 expression is higher in NPCs compared to hepatocytes. However, the absolute contribution to WISP expression is rather low, because NPCs comprise only 20% of the liver mass compared to 80% by the hepatocytes.

3.2.1 WISP1 expression is induced in hepatocytes and NPCs upon CCl_4 administration

To investigate WISP1 expression in hepatocytes and NPCs after administration of CCl_4, C57Bl/6N mice were treated intraperitoneally with either olive oil as control vehicle or 1.6 g/kg CCl_4. After 24h, hepatocytes and non-parenchymal cells were isolated and WISP1 RNA was quantified by qRT-PCR. The corresponding control cell populations were used as

references. The results showed approximately 40-fold induction of WISP1 RNA in hepatocytes compared to a 3-fold induction in non-parenchymal cells (Figure 23).

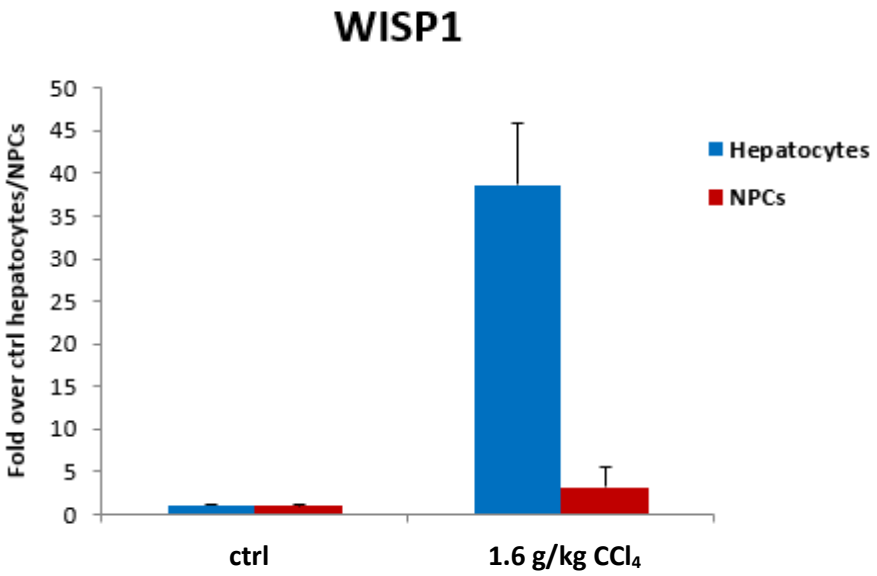

Figure 23: Real time qPCR analysis of WISP1 expression in isolated primary mouse hepatocytes versus non-parenchymal cells. Mice were pretreated with either oilve oil as control vehicle or 1.6 g/kg CCl_4. The results indicate stronger induction of WISP1 RNA in hepatocytes compared to in NPCs. Data represent mean values ± S.E. of three independent biological replicates per time point.

The results indicated an induction of WISP1 in both hepatocytes and NPCs. However, the induction was much stronger in hepatocytes compared to NPCs after administration of 1.6 g/kg CCl_4. This suggests that WISP1 expression is mainly derived from hepatocytes after administration of CCl_4. Moreover, hepatocytes make up the main cell type (about 80%) in the liver and the NPCs compose only 20% of liver mass, which further supports our hypothesis.

3.3 WISP1 expression is induced in human liver diseases

The previous results showed a strong induction of WISP1 in a mouse model of acute liver injury. In a next step, an analysis of WISP1 mRNA was performed in liver biopsies from human donors to establish whether WISP1 expression is also altered in the course of human liver disease. RNA was received from human liver tissue of 132 patients (kindly donated by Prof. Dr. Thomas Weiß, University hospital Regensburg). Quantitative RT-PCR was performed to analyse WISP1 expression. The expression of WISP1 was compared to control (healthy) samples and further clustered into three groups according to the type of liver injury - from fibrosis to hepatocellular carcinoma (HCC). The analysis revealed a significant induction of

WISP1 expression in the group of cirrhosis and HCC in comparison to the control group (Figure 24).

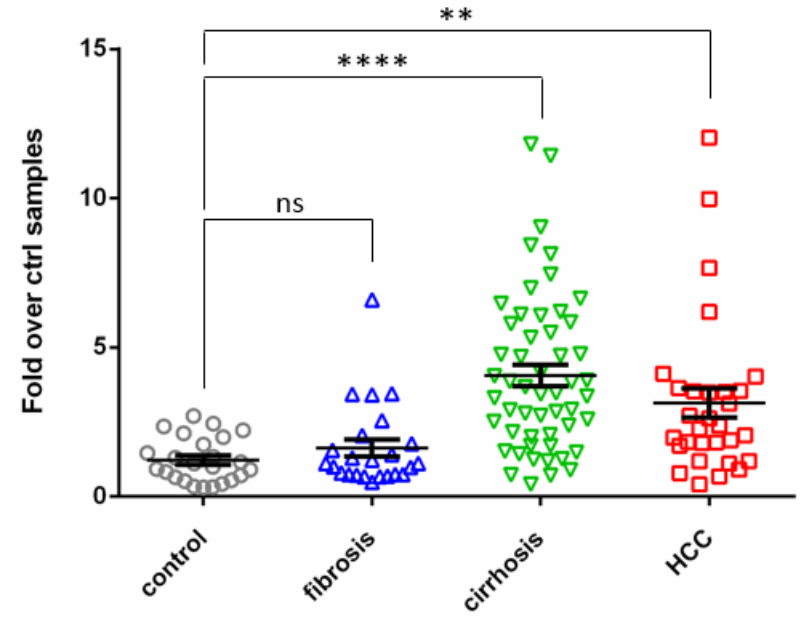

Figure 24: Quantitative RT-PCR of WISP1 expression in human liver disease tissue. Results revealed a significant induction of WISP1 expression in the group of cirrhosis and HCC. The data include 24 samples in the control group; 24 samples in the group of fibrosis; 53 samples in the group of cirrhosis and 30 samples in the group of HCC. Error bars indicate mean ± S.E., ns not significant, ****P<0.0001, **P<0.01 to control group, unpaired t-test.

Taken together, the increased expression in the different disease conditions suggests that WISP1 may be also important in human liver disease.

3.4 Establishment of a WISP1 knockout mouse line

The previous results showed an upregulation of WISP1 during acute liver injury induced by CCl_4 as well as in human liver disease tissue. To investigate whether WISP1 has an influence during acute liver injury, a knockout mouse line was established.

All WISP1 knockout and wild type mice were examined for the correct genotype using Phire Animal Tissue Direct PCR Kit (Thermo Scientific), as described in the material and methods section (Chapter 2.2.1.1). Gel electrophoresis showed clear bands for both PCR products. The first lane shows a PCR product at 459 bp in the mutant PCR, which indicates that this mouse was a homozygous WISP1 knockout (Figure 25 b). A 363 bp PCR product indicative of the wild type mouse is observed in the second lane of the wild type PCR blot. Finally, the third lane showed both PCR products, concluding that this mouse was a heterozygote carrying the wild type allele and the mutant allele, which contains the puromycin cassette and a stop codon to inhibit the transcription of WISP1.

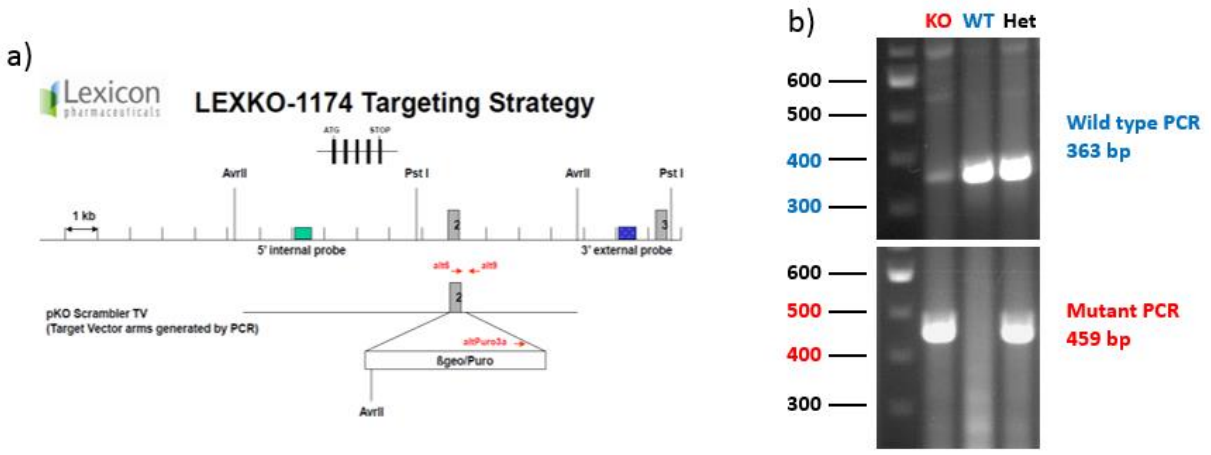

Figure 25: Establishment of WISP1 knockout mouse line a) Generation of WISP1 knockout mice. Exon 2 of WISP1 was replaced by a construct containing a puromycin resistant cassette and a stop codon in its 3` end region resulting in the inhibition of the transcription of WISP1. **b) Genotyping of WISP1 mice.** The first lane corresponds to knockout, second to wild type and third to heterozygous genotypes respectively. The mutant PCR product can be detected at 459 bp and the wild type PCR product at 363 bp. Images are representative for all PCR analyses done.

3.4.1 Validation of WISP1 expression in different organs of mice confirmed successful knockout of WISP1

The next step was to investigate WISP1 expression in various organs in both the wild type and WISP1 knockout mice. For this reason, RNA was isolated from liver, brain, kidney, spleen, heart, lung, and intestine as well as muscle tissue. WISP1 expression was found to be highest in lung tissue (about 12-fold) followed by brain (about 4-fold), spleen (about 3-fold) and intestine (2-fold). WISP1 RNA was comparable in heart (about 1-fold), kidney (about 1.5-fold) and liver (1-fold). Almost no expression was detected in muscles (about 0.08-fold) (Figure 26). All WISP1 knockout organs were undetermined for WISP1 expression, confirming the efficient deletion of WISP1. Taken together, WISP1 was expressed in the wild type mice with different levels in almost all tissues tested.

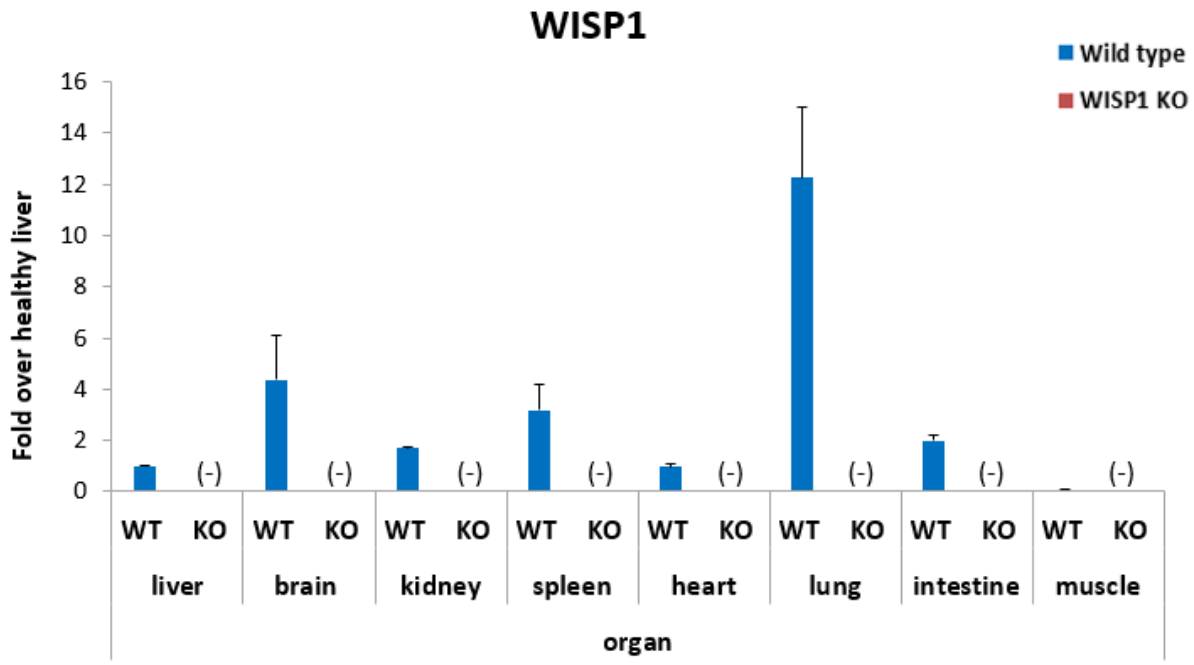

Figure 26: Organ specific quantitative RT-PCR of WISP1 mRNA of untreated wild type mice and WISP1 knockout mice. The highest expression level of WISP1 was found in lung, followed by brain, spleen and intestine. WISP1 expression was comparable in the heart, kidney and liver. Liver tissue was used as a reference for all organs. Data represent mean of three biological replicates ± S.E. (-) No expression was detectable in the WISP1 knockout mice.

The qRT-PCR did not provide any information about the possible zonation and localization of WISP1 expression in the different tissues. Therefore, immunohistochemical staining of WISP1 in different organs was performed (Figure 27). Unfortunately, IHC staining detected comparable signals in WISP1 knockout and wild type mice, revealing unspecific signals in all organs.

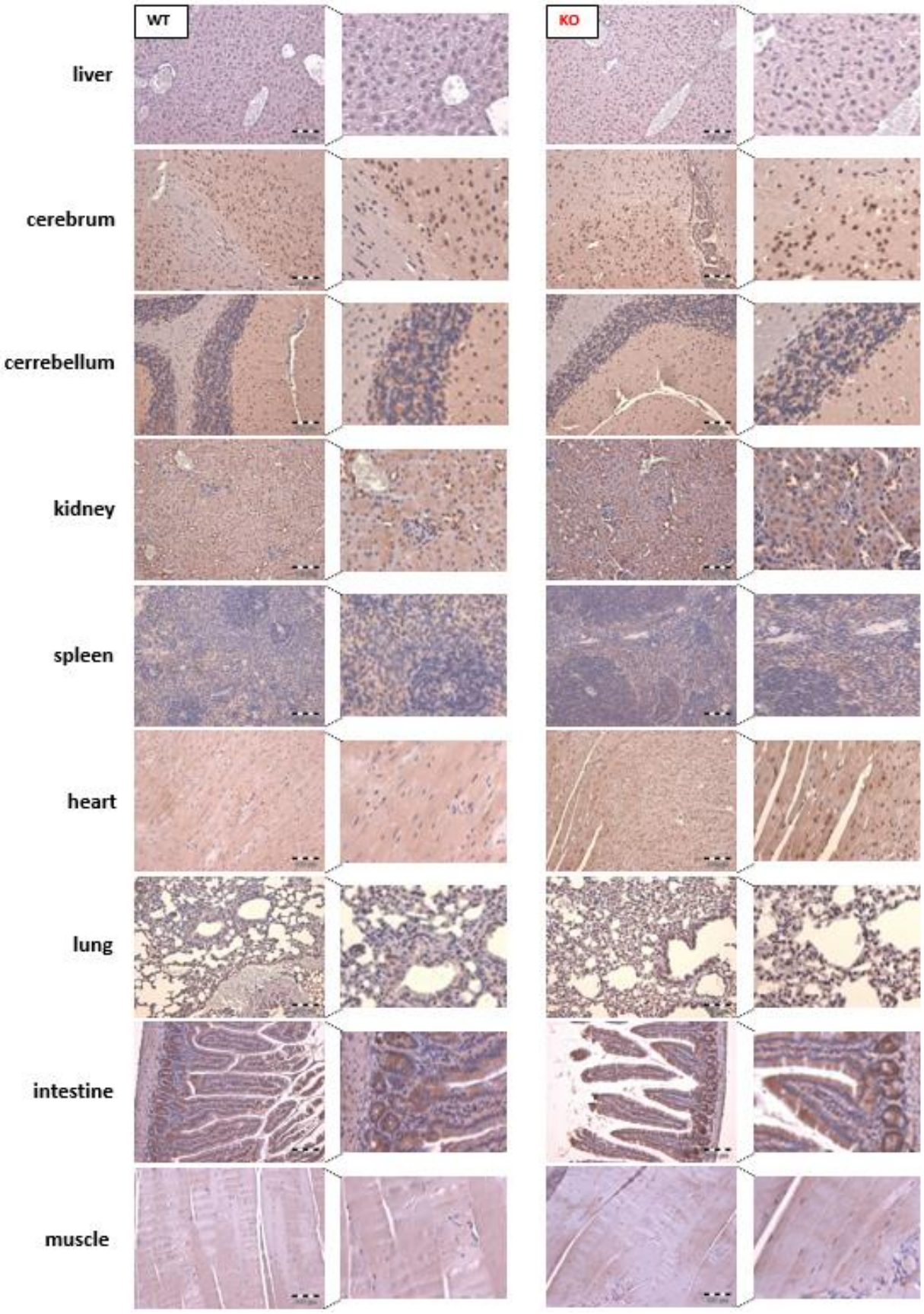

Figure 27: Immunohistochemical staining of WISP1 in various tissues of wild type mice and WISP1 knockout mice. The results show no difference in the wild type mice compared to WISP1 knockout mice, revealing that the staining was not successful. WISP1 knockout mice were used as negative control. Representative images of three mice per organ, scale bars represent 100 µm.

In conclusion, qRT-PCR detected different levels of WISP1 RNA in various organs of wild type mice. However, localization of WISP1 was not possible to determine, because IHC staining was not successful, due to antibody unspecificity. Nevertheless, the results revealed the successful establishment of WISP1 knockout mouse model which could be used for further investigation of WISP1 phenotype. For example, *in vivo* studies to examine the potential role of WISP1 during acute liver injury by administration of CCl_4 or APAP in a time- and concentration-dependent manner. Moreover, the WISP1 knockout mice also allow the investigation of WISP1 in the context of liver regeneration after administration of hepatotoxic compounds. Furthermore, *in vitro* experiments using isolated hepatocytes and NPCs could be used to study the influence of WISP1 in liver cell subpopulations.

3.5 WISP1 knockout mice exhibit higher susceptibility to CCl_4-induced liver damage

The previous validation of WISP1 deletion in knockout mice provided a good precondition for assessing the potential role of WISP1 in acute liver injury.

First, a titration of CCl_4 was performed to investigate the potential effects of WISP1 deletion in knockout mice compared to wild type mice during acute liver damage in a dose-dependent manner. Therefore, the mice were challenged with different concentrations of CCl_4 (1.6 g/kg, 920 mg/kg, 460 mg/kg, 132.4 mg/kg, 0.076 mg/kg) or control vehicle (olive oil). Blood and liver tissue samples were collected after 24h. For each time point, 3 mice were used. The genotype was confirmed by Phire Animal Tissue Direct PCR Kit as described in the method section.

CCl_4 intoxication caused macroscopically-visible hepatic alterations in forms of white spots in all concentrations in both mice. However, more extensive white puncta were observed in the WISP1 knockout mice afteronly mild concentrations of CCl_4 compared to wild type mice (Figure 28).

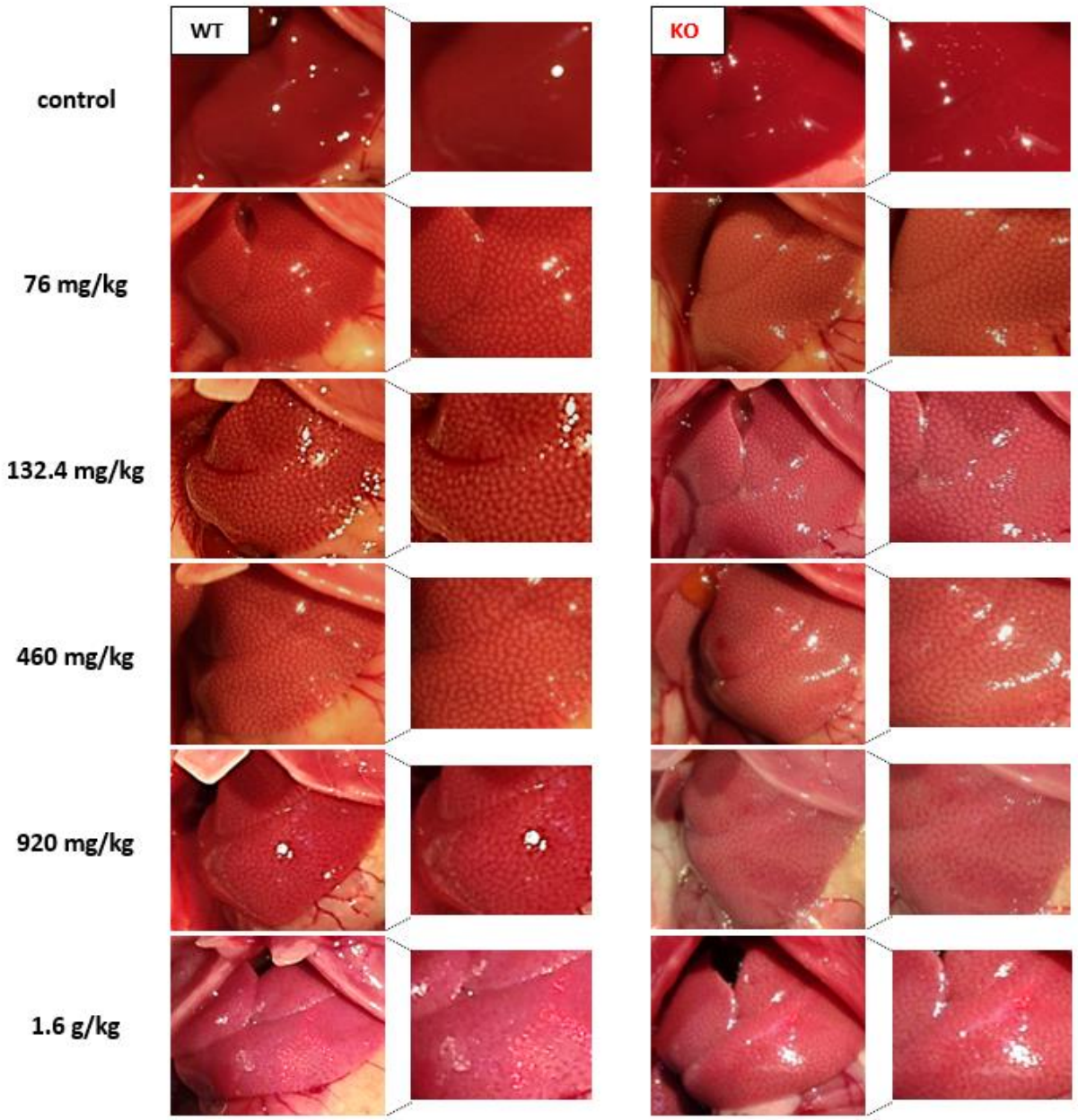

Figure 28: Concentration-dependent analysis of gross appearance of WISP1 knockout and wild type mouse liver after administration of CCl_4 for 24h. Both control livers show a smooth appearance and intense red color. At lower concentrations of CCl_4 (76 mg/kg up to 460 mg/kg), an enhanced characteristic white spotted pattern was observed in WISP1 knockout mice compared to wild type mice, indicating a more advanced stage of liver injury. Representative images of three mice per concentration.

In order to assess the microscopic hepatic lesions induced by CCl_4, paraffin embedded liver sections were stained with hematoxylin and eosin. WISP1 knockout and wild type mice showed a concentration-dependent increase in the dead cell areas around the central veins up to a concentration of 460 mg/kg. However, at lower concentrations of CCl_4 (76 mg/kg, 132.4 mg/kg, 460 mg/kg), the WISP1 knockout mice displayed an enlarged dead cell area compared to wild type mice (Figure 29). Moreover, qualitative differences were observed in the dead cell area of wild type mice treated with 920 mg/kg CCl_4. The yellow

arrow indicates still visible nuclei of hepatocytes in the dead cell area, which were not visible in the dead cell areas of WISP1 knockout mice.

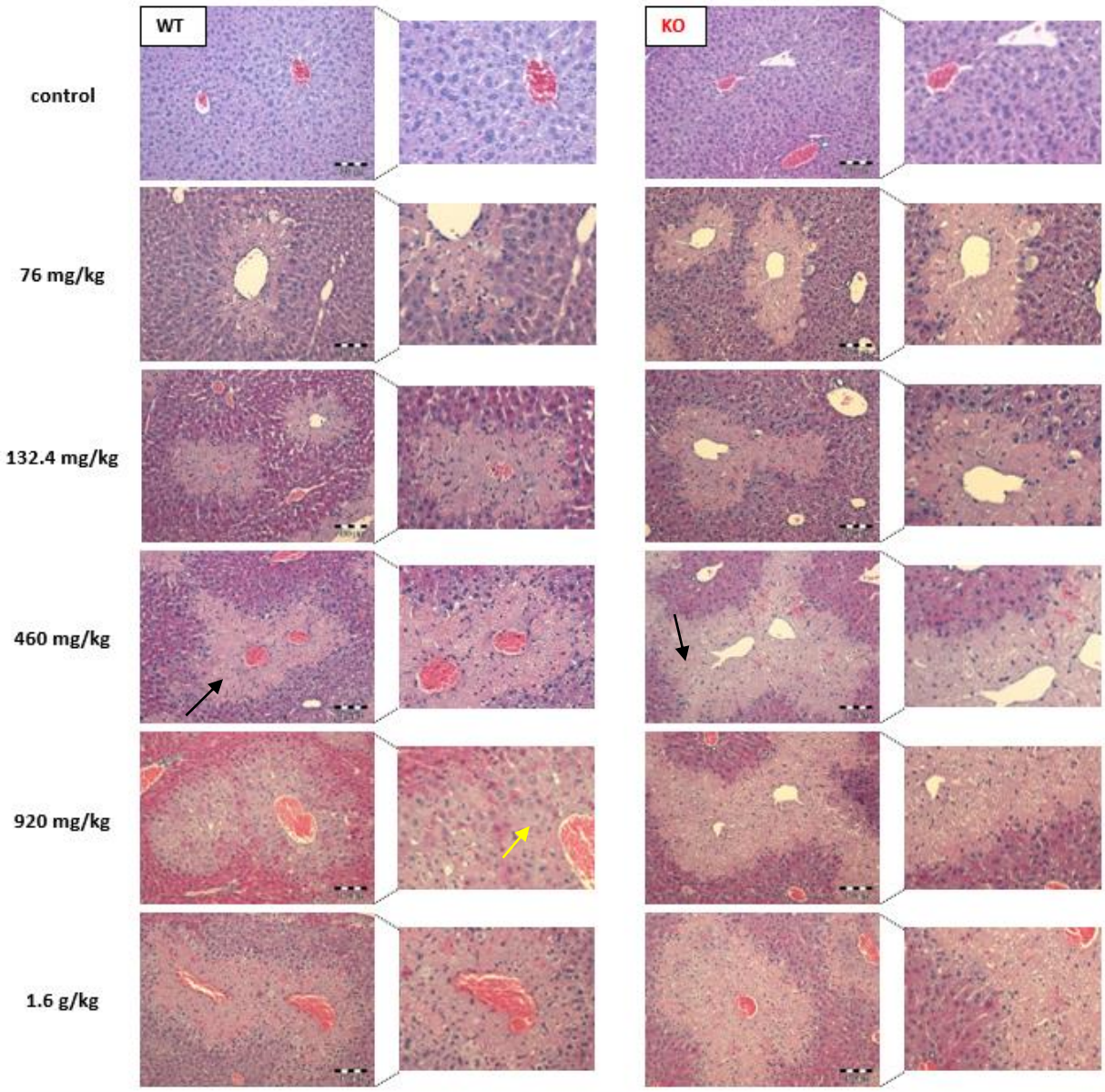

Figure 29: H&E staining of WISP1 knockout and wild type mouse liver after administration of various concentrations of CCl_4 for 24h. The area of centrilobular liver damage (black arrows) was identified in a concentration-dependent manner in WISP1 knockout and wild type mice. Enlarged dead cell areas were observed at lower concentrations in the WISP1 knockout mice compared to wild type mice. At a concentration of 920 mg/kg of CCl_4, hepatocyte nuclei were still visible in the wild type mice (yellow arrow), whereas WISP1 knockout mice displayed a clear dead cell area. Representative images of three mice per condition, scale bars represent 100 µm.

In order to obtain quantitative measurements of liver injury in the WISP1 knockout and wild type mice, the dead cell areas were quantified using image analysis software. The quantification indicated a concentration-dependent increase in the dead cell areas in both

WISP1 knockout and wild type mice (Figure 30). However, the WISP1 knockout mice showed a significant increase in the dead cell areas at lower concentrations of CCl_4 (76 mg/kg up to 460 mg/kg) compared to wild type mice. Moreover, WISP1 knockout mice showed a maximal dead cell area of about 50 % already at a dose of 460 mg/kg CCl_4; whereas, the wild type mice displayed a dead cell of about 25 %.

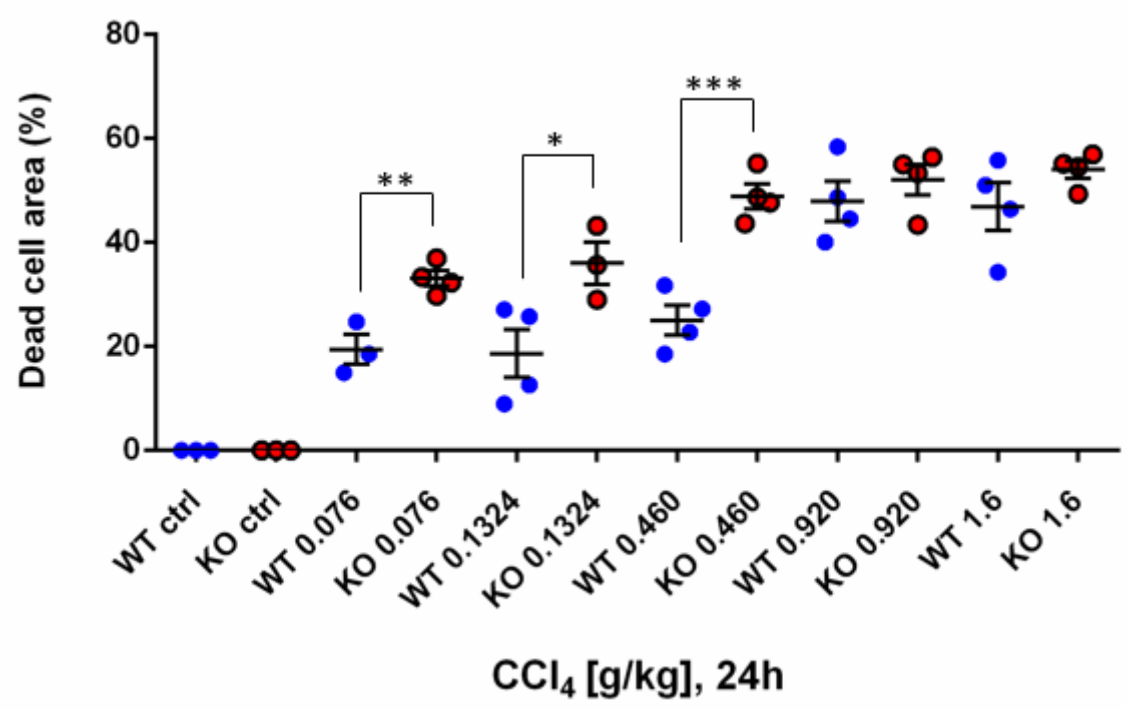

Figure 30: Concentration-dependent quantification of the dead cell areas of WISP1 knockout and wild type mice after administration of CCl_4 for 24h. The extent of the dead cell areas was quantified as described in the method section. The quantification revealed a concentration-dependent increase in the dead cell areas in wild type and WISP1 knockout mice. At lower concentrations of CCl_4 enlarged dead cell areas were observed in the WISP1 knockout mice compared to wild type mice. The data represent at least three mice per concentration. Error bars indicate mean values ± S.E. ***P<0.001 to wild type condition, **P<0.01 to wild type condition, *P<0.05 to wild type condition, unpaired t-test.

The extent of liver damage was also assessed by measuring the plasma concentrations of hepatic damage marker alanine transaminase (ALT). Consistent with the quantification of the dead cell areas, the liver enzymes were elevated with increased CCl_4 concentrations in both wild type and WISP1 knockout mice. Importantly, this analysis was more sensitive than the quantification of dead cell areas, showing higher ALT values in WISP1 knockout mice at all concentrations (Figure 31). A significant difference compared to the wild type mice was observed at 920 mg/kg of CCl_4.

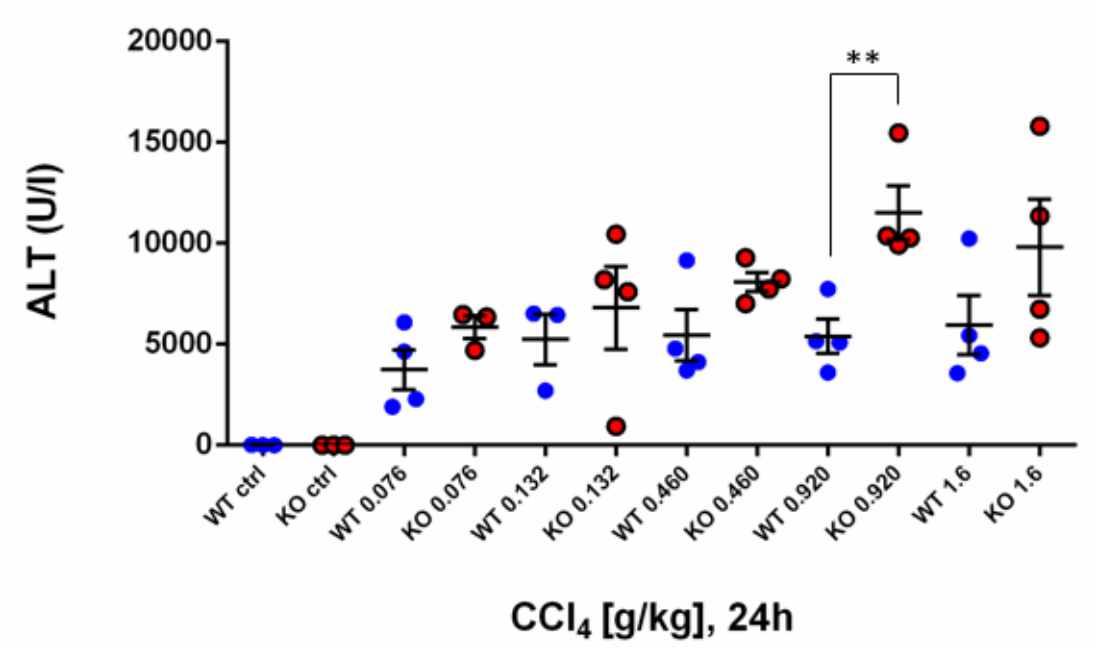

Figure 31: Plasma transaminase activity after different doses of CCl_4 in WISP1 knockout and wild type mice. Increased ALT activity was observed for the wild type and WISP1 knockout mice in a concentration-dependent manner. However, the WISP1 knockout mice showed higher ALT values compared to wild type mice at all concentrations. Data obtained from at least three mice per condition. Error bars indicate mean values ± S.E. **P<0.01 to wild type condition, unpaired t-test.

In conclusion, the histological features of liver injury (i.e. dead cell areas) and the increased activity of liver enzymes in wild type and WISP1 knockout mice indicated that a robust and reproducible experimental setup was achieved, similar to what has been reported in previous studies [14]. Moreover, the titration of CCl_4 was a useful tool to deliver a first robust and reproducible insight into the effect of the absence WISP1 upon liver injury. It was beneficial to establish an optimal concentration for further time-dependent and kinetic analysis of WISP1 knockout mice. Interestingly, the WISP1 knockout mice exhibited an enhanced liver damage at all concentrations of CCl_4 compared to wild type mice. This led to the hypothesis that WISP1 is a protective mediator during acute liver injury in mice.

3.6 Time-resolved challenge using CCl_4 revealed different kinetics of liver damage in WISP1 knockout mice

The previous concentration-dependent analysis of WISP1 knockout and wild type mice challenged with CCl_4 suggested that WISP1 may play a protective role in the acute liver injury model. Titration of CCl_4 revealed that a dose of 460 mg/kg CCl_4 leads to the most robust phenotype with the highest quantitative differences between WISP1 knockout mice and wild type mice. Therefore, to further investigate kinetic and molecular events leading to an advanced liver damage, WISP1 knockout mice and wild type mice were treated with 460mg/kg CCl_4 for 30min, 2h, 8h, 12h, 18h and D1. For the vehicle control, mice were treated with olive oil for 24h.

WISP1 knockout and wild type livers both showed the typical intense red coloration in the control situation, which did not change until 8h after CCl_4 treatment (Figure 32). After 12h of 460 mg/kg CCl_4 WISP1 knockout livers exhibited small white spots, which became more prominent after 18h and 24h of treatment. In contrast, the wild type mice displayed initial white spots after 18h of treatment, which became more prominent after 24h. However, WISP1 knockout mice showed more extensive white spots at 18h and D1 compared to wild type mice, indicating a more advanced stage of liver damage.

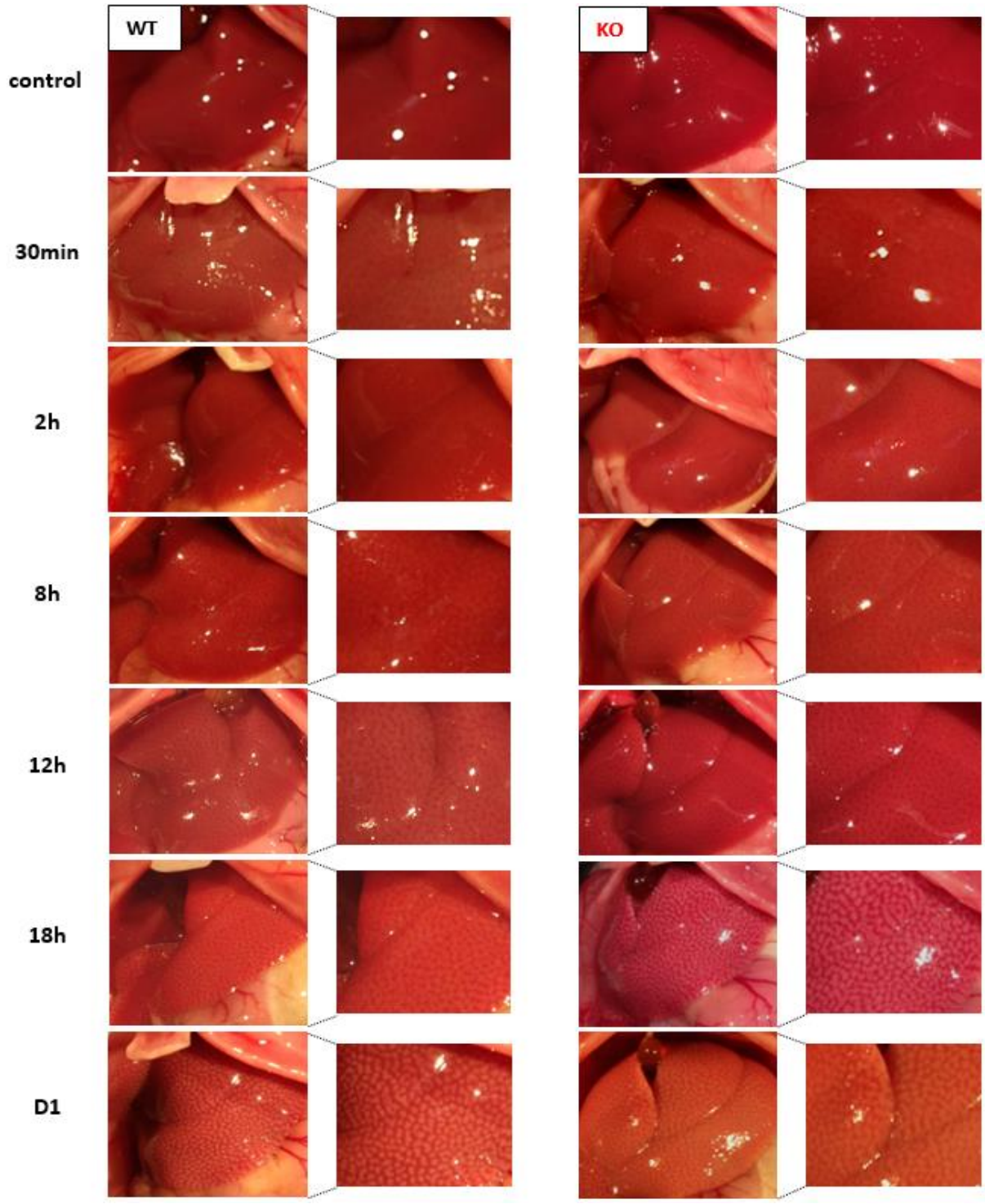

Figure 32: Time-dependent analysis of gross pathology appearance of WISP1 knockout and wild type mouse liver after administration of 460 mg/kg CCl_4 for the indicated time points. Both wild type and WISP1 knockout control livers showed a smooth appearance and an intense red coloration. An enhanced characteristic white spotted pattern was observed in the WISP1 knockout mice compared to wild type mice, indicating a more severe liver injury already at 18h after administration of CCl_4. Representative images of three mice per concentration.

In order to microscopically assess the pericentral necrotic lesions, H&E staining was performed from paraffin embedded liver tissue. According to gross pathology images, no

necrotic lesions were observed until 8h after CCl_4 treatment (Figure 33). Initial necrotic lesions were observed at 18h in the wild type mice and already at 12h in the WISP1 knockout mice after treatment (black arrows). Clear dead cell areas, indicating the peak of liver damage, were detected at D1 in the wild type mice and already at 18h in the WISP1 knockout mice. These observations suggested a time shift in the induction of liver damage in WISP1 knockout mice that is approximately 6h earlier compared to wild type mice. According to the previous concentration series, WISP1 knockout mice displayed an enlarged dead cell area, which is almost doubled in size at D1. Interestingly at 18h, the size of the affected area around the central vein is comparable in both wild type and WISP1 knockout mice.

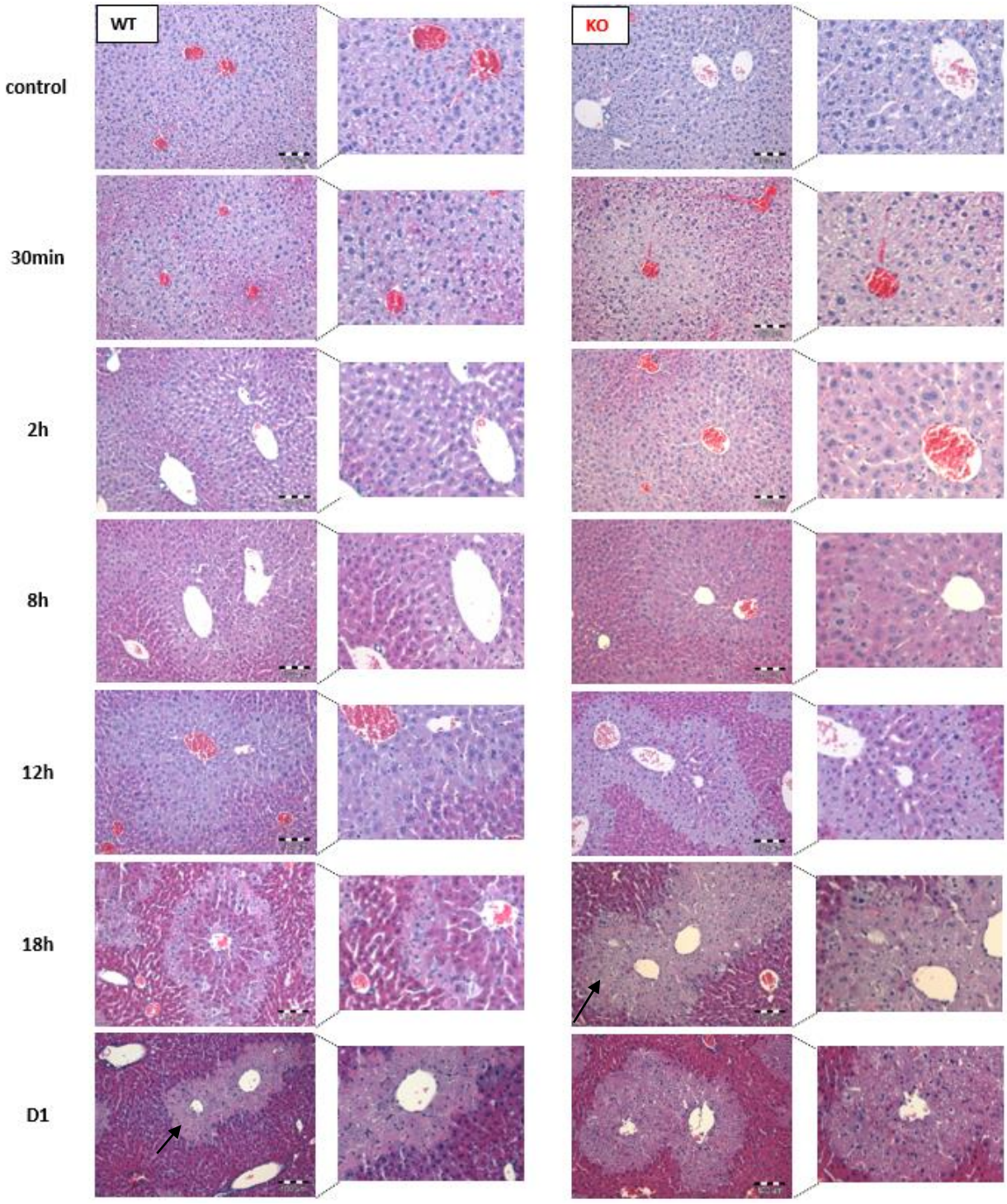

Figure 33: Time-dependent H&E staining of WISP1 knockout and wild type mouse livers after administration of 460 mg/kg CCl_4 for the indicated time points. Initial necrotic lesions were observed around the central veins (black arrows) in the wild type mice after 18h, leading to a full dead cell area after 24h of treatment. WISP1 knockout mice showed initial affected areas already at 12h, followed by a full necrotic area at 18h after administration of CCl_4. Representative images of three mice per condition, scale bars represent 100 µm.

This time-dependent analysis not only supports the previous results of the concentration-dependent analysis, but also revealed differences in the kinetics of developing acute liver damage after CCl_4 in WISP1 knockout mice compared to their wild type

littermates. Moreover, hepatotoxicity also appears to occur earlier in the WISP1 knockout mice.

3.6.1 Molecular markers of cell death revealed earlier stage of liver damage in WISP1 knockout mice

As shown in time-dependent analysis after CCl_4 administration, WISP1 knockout exhibited an already a clear necrotic area at 18h; whereas, wild type littermates showed dead cells only at the border of pericentral areas (Figure 33). In order to clarify the advanced stage of liver damage in WISP1 knockout mice, TUNEL assay and HMGB1 staining were performed. HMGB1 is a nuclear ubiquitously expressed protein in eukaryotes. Upon necrosis, it is passively released by cells and functions as a damage-associated molecular pattern (DAMP) [172, 173]. The terminal transferase uridyl nick end labelling (TUNEL) assay is used to detect DNA fragmentation, which is an indicator of apoptosis in cells. HMGB1 staining displayed its translocation to the cytoplasm at 18h in wild type mice, illustrating the time at which the hepatocytes started to undergo cell death (Figure 34). At the same time point, WISP1 knockout mice exhibited no positive staining of nuclei or cytoplasm, indicating that all hepatocytes in the centrilobular region were already dead. TUNEL assay revealed few cells that were positively stained at the border of the centrilobular regions at 18h in wild type mice (Figure 35). Conversely, all hepatocytes in the WISP1 knockout mice were stained positive in the centrilobular region at the same time point.

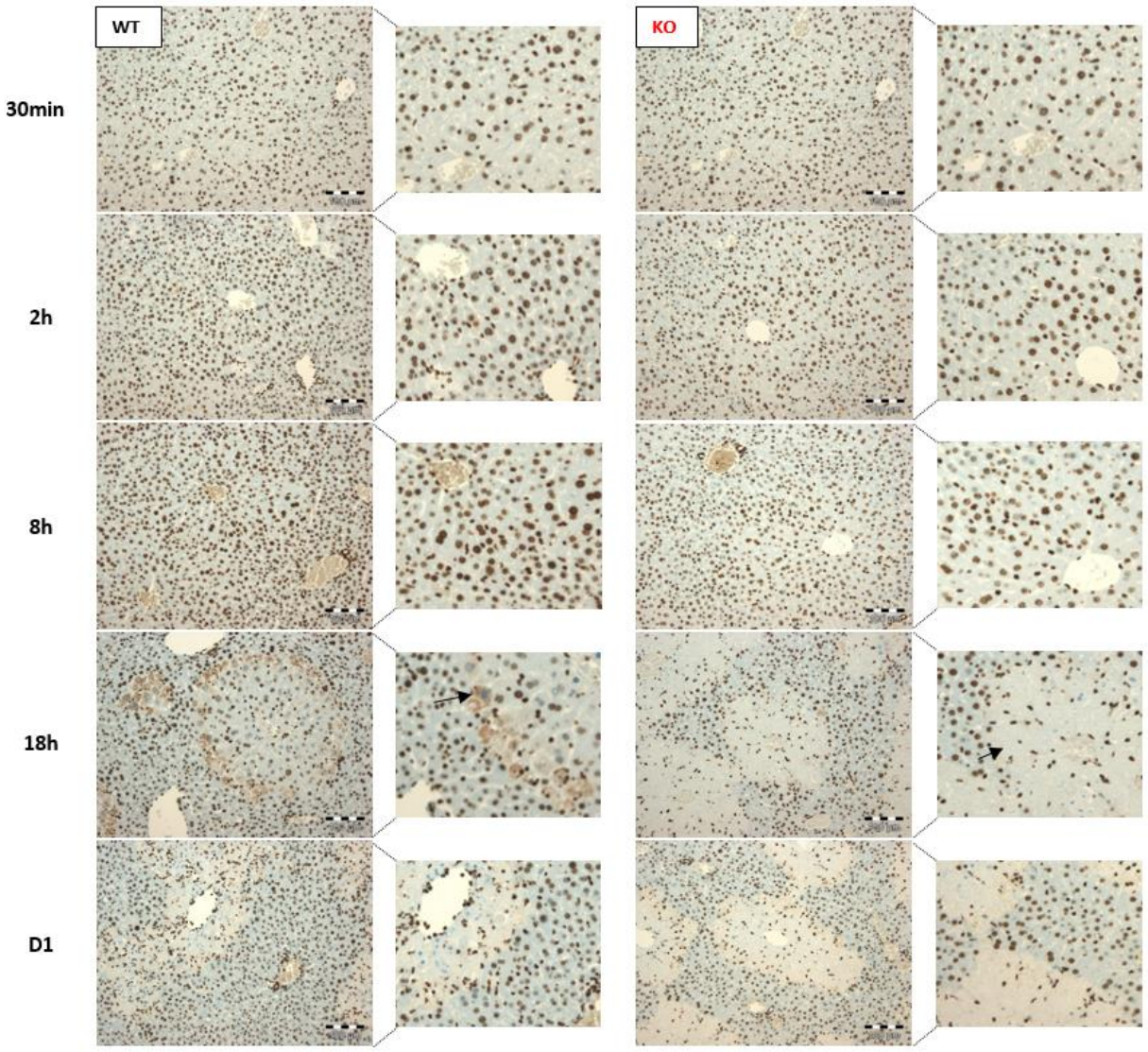

Figure 34: HMGB1 staining in WISP1 knockout and wild type mice after administration of 460 mg/kg CCl_4 for the indicated time points. At 30min, 2h and 8h all nuclei were stained positive, thus indicating no translocation of HMGB1 to the cytoplasm. Wild type mice revealed positive stained cytoplasm at the borders of the centrilobular regions after 18h (black arrow); whereas, WISP1 knockout mice showed no positively stained hepatocyte nuclei or cytoplasm. Representative images of three mice per condition, scale bars represent 100 µm.

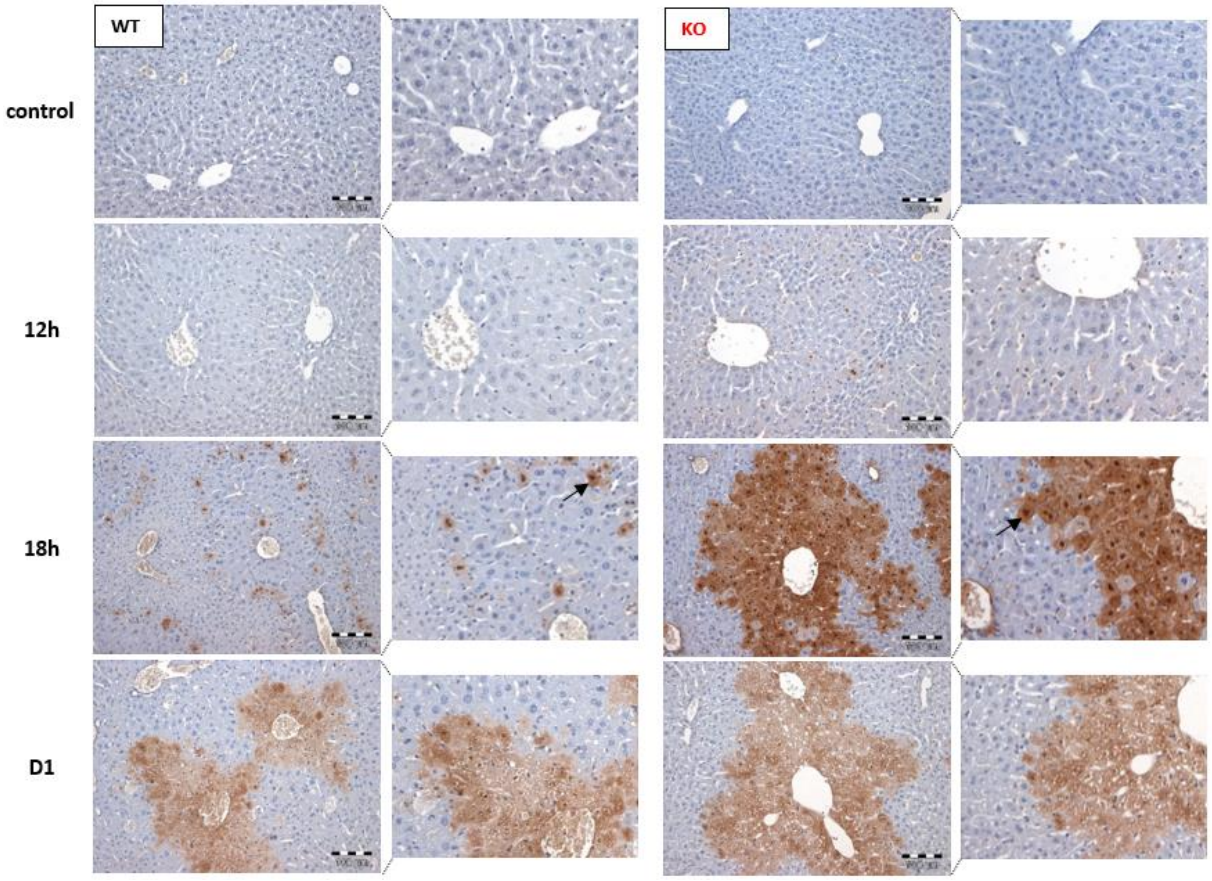

Figure 35: Terminal transferase uridyl nick end labelling (TUNEL) assay in WISP1 knockout and wild type mice after administration of 460 mg/kg CCl_4 for the indicated time points. TUNEL positive staining (brown nuclei) was observed in the wild type mice at the border of centrilobular regions at 18h (black arrows). First single positive-stained hepatocytes were observed in the WISP1 knockout mice after 12h, followed by a completely positive-stained area at 18h. Representative images of three mice per condition, scale bars represent 100 µm.

These data indicate an advanced stage of liver damage in the WISP1 knockout mice compared to wild type mice already at 18h after CCl_4 administration. Both approaches showed full dead cell areas around the central veins in the WISP1 knockout mice at 18h after CCl_4 administration; whereas, the wild type mice still displayed healthy hepatocytes within the centrilobular area. In conclusion, this approach not only showed an enhanced damage of the liver in WISP1 knockout mice, but also that the progress of liver damage occurred earlier in mice lacking WISP1.

3.7 WISP1 knockout mice exhibit higher susceptibility to paracetamol-induced liver damage

The initial results using CCl_4 as a model compound to induce acute liver damage suggested a higher susceptibility of WISP1 knockout mice compared to wild type mice. In order to clarify if this phenotype is unique for CCl_4, paracetamol was used as another hepatotoxic model. Therefore, wild type and WISP1 knockout mice were treated using a dose of 300 mg/kg APAP for 30min, 1h, 2h, 4h, 8h, 12h and D1. PBS was used as the vehicle

control. Wild type and WISP1 knockout mice exhibited the typical intense red color in the control condition of both the wild type and knockout mice, which started to become pale 1h and 2h after administration of APAP (Figure 36). Severe hemorrhage and characteristic white spots were visible in wild type and WISP1 knockout mice after 4h and 8h. An attenuated white spotted pattern was detected at 12h and D1 in the wild type mice compared to WISP1 knockout mice. At the same time points, hemorrhage was still visible in the WISP1 knockout mice.

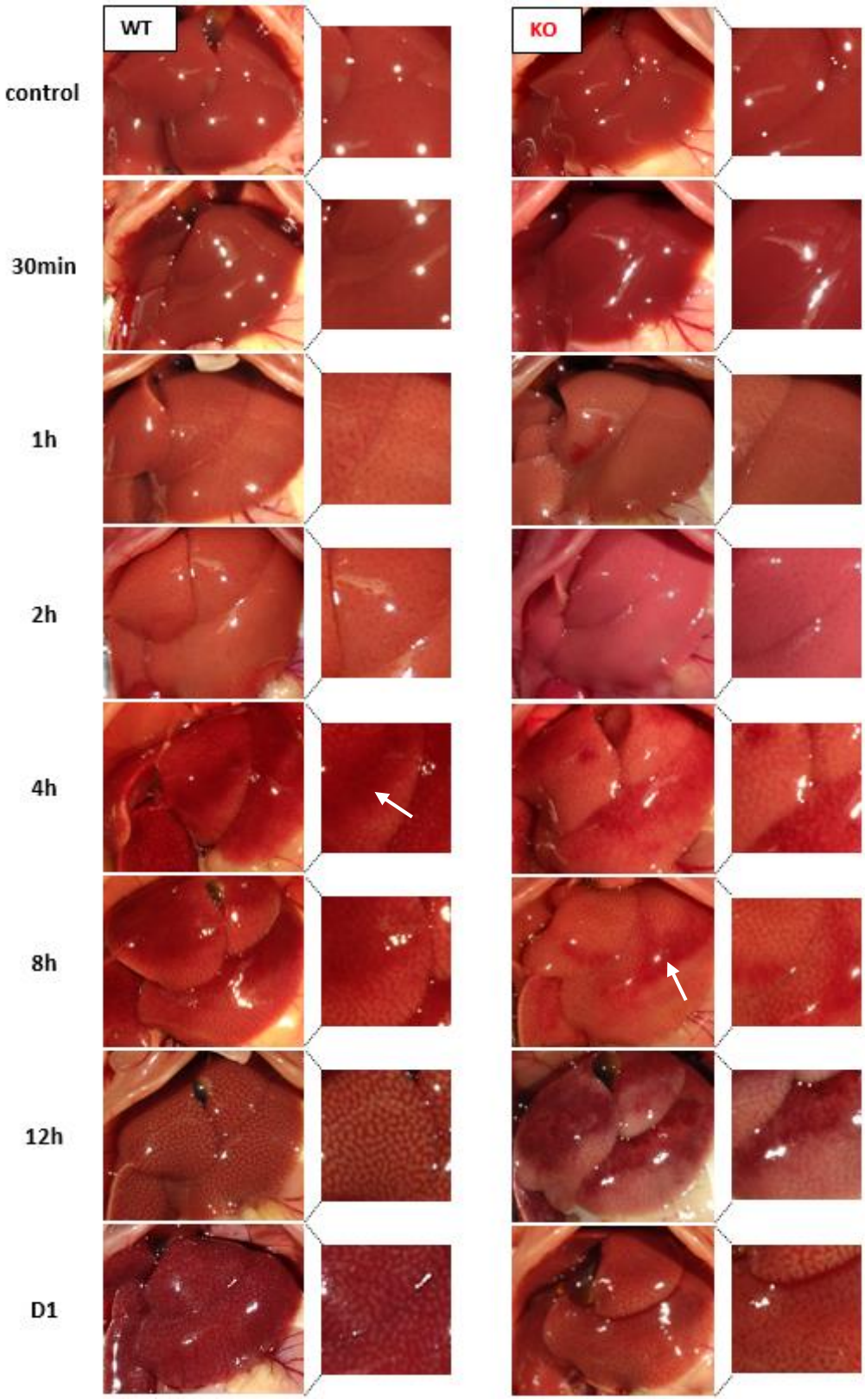

Figure 36: Time-dependent analysis of gross pathology appearance of WISP1 knockout and wild type mouse livers after administration of 300 mg/kg APAP for the indicated time points. Both wild type and WISP1 knockout control livers show a smooth appearance and intense red coloration. Characteristic white spotted pattern was observed in the wild type and WISP1 knockout mice starting 1h after administration of APAP. After 4h and 8h, severe hemorrhage was observed in both mice (white arrows). After 12h and at D1, characteristic white spotted pattern is attenuated in the wild type mice compared to the WISP1 knockout mice. Moreover, severe hemorrhage was detected only in the WISP1 knockout mice at later time points. Representative images of at least three mice per time point.

To assess the pericentral dead cell area in wild type and WISP1 knockout mice after APAP administration, H&E staining was performed using paraffin embedded liver tissue (Figure 37). Consistent with gross pathology images, the first necrotic lesions were observed after 4h in wild type and WISP1 knockout mice. However, the area necrotic lesions in the WISP1 knockout mice were slightly enhanced compared to the wild type mice up to D1. The wild type mice exhibited severe hemorrhage at 4h and 8h after administration of APAP.

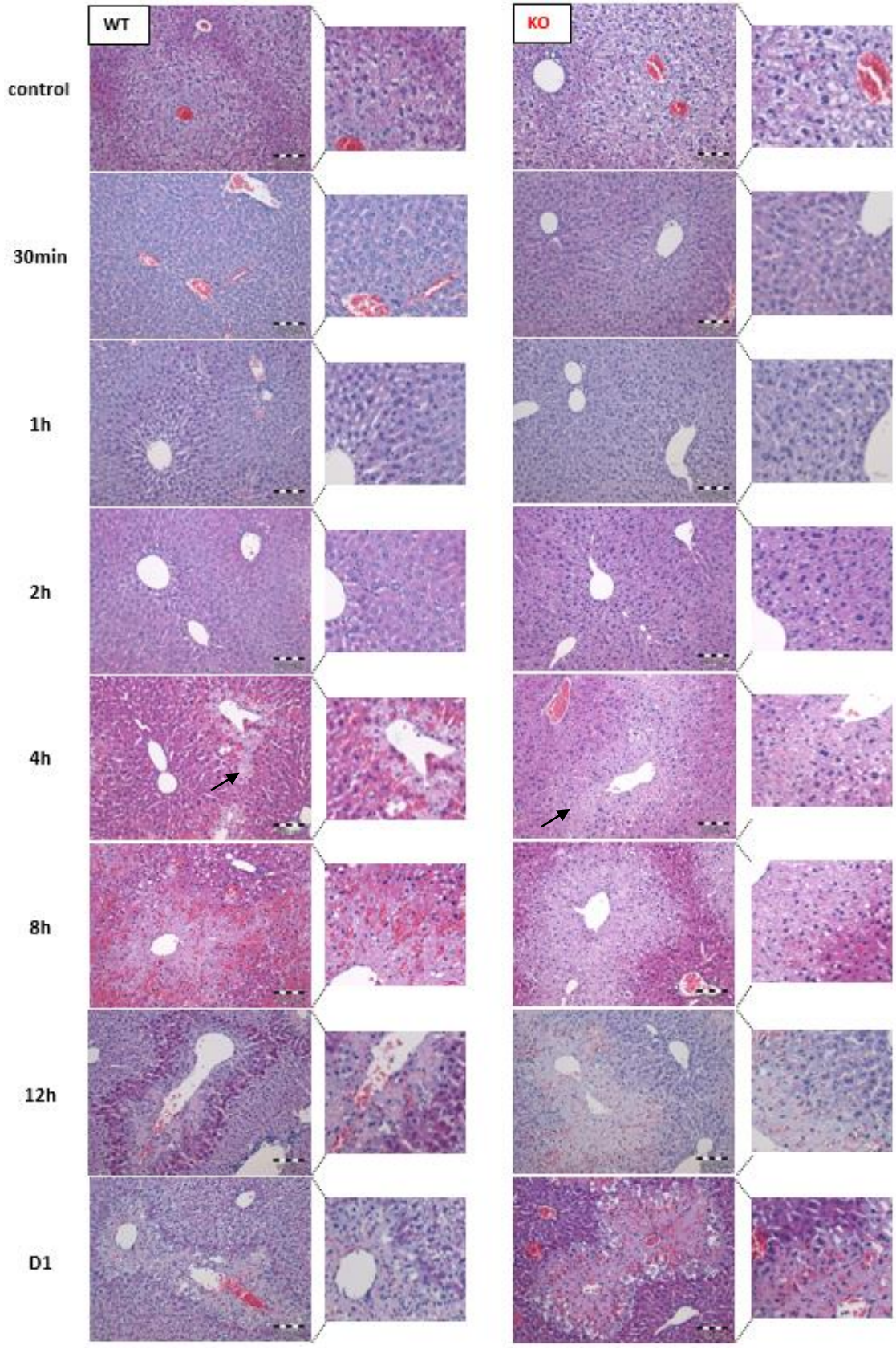

Figure 37: Time-dependent H&E staining of WISP1 knockout and wild type livers after administration of 300 mg/kg APAP for the indicated time points. Initial necrotic lesions were detected in the wild type mice after 4h of APAP administration (black arrows). Slightly enhanced necrotic lesions were observed in the WISP1 knockout mice at 4h until D1 compared to the wild type mice. However, the wild type mice displayed severe hemorrhage at 4h and 8h after intoxication. Representative images of three mice per time point, scale bars represent 100 µm.

By measuring alanine transaminase activity (ALT) in the plasma samples of wild type and WISP1 knockout mice, the extent of liver damage was assessed quantitatively. Elevated liver enzymes were detected starting at 4h after administration of APAP in wild type and WISP1 knockout mice (Figure 38). However, high variances between the biological replicates were observed in the wild type and WISP1 knockout mice at 8h, which made it challenging to determine differences between both mice. After 12h and D1, WISP1 knockout mice exhibited significantly enhanced liver enzymes compared to wild type mice.

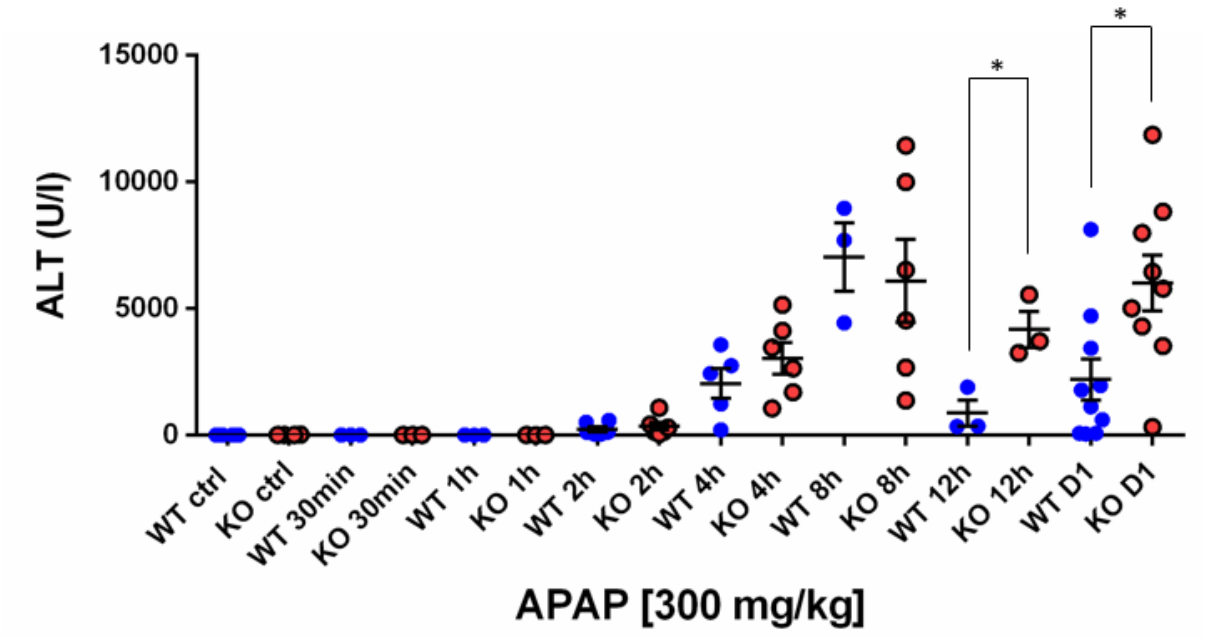

Figure 38: Time-dependent analysis of plasma transaminase activity after 300 mg/kg APAP in WISP1 knockout and wild type mice for the indicated time points. Increased liver enzymes were observed in the wild type and WISP1 knockout mice starting at 4h after APAP administration. However, significantly enhanced ALT activity was detected at 12h and D1 in the WISP1 knockout mice. Data obtained from at least three mice per condition. Error bars indicate mean values ± S.E. *P<0.05 to wild type condition, unpaired t-test.

3.8 WISP1 expression is induced after administration of CCl_4 as well as after paracetamol in wild type mice

Previous results from quantitative RT-PCR (Chapter 3.1) revealed an induction of WISP1 expression in C57Bl/6N after CCl_4 administration. However, wild type and WISP1 knockout mice have a different genetic background (129S5/SvEvBrd * C57BL/6J, EMMA mouse repository EM:02344) compared to the mice used in previous experiments (C57Bl/6N). Therefore, in order to determine whether CCl_4 or APAP treatment of wild type mice would also lead to an increase in WISP1 expression, RNA was isolated from CCl_4 and APAP treated wild type and WISP1 knockout mice and transcribed into cDNA to measure WISP1 RNA. WISP1 expression increased after mild dose of CCl_4 (460 mg/kg) at 8h, with the maximal induction of about 80-fold observed at 12h. On D1, the levels returned to the control levels in wild type mice (Figure 39). After administration of 300 mg/kg APAP, the

expression of WISP1 first decreased until 1h and increased at 8h after treatment with a maximal induction of about 2.5-fold at 12h. On D1, WISP1 levels decreased again to half of control levels. WISP1 expression was undetectable in the WISP1 knockout mice at all time points, confirming the successful deletion of WISP1.

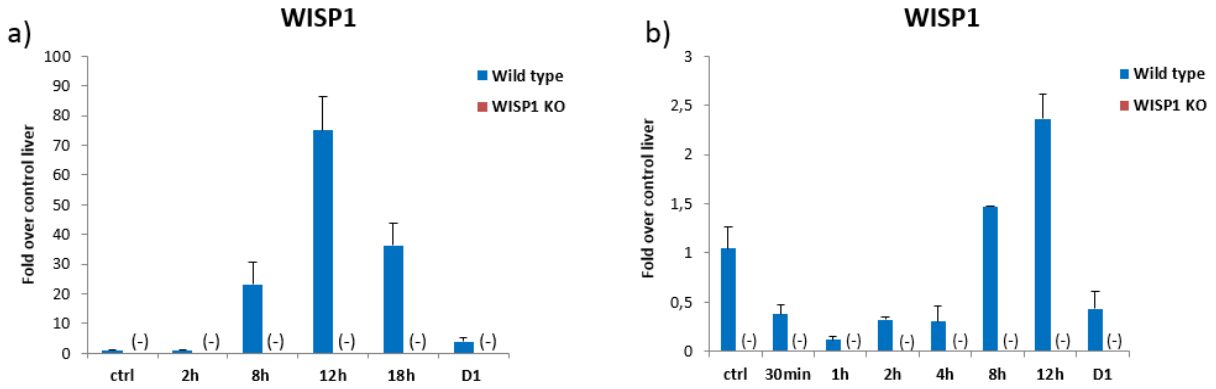

Figure 39: Time-dependent quantitative RT-PCR of WISP1 expression in wild type and WISP1 knockout mice after 460 mg/kg CCl_4 and 300 mg/kg APAP for the indicated time points. WISP1 expression increased upon CCl_4 administration with the maximal inductuion of about 80-fold at 12h. WISP1 RNA turned back to control levels at D1. After administration of APAP, WISP1 RNA decreased until 1h and further increased with the maximal induction of about 2-fold at 12h. Data represent mean of at least four biological replicates ± S.E. (-) No expression was detectable in the WISP1 knockout mice.

The results confirmed gene array data from the Bl6N mice and qRT-PCR of WISP1 expression showing an induction after CCl_4 administration (Figure 21). However, there was a time shift in the maximal induction of WISP1 expression after mild doses of CCl_4 in the wild type mice. Interestingly, a decrease in RNA levels was observed at early time points after APAP administration followed by an increase in WISP1 expression upon the development of liver damage. However, the induction after APAP administration was much lower compared to the induction after administration of CCl_4.

The next step was to clarify if WISP1 protein levels were also altered after the induction of liver damage. Therefore, plasma samples and liver tissue from 3 mice per time point were analyzed using Quantikine® ELISA Mouse/Rat WISP-1/CCN4 immunoassay. High basal levels of WISP1 protein were detected in the plasma samples, including an increase at 2h and D1 after CCl_4 (Figure 40). However, the increase in plasma concentrations was not as high as the increase in RNA levels; and, the peak in WISP1 expression (12h) did not match the peaks in plasma levels. In contrast, liver tissue samples had low levels of WISP1, with increased protein levels detectable at both early time points (30min, 2h) and later time points (18h, D1).

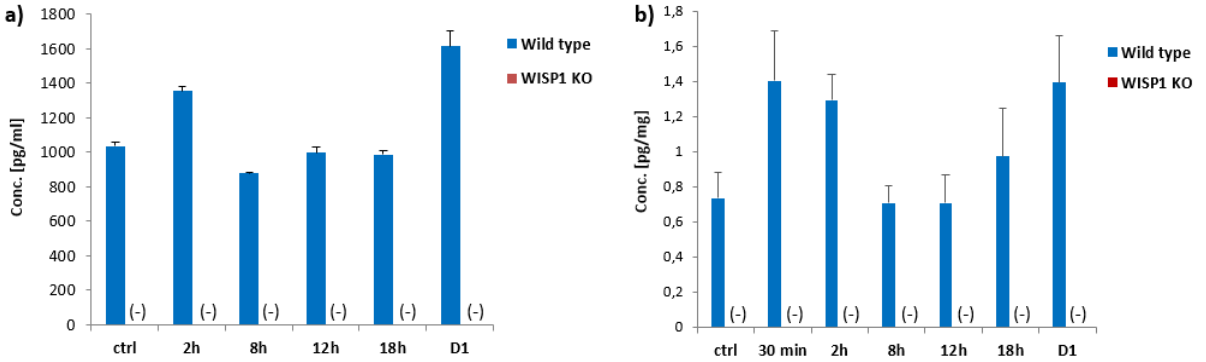

Figure 40: Time-dependent analysis of WISP1 protein concentrations in plasma a) and liver tissue b) of wild type and WISP1 knockout mice after administration of 460 mg/kg CCl_4. ELISA revealed high concentrations of WISP1 protein (about 1000 pg/ml) in the plasma which increased after 2h and D1 to about 1400 pg/ml. The concentrations in liver tissue samples increased at early time points after CCl_4, turned back to control levels at 8h and 12h and increased again at later time points (18h, D1). Data represent mean of at least three biological replicates ± S.E. (-) No protein concentrations were detectable in the WISP1 knockout mice.

Taken together, the qRT-PCR data suggested that WISP1 expression is induced upon CCl_4 intoxication as well as after APAP administration. Compared to the maximal dose, using a low dose of CCl_4 shifted the time when a maximal induction of WISP1 was observed to an earlier time point. However, previous results (maximal dose of CCl_4) were performed using a different mouse strain (C57Bl/6N), which could explain the differences in the expression of WISP1, because WISP1 knockout and wild type mice have a different and mixed genetic background (129S5/SvEvBrd * C57BL/6J).

3.9 Liver regeneration is not impaired by the absence of WISP1

In order to study whether liver regeneration is impaired by the absence of WISP1, wild type and WISP1 knockout mice were treated with either olive oil as the control vehicle, or with 460 mg/kg CCl_4 intraperitoneally for D1, D2, D3 and D4. Gross pathology revealed that under control conditions, livers from both wild type and WISP1 knockout mice exhibited the characteristic dark red coloration of a healthy liver (Figure 41). After D1 of CCl_4 treatment, liver of the wild type mice showed the characteristic white spots (puncta), indicating localized areas of cell damage. This was more intensive in the WISP1 knockout mice at the same time point, reflecting an advanced stage of liver damage. On D4 of treatment, almost no white puncta were observed in the wild type mice, showing a successful recovery from liver injury. However, WISP1 knockout mice displayed an increased size of white puncta at D2 up to D4, when compared to wild type mice.

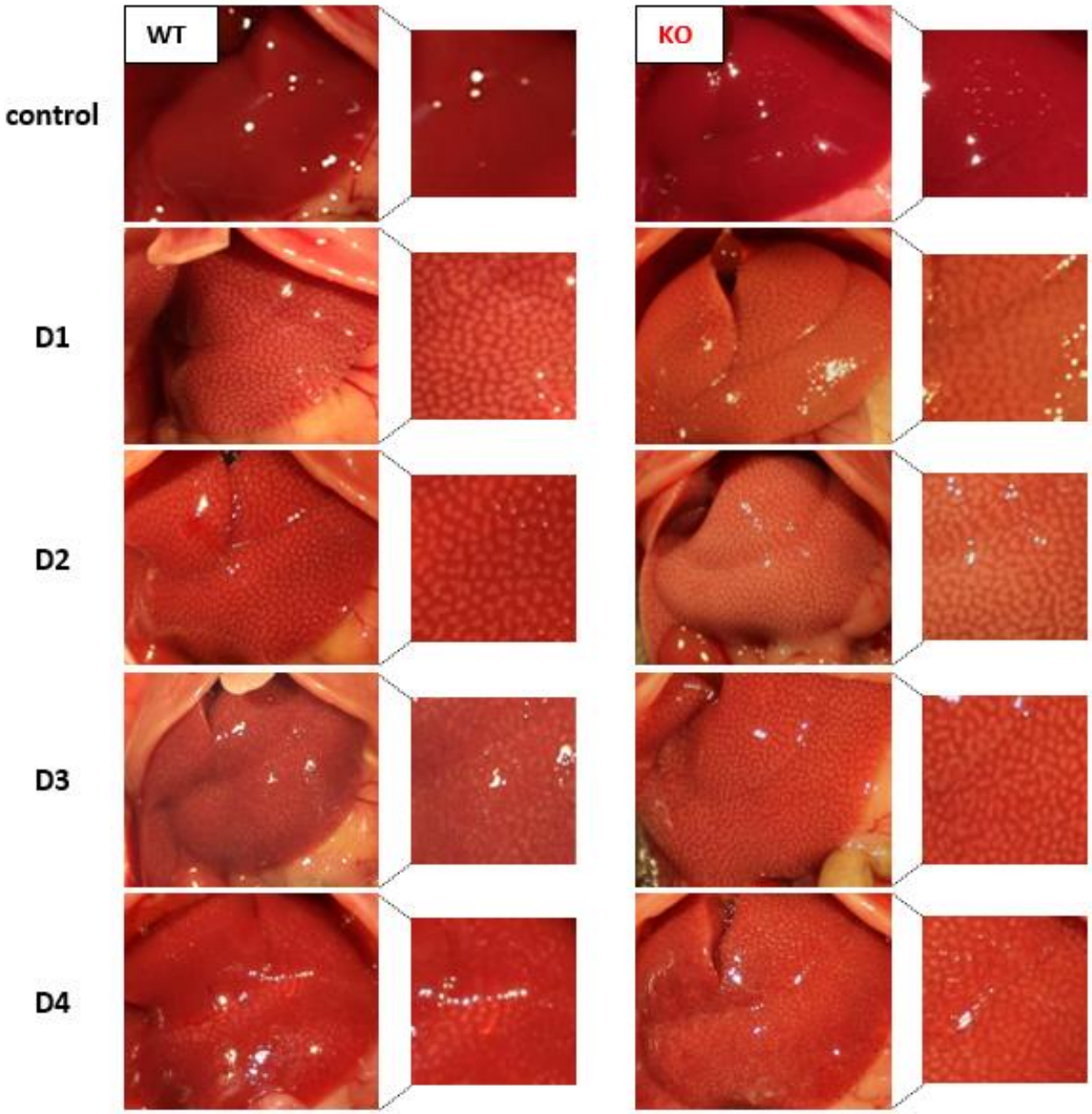

Figure 41: Time-dependent analysis of gross pathology appearance of WISP1 knockout mouse liver and wild type mouse liver after administration of 460 mg/kg CCl_4 for the indicated time points. Wild type mice and WISP1 knockout mice showed a characteristic intense red color under control condition. At D1 up to D4, an increased size of white puncta was observed in the liver of WISP1 knockout mice compared to the liver of wild type mice. On D4, only slight white puncta were observed in wild type mice. Representative images of five mice per time point.

Macroscopic alterations revealed enhanced liver damage in WISP1 knockout mice upon liver regeneration. In order to visualize the necrotic lesions microscopically, H&E staining was performed, using paraffin embedded liver sections of wild type mice and WISP1 knockout mice. The H&E staining showed enhanced pericentral necrosis in the livers of WISP1 knockout mice at all the indicated time points compared to the livers of wild type mice (Figure 42). An enhanced immune cell infiltration was observed around the central veins in wild type mice on day 4 in contrast to the WISP1 knockout mice that still showed a small

necrotic lesion, which was associated with less infiltration of immune cells. Overall, these results suggest that the capacity to recover from liver injury is not impaired by the absence of WISP1. However, WISP1 knockout mice seem to require a longer time period to recover from liver damage.

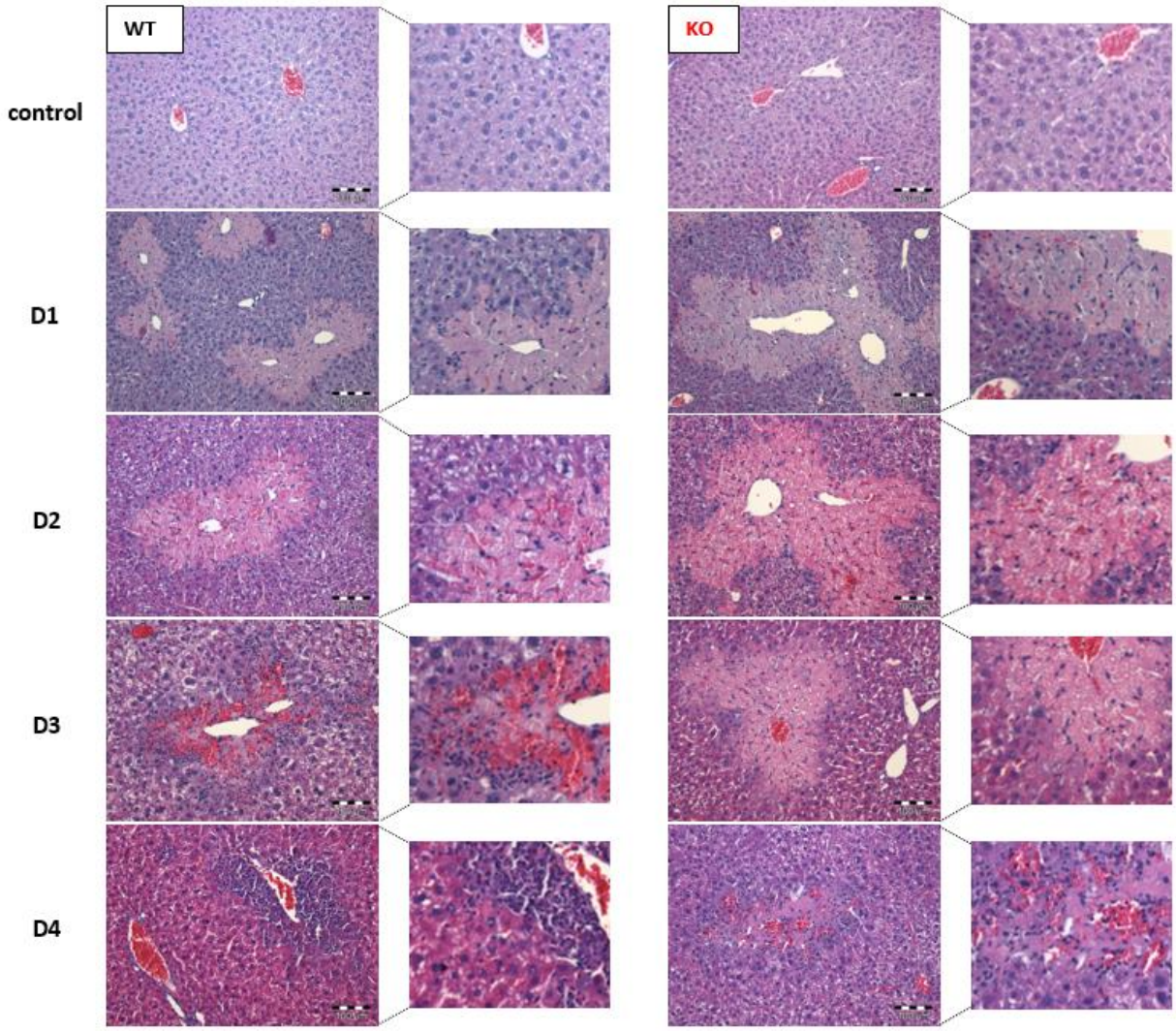

Figure 42: Time-dependent H&E staining of WISP1 knockout mice and wild type mice upon liver regeneration after administration of CCl_4. H&E staining of livers from WISP1 knockout mice showed an increased size of the dead cell areas, when compared to wild type mice at the indicated time points. The necrotic lesions are not fully recovered at D4 in the WISP1 knockout mice; whereas, in the wild type mice only a strong immune cell infiltration was observed. Representative images of five mice per time point, scale bars represent 100 µm.

Dead cell areas of WISP1 knockout and wild type mice were quantified using image analysis software. The quantification revealed enlarged dead cell areas at all indicated time points in the WISP1 knockout mice (Figure 43). However, the dead cell areas in wild type mice, as well as in WISP1 knockout mice decreased with comparable kinetics starting from D2 to D4.

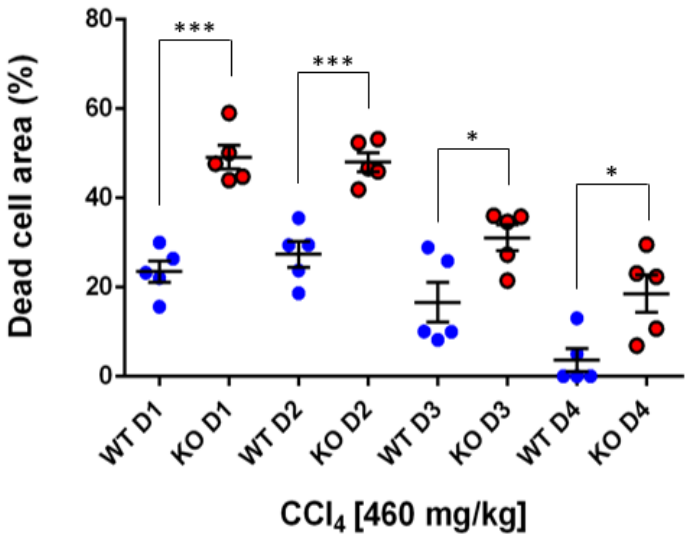

Figure 43: Time-dependent quantification of dead cell areas of WISP1 knockout mice and wild type mice after administration of 460 mg/kg CCl_4 for the indicated time points. The quantification revealed enlarged dead cell areas in the WISP1 knockout mice upon liver regeneration. However, wild type and WISP1 knockout mice seemed to recover with comparable kinetics from liver injury. Data represent at least three mice per concentration. Error bars indicate mean ± S.E. ***P<0.001 to wild type condition, **P<0.01 to wild type condition, *P<0.05 to wild type condition, unpaired t-test.

Taken together, this experiment revealed that both the WISP1 knockout mice and wild type mice recover from acute liver injury after CCl_4 administration with comparable kinetics. However, liver regeneration in the WISP1 knockout mice is delayed, when compared to wild type mice. One potential explanation is that the WISP1 knockout mice had twice the dead cell area after one day intoxication, and thus require a longer recovery period from acute liver injury.

3.9.1 Proliferation is not altered during liver regeneration by the absence of WISP1

Previous observations revealed no difference in the capacity of WISP1 knockout and wild type mice to recover from acute liver injury. In order to examine whether proliferating cell nuclear antigen (PCNA) signaling and gene expression is altered during liver regeneration by the absence of WISP1, western blot analysis and qRT-PCR of liver homogenates were performed.

Proliferating cell nuclear antigen (PCNA) is a nuclear protein, which is involved in cell cycle progression, serving as a cofactor for DNA polymerase-δ [174]. Bhushan et al showed that most of the PCNA-positive stained cells can be observed during S-phase after administration of APAP at D2, indicating that PCNA is involved in DNA replication [86]. Thus, PCNA is used as a marker for proliferating cells [175].

Wild type and WISP1 knockout mice were injected intraperitoneally using 460 mg/kg CCl_4 for D1, D2, D3 and D4. Olive oil was used as the control vehicle. Western blot analysis displayed activation of PCNA signaling in both wild type and WISP1 knockout mice starting at D2 until D4 (Figure 44). Quantification of signal volumes revealed no differences in the activation of PCNA in wild type mice compared to WISP1 knockout mice.

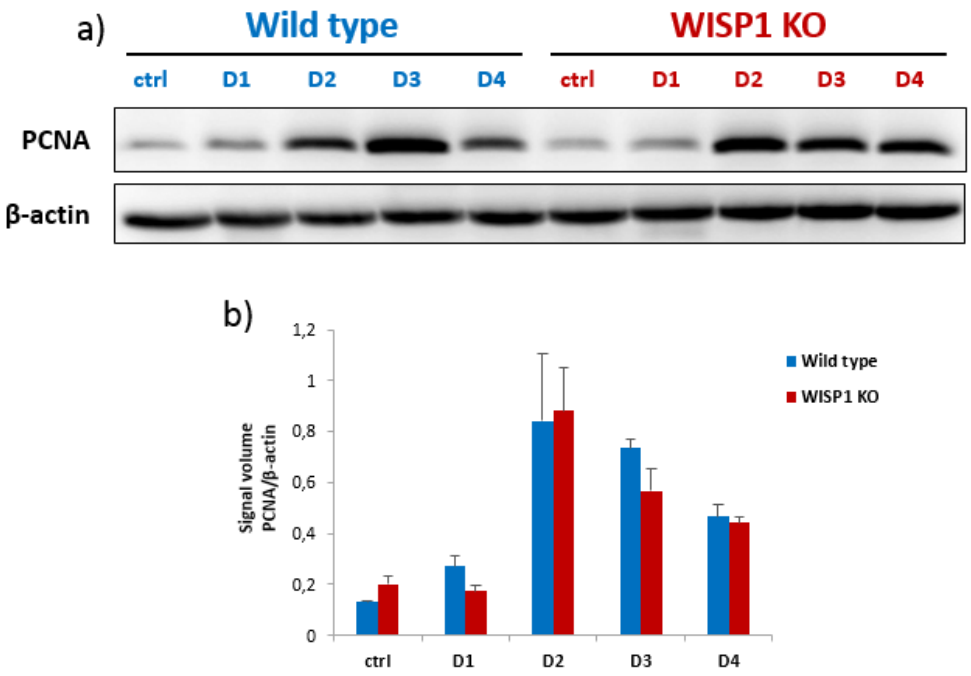

Figure 44: Time-dependent western blot analysis of PCNA levels after administration of 460 mg/kg CCl_4 during liver regeneration. Results revealed no difference in PCNA levels in WISP1 knockout and wild type mice. a) Western blot, b) Quantification shows mean values of three independent biological replicates ± S.E. β-actin was used as loading control.

PCNA expression was increased upon liver regeneration to comparable levels in both wild type and WISP1 knockout mice (Figure 45). On D4, the expression of PCNA was slightly increased compared to wild type mice, most likely because proliferation is still needed in the WISP1 knockout mice, as the wound is not fully recovered.

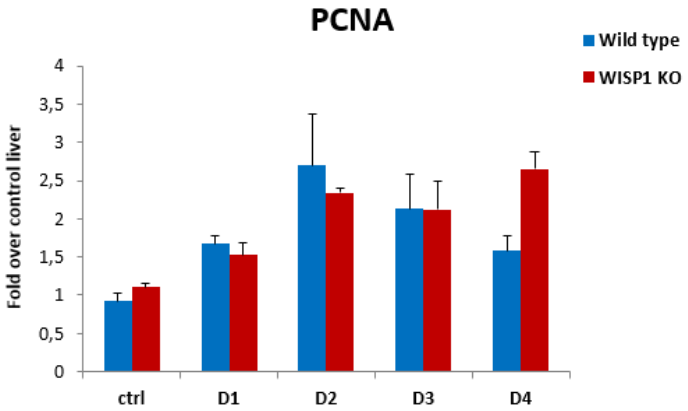

Figure 45: Time-dependent quantitative RT-PCR of PCNA RNA after administration of 460 mg/kg CCl_4 for the indicated time points. PCNA expression is increased to comparable levels in both wild type and WISP1 knockout mice. However, at D4 expression was slightly higher in the WISP1 knockout mice. Data represent mean values of five biological replicates ± S.E.

In summary, these results suggest that proliferation was not impaired by the deletion of WISP1. On D4, WISP1 knockout mice seemed to have higher PCNA expression, because on D4 the wound is not fully regenerated in the WISP1 knockout mice compared to wild type mice.

3.9.2 Cell cycle-dependent genes are slightly higher expressed when WISP1 is deleted

To study whether cell cycle dependent genes were altered by deletion of WISP1 during liver regeneration, quantitative RT-PCR was performed. Therefore, RNA was isolated from wild type and WISP1 knockout mice and cell cycle-dependent RNA expression was quantified by quantitative RT-PCR. CycG2 is known to block cell cycle entry [176]; therefore, a comparable decrease in CycG2 expression was observed during liver regeneration in wild type and WISP1 knockout mice. Cytokines act as precursors to drive quiescent hepatocytes into the cell cycle (G_0 to G_1). Cell cycle progression is then driven by growth factors to override a restriction point in late G_1-phase. Increased expression of cyclins, such as cyclin D, E and A, are associated with the passage from G_1 to S phase [82, 116, 177, 178]. WISP1 knockout and wild type mice showed similar expression pattern of CycD1, CycE2 and CycA2 with increased induction on D2 and downregulation by D4 (Figure 46). Thereby, WISP1 knockout mice displayed a slightly increased induction of cell cycle genes during liver regeneration, which could be due to a compensatory mechanism or to the fact that enhanced cell proliferation is needed in WISP1 knockout mice to overcome the enlarged dead cell areas.

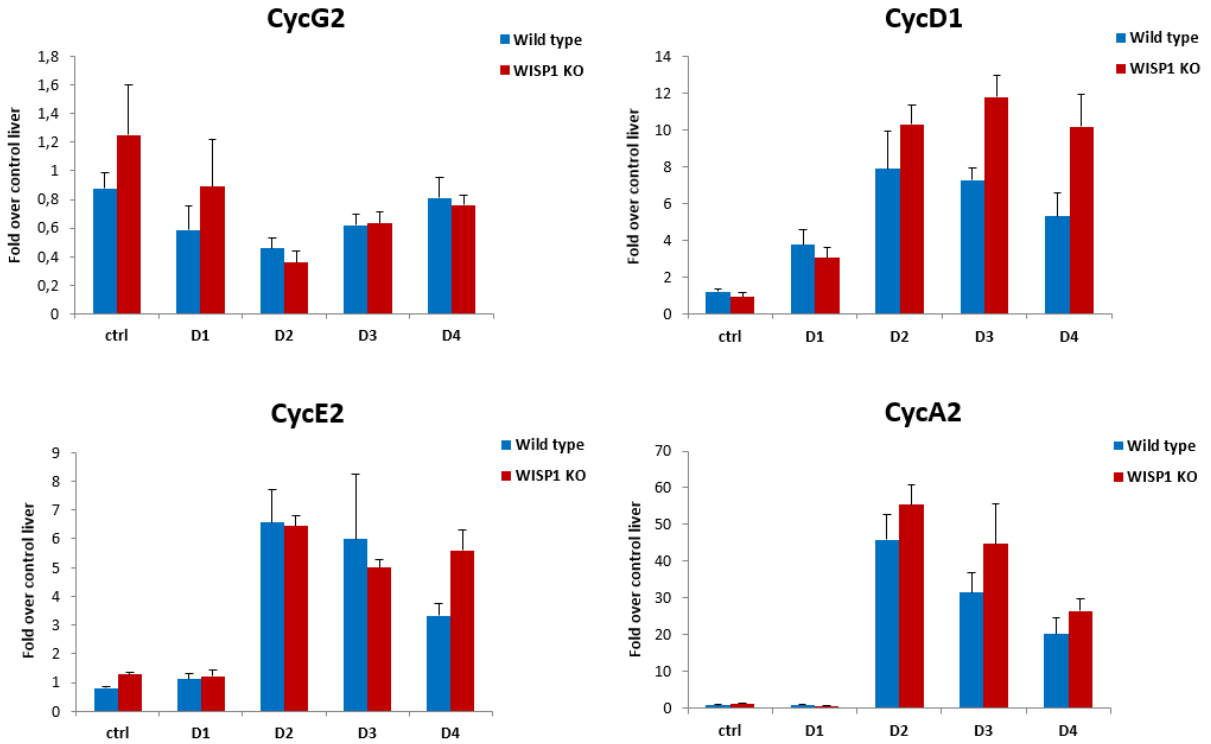

Figure 46: Time-dependent quantitative RT-PCR of cell cycle-dependent genes CycG2, CycD1, CycE2, and CycA2 after administration of CCl_4 for the indicated time points. CycG2 expression was downregulated to same extent in the wild type and WISP knockout mice. CycD1, CycE2 and CycA2 followed a similar expression pattern of an induction at D2 and a decrease during liver regeneration up to D4. Quantitative RT-PCR revealed slightly higher expression of cell cycle-dependent genes in WISP1 knockout mice during liver regeneration. Data represent mean values of five biological replicates ± S.E.

Taken together, these analyses revealed that cell cycle-dependent genes were not altered by the deletion of WISP1 upon liver regeneration. WISP1 knockout mice exhibited increased induction of cell cycle-dependent genes, which might be due to the fact that the wound is enlarged in these mice and enhanced proliferation is needed for recovery.

Because liver regeneration was not impaired by the absence of WISP1, and a clear and robust protective phenotype was observed upon acute liver injury, the focus was to investigate WISP1 function upon acute liver injury.

3.10 WISP1 knockout enhanced sensitivity is not caused by altered redox state or Cyp2e1 metabolism

The differential sensitivity of WISP1 knockout mice compared to wild type mice could be due to a basal reduction in antioxidant metabolites, such as GSH or an enhanced metabolic activation of CCl_4 by Cyp2E1. Therefore, the next step was to examine GSH content in WISP1 knockout and wild type mice upon APAP and CCl_4 administration, as well as the Cyp2E1 levels.

Quantification of GSH levels were performed after administration of 300 mg/kg APAP or 460 mg/kg CCl_4. Moreover, IHC staining was used to quantify Cyp2E1 areas around the central veins. Quantitative RT-PCR and western blotting were used to assess the expression of Cyp2E1 during acute liver damage caused by CCl_4.

As seen in figure 27, GSH content did not differ in the control condition in wild type mice compared to WISP1 knockout mice. Moreover, depletion and recovery of GSH content was also comparable in the WISP1 knockout and wild type mice after treatment using 300 mg/kg APAP (Figure 47 a). Depletion of GSH after administration of CCl_4 was not as strong as in the APAP model (Figure 47 b). However, depletion and recovery of GSH was comparable in both the wild type and WISP1 knockout mice upon CCl_4 administration.

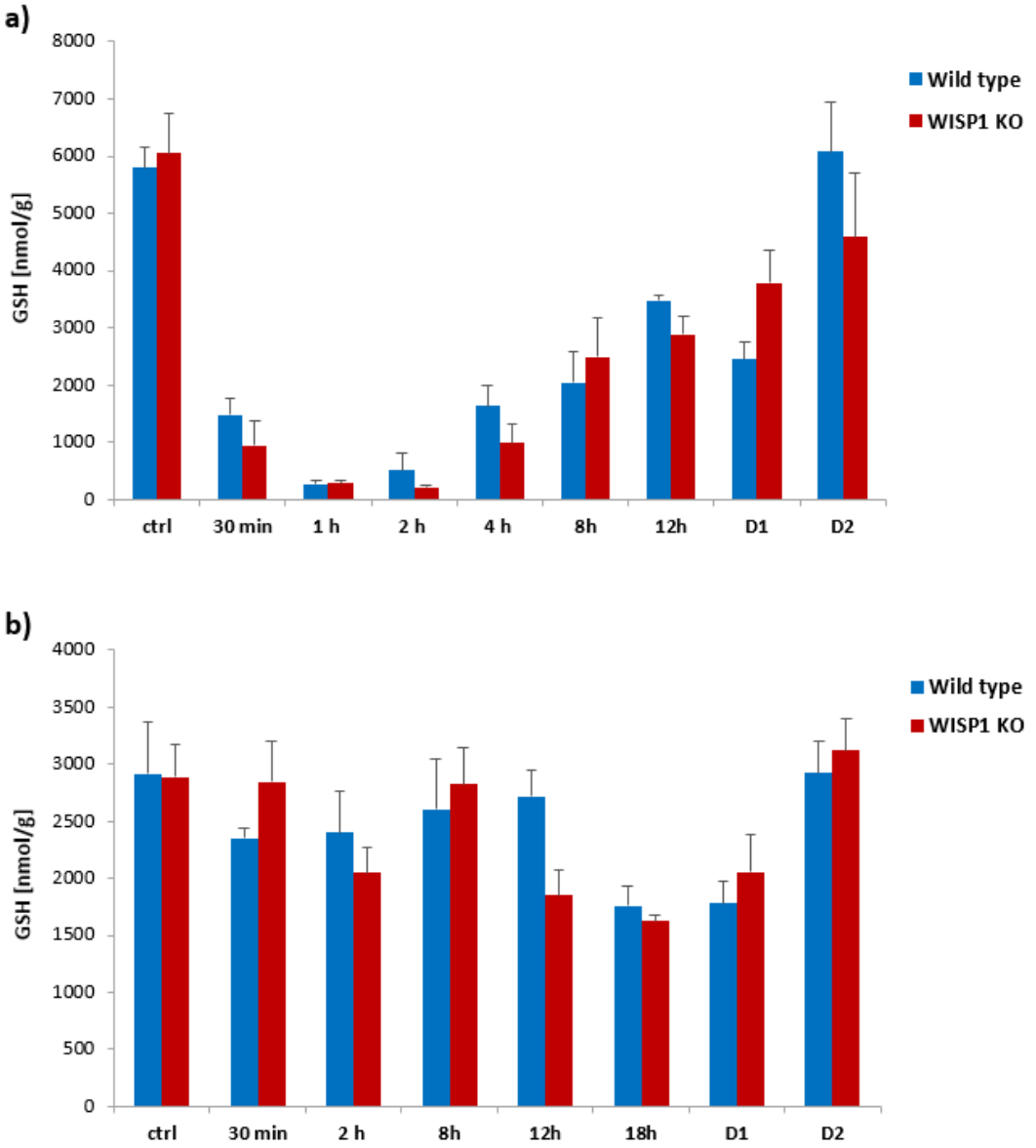

Figure 47: Time-dependent analysis of GSH content in wild type and WISP1 knockout mouse liver tissue after administration of a) 300 mg/kg APAP and b) 460 mg/kg CCl_4. GSH content showed no significant difference in the wild type and WISP1 knockout mice after APAP administration. Data represent mean of at least three biological replicates ± S.E.

The next step was to determine the Cyp2E1 positive area around the central veins in WISP1 knockout and wild type mice. Immunohistochemical staining of Cyp2E1 in control liver tissue (vehicle control) showed no difference between wild type and WISP1 knockout mice (Figure 48 a). Furthermore, the quantification revealed no significant difference in the size of Cyp2E1 stained positive area (Figure 48 b). Figure 48 c shows the result from qRT-PCR of Cyp2E1 in wild type and WISP1 knockout mice after administration of 460 mg/kg CCl_4. Cyp2E1 expression was not significantly altered in the control condition, and the depletion of Cyp2E1 was comparable between wild type and WISP1 knockout mice.

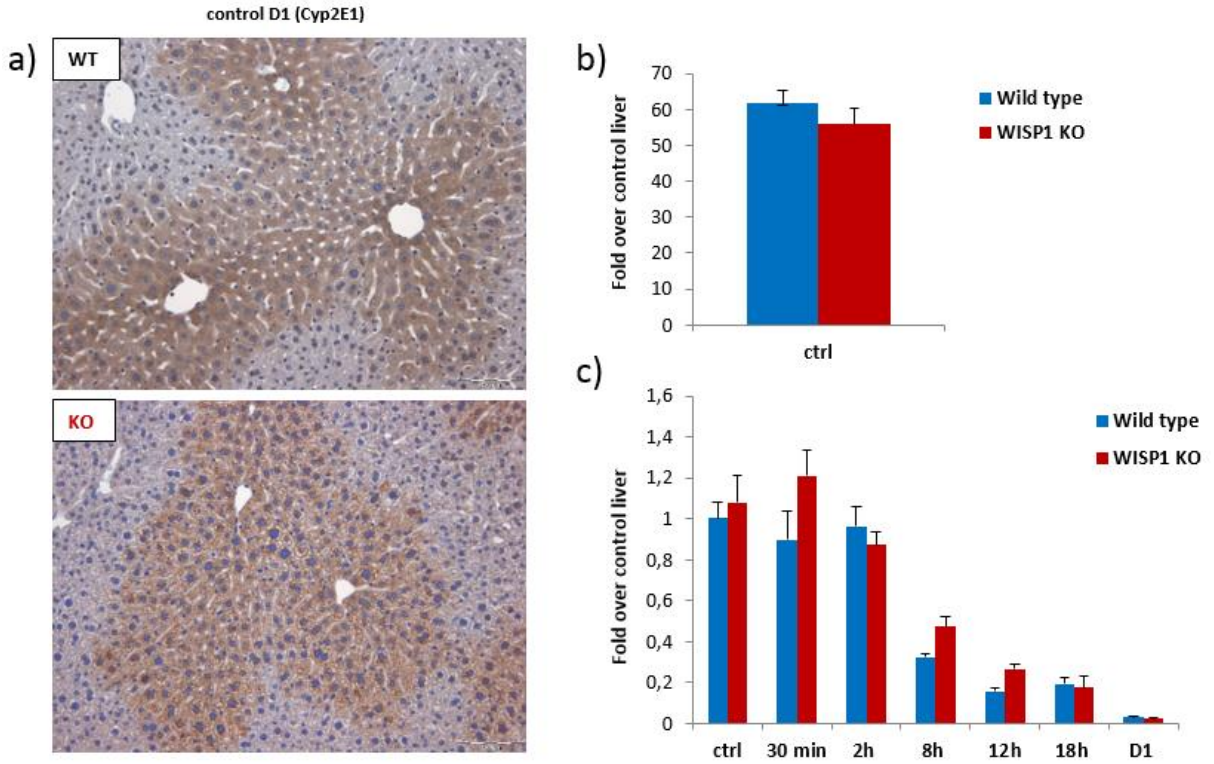

Figure 48: Analysis of Cyp2E1 expression showed no difference in wild type mice compared to WISP1 knockout mice. a) Immunohistochemistry staining of Cyp2E1 in wild type and WISP1 knockout mice under control conditions at D1. Representative images of three mice per condition. Scale bars represent 100 µm. **b) Quantification of Cyp2E1 positive stained area around the central veins.** Results revealed no significant difference in the size of Cyp2E1 area in the wild type mice versus WISP1 knockout mice. Quantification was done using three biological replicates and five images were quantified from each biological replicate. Data represent mean ± S.E. **c) Time-dependent quantitative RT-PCR of Cyp2E1 expression after administration of 460 mg/kg CCl_4 for the indicated time points.** Cyp2E1 expression was decreased in both the wild type and WISP1 knockout mice in acute liver damage and no significant difference was observed. Data represent mean of at least five biological replicates ± S.E.

Finally, western blot analysis was used to determine protein levels of Cyp2E1 in liver homogenates after induction of liver damage by CCl_4. This result indicated no significant difference in wild type and WISP1 knockout mice regarding Cyp2E1 protein levels in control conditions as well as during induction of liver damage (Figure 49 a, b).

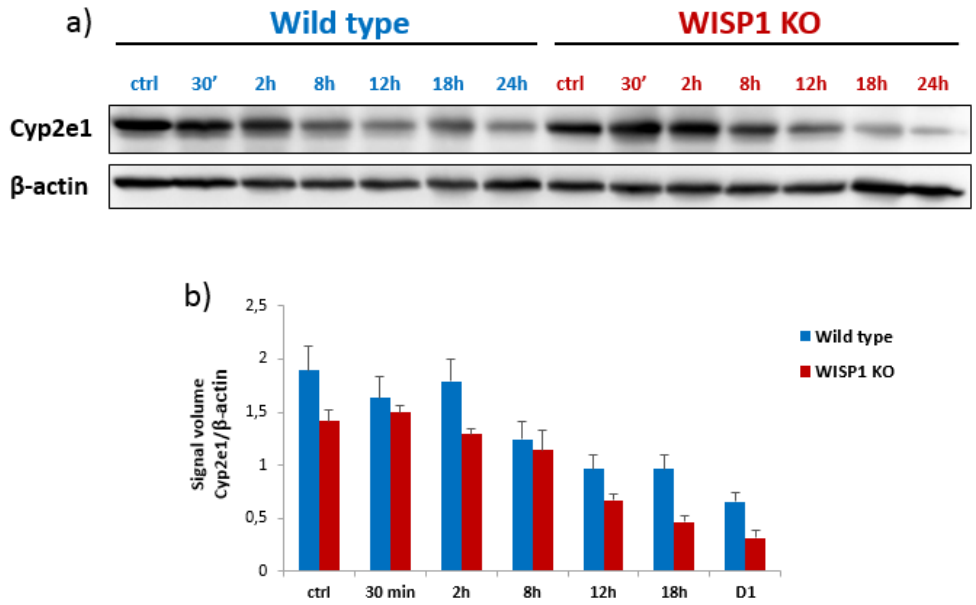

Figure 49: Time-dependent analysis of Cyp2E1 protein levels in wild type and WISP1 knockout mice. a) Western blot analysis of Cyp2E1 levels in liver homogenates after induction of liver damage using 460 mg/kg CCl_4. ß-actin was used as loading control. **b) Quantification of western blot analysis.** Western blot analysis and quantification of western blots revealed no difference in the protein levels of Cyp2E1 in wild type mice versus WISP1 knockout mice. Results are representative of three independent biological replicates per time point. Data are mean values ± S.E. β-actin was used as loading control.

In conclusion, these analyses revealed no differences regarding the redox state and metabolism of hepatotoxic substances in wild type and WISP1 knockout mice. Therefore, the hypothesis that altered metabolism or differences in redox state may be responsible for the enhanced liver damage in WISP1 knockout mice could be excluded.

3.11 Gene expression of CCN family members revealed alterations by the absence of WISP1

CCN family members were reported to interact with cytokines, like TNFα, converting their proliferation-promoting effect into an apoptotic inducing potential [112]. Therefore, the next step was to investigate whether the expression of CCN family members is altered during liver injury by the deletion of WISP1 in knockout mice, which could influence the outcome of liver injury. RNA was isolated from CCl_4 time series and qRT-PCR was performed for Cyr61 (CCN1), CTGF (CCN2) and Nov (CCN3). As seen in figure 50, Cyr61 was upregulated in all samples for all treated time points. However, the induction was higher in the WISP knockout mice at 2h and D1 compared to wild type mice. CTGF expression was increased at 18h and D1 after CCl_4 in both wild type and WISP1 knockout mice, but higher induction was observed in the WISP1 knockout mice. Nov expression only increased in the WISP1 knockout mice at all indicated time points.

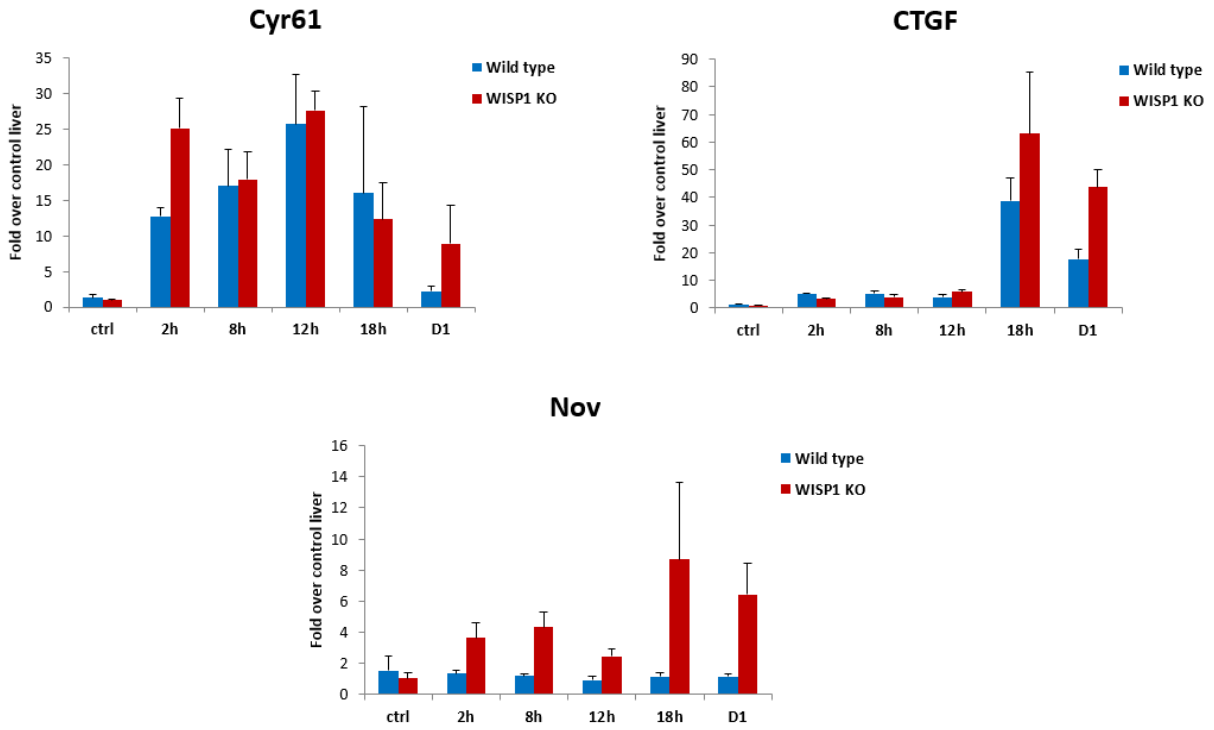

Figure 50: Time-dependent quantitative RT-PCR of CCN family members after administration of 460 mg/kg CCl_4 for the indicated time points. Cyr61 expression was induced at all time points. However, stronger induction was observed in the WISP1 knockout mice at 2h and D1. CTGF expression was induced in wild type and WISP1 knockout mice at 18h and D1, however, stronger induction was detected in the WISP1 knockout mice. Nov expression was induced only in the WISP1 knockout mice with the highest induction at 18h after CCl_4 treatment. Data represent mean of at least three biological replicates ± S.E.

This approach displayed that not only WISP1 is induced during acute liver damage, but also the CCN family members. Quantitative RT-PCR results revealed altered expression of CCN family members in the absence of WISP1. This led to the hypothesis that WISP1 knockout mice tried to compensate for the loss of WISP1 by upregulating other CCN family members.

3.12 Signal transduction analyses of WISP1 knockout and wild type mice during acute liver injury

3.12.1 Deletion of WISP1 leads to stronger induction of stress signaling pathway JNK

MAPK associated signaling pathways are known to be activated upon various stimuli, such as ROS, growth factors, environmental stress or cytotoxic drugs. Activation of signaling cascade can trigger different cellular responses, including differentiation, migration and proliferation. However, apoptosis or inflammation could also be consequences of MAPK signaling [88, 179].

In order to study whether c-Jun N terminal kinases (JNKs) were altered upon CCl_4 administration in WISP1 knockout mice compared to wild type mice, western blot analysis was performed. Protein lysates were prepared using liver harvested from wild type and WISP1 knockout mice after administration of 460 mg/kg CCl_4 for 30min, 2h, 8h, 18h and 24h. Figure 51 represents results from western blot analysis of JNK levels. Stronger JNK activation was observed in WISP1 knockout mice at 2h after administration of 460 mg/kg CCl_4.

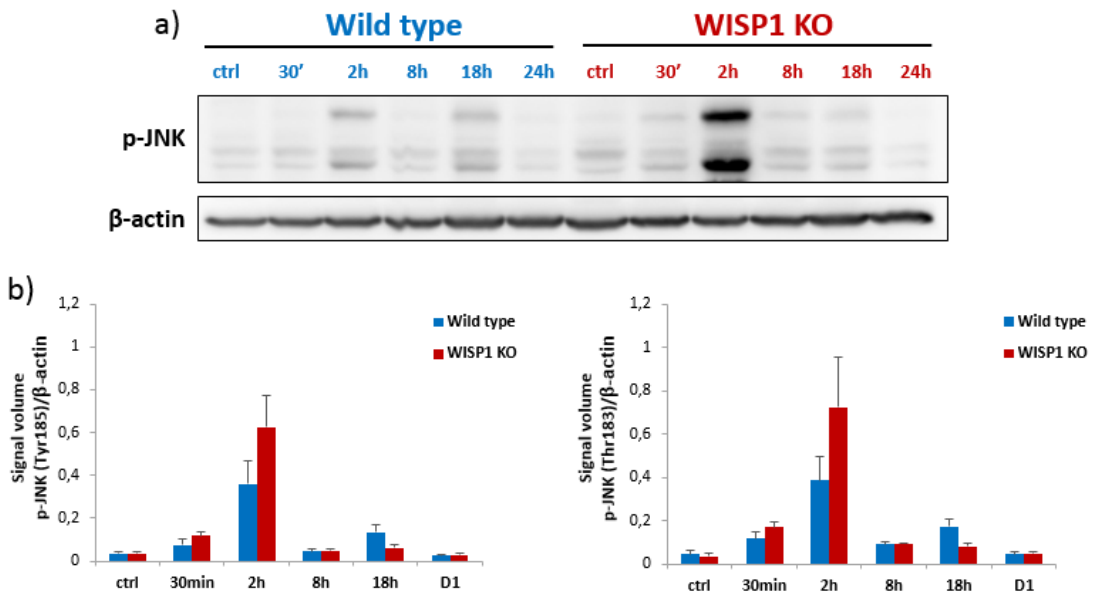

Figure 51: Activation of JNK protein in wild type mice and WISP1 knockout mice upon CCl_4 administration. a) Western blot analysis of JNK levels in wild type and WISP1 knockout mice after administration of 460 mg/kg CCl_4. b) Quantification of western blot analysis from wild type mice versus WISP1 knockout mice. Phosphorylation of JNK was stronger induced at 2h in WISP1 knockout mice. β-actin was used as loading control. Results are representative of six independent biological replicates per time point. Data are mean values ± S.E.

Taken together, these results show that the deletion of WISP1 resulted in a higher activation of stress signaling in WISP1 knockout mice.

3.12.1.1 Upstream regulator of JNK signaling, growth arrest and DNA damage-inducible 45 beta (GADD45β) is not suppressed by the deletion of WISP1

Growth arrest and DNA damage-inducible 45 beta (GADD45β) was shown to inhibit JNK phosphorylation and thereby protecting against APAP-induced toxicity in mice [110, 180]. In order to address the question whether GADD45β was involved in the protective phenotype of wild type mice, qRT-PCR was performed using RNA isolated from liver homogenates after CCl_4 administration (Figure 52). GADD45β expression was increased at 2h and 18h after CCl_4 administration. However, enhanced induction was observed at 2h and on D1 in WISP1 knockout mice.

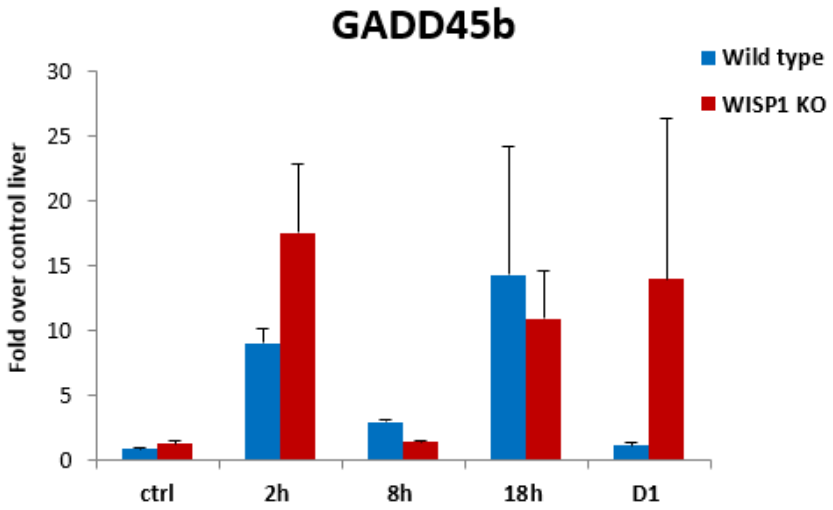

Figure 52: Time -ependent quantitative RT-PCR of GADD45β in WISP1 knockout and wild type mice after 460 mg/kg CCl_4 for the indicated time points. GADD45β expression was observed to be increased in the WISP1 knockout mice at 2h and D1 after administration of CCl_4. Data represent mean of three independent biological replicates ± S.E.

Surprisingly, this result was contrary to our hypothesis, which proposed higher expression in the wild type mice leading to attenuated JNK signaling. Taken together, GADD45β was not the cause for lower JNK activation in the wild type mice.

3.12.1.2 Stress-induced activating transcription factor 3 (ATF3) is not influenced by the absence of WISP1

ATF3 is known to be expressed at low levels under physiological conditions [181, 182]. However, upon cellular growth or stress, such as exposure to CCl_4 or APAP [183] the expression greatly increases, indicating ATF3 as a key regulator in cellular stress responses. ATF3 expression was linked to cell cycle progression, metabolism, as well as cell death [181-183]. To examine whether ATF3 expression was altered upon genetic deletion of WISP1, quantitative RT-PCR was performed using RNA from wild type and WISP1 knockout mice treated with 460 mg/kg CCl_4. Results showed a biphasic induction of ATF3 expression, which peaked at 2h and 12h after treatment (Figure 53). Levels of AFT3 RNA were comparable in both wild type and WISP1 knockout mice.

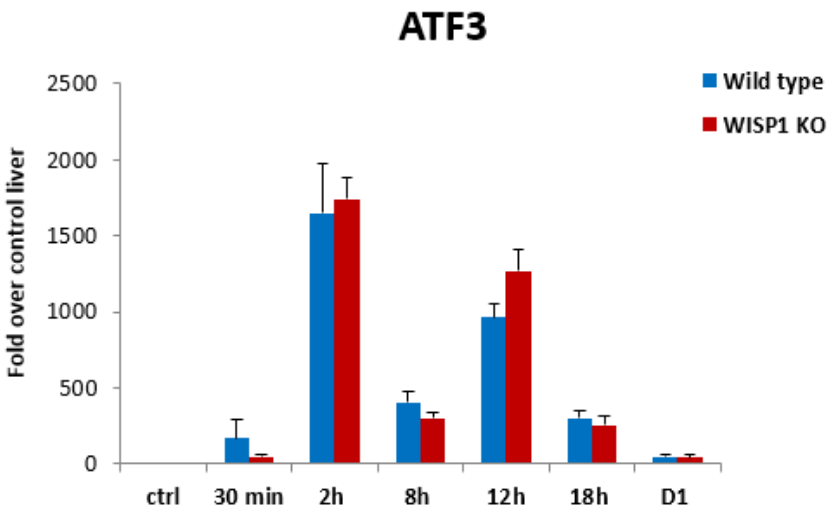

Figure 53: Time-dependent quantitative RT-PCR of ATF3 expression in wild type and WISP1 knockout mice after administration of 460 mg/kg CCl_4 for the indicated time points. Results revealed a biphasic induction of ATF3 at 2h and 12h after CCl_4 administration. However, no difference was detected in the wild type mice compared to WISP1 knockout mice. Data represent mean of six independent biological replicates ± S.E.

In summary, induction of AFT3 expression, an early response gene induced by cellular growth or stress, was not impaired by the absence of WISP1.

3.12.2 Biphasic phosphorylation of ERK1/2 is attenuated in WISP1 knockout mice

In order to study whether extracellular-signal regulated kinase (ERK) was altered in WISP1 knockout mice compared to wild type mice, western blot analysis of liver tissue homogenates was performed after CCl_4 administration (Figure 54). Biphasic activation of ERK1/2 was observed in the wild type mice at 30min until 2h, and at 18h after CCl_4 administration; whereas, in the WISP1 knockout mice ERK1/2 activation was observed only at 30 min and 2h.

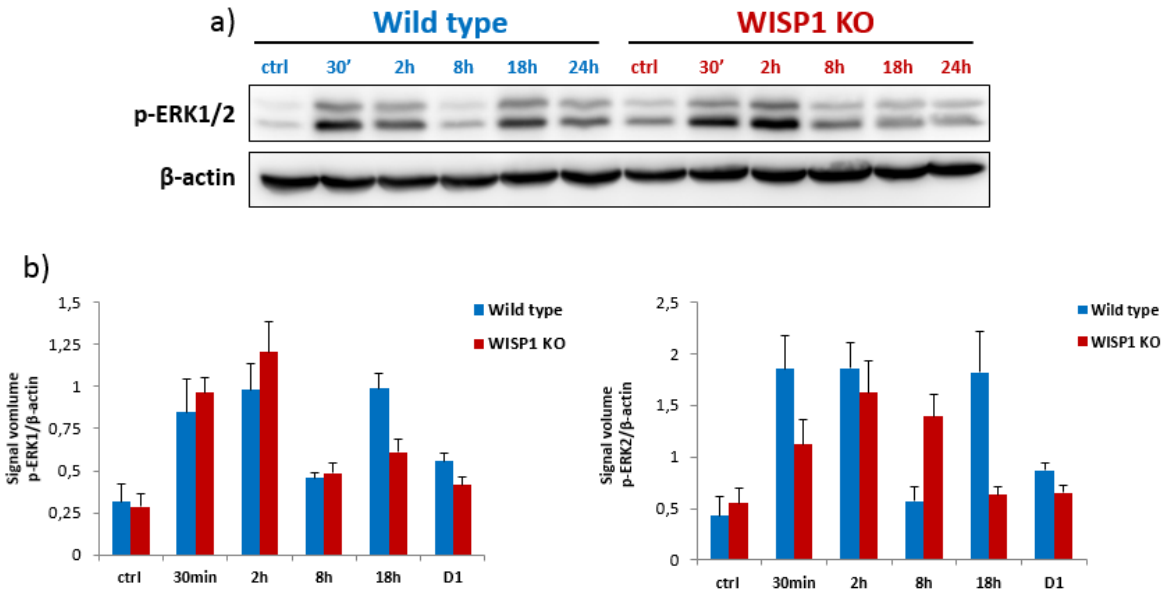

Figure 54: Activation of ERK1/2 in wild type mice and WISP1 knockout mice upon CCl_4 administration. a) Western blot analysis of p-ERK1/2 in liver homogenates of wild type and WISP1 knockout mice after administration of CCl_4 for the indicated time points. b) Quantification of western blot analysis. Results show a biphasic phosphorylation of ERK1/2 in the wild type mice, which peaked at early time points (30 min and 2h) and at later time point (18h). The second phosphorylation of ERK1/2 was attenuated in the WISP1 knockout mice. Results are representative of six independent biological replicates per time point. Data are mean values ± S.E. β-actin was used as loading control

Analysis of ERK1/2 signaling revealed comparable activation levels at early time points in both wild type and WISP1 knockout mice. However, the second peak of activation at 18h was diminished in the WISP1 knockout mice.

3.12.2.1 Absence of WISP1 does not influence the induction of early activated transcription factor c-Myc

ERK1/2 has been shown to phosphorylate numerous substrates as well as nuclear transcription regulators, such as c-Myc [93]. This transcription factor is known to be an early activated transcription factor associated with hepatocyte proliferation, cell growth and loss of differentiation [94-97]. In order to study whether the expression of c-Myc is altered upon the deletion of WISP1, RNA was quantified from the livers of wild type and WISP1 knockout mice treated with 460 mg/kg CCl_4. Expression of c-Myc increased starting at 2h up to 18h treatment, before decreasing to control levels at D1 (Figure 55). However, the expression of c-Myc was slightly higher in the WISP1 knockout mice compared to wild type mice on D1.

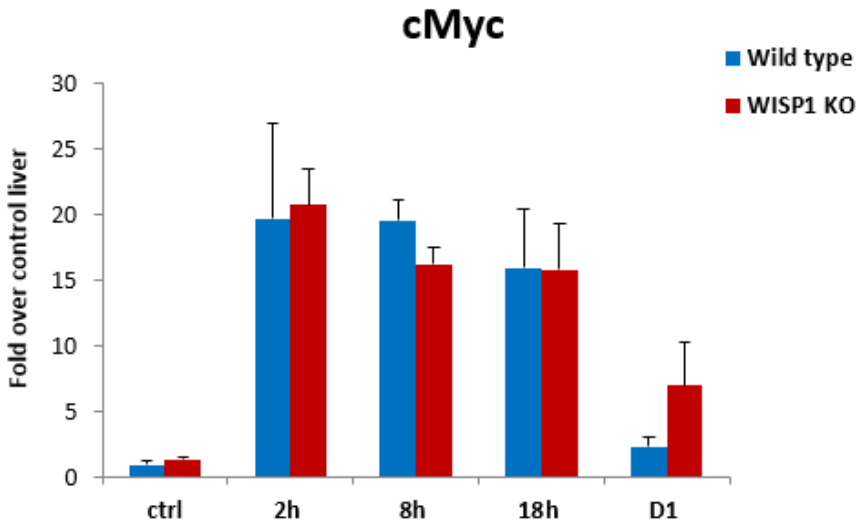

Figure 55: Time-dependent quantitative RT-PCR of cMyc expression in wild type mice and WISP1 knockout mice after CCl_4 administration for the indicated time points. cMyc expression was increased in both wild type and WISP1 knockout mice at 2h up to 18h. Slightly higher expression was detected in the WISP1 knockout mice on D1. Data represent mean of three independent biological replicates ± S.E.

Promotion of cell cycle progression is one of the key biological functions of c-Myc [97]. Therefore, the general lack in alteration of cMyc expression confirms previous findings (Chapter 3.9) showing no impairment of liver regeneration in the WISP1 knockout mice.

3.12.3 Activation of Akt kinase, a cell survival mediator, is not altered by deletion of WISP1 in mouse liver

More than a decade ago, WISP1 was shown to decrease p53-mediated apoptosis by the activation of Akt kinase through inhibiting cytochrome C release and the up-regulation of anti-apoptotic Bcl-X_L [106]. This led to the hypothesis that Akt kinase is involved in the protective phenotype of wild type mice. To investigate Akt signaling in wild type mice compared to WISP1 knockout mice, western blot analysis was performed using protein lysates from the livers of mice treated with CCl_4. A time-dependent increase in the phosphorylation of Akt was observed in both wild type and WISP1 knockout mice starting at 12h and lasting until D1. However, the activation was stronger at 18h in the WISP1 knockout mice (Figure 56).

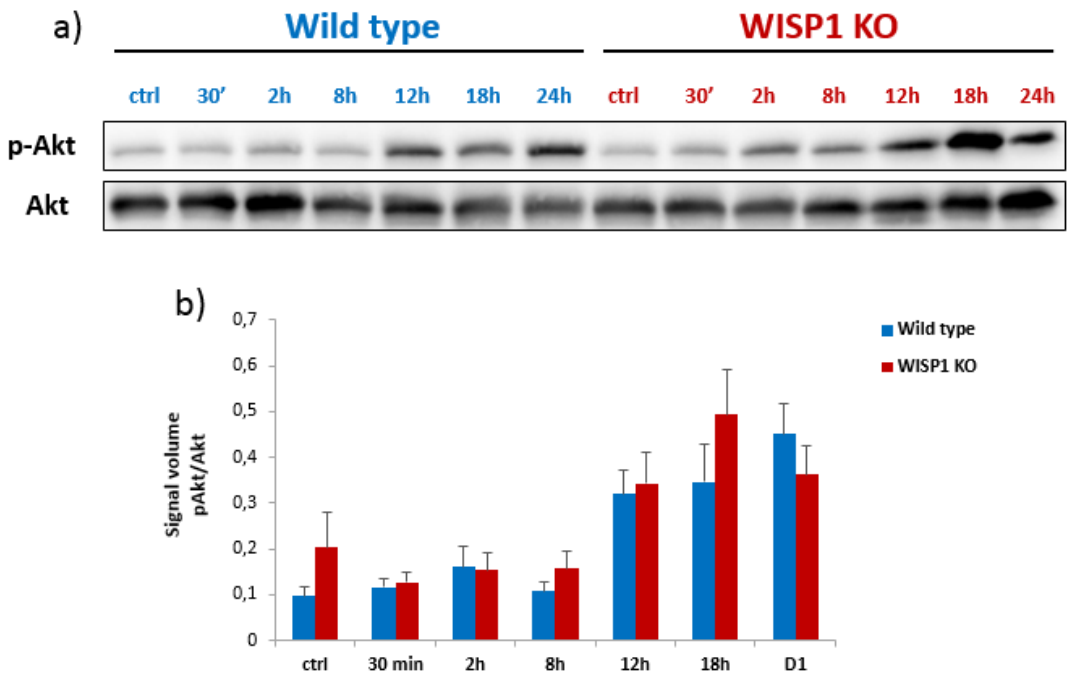

Figure 56: Activation of Akt in wild type mice and WISP1 knockout mice. a) Western blot analysis of Akt levels after administration of 460 mg/kg CCl_4 in wild type and WISP1 knockout mice. b) Quantification of western blot analysis. Phosphorylation was stronger induced in the WISP1 knockout mice at 18h. At D1, a similar phosphorylation was observed in both wild type and WISP1 knockout mice. Total Akt was used as a reference control. Results are representative of six independent biological replicates per time point. Data are mean values ± S.E.

Surprisingly, contrary to previous reports [106] and to our hypothesis, western blot analysis of WISP1 knockout mice showed slightly stronger activation of Akt kinase. This suggests that Akt kinase signaling was not mainly involved in the protective phenotype, which was observed in wild type mice.

3.12.4 Deletion of WISP1 leads to the activation of p38 mitogen-activated protein kinase (p38) upon CCl_4 administration

The previous results indicated alterations in extracellular signal-regulated kinase (ERK1/2). To examine if further MAPK signaling was impaired, p38 mitogen-activated protein kinase (p38) and c-Jun N-terminal kinase (JNK) were investigated. Therefore, western blot analysis was performed using liver tissue homogenates from wild type and WISP1 knockout mice treated with CCl_4. Phosphorylation of p38 was stronger activated in the wild type mice under control condition compared to WISP1 knockout mice (Figure 57). At 12h, slightly enhanced activation of p38 was observed in the WISP1 knockout mice.

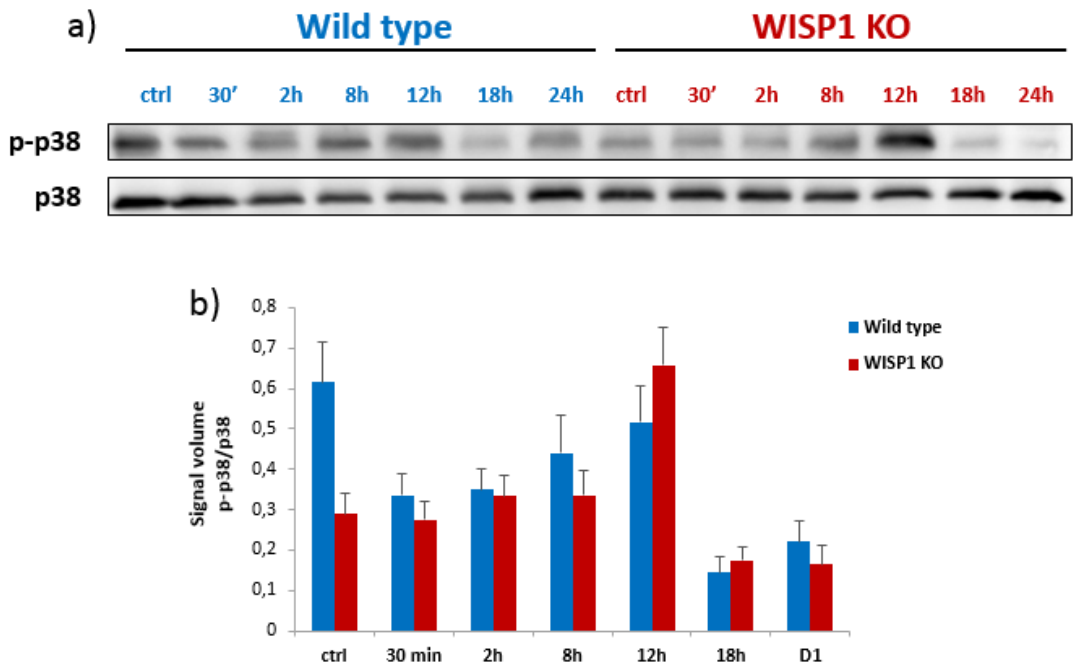

Figure 57: Activation of p38 in wild type mice and WISP1 knockout mice. a) Western blot analysis of p38 levels in wild type and WISP1 knockout mice after 460 mg/kg CCl_4. b) Quantification of western blot analysis. Activation of p38 was stronger induced in the wild type mice under control condition. At 12h, activation was enhanced in the WISP1 knockout mice compared to wild type mice. Total p38 was used as a reference control. Results are representative of six independent biological replicates per time point. Data are mean values ± S.E.

3.12.5 Early mediator of necrotic cell death receptor interacting protein kinase (RIP3) is not altered in WISP1 knockout mice compared to wild type mice

Receptor interacting protein kinase (RIP3) was recently identified as an early mediator of APAP toxicity in mice, while modulating mitochondrial dysfunction and oxidative stress [51]. Western blot analysis was performed to examine whether RIP3 kinase is involved in the development of advanced liver damage in WISP1 knockout mice. The results revealed no difference in RIP3 protein levels in both WISP1 knockout and wild type mice (Figure 58).

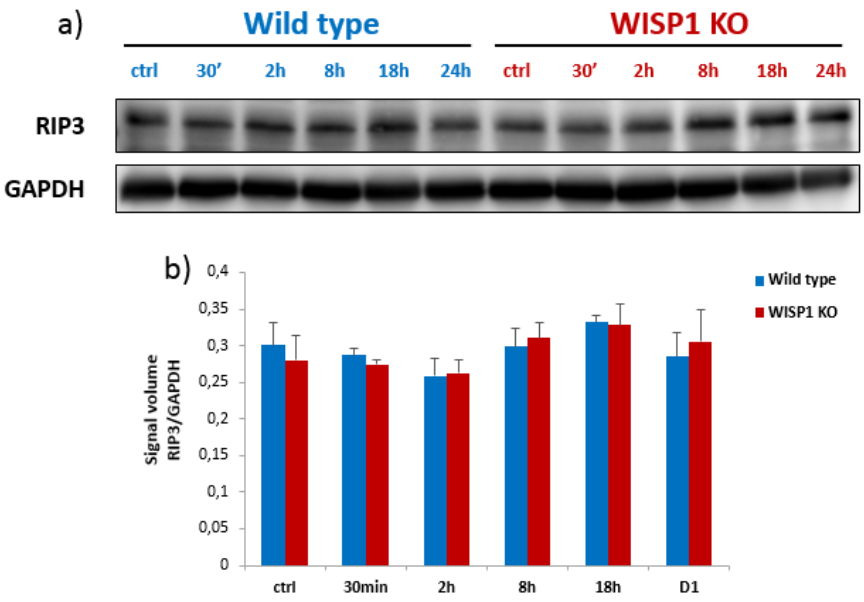

Figure 58: RIP3 levels in wild type mice and WISP1 knockout mice. a) Western blot analysis of RIP3 levels after administration of 460 mg/kg CCl_4 in wild type and WISP1 knockout mice. b) Quantification of western blot analysis. No difference was detectable in the wild type mice compared to WISP1 knockout mice. GAPDH was used as loading control. Results are representative of three independent biological replicates per time point. Data are mean values ± S.E.

In conclusion, the analysis revealed significant differences in the activation of signaling proteins in wild type and WISP1 knockout mice after induction of liver damage. Enhanced activation of MAPK-associated signaling may be responsible for the increased susceptibility of the WISP1 knockout mice to liver damage. However, stronger activation of the pro-survival PI3K/Akt signaling pathway was observed in WISP1 knockout mice. Furthermore, RIP3 seemed to be not involved in the progression of liver damage in wild type and WISP1 knockout mice.

3.12.6 CCl_4-induced ER-stress activation is not altered by the deletion of WISP1

The accumulation of misfolded proteins is known to activate three sensors in the ER lumen: IRE1α, PERK, and ATF6. The induction of IRE1α leads to the splicing of Xbp1 to a potent transcription factor, sXbp1, which controls genes involved in protein folding and quality control. However, prolonged or massive ER-stress is known to induce apoptosis via the upregulation of the transcription factor CHOP, which can induce the expression of pro-apoptotic genes, such as Bim and Erol1, and suppress the anti-apoptotic genes, such as Bcl-2 [99]. Therefore, the involvement of ER stress was investigated in wild type and WISP1 knockout mice. Results from the PCR analysis of Xbp1 splicing revealed no difference between wild type and WISP1 knockout mice (Figure 59).

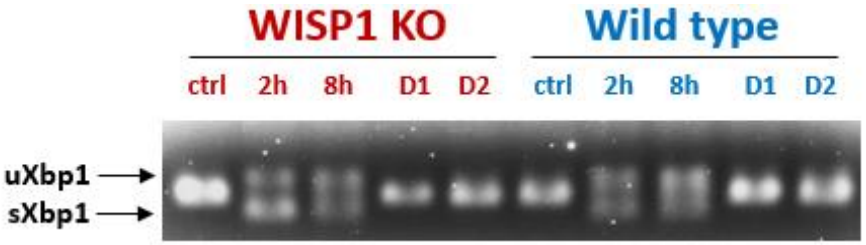

Figure 59: PCR analysis of ER-stress marker Xbp1 after administration of 460 mg/kg CCl_4 in wild type and WISP1 knockout mice. Splicing of Xbp1 was detected at 2h and 8h after CCl_4 administration with no difference between wild type and WISP1 knockout mice. The results are representative for three mice per condition.

Moreover, the transcription factor CHOP was analyzed using quantitative RT-PCR. CHOP expression was induced at 2h and 8h after induction of liver damage in both the wild type and WISP1 knockout mice. However, no significant difference could be observed.

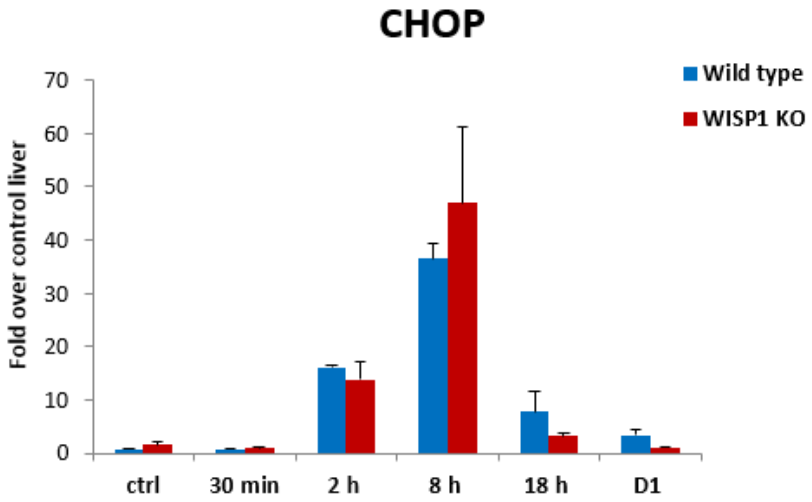

Figure 60: Time-dependent quantitative RT-PCR of CHOP expression in WISP1 knockout and wild type mice after administration of 460 mg/kg CCl_4 for the indicated time points. CHOP expression was not altered in wild type mice compared to WISP1 knockout mice after induction of liver damage. Data represent mean of three independent biological replicates ± S.E.

Taken together, these results showed that ER stress is involved in liver damage after CCl_4; [99], however it may not be the reason for the enhanced susceptibility in WISP1 knockout mice.

3.12.7 MAPK and inflammation-associated signaling pathways are not altered in WISP1 knockout and wild type mice after paracetamol administration

Previous results suggested alterations in MAPK associated signaling pathways after administration of CCl_4 in wild type mice compared to WISP1 knockout mice. In order to clarify whether signaling pathways were also altered upon APAP administration, western blot analysis was performed. Therefore, wild type and WISP1 knockout mice were injected intraperitoneally using 300 mg/kg APAP for 30min, 2h, 4h, 8h, 12h and 24h. PBS was used as vehicle control for 24h. Western blot analysis showed a strong activation of JNK at 2h and 4h after APAP administration (Figure 61). The phosphorylation decreased at 8h and 12h, returning back to control levels at D1. However, quantifications of signal volumes revealed no differences in the activation of JNK in wild type mice compared to WISP1 knockout mice.

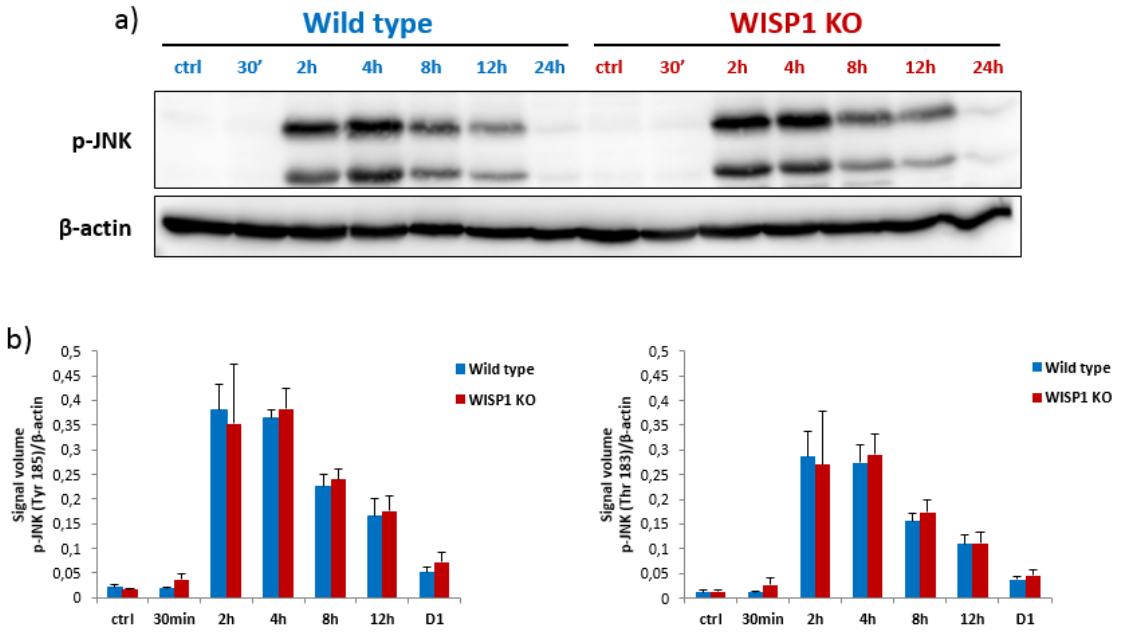

Figure 61: Activation of JNK in wild type mice and WISP1 knockout mice upon APAP administration. a) Western blot analysis of JNK levels after administration of 300 mg/kg APAP in wild type and WISP1 knockout mice for the indicated time points. b) Quantification of western blot analysis. Phosphorylation of JNK was detected as early as 2h and decreased until 12h after APAP administration. β-actin was used as loading control. Results are representative of three independent biological replicates per time point. Data are mean values ± S.E.

Strong phosphorylation of ERK1/2 was observed at 2h up to 12h after APAP administration (Figure 62). Western blot quantification of three independent biological replicates did not reveal significant differences in wild type mice compared to WISP1 knockout mice.

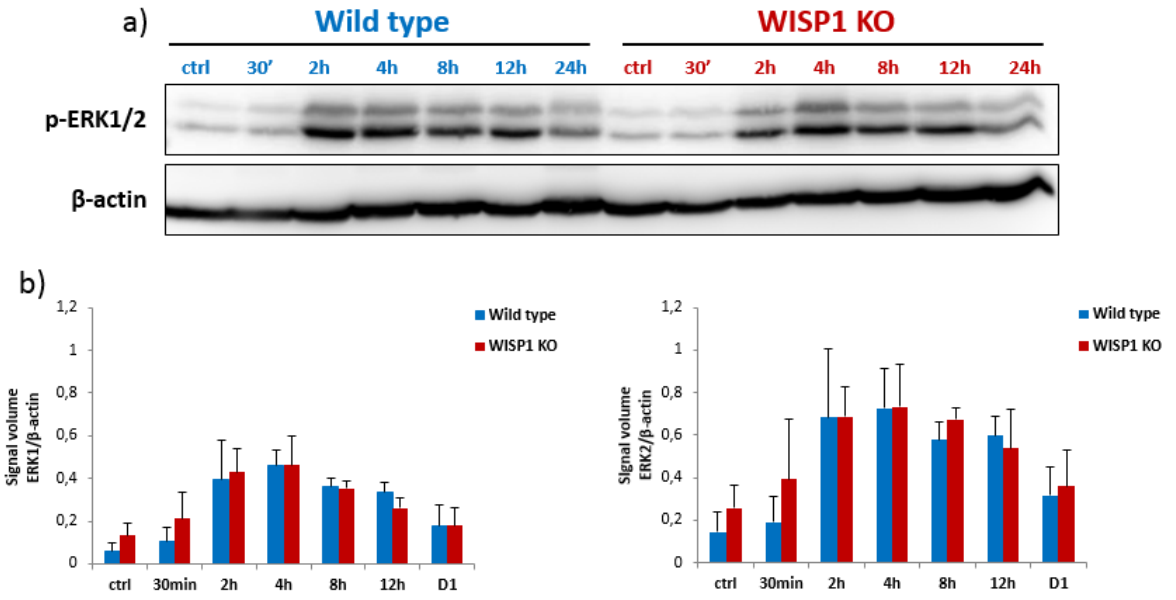

Figure 62: Activation of ERK1/2 in wild type mice and WISP1 knockout mice upon APAP administration. Western blot analysis of ERK1/2 levels after administration of 300 mg/kg APAP in wild type and WISP1 knockout mice. b) Quantification of western blot analysis. Phosphorylation of ERK1/2 was observed at 2h up to D1 after APAP administration. However, no significant difference was observed in the wild type mice compared to WISP1 knockout mice. β-actin was used as loading control. Results are representative of three independent biological replicates per time point. Data are mean values ± S.E.

Taken together, these results demonstrated that the activation of MAPK associated signaling pathways was not significantly altered upon APAP administration in wild type mice compared to WISP1 knockout mice. These results led to the hypothesis that protective effects of WISP1 are not mediated through these signaling pathways after APAP administration.

3.12.8 Activation of hepatoprotective signaling (STAT3) is enhanced in WISP1 knockout mice compared to wild type mice

Previous results for MAPK associated signaling pathways revealed differences upon the deletion of WISP1 after administration of 460 mg/kg CCl_4. Since these pathways are known to be induced by growth factors, cytokines or cellular stress, the hypothesis was that inflammation plays an important role when regarding WISP1 phenotype [88, 179].

The hepatoprotective signal transducer and activator of transcription 3 (STAT3) is known to be induced by pro-inflammatory interleukin 6 (IL6) [55]. In order to study the activation of STAT3 signaling in wild type and WISP1 knockout mice, western blot analysis was performed using liver homogenates after CCl_4 administration. Analysis revealed an enhanced and prolonged STAT3 activation in the WISP1 knockout mice starting at 12h until D1 after induction of liver damage (Figure 63).

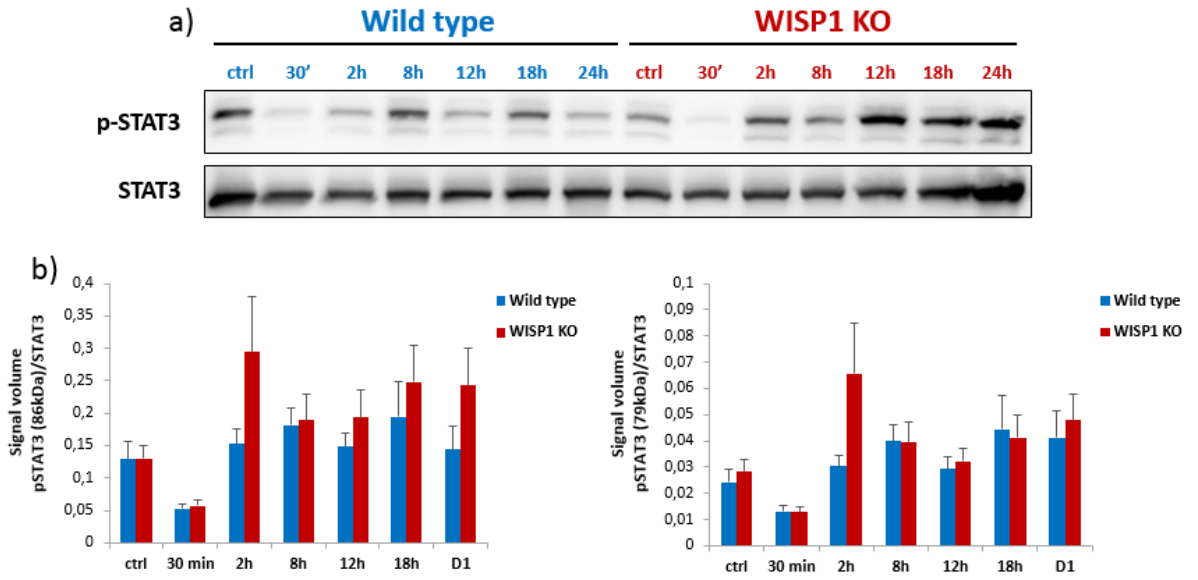

Figure 63: Activation of STAT3 in wild type mice and WISP1 knockout mice upon CCl_4 administration. a) Western blot analysis of STAT3 levels after administration of 460 mg/kg CCl_4 in wild type and WISP1 knockout mice. b) Quantification of western blot analysis. Activation of STAT3 signaling was observed starting at 8h until 18h in the wild type mice. Furthermore the analysis showed a prolonged and enhanced activation of STAT3 in the WISP1 knockout mice starting at 12h until D1. Total STAT3 was used as reference control. Results are representative of six independent biological replicates per time point. Data are mean values ± S.E.

Interestingly, western blot analysis of STAT3 signaling revealed even stronger activation of the hepatoprotective signaling in WISP1 knockout mice, although those mice exhibited enhanced liver damage. Besides the hepatoprotective effect of STAT3, its activation is also linked to inflammation. This led to the hypothesis that WISP1 knockout mice may display a higher inflammatory state, since phosphorylation of STAT3 can be induced by pro-inflammatory cytokines, such as interleukin 6 (IL6) [55].

3.12.9 Deletion of WISP1 does not alter inflammation-associated signaling upon APAP administration

Previous results suggested alterations regarding phosphorylation of STAT3 in WISP1 knockout mice after administration of 460 mg/kg CCl_4. In order to study the activation of STAT3 after administration of 300 mg/kg APAP, western blot analysis was performed. Protein lysates were prepared from wild type and WISP1 knockout mice treated for 30min, 2h, 4h, 8h, 12h and 24h. Activation of STAT3 signaling was enhanced at 2h until 12h upon APAP administration (Figure 64). At 4h, western blot analysis showed a slightly stronger activation of STAT3 signaling in WISP1 knockout mice compared to wild type mice.

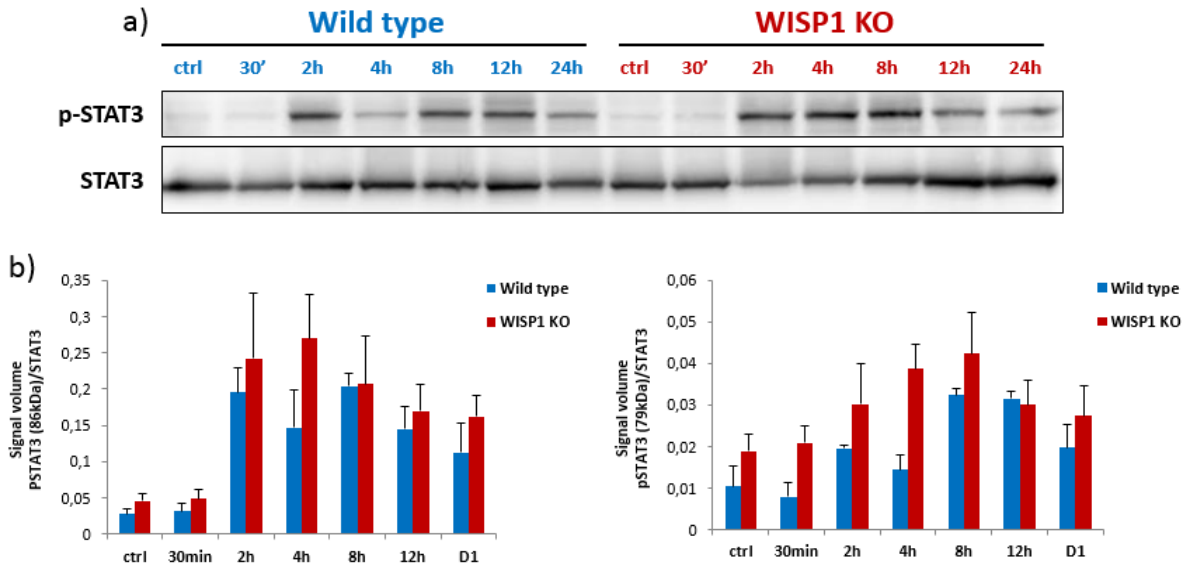

Figure 64: Activation of STAT3 in wild type mice and WISP1 knockout mice upon APAP administration. Western blot analysis of STAT3 levels after administration of 300 mg/kg APAP in wild type and WISP1 knockout mice. b) Quantification of western blot analysis. Results revealed phosphorylation of STAT3 at 2h until 12h after APAP administration. Stronger activation of STAT3 was observed in WISP1 knockout mice at 4h. Total STAT3 was used as loading control. Results are representative of three independent biological replicates per time point. Data are mean values ± S.E.

In conclusion, western blot analysis revealed slightly stronger activation of STAT3 only at 4h in WISP1 knockout mice compared to wild type mice.

3.13 Inflammation-associated genes are stronger induced by the absence of WISP1

Sterile inflammation is a well-known factor during various acute and chronic liver diseases [52, 53]. However, its contribution to liver regeneration versus enhancing liver injury is not well-known and still under debate [52, 184]. For example, inhibition of DAMP receptors or antagonism of TLRs during liver ischemia-reperfusion were shown to protect against hepatic ischemia-reperfusion injury [70, 71], suggesting a pro-damaging role of inflammation. In contrast, depletion of macrophages by clodronate liposomes led to enhanced liver damage after administration of APAP, suggesting a pro-regenerative role upon acute liver damage [185].

First, in order to study cytokine expression upon CCl_4-induced liver injury in wild type and WISP1 knockout mice, quantitative RT-PCR was performed. Results revealed an increase of TNFα, Il6, Lcn2 and IFNγ expression at 12h and 18h (Figure 65). Interestingly, the induction of TNF and IL-6 was stronger in WISP1 knockout mice at 12h and 18h after administration of CCl_4, with a slight increase in IFNγ expression at 12h.

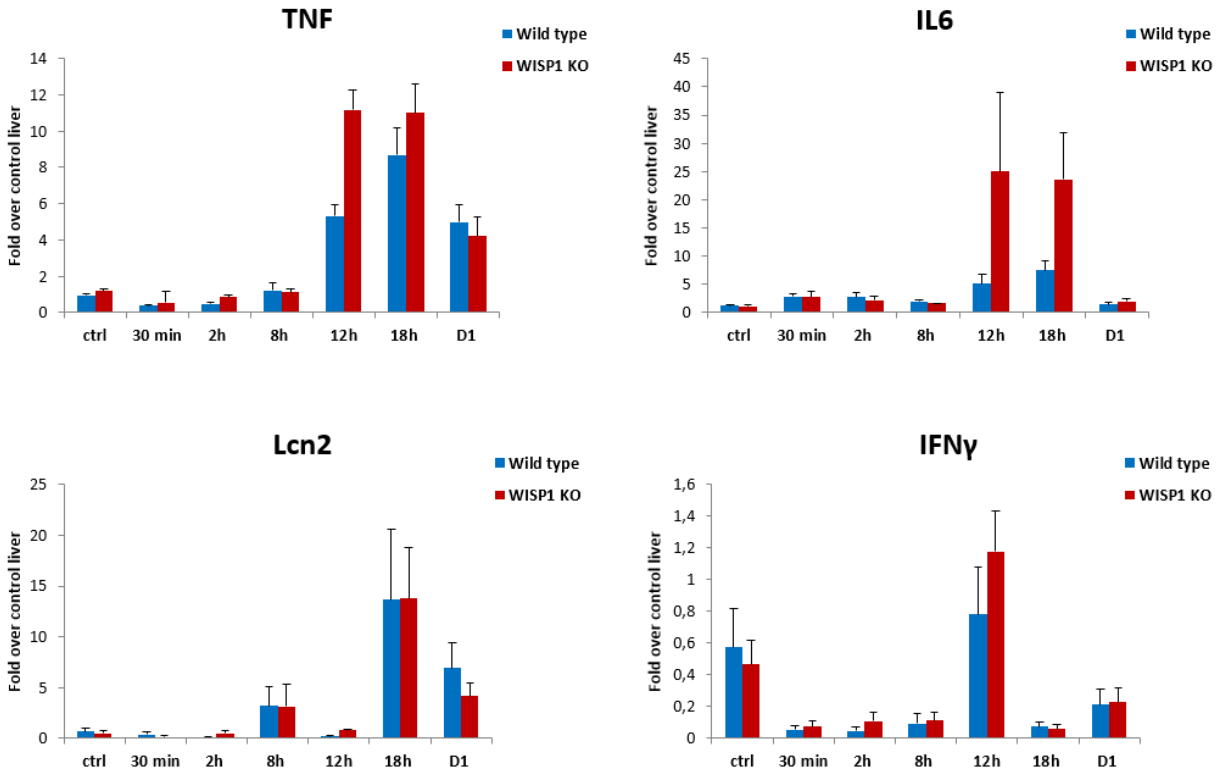

Figure 65: Time-dependent quantitative RT-PCR of inflammatory cytokines TNFα, Il6, Lcn2 and IFNγ in wild type mice and WISP1 knockout mice for the indicated time points. Induction of cytokine expression was observed for all targets between 12h and D1. However, quantitative RT-PCR showed an enhanced expression of TNFα and Il6 after 12h and 18h in WISP1 knockout mice compared to wild type mice. At 12h, a slight increase in IFNγ expression was observed after CCl_4 administration. Data represent mean of six independent biological replicates ± S.E.

These results suggest that the induction of inflammation upon CCl_4 intoxication is enhanced in livers of WISP1 KO mice.

3.13.1 Expression of neutrophil recruitment-associated chemokines are increased in WISP1 knockout mice

The next step was to investigate the expression of different chemokines since they are known to be involved in leukocytes chemoattraction to the site of injury. Moreover, low concentration levels of CXC chemokines, such as CXCL1-2, CXCl3 or CXCL5-8, were associated with proliferation and liver repair; whereas, high levels were related to hepatotoxicity, upon binding to their receptor CXCR2 [178]. The results show an induction in chemokines´ expression for all targets after the induction of liver damage in wild type and WISP1 knockout mice (Figure 66). However, an enhanced expression in WISP1 knockout mice was observed for CCl3 and CCl4 at 12h, for CCl2 at 8h, for CCl5, Cxcl1 and Cxcl5 at 18h respectively.

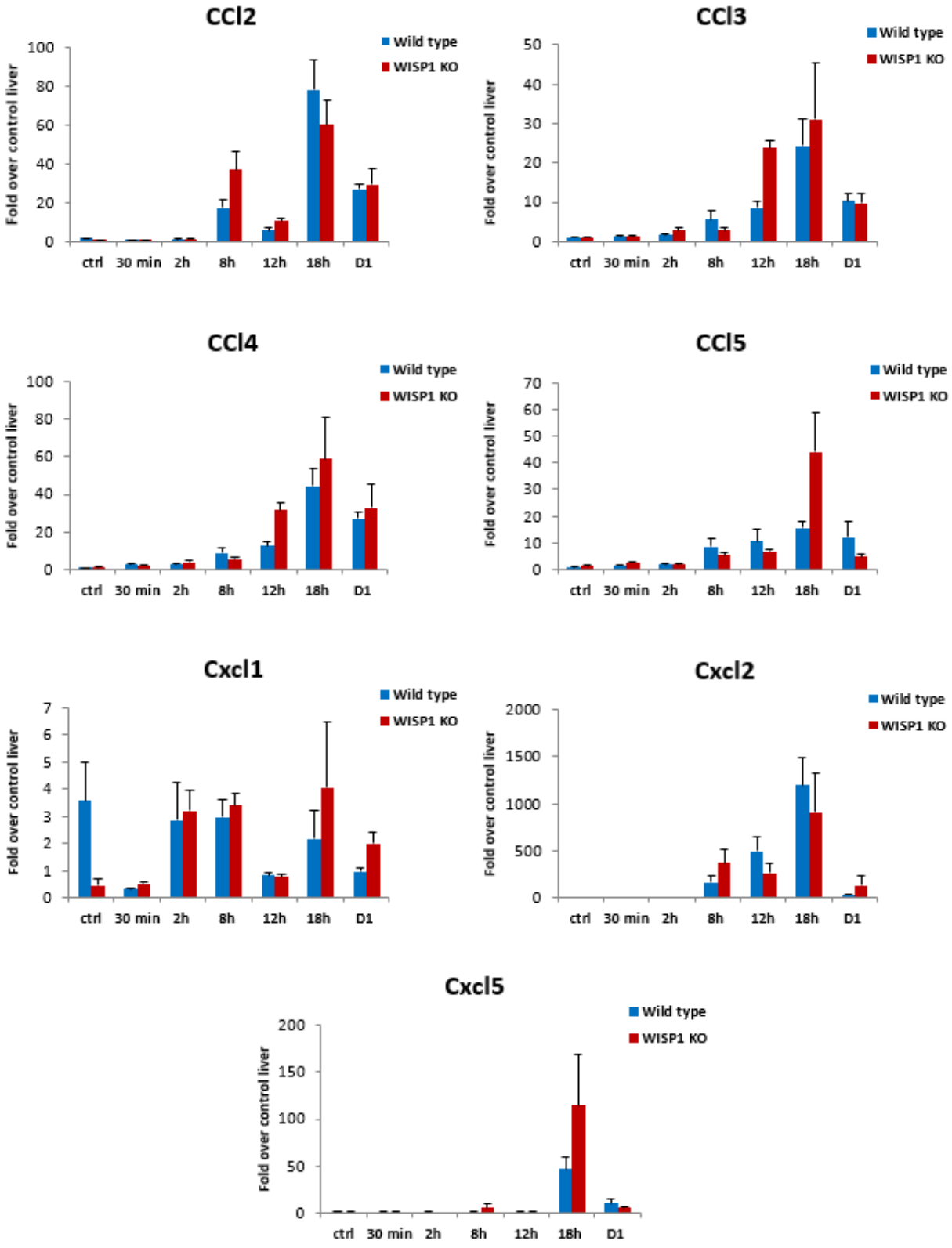

Figure 66: Time-dependent quantitative RT-PCR of various chemokines after administration of 460 mg/kg CCl_4 in wild type mice and WISP1 knockout mice for the indicated time points. Results revealed enhanced expression of CCl2, CCl3, CCl4, CCl5, Cxcl1 and Cxcl5 in WISP1 knockout mice compared to wild type mice at 8h up to 18h respectively. Data represent mean of six independent biological replicates ± S.E.

In conclusion, the levels of almost all chemokines investigated were stronger induced in WISP1 knockout mice upon CCl_4 intoxication, suggesting that deletion of WISP1 enhances the inflammatory response during acute liver injury.

3.13.2 WISP1 knockout mice shows enhanced immune cell infiltration compared to wild type mice

Signal transduction and quantitative RT-PCR revealed a higher inflammatory response in WISP1 knockout mice after induction of liver damage using 460 mg/kg CCl_4. In order to clarify if immune cell infiltration was altered upon deletion of WISP1, immunohistochemical staining was performed with antibodies targeting markers for all leukocytes (CD45), neutrophils (Ly6G) and Kupffer cells (F4/80).

Leukocytes (CD45 positive cells) were uniformly distributed in the control condition of both the wild type and WISP1 knockout mice (Figure 67). In the early time points after CCl_4 administration (30min until 8h), there were no differences between the wild type and WISP1 knockout mice. At 18h and on D1, a strong immune cell infiltration was detected at the site of injury in both mice (black arrows indicate positively-stained leukocytes).

Immunohistochemical analysis (Figure 68) revealed just few positive neutrophils in the control condition and in the early time points after CCl_4 administration (30min up to 8h). At 18h and D1, there was a strong neutrophil infiltration at the site of injury in both the WISP1 knockout as well as wild type mice (black arrows indicate positively stained neutrophils).

Figure 69 shows immunohistochemical analysis of Kupffer cells in wild type and WISP1 knockout mice. In the control conditions and at early time points after administration of CCl_4 (30min until 8h), Kupffer cells were uniformly distributed in wild type and WISP1 knockout mice. At 18h, there was an accumulation of Kupffer cells at the borders of the pericentral regions in wild type mice. WISP1 knockout mice exhibited enhanced Kupffer cell infiltration towards the pericentral dead cell area, as well as the periportal area. Furthermore, both wild type and WISP1 knockout mice showed attenuated Kupffer cell infiltration on D1 of treatment.

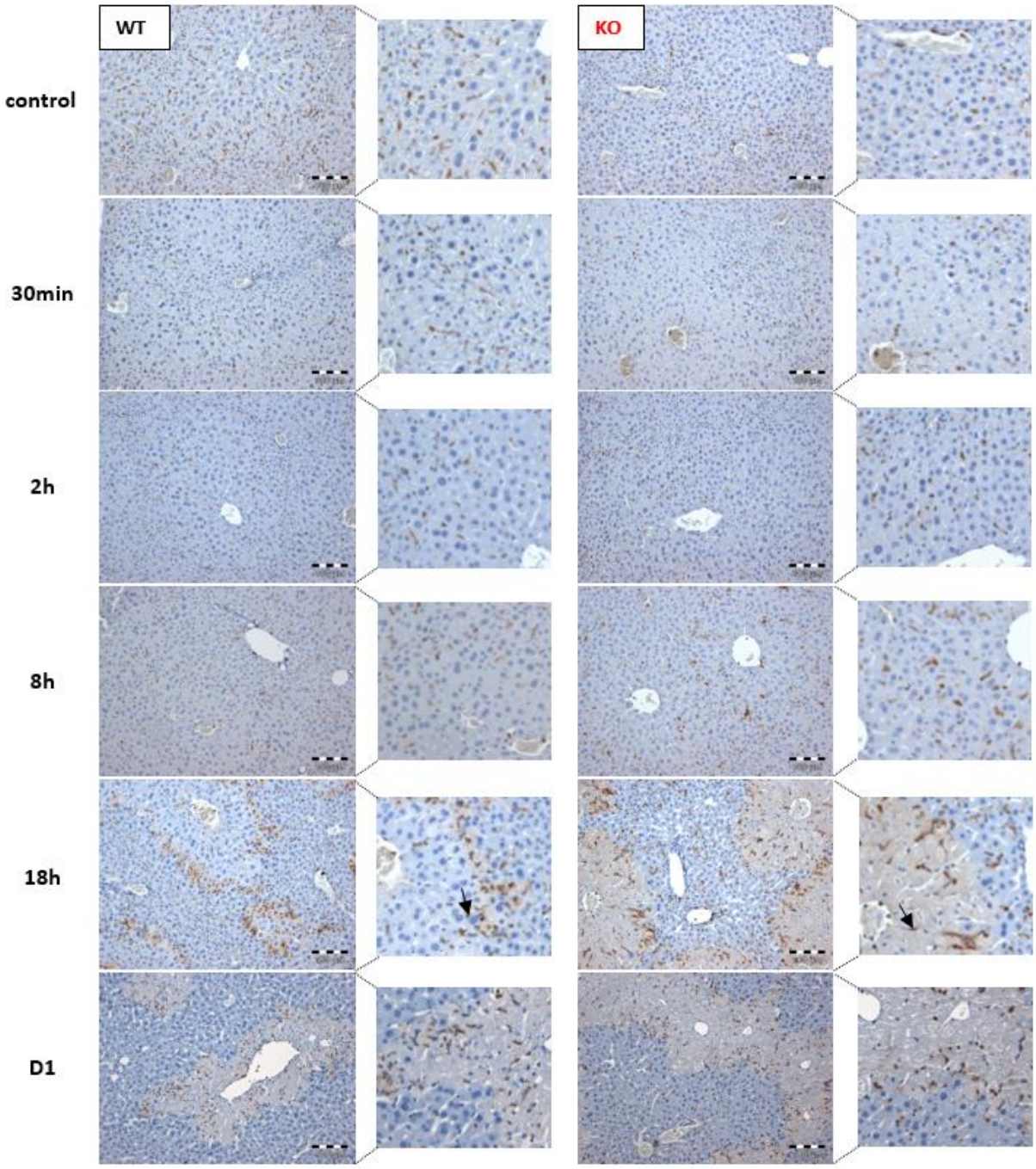

Figure 67: Immunohistochemical staining of leukocytes (CD45) in wild type and WISP1 knockout mice after administration of 460 mg/kg CCl_4 for the indicated time points. Leukocytes were detected and found to be homogenously distributed in the control livers of wild type and WISP1 knockout mice (black arrows indicate positively stained brown leukocytes). Although, the signal in WISP1 knockout mice seemed to be less pronounced. At 18h and D1 after intoxication, leukocytes accumulated at the border of the pericentral area. Representative images of three biological replicates per time point, scale bars represent 100 µm.

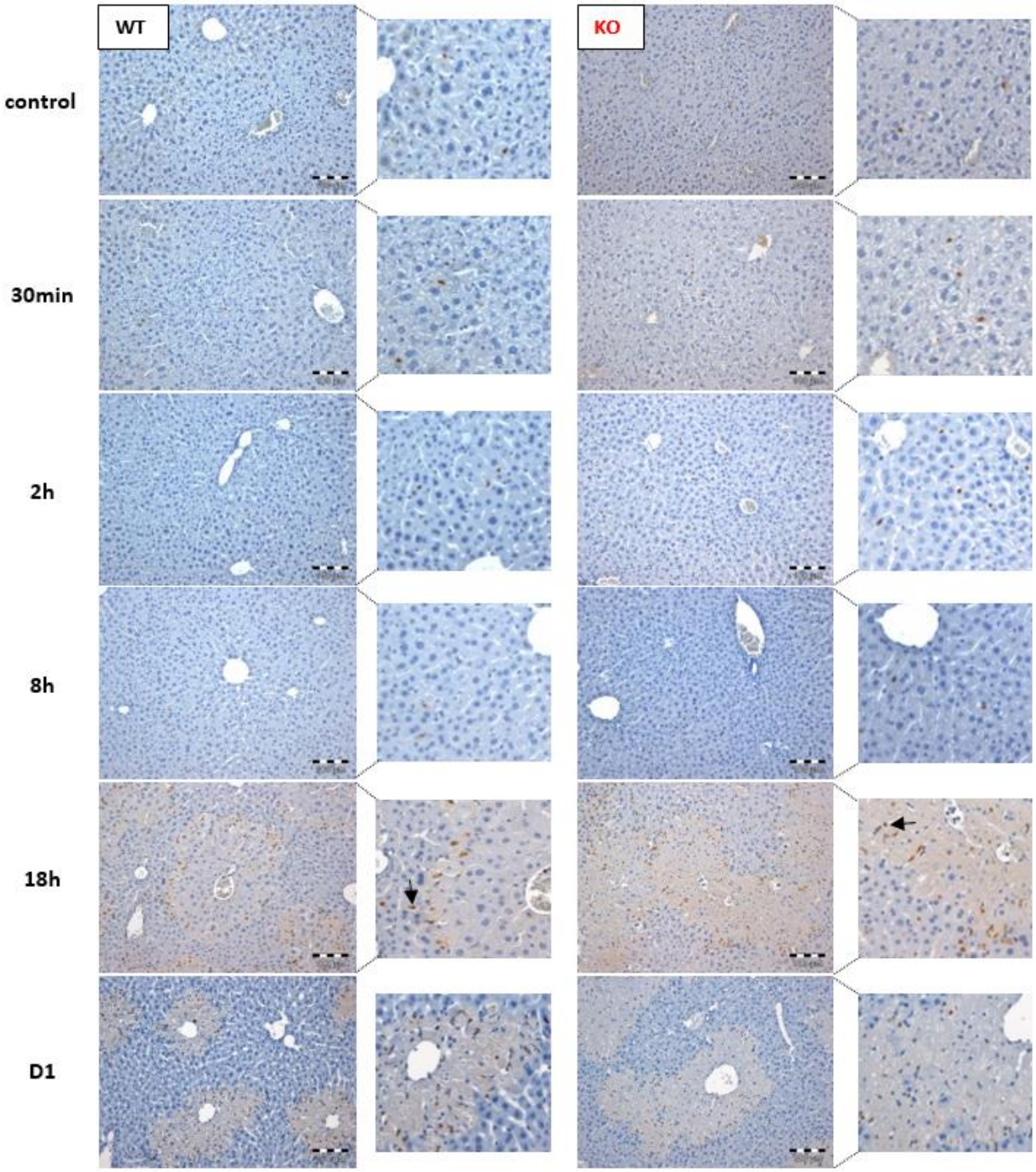

Figure 68: Immunohistochemical staining of Neutrophils (Ly6G) in wild type mice and WISP1 knockout mice after administration of 460 mg/kg CCl_4 for the indicated time points. Only few neutrophils were observed in the control tissue, as well as at 30min up to 8h after administration of CCl_4. At 18h and D1, neutrophils infiltrated in the liver to the site of injury (black arrows indicate positively stained brown neutrophils). Representative images of three mice per time point, scale bars represent 100 µm.

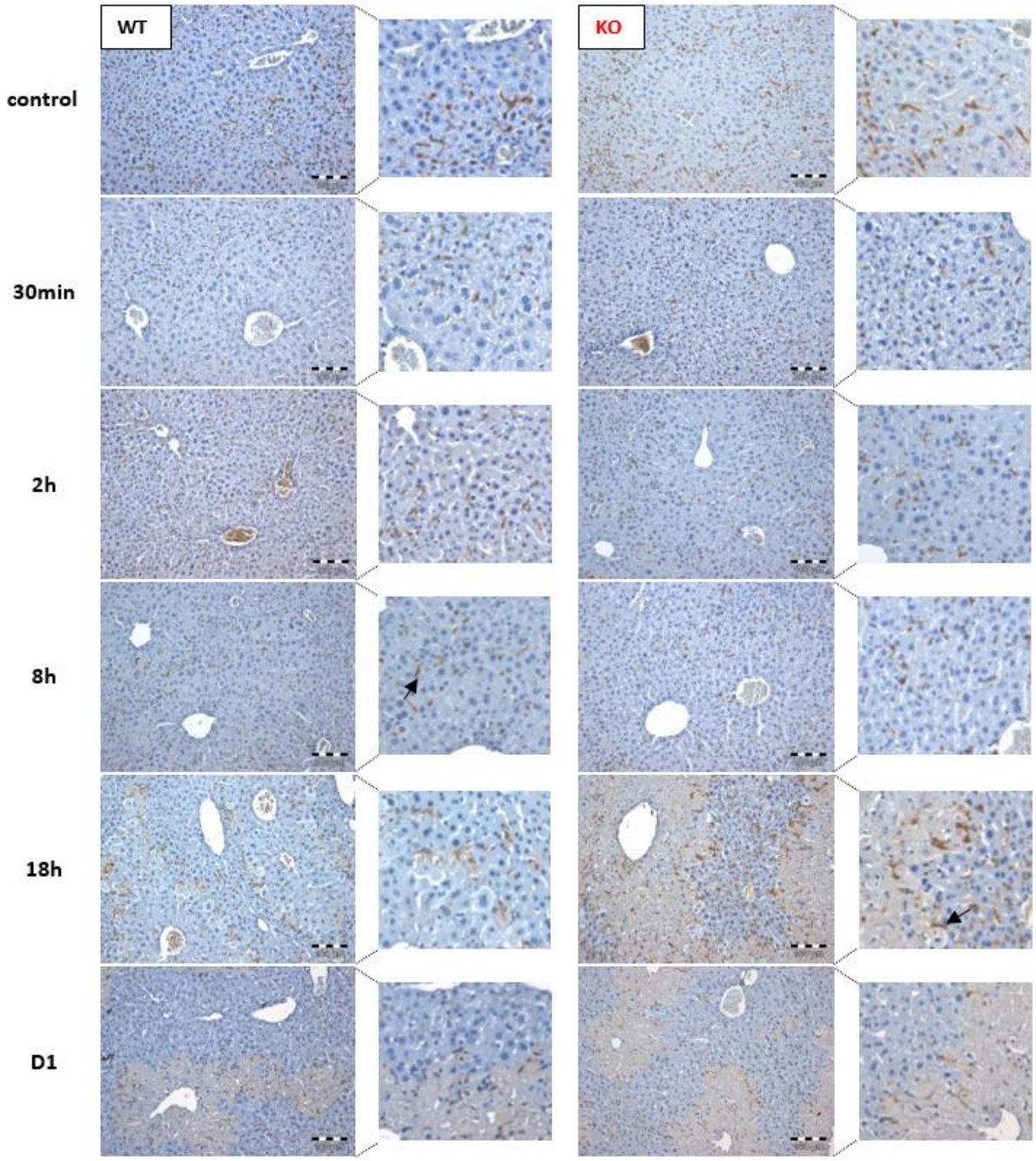

Figure 69: Immunohistochemical staining of Kupffer cells (F4/80) in wild type and WISP1 knockout mice after administration of 460 mg/kg CCl_4 for the indicated time points. Homogenous distribution of Kupffer cells was observed in the control tissue, as well as at 30min up to 8h after administration of CCl_4. At 18h, Kupffer cells infiltrate at the border of the pericentral area in wild type mice (black arrows indicate brown stained Kupffer cells). Infiltration was observed to be enhanced in the WISP1 knockout mice at 18h. Representative images of three mice per time point, scale bars represent 100µm.

Immunohistochemical analyses revealed strong immune cell infiltration upon CCl_4 administration in wild type and WISP1 knockout mice. In order to quantify the number of infiltrating leukocytes and neutrophils, 10 images were counted per biological replicate for positively-stained cells. Quantification of leukocytes revealed a reduced numbers in WISP1 knockout mice in the control condition compared to wild type mice (Figure 70). However, more leukocytes were counted in WISP1 knockout mice at 18h after CCl_4 administration.

There was also increased neutrophil infiltration in WISP1 knockout mice as early as 8h, compared to wild type counterparts, particularly at 8h and 18h after induction of liver injury.

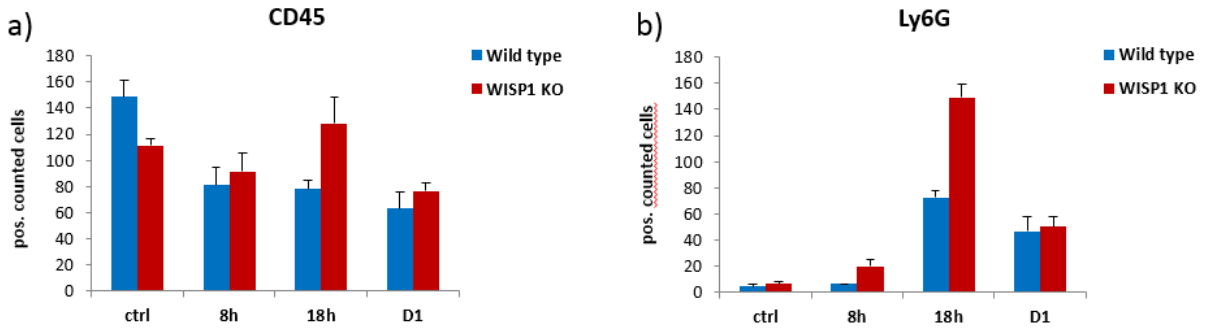

Figure 70: Time-dependent quantifications of immunohistochemical analysis of a) leukocytes and b) neutrophils. Results for CD45 revealed less leukocytes in WISP1 knockout mice in the control condition. However, at 18h more leukocytes were detected in the WISP1 knockout mice. More neutrophils were determined in WISP1 knockout mice already at 8h after CCl_4 administration. At 18h, the number of neutrophils is doubled in WISP1 knockout mice compared to wild type mice. Data represent mean of 10 images counted per biological replicate, three biological replicates were used per time point ± S.E.

Taken together, these investigations indicated that there is a higher immune cell infiltration in WISP1 knockout mice upon CCl_4 intoxication.

3.14 WISP1 knockout hepatocytes reveal higher susceptibility to cytokine-induced cell death

The previous results revealed an enhanced inflammatory response in WISP1 knockout mice after administration of 460 mg/kg CCl_4. To gain insights into whether inflammation could be the cause for enhanced liver damage in WISP1 knockout mice, primary hepatocytes from wild type and WISP1 knockout mice were isolated and cultivated in collagen monolayer configuration. Hepatocytes were stimulated using TNFα and TGFβ in combination with actinomycin D to block transcription and DNA replication [186] in order to induce apoptosis.

Microscopically, no difference could be observed in WISP1 knockout hepatocytes regarding the morphology and viability in the control condition compared to wild type hepatocytes (Figure 71, 72). Upon stimulation with TNFα, apoptosis was observed in wild type and WISP1 knockout hepatocytes at already low concentrations. However, the WISP1 knockout hepatoyctes revealed enhanced apoptosis starting from 5 ng/ml up to 10 ng/ml TNFα (indicated by red circles) compared to wild type hepatocytes.

TGFβ stimulation also caused an increase in apoptosis in both wild type and WISP1 knockout hepatocytes in a concentration-dependent manner (Figure 72). Importantly, the

WISP1 knockout hepatocytes exhibited more apoptotic cells starting at concentrations of 5 ng/ml up to 10 ng/ml of TGFβ (indicated by red circles).

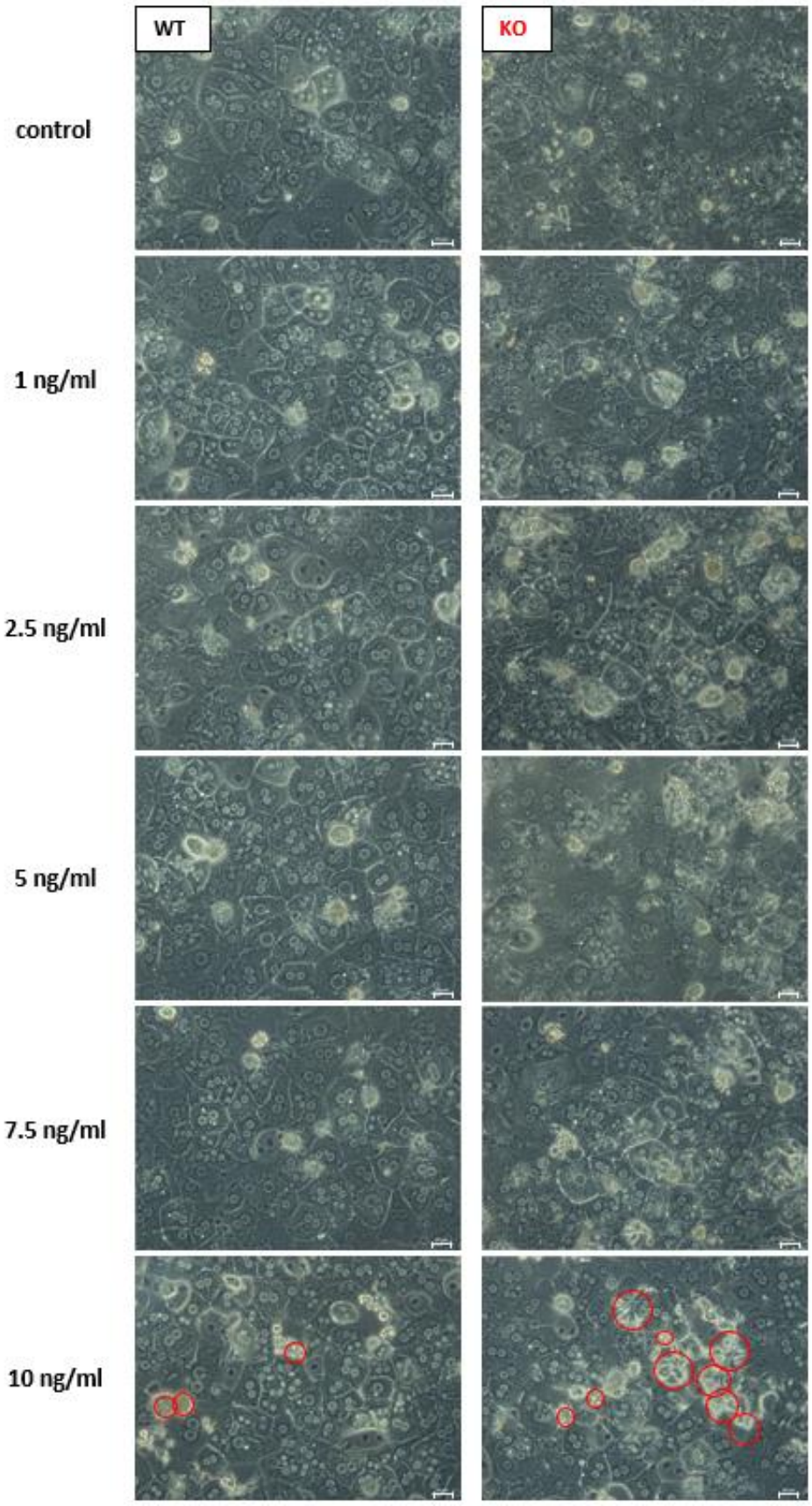

Figure 71: Concentration-dependent *in vitro* stimulation of primary wild type and WISP1 knockout hepatocytes using TNFα for 8h. *In vitro* stimulation using different concentrations of TNFα revealed more dead cells at 5 ng/ml up to 10 ng/ml in the WISP1 knockout hepatocyte culture compared to wild type hepatocyte culture (indicated by red circles). Representative images of four independent biological replicates per concentration. Scale bars represent 20 µm.

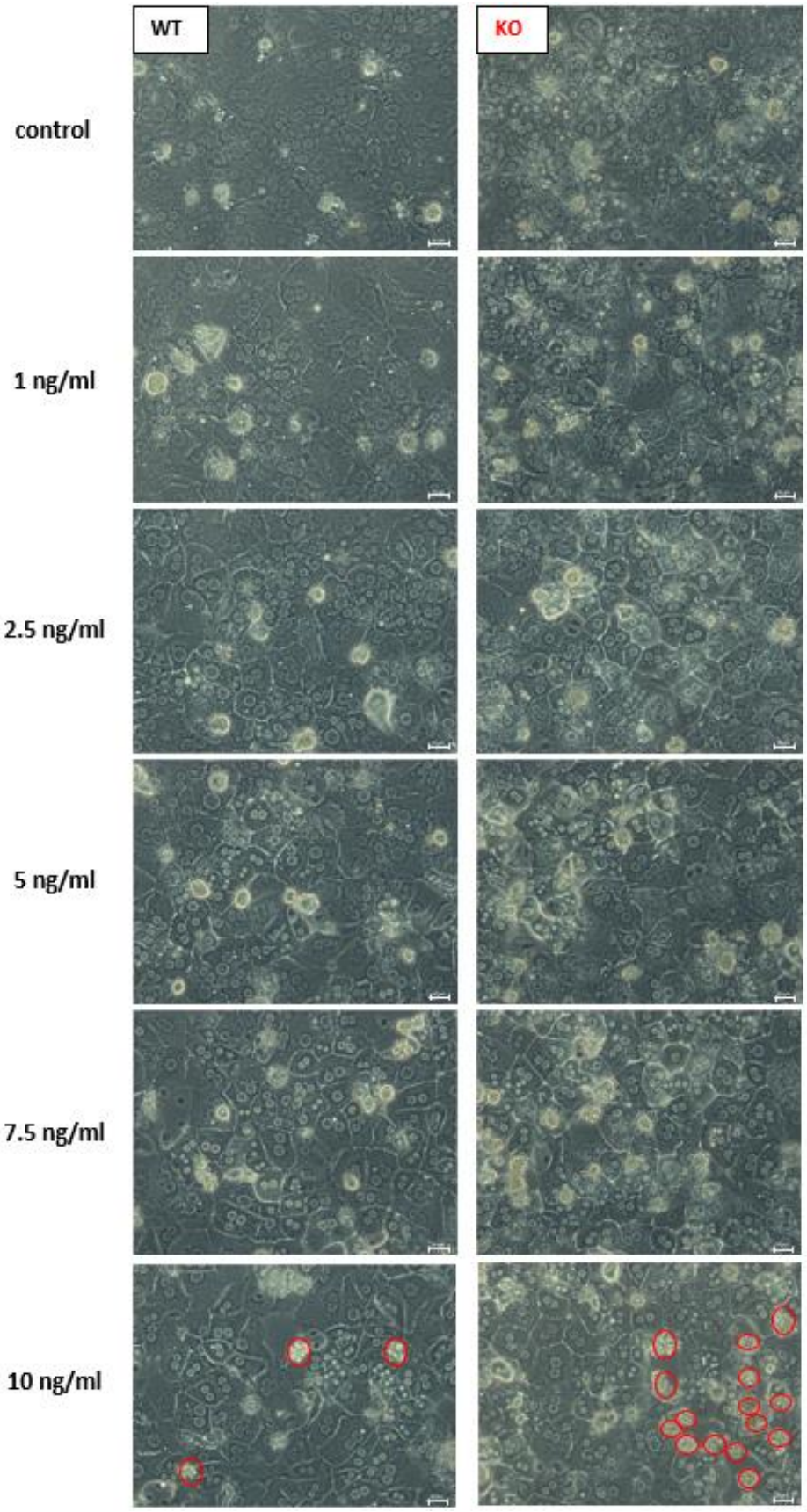

Figure 72: Concentration-dependent *in vitro* stimulation of primary wild type and WISP1 knockout hepatocytes using TGFβ for 24h. *In vitro* stimulation using different concentrations of TGFβ revealed more dead cells at 5 ng/ml up to 10 ng/ml in the WISP1 knockout hepatocyte culture compared to wild type hepatocyte culture (indicated by red circles). Representative images of three independent biological replicates per concentration. Scale bars represent 20 µm.

Microscopic assessment of apoptosis induction revealed enhanced susceptibility to TNFα as well as TGFβ stimulation in both the wild type and WISP1 knockout hepatocytes. For quantitative assessment, apoptotic cells of wild type and WISP1 knockout conditions were quantified. In this case, 5 images per concentration and biological replicate were counted. Quantification revealed a significant increase in apoptotic cells upon TNFα stimulation in the WISP1 knockout hepatocyte culture at all concentrations (Figure 73 a) compared to wild type conditions. Analyses of TGFβ stimulation (Figure 73 b) showed significantly enhanced apoptosis in the WISP1 knockout hepatocyte culture at just 7.5 ng/ml and 10 ng/ml.

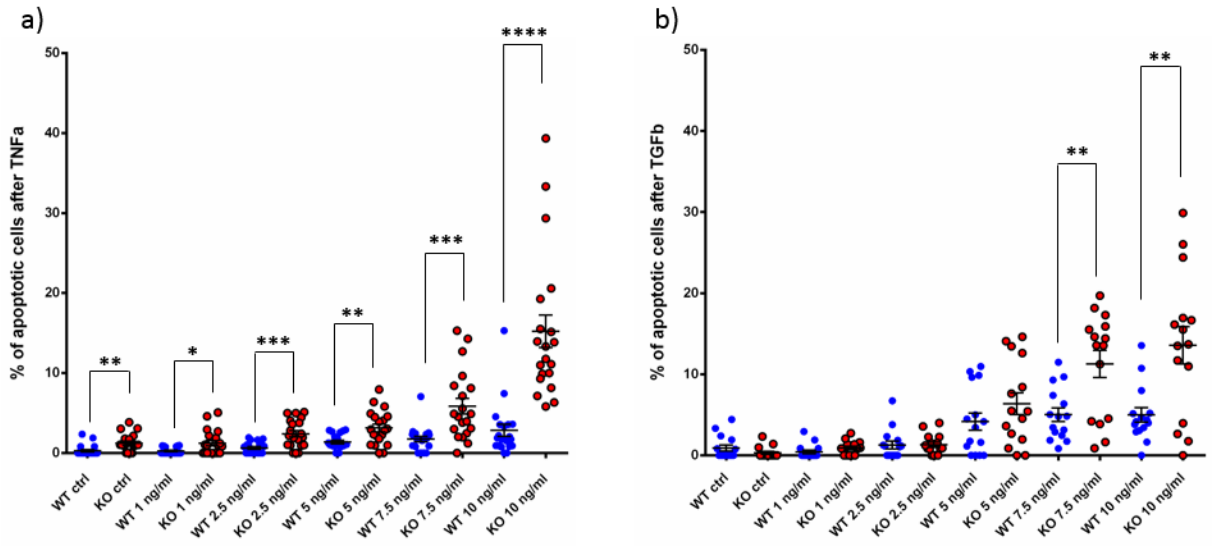

Figure 73: Concentration-dependent quantification of apoptotic cells after *in vitro* stimulation using a) TNFα and b) TGFβ. Stimulations using TNFα revealed a significant increase in the percentage of apoptotic cells at all concentrations in the WISP1 knockout hepatocyte culture. TGFβ stimulation showed a significant increase in the percentage of apoptotic cells at just 7.5 ng/ml and 10 ng/ml in the WISP1 knockout hepatocyte culture. Data represent mean of four (TNFα); and three (TGFβ) biological replicates ± S.E., five images were counted for each biological replicate, ****P<0.0001, ***P<0.001, **P<0.01, *P<0.05 to wild type condition, unpaired t-test.

Taken together, this investigation showed enhanced apoptosis upon TNFα and TGFβ stimulation in WISP1 knockout hepatocytes culture compared to wild type hepatocytes culture. However, TGFβ stimulation showed higher variances between the biological replicates than after stimulation with TNFα. These results supported the hypothesis that inflammation is involved in the development of enhanced liver damage in WISP1 knockout mice.

3.14.1 Cleaved caspase 3 is stronger induced in WISP1 knockout hepatocytes upon stimulation with TNFα

In order to study the differential sensitivity to induction of apoptosis in wild type and WISP1 knockout hepatocytes, western blot analysis of cleaved caspase 3 was performed using protein lysates from WISP1 knockout and wild type hepatocytes. Cleaved caspase 3

was observed upon TNFα stimulation in a time-dependent manner in both wild type and WISP1 knockout hepatocytes (Figure 74). However, quantification of the western blot analysis revealed higher levels upon deletion of WISP1 in hepatocytes.

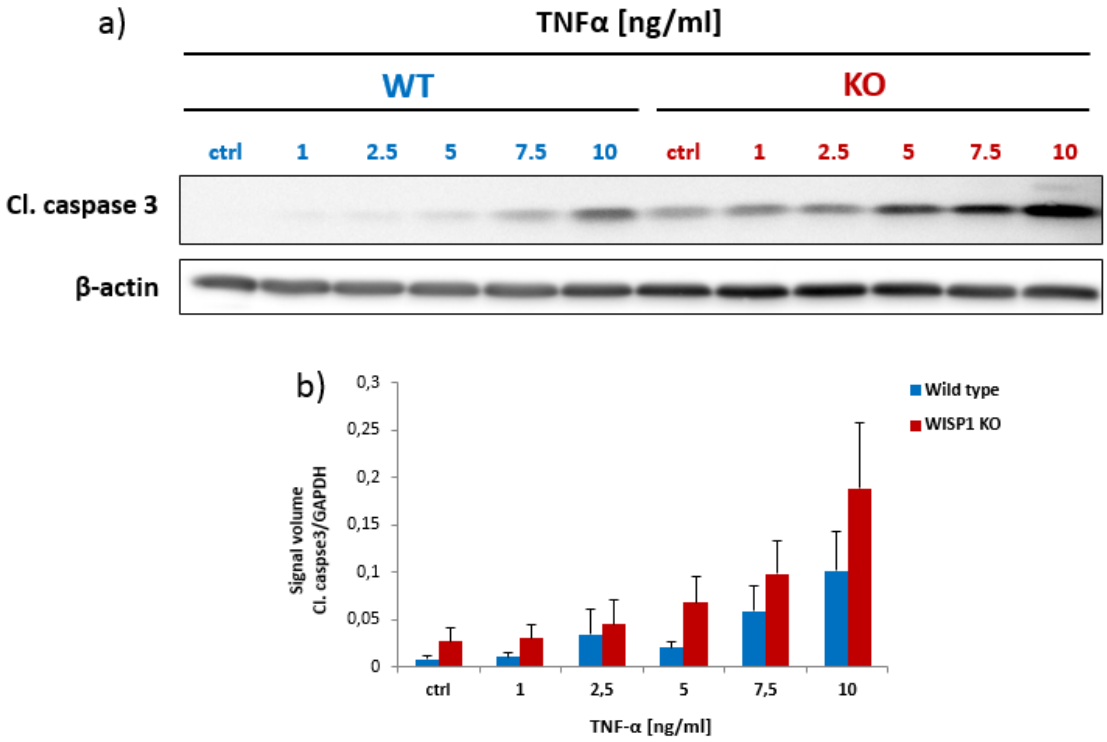

Figure 74: Cleaved caspase 3 levels in wild type and WISP1 knockout hepatocytes upon TNFα stimulation. a) Western blot analysis of cleaved caspase 3 levels in wild type and WISP1 knockout hepatocytes after stimulation using TNFα for 8h for the indicated concentrations. b) Quantification of western blot analysis. Analysis shows a concentration-dependent increase in the cleaved caspase 3 levels in wild type and WISP1 knockout hepatocytes. However, higher levels of cleaved caspase 3 were observed in WISP1 knockout hepatocytes compared to wild type hepatocytes. β-actin was used as loading control. Data represent mean of three independent biological replicates ± S.E.

In conclusion, this result confirmed the microscopic observation of enhanced apoptosis in WISP1 knockout hepatocytes upon TNFα stimulation.

3.14.2 TGFβ stimulation displays no clear difference in cleaved caspase 3 signaling

Since TGFβ stimulation revealed higher sensitivity of WISP1 knockout hepatocytes compared to wild type hepatocytes, protein expression analysis was performed to investigate the cleavage of caspase 3 as a marker of apoptosis. Protein lysates were prepared from primary wild type and WISP1 knockout hepatocytes after stimulation using different concentrations of TGFβ. Results revealed activation of cleaved caspase 3 in both WISP1 knockout and wild type hepatocytes (Figure 75). There were no differences in the

activation of cleaved caspase 3 signaling in wild type hepatocytes compared to WISP1 knockout hepatocytes.

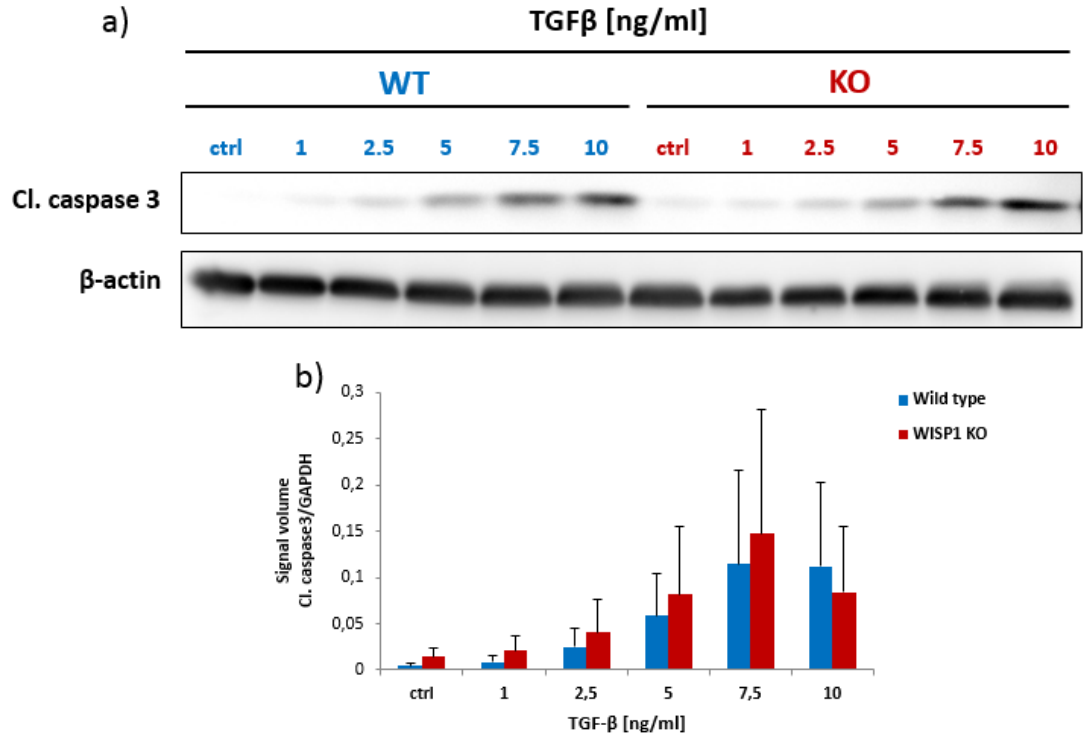

Figure 75: Cleaved caspase 3 levels in wild type and WISP1 knockout hepatocytes upon TGFβ stimulation. a) Western blot analysis of cleaved caspase 3 levels in wild type and WISP1 knockout hepatocytes after stimulation using TGFβ for 24h for the indicated concentrations. b) Quantification of western blot analysis. Results revealed no difference in the activation of cleaved caspase 3 upon TGFβ stimulation in wild type and WISP1 knockout hepatocytes. β-actin was used as loading control. Data represent mean of three independent biological replicates ± S.E.

Taken together, it was shown that there is a comparable activation of cleaved caspase 3 upon TGFβ stimulation in wild type and WISP1 knockout mice. This is may be due to high variability between biological replicates which were already seen upon the quantification of apoptotic cells.

3.15 WISP1 knockout hepatocytes are more susceptible to paracetamol toxicity *in vitro*

The previous analyses revealed enhanced susceptibility of WISP1 knockout mice upon 300 mg/kg APAP administration. Hepatocytes which make up about 80 % of the liver mass [8], were shown to be the main source of WISP1 expression upon CCl_4 administration in mice. Furthermore, pervious investigations by our group revealed that WISP1 is secreted by hepatocytes upon TGFβ stimulation *in vitro* (Campos, unpublished data). Therefore, the next step was to investigate wild type and WISP1 knockout cells upon stimulation using APAP *in vitro* in a collagen sandwich configuration. The first approach was to stimulate the cells using

a concentration range of 1 mM up to 10 mM directly after 3h of plating the cells, followed by 24h of incubation. The second approach was to stimulate the hepatocytes on D1 in culture using the same concentrations for 24h incubation. Propidium iodide staining was performed directly after 24h of stimulation to visualize the dying hepatocytes.

Figure 76 shows results from propidium iodide staining of wild type and WISP1 knockout hepatocytes after stimulation. Hepatocytes are stained positive for propidium iodide already at low (1 mM) concentrations of APAP. Cell death occurred in a concentration-dependent manner in wild type and WISP1 knockout hepatocytes. However, the deletion of WISP1 led to increased cell death upon APAP stimulation compared to wild type hepatocytes.

Stimulation on D1 in culture also led to cell death starting at 1 mM of APAP (Figure 77). Increased concentration induced enhanced cell death in both wild type hepatocytes and WISP1 knockout. The toxic effect of APAP appeared to be more prominent in the WISP1 knockout hepatocytes, where all hepatocytes were shown to be dead at 7.5mM and 10 mM of APAP stimulation.

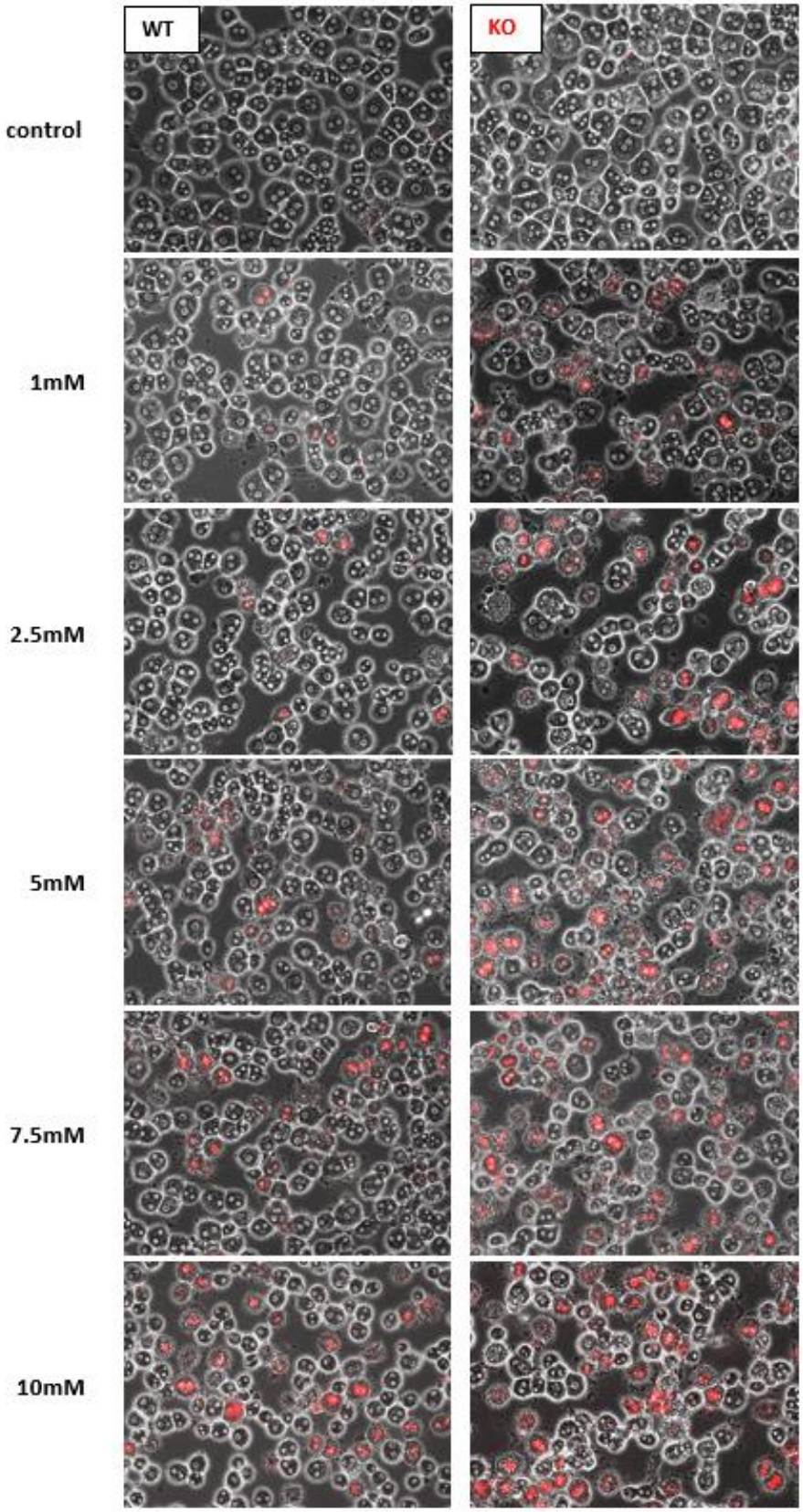

Figure 76: Propidium iodide staining of wild type and WISP1 knockout hepatocytes after stimulation using various concentrations of APAP (3h after plating for 24h). Results show no alterations under control condition in both the wild type culture and WISP1 knockout culture. The number of dead cells increased in a concentration-dependent manner (nuclei were stained red upon cell death). Though, the WISP1 knockout hepatocytes showed an increased number of dead cells compared to wild type hepatocytes. Representative images of three biological replicates, magnification of 20X.

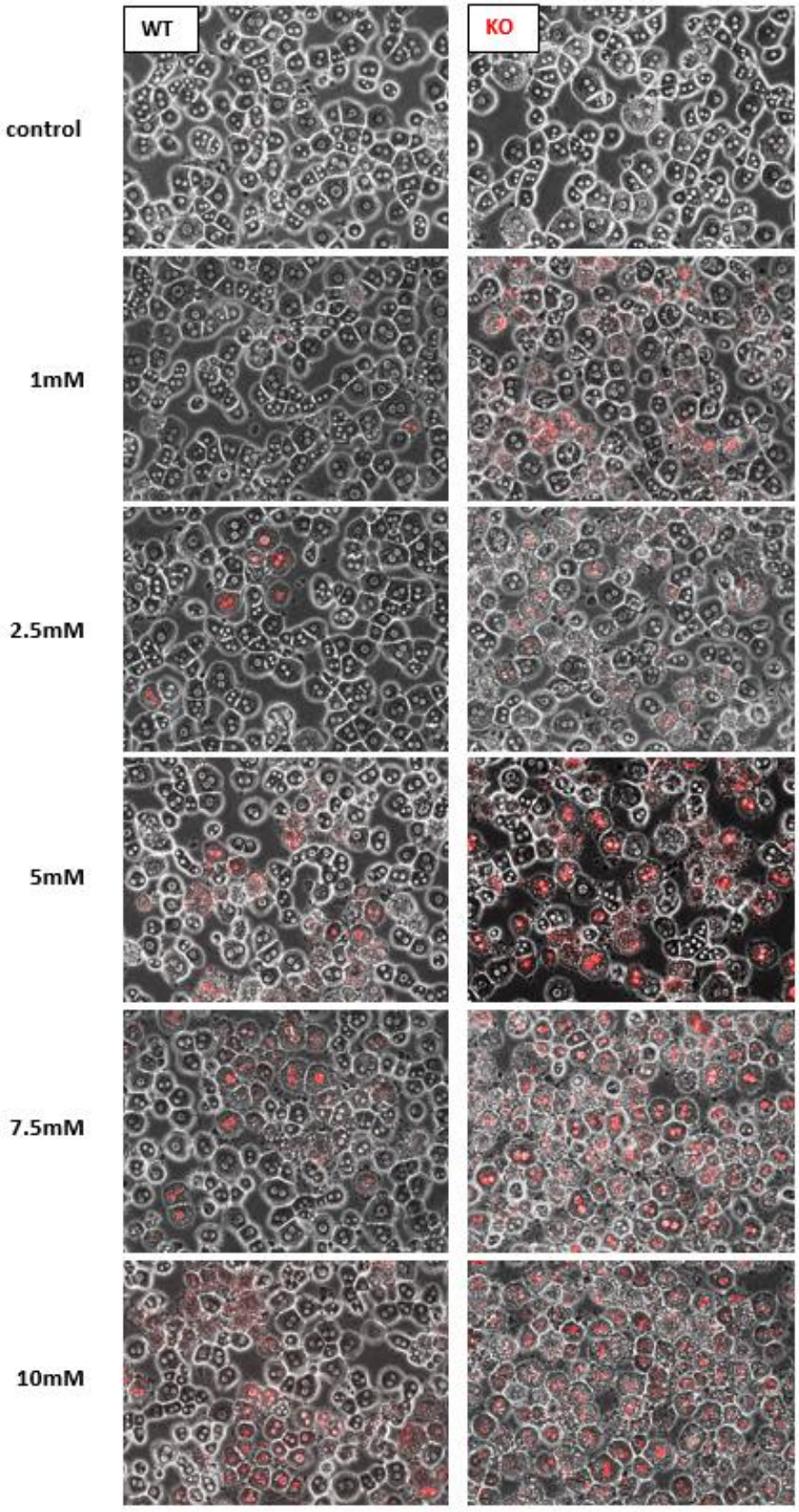

Figure 77: Propidium iodide staining of wild type and WISP1 knockout hepatocytes after stimulation using different concentrations of APAP (24h after plating for 24h). Propidium iodide staining revealed the first dead cells already at 1 mM of APAP. Cell death of hepatocytes (nuclei were stained red upon cell death) increased in a concentration-dependent manner in wild type and WISP1 knockout hepatocytes. Though, the deletion of WISP1 in hepatocytes led to an increased number of dead cells compared to wild type hepatocytes. Representative images of three biological replicates, magnification of 20X.

In order to obtain quantitative measurements of cell death in wild type and WISP1 knockout hepatocytes, propidium iodide staining was quantified. Stimulation after 3h in culture (for 24h) revealed a significant increase in the percentage of dead cells in the WISP1 knockout culture at all the indicated concentrations compared to the wild type culture. Stimulation after 24h in culture (for 24h) also showed a significant increase in the percentage of dead cells at all concentrations in the WISP1 knockout culture compared to wild type culture.

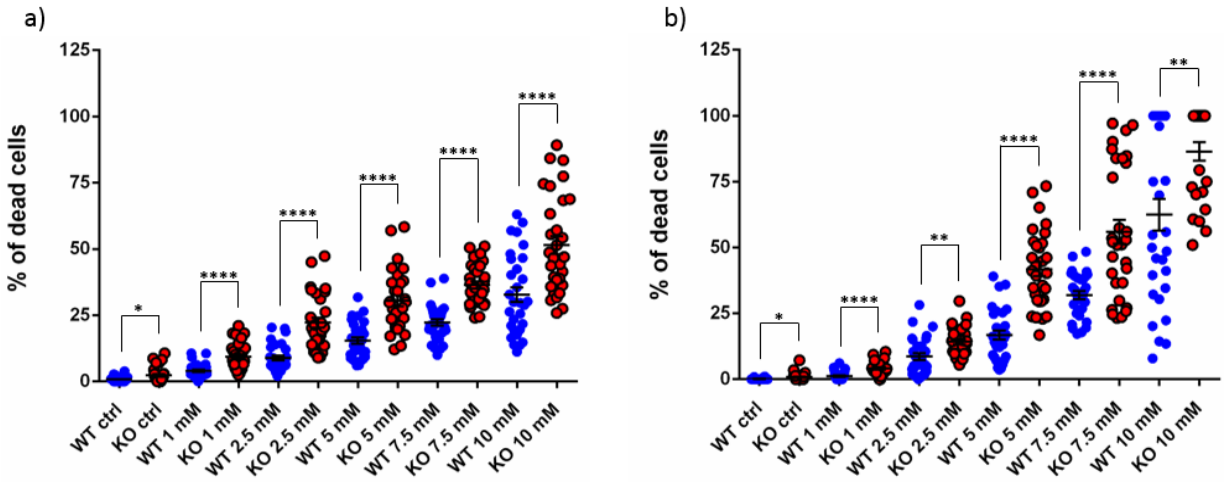

Figure 78: Quantification of dead cells after APAP stimulation a) Stimulation at 3h after plating for 24h. Quantification of dead cells revealed a significant increase in the percentage of dead cells in the WISP1 knockout culture compared to the wild type culture. **b) Stimulation at D1 in culture for 24h.** Quantification detected a significant increase in the percentage of dead cells in the WISP1 knockout culture compared to the wild type culture. Data represent mean of three independent biological replicates ± S.E., 10 images were counted for each biological replicate, ****P<0.0001, **P<0.01, *P<0.05 to wild type condition, unpaired t-test.

Taken together, these results revealed a higher susceptibility of WISP1 knockout hepatocytes to APAP-induced cell death *in vitro*.

3.16 Affymetrix gene array analysis of WISP1 knockout mice revealed alterations in gene expression compared to wild type mice

In order to study gene expression alterations in wild type and WISP1 knockout mice, a time resolved global gene expression profiling using Affymetrix microarrays was performed. For this purpose, wild type and WISP1 knockout mice received a single dose of 460 mg/kg CCl_4 or olive oil as control vehicle intraperitoneally. Liver tissue was collected after early (8h and 12h) and late time points (D1 and D3). For each time point, five wild type and five WISP1 knockout mice were used. Initially, expression levels after 8h, 12h, D1 and D3 of wild type and WISP1 knockout mice were compared to their respective controls. The analysis detected 3,648 genes that were at least 2-fold deregulated in wild type and 4,617 genes deregulated in WISP1 knockout mice, when compared to their corresponding control

group (pValue (FDR) < 0.05). The strongest up-regulated gene was the small proline-rich protein 1A (Sprr1a) with a 205-fold increase in expression at 12h in wild type mice and 231-fold in WISP1 knockout mice (Figure 79). The strongest down-regulated gene was cytochrome P450, family 7, subfamily a, polypeptide 1 (Cyp7a1) with a 35-fold down-regulation in wild type mice and 93-fold down-regulation in WISP1 knockout mice. Inflammation- and stress associated genes were among the strongest up-regulated genes, such as Hspa1a and 1b (heat shock protein 1a and 1b), member 2), Tnfrsf12a (tumor necrosis factor receptor superfamily, member 12a), Atf3 (activating transcription factor 3), Ifrd1 (interferon-related developmental regulator 1), CD14 (CD14 antigen), Ier3 (immediate early response 3) and Ddit3 (DNA-damage inducible transcript 3). Likewise, metabolism-associated genes like Hsd3b5 (hydroxyl-delta-5-steroid dehydrogenase, 3 beta- and steroid delta-isomerase 5), Cyp2c37 (cytochrome P450, family 2, subfamily c, polypeptide 37), Cyp2c38 (cytochrome P450, family 2, subfamily c, polypeptide 38) and Sult2a8 (sulfotransferase family 2A, dehydroepiandrosterone (DHEA) – preferring, member 8) were among the most down-regulated genes.

pValue(FDR) < 0.05			Wild type (WT)								WISP1 knockout (KO)								
			8h vs ctrl		12h vs ctrl		D1 vs ctrl		D3 vs ctrl		8h vs ctrl		12h vs ctrl		D1 vs ctrl		D3 vs ctrl	
EntrezID	Symbol	Description	Fold	pValue	Fold	pValue	Fold	pValue	Fold	pValue	Fold	pValue	Fold	pValue	Fold	pValue	Fold	pValue
20753	Sprr1a	small proline-rich protein 1A	142,2	2,00E-16	205,4	1,48E-17	47,68	1,26E-12	13,76	7,80E-08	184,1	3,67E-17	231,9	4,39E-18	44,27	6,79E-13	21,16	2,72E-09
11910	Atf3	activating transcription factor 3	19,72	8,63E-15	41,39	7,35E-18	4,18	1,36E-06	2,85	4,73E-04	16,76	6,75E-14	55,51	7,96E-19	4,15	1,51E-06	2,74	1,13E-03
240672	Dusp5	dual specificity phosphatase 5	20,81	1,01E-15	29,36	3,15E-17	3,14	2,43E-05	2,28	3,67E-03	28,75	3,59E-17	36,76	1,62E-18	5,43	4,49E-09	2,36	2,54E-03
12306	Anxa2	annexin A2	8,84	1,47E-14	20,82	3,26E-19	15,95	5,02E-17	8,97	1,39E-13	10,81	4,70E-16	23,88	4,04E-20	21,9	1,87E-19	11,69	1,48E-15
12475	Cd14	CD14 antigen	13,65	1,35E-11	24,52	3,23E-14	8,58	4,92E-09	2,76	3,78E-03	14,54	4,69E-12	33,72	9,33E-16	14,55	6,77E-12	2,9	2,41E-03
79201	Tnfrsf23	tumor necrosis factor receptor superfamily, member 23	6,32	1,08E-06	20,72	8,01E-12	6,06	2,59E-06	2,73	1,17E-02	8,99	2,34E-08	24,24	1,38E-12	8,75	3,65E-08	4,18	3,14E-04
27279	Tnfrsf12a	tumor necrosis factor receptor superfamily, member 12a	13,1	9,17E-17	11,81	1,78E-16	7,8	3,41E-13	2,4	1,17E-04	14,43	1,05E-17	16,54	7,96E-19	12,2	1,36E-16	3,23	6,48E-07
107272	Psat1	phosphoserine aminotransferase 1	12,44	1,29E-17	15,03	6,67E-19	6,07	7,32E-13	2,1	3,32E-04	12,75	7,97E-18	18,14	6,60E-20	6,95	2,74E-14	2,76	2,35E-06
67951	Tubb6	tubulin, beta 6 class V	7,79	6,34E-16	10,34	5,62E-18	7,12	7,78E-15	2,68	9,80E-07	12,51	2,02E-18	16,14	6,41E-20	10,96	1,20E-17	3,69	4,34E-09
17869	Myc	myelocytomatosis oncogene	16,44	2,68E-16	16,52	1,66E-16	2,77	2,30E-05	2,26	1,39E-03	12,53	5,04E-15	15,84	2,03E-16	2,2	6,89E-04	1,91	1,29E-02
11770	Fabp4	fatty acid binding protein 4, adipocyte	10,48	6,45E-12	11,71	1,31E-12	6,98	2,31E-09	4,79	1,08E-06	10,43	5,09E-12	14,21	1,14E-13	6,56	1,98E-09	3,78	2,04E-05
654432	Gm7334	predicted gene 7334	11,14	1,13E-13	9,91	3,54E-13	7,09	9,85E-11	2,07	7,85E-03	13,01	5,83E-15	14,02	1,22E-15	9,17	6,15E-13	1,92	1,84E-02
23849	Klf6	Kruppel-like factor 6	12,88	4,02E-17	15,2	2,79E-18	2,36	2,09E-05	2,51	2,04E-05	9,69	8,18E-16	14,44	2,73E-18	2,51	4,56E-06	2,5	2,37E-05
13086	Cyp2a4	cytochrome P450, family 2, subfamily a, polypeptide 4	16,81	3,19E-09	6,17	2,02E-05	11,07	1,72E-07	3,79	4,78E-03	6,51	7,01E-06	5,53	2,99E-05	7,56	1,85E-06	4,07	1,63E-03
11504	Adamts1	a disintegrin-like and metallopeptidase (reprolysin type) with thrombospondin type 1	7,37	1,60E-13	8,17	3,16E-14	2,72	5,18E-06	1,78	1,17E-02	10,65	8,17E-16	21,14	2,42E-19	4,95	6,96E-11	1,95	3,20E-03
54720	Rcan1	regulator of calcineurin 1	11,34	1,45E-21	11,89	1,10E-21	3,53	1,89E-12	1,88	3,58E-05	12,39	3,77E-22	10,88	1,61E-21	3,41	9,53E-13	1,7	4,62E-04
228413	Prrg4	proline rich Gla (G-carboxyglutamic acid) 4 (transmembrane)	6,94	1,45E-13	9,03	2,79E-15	3,66	1,02E-08	2,2	3,06E-04	7,79	1,72E-14	12,27	3,13E-17	6,06	1,14E-12	2,86	3,15E-06
15937	Ier3	immediate early response 3	2,59	6,98E-05	11,94	2,03E-14	2,08	2,22E-03	1,92	1,28E-02	4,02	6,40E-08	20,71	4,51E-17	4,82	4,49E-09	2,52	4,44E-04
171210	Acot2	acyl-CoA thioesterase 2	5,88	3,22E-09	10,31	2,32E-12	3,98	1,47E-06	3,55	2,02E-05	4,86	2,63E-08	10,62	5,77E-13	8,07	3,66E-11	2,67	6,70E-04
17768	Mthfd2	methylenetetrahydrofolate dehydrogenase (NAD+ dependent), methenyltetrahydrofolate cyclohydrolase	5,81	9,29E-12	8,61	2,20E-14	4,25	3,50E-09	1,61	4,43E-02	6,76	9,74E-13	12,15	1,82E-16	5,19	6,37E-11	2,02	2,66E-03

Figure 79: Analysis of groups of similar regulated genes. The figure shows a snapshot of the results obtained for groups of similar regulated genes. Results show the fold change over wild type control or WISP1 knockout control respectively. Data are attached in the supplement 1.

Interestingly, gene array of wild type and WISP1 knockout mice did not reveal an up-regulation of lipocalin 2 (Lcn2), which was one of the most up-regulated genes detected in previous gene array studies by our group [171]. However, typical gene expression patterns, such as the up-regulation of inflammation- and stress associated genes, and the down-regulation of metabolism, were detected as previously reported by [171].

Principal component analysis indicated a good clustering of gene expression in wild type and WISP1 knockout control and after 8h of CCl_4 administration (Figure 80). However,

at 12h, the WISP1 knockout samples clearly deviated from the corresponding wild type samples. At 24h and 72h, samples from wild type and WISP1 knockout mice clustered in a more diffuse way. This transcriptional regulatory network can be associated to corresponding biological features, already described by Campos [171], such as the activation of MAPK and ER-stress associated pathways (2h-8h) followed by an inflammation response on D1. These events are followed by the repression of metabolism-associated genes. Finally, regenerative processes take place, which are characterized by proliferating hepatocytes to restore tissue homeostasis (D2-D4).

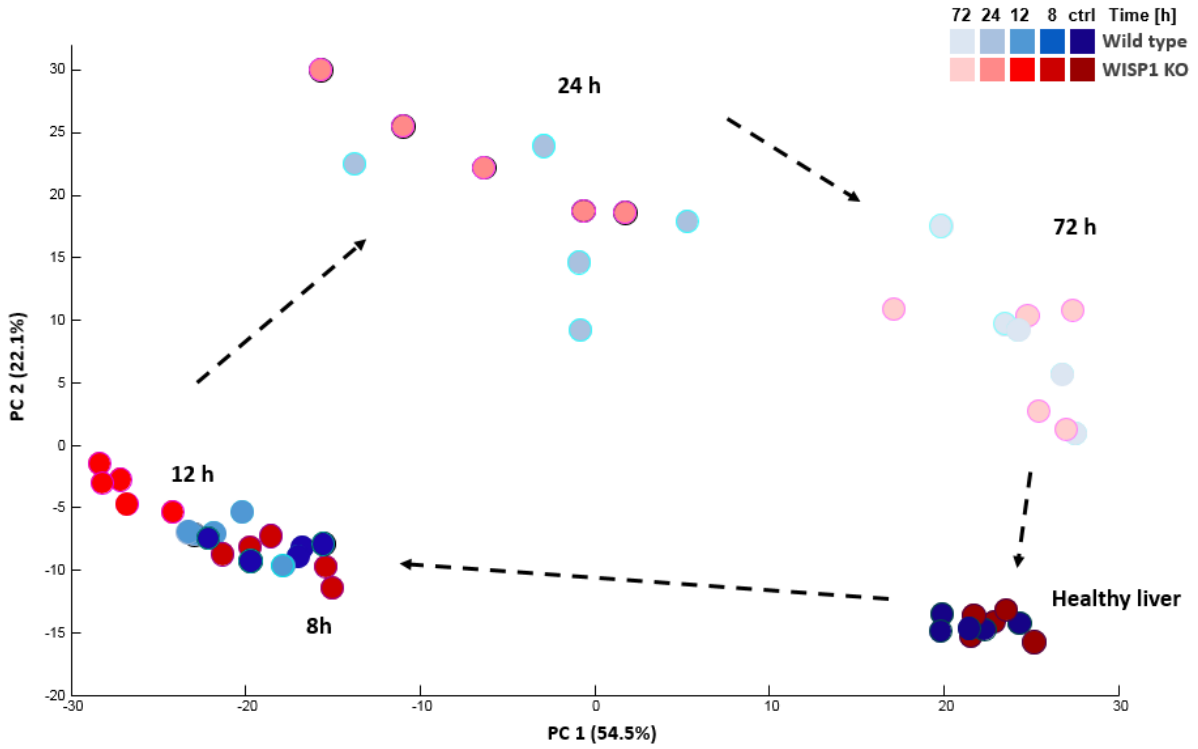

Figure 80: Principal component analysis of gene expression in wild type and WISP1 knockout livers after administration of 460 mg/kg CCl_4. The graph represents the coordinates of the principal component 1 (PC1) and principal component 2 (PC2), which account for 54.5 % and 22.1 % of the deregulated genes in the transcriptional response after CCl_4, respectively. The position of control and 8h samples revealed a robust and time-dependent clustering of 5 independent biological replicates per time point. However at 12h, WISP1 knockout samples clustered clearly away from the corresponding wild type samples. At 24h and 72h, samples clustered in a more diffuse way, finally returning back to almost control conditions.

Taken together, the principal component analysis revealed a good clustering within the time-matched samples from both the wild type and WISP KO mice after CCl_4 administration. Importantly, at 12h WISP1 knockout samples clearly deviated from the wild type samples. Nonetheless, at the peak of liver damage (24h), samples clustered in a more diffuse way, thus showing no shift between wild type and WISP1 knockout mice. This was also observed for the regenerative process (72h) which seemed to be comparable in WISP1 knockout and wild type mice. Further bioinformatics analyses were applied to identify the differences in transcriptional responses of wild type and WISP1 knockout mice.

3.16.1 Fuzzy C-Means clustering established 15 gene expression clusters

Fuzzy C-Means clustering allows pattern recognition in a large set of data [170], and was therefore used to analyze differentially expressed genes of WISP1 knockout and wild type mice. Here, the gene expression values from WISP1 knockout mice were used to calculate the differences in fold change relative to the wild type mice, according to the different time points measured. Subsequently, results were clustered using Fuzzy C means algorithm. Analysis revealed 15 main gene expression clusters, which consisted of a maximum of 21 genes (Figure 81).

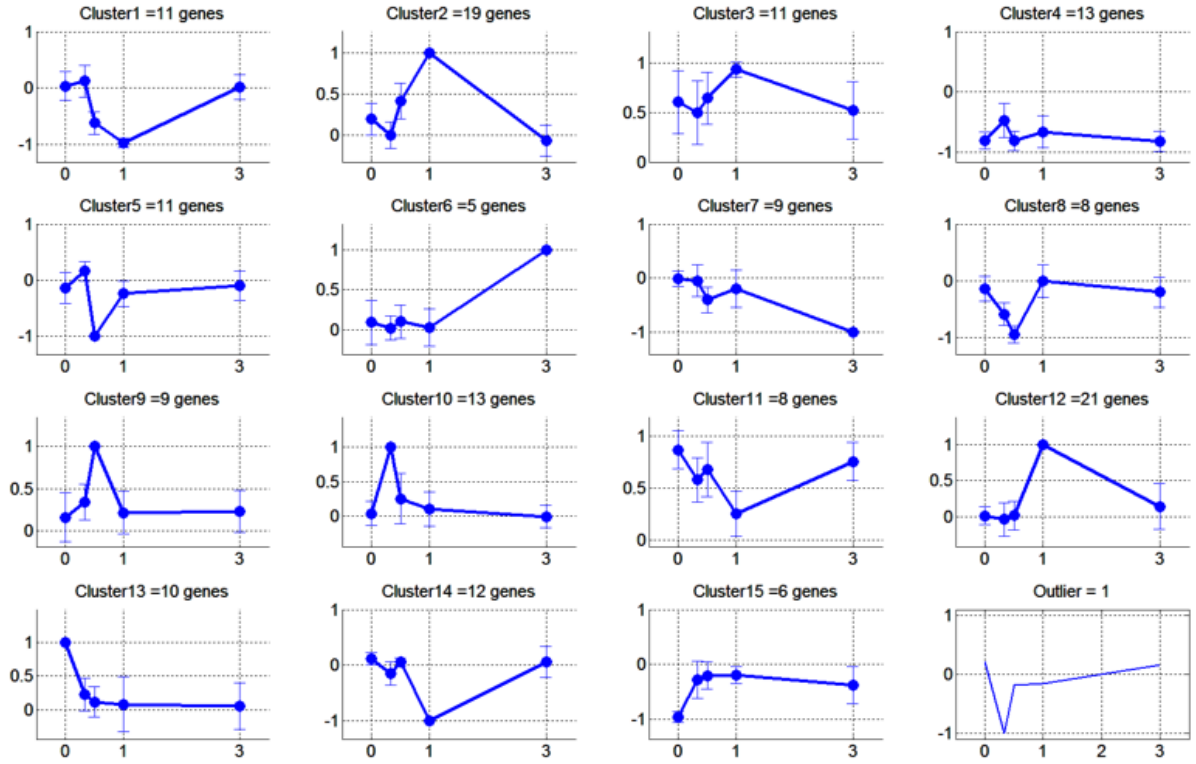

Figure 81: Fuzzy C-Mean clustering analysis of WISP1 knockout versus wild type mice identified 15 gene expression clusters. Fuzzy C-Mean clustering was used to analyze differential expressed genes in WISP1 knockout mice. The analysis identified 15 main gene expression clusters, Fold = 1.5, p-value (FDR) < 0.05, data are attached in the supplement 2.

3.16.2 Gene ontology and KEGG analyses revealed alterations in lipid metabolism in WISP1 knockout mice

Gene ontology (GO, http://www.geneontology.org/), an expert curated database assigning genes to various functional categories, was used to obtain biologically meaningful contexts from the gene list [187]. This database assigned genes to various functional categories [187] divided into three main categories: biological process (BP), molecular function (MF) and cellular component (CC). This method was applied to identify enriched

biological motifs within the time-dependent analysis. Therefore, data obtained from Fuzzy C-Mean clustering were used.

Analysis of GO "biological process" revealed high enrichment of metabolism associated terms in cluster 1, such as "carboxylic metabolic process" (p = 3.62E-10), "oxoacid metabolic process" (p = 5.88E-10) and "small molecule metabolic process" (p = 5.78E-08) (Figure 82). Cluster 1 contained down-regulated genes for the 8h and D1 time points, indicating an intense loss in metabolic functions in both the WISP1 knockout and wild type mice after induction of liver damage. Moreover, cluster 2 and 12 depicted a high enrichment in lipid metabolic processes, such as "single-organism metabolic process" (p = 1.63E-08), "cellular lipid metabolic process" (p = 1.08E-09) and "organic substance metabolic process" (p = 1.13E-06) (Figure 62). These clusters showed an up-regulation of genes at 8h and D1, indicating a strong induction of lipid metabolism associated genes during the formation of acute liver damage.

	A	B	C	D	E	F	G	H	I	J	K	Z	AA
1				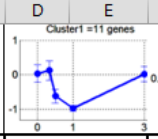		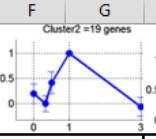		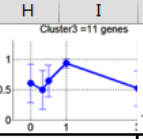		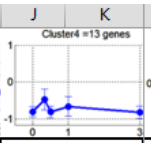		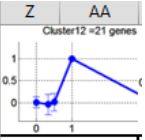	
2				Cluster-1		Cluster-2		Cluster-3		Cluster-4		Cluster-12	
3	GO-ID	Description	Size	Count	pValue	Count	pValue	Count	pValue	Count	pValue	Count	pValue
4	GO:0032787	monocarboxylic acid metabolic process	549	5	1,90E-07	8	3,42E-11					4	3,03E-04
5	GO:0006631	fatty acid metabolic process	354	2	6,48E-03	7	1,03E-10					4	5,51E-05
6	GO:0006629	lipid metabolic process	1134	4	2,03E-04	9	2,77E-10					6	2,40E-05
7	GO:0009062	fatty acid catabolic process	80			5	2,97E-10					3	2,03E-05
8	GO:0019752	carboxylic acid metabolic process	846	7	3,62E-10	8	1,05E-09					4	1,58E-03
9	GO:0043436	oxoacid metabolic process	907	7	5,88E-10	8	1,81E-09					4	2,05E-03
10	GO:0006082	organic acid metabolic process	923	7	6,63E-10	8	2,08E-09					4	2,19E-03
11	GO:0072329	monocarboxylic acid catabolic process	95	1	4,90E-02	5	7,14E-10					3	3,40E-05
12	GO:0016042	lipid catabolic process	252	1	1,28E-01	6	1,08E-09					3	6,20E-04
13	GO:0044255	cellular lipid metabolic process	849	2	3,51E-02	8	1,08E-09					5	9,61E-05
14	GO:0044242	cellular lipid catabolic process	160			5	9,96E-09					3	1,62E-04
15	GO:0044281	small molecule metabolic process	1760	7	5,78E-08	9	1,31E-08					6	2,84E-04
16	GO:0044710	single-organism metabolic process	4526	7	3,50E-05	12	1,63E-08					8	1,43E-03
17	GO:0016054	organic acid catabolic process	183	2	1,76E-03	5	1,95E-08					3	2,41E-04
18	GO:0046395	carboxylic acid catabolic process	183	2	1,76E-03	5	1,95E-08					3	2,41E-04
19	GO:0044283	small molecule biosynthetic process	460	5	7,90E-08					2	3,92E-02	3	3,58E-03
20	GO:0001676	long-chain fatty acid metabolic process	91			4	1,13E-07					2	2,55E-03
21	GO:0044282	small molecule catabolic process	264	2	3,64E-03	5	1,22E-07					4	1,74E-05
22	GO:0008152	metabolic process	11355	8	1,81E-03	15	4,81E-07					13	7,13E-04
23	GO:0055114	oxidation-reduction process	994	3	2,93E-03	5	8,04E-05					7	5,03E-07
24	GO:0071704	organic substance metabolic process	9985	7	5,66E-03	14	1,13E-06					10	1,91E-02

Figure 82: Analysis of GO "biological process" overrepresentation in a time-dependent gene clusters. The figure shows a snapshot of the results obtained from the overrepresentation of GO "biological processes". The strongest overrepresentations of GO motifs were observed in cluster 1 containing down-regulated genes; clusters 2 and 12 containing up-regulated genes. Cluster 1 showed a high enrichment of GO terms associated with metabolism; clusters 2 and 12 were associated with lipid metabolism and oxidation-reduction processes, gray colored boxes indicate p-value<10^{-5}, data are attached in the supplement 3.

Previous analysis of GO “biological process” showed a high enrichment of lipid metabolic processes in clusters 2 and 12. In line with this, analysis of GO “molecular function” revealed an enrichment of metabolism in up-regulated gene clusters (Figure 83). Among these genes clusters, GO terms such as “catalytic activity” (p = 2.90E-06) and “oxireductase activity” (p = 2.74E-06) were detected, suggesting that enzymes involved in these processes, like cytochrome P450 [188], are induced in these clusters.

	A	B	C	D	E	F	G	H	I	J	K	Z	AA
1				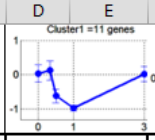		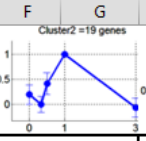		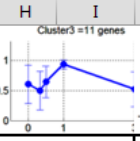		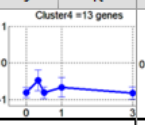		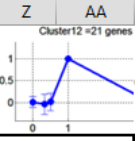	
2				Cluster-1		Cluster-2		Cluster-3		Cluster-4		Cluster-12	
3	GO-ID	Description	Size	Count	pValue	Count	pValue	Count	pValue	Count	pValue	Count	pValue
4	GO:0003674	molecular_function	21487	10	4,76E-03	17	3,72E-05	9	2,09E-02	11	7,03E-03	21	1,60E-07
5	GO:0016491	oxidoreductase activity	778	2	2,97E-02	4	5,45E-04					6	2,74E-06
6	GO:0003824	catalytic activity	5699	7	1,60E-04	11	2,90E-06	4	1,12E-01			11	2,56E-05
7	GO:0005488	binding	15867	9	2,89E-03	13	2,41E-03	7	9,08E-02	9	2,49E-02	17	3,12E-05
8	GO:0016290	palmitoyl-CoA hydrolase activity	13			2	3,23E-05						
9	GO:0052689	carboxylic ester hydrolase activity	133			3	5,14E-05						
10	GO:0047617	acyl-CoA hydrolase activity	18			2	6,32E-05						
11	GO:0016289	CoA hydrolase activity	21			2	8,67E-05						
12	GO:0000062	fatty-acyl-CoA binding	31			2	1,92E-04						
13	GO:0043548	phosphatidylinositol 3-kinase binding	31									2	2,94E-04
14	GO:0016788	hydrolase activity, acting on ester bonds	686			4	3,36E-04						
15	GO:0016790	thiolester hydrolase activity	41			2	3,37E-04						
16	GO:0043168	anion binding	2624	5	3,86E-04	5	7,13E-03	4	6,96E-03	3	1,71E-01		
17	GO:0004123	cystathionine gamma-lyase activity	1	1	5,21E-04								
18	GO:0044540	L-cystine L-cysteine-lyase (deaminating)	1	1	5,21E-04								
19	GO:0047568	3-oxo-5-beta-steroid 4-dehydrogenase activity	1	1	5,21E-04								
20	GO:0080146	L-cysteine desulfhydrase activity	1	1	5,21E-04								
21	GO:0098600	selenomethionine gamma-lyase activity	1	1	5,21E-04								
22	GO:0004058	aromatic-L-amino-acid decarboxylase activity	1										
23	GO:0008123	cholesterol 7-alpha-monooxygenase activity	1										

Figure 83: Analysis of GO “molecular function” overrepresentation in time-dependent gene clusters. The figure represents a snapshot of results obtained for overrepresentation of GO “molecular function”. According to previous analyses “biological process”, strong overrepresentations of GO motifs were observed in clusters 2 and 12, containing up-regulated genes with GO terms such as enzyme activity, gray colored boxes indicate p-value<10^{-5}, data are attached in the supplement 3.

Further analysis of GO “cellular component” confirmed previous results showing an up-regulation of lipid metabolic processes (Figure 84). Clusters 2 and 12 revealed an enrichment in GO terms, such as “membrane-bounded organelle” (p = 3.43E-07) and “cytoplasm” (p = 7.90E-06).

	A	B	C	D	E	F	G	H	I	J	K	Z	AA
1				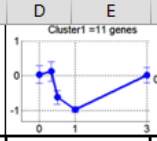		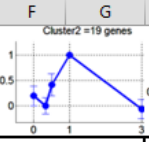		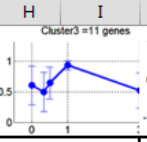		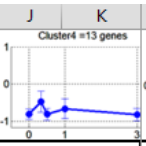		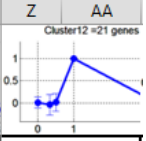	
2				Cluster-1		Cluster-2		Cluster-3		Cluster-4		Cluster-12	
3	**GO-ID**	**Description**	**Size**	**Count**	**pValue**	**Count**	**pValue**	**Count**	**pValue**	**Count**	**pValue**	**Count**	**pValue**
4	GO:0044464	cell part	16086	**9**	**3,24E-03**	**15**	**6,15E-05**	7	9,83E-02			**20**	**1,57E-08**
5	GO:0005623	cell	16133	**9**	**3,31E-03**	**15**	**6,40E-05**	7	1,00E-01			**20**	**1,66E-08**
6	GO:0043227	membrane-bounded organelle	11087	6	5,34E-02	**15**	**3,43E-07**	6	6,45E-02			**14**	**9,11E-05**
7	GO:0043226	organelle	12038	6	7,89E-02	**15**	**1,10E-06**	6	9,72E-02	7	1,00E-01	**14**	**2,45E-04**
8	GO:0005737	cytoplasm	9613	6	2,66E-02	**13**	**7,90E-06**	6	3,11E-02			**15**	**1,80E-06**
9	GO:0005575	cellular_component	20970	**10**	**3,79E-03**	**17**	**2,51E-05**	**10**	**1,22E-03**	**11**	**5,46E-03**	**20**	**2,71E-06**
10	GO:0044424	intracellular part	12590	6	9,71E-02	**13**	**1,83E-04**	6	1,21E-01			**16**	**8,57E-06**
11	GO:0044444	cytoplasmic part	6642	5	2,56E-02	**11**	**1,36E-05**	**6**	**4,32E-03**	5	1,19E-01	**11**	**1,13E-04**
12	GO:0005622	intracellular	13199	7	2,98E-02	**13**	**3,14E-04**	6	1,52E-01			**16**	**1,69E-05**
13	GO:0005783	endoplasmic reticulum	1397			**6**	**2,57E-05**			3	3,07E-02	3	7,74E-02
14	GO:0044421	extracellular region part	3721	3	1,09E-01	5	3,17E-02	4	2,51E-02	**7**	**6,44E-05**		
15	GO:0043231	intracellular membrane-bounded organelle	9889			**12**	**9,51E-05**	5	1,79E-01			**13**	**1,57E-04**
16	GO:0016020	membrane	9951			**12**	**1,02E-04**	**7**	**5,26E-03**	**8**	**5,16E-03**	**12**	**9,62E-04**
17	GO:0005576	extracellular region	4292	3	1,55E-01	5	5,66E-02	4	4,19E-02	**7**	**1,66E-04**		
18	GO:0043229	intracellular organelle	10952			**12**	**2,78E-04**					**13**	**4,82E-04**
19	GO:0098805	whole membrane	1775			3	8,48E-02					**6**	**2,98E-04**
20	GO:0098588	bounding membrane of organelle	1896			4	1,48E-02					**6**	**4,28E-04**
21	GO:0044425	membrane part	7788			**10**	**4,81E-04**					9	1,22E-02
22	GO:0005789	endoplasmic reticulum membrane	780			**4**	**5,51E-04**					2	1,58E-01
23	GO:0042175	nuclear outer membrane-endoplasmic reticulum membrane network	796			**4**	**5,95E-04**					2	1,64E-01
24	GO:0031982	vesicle	3456	4	1,33E-02	5	2,33E-02	3	1,48E-01	**6**	**6,05E-04**		
25	GO:0044432	endoplasmic reticulum part	890			**4**	**9,10E-04**						
26	GO:0005967	mitochondrial pyruvate dehydrogenase complex	3	**1**	**1,56E-03**								

Figure 84: Analysis of GO "cell component" overrepresentation in the time-dependent gene clusters. The snapshot represents the results obtained for overrepresentation of GO "cell component". The strongest overrepresentations of GO motifs were observed in clusters 2 and 12, showing a high enrichment of GO terms associated with membrane-bounded organelle and cytoplasm, gray colored boxes indicate p-value<10^{-5}, data are attached in the supplement 3.

However, to gain more precise information about altered pathways in this model, the Kyoto Encyclopedia of Genes and Genomes (KEGG http://www.genome.jp/kegg/) was used to identify biological motifs [189]. KEGG is a curated database that integrates current knowledge on molecular interactions, such as pathways, with databases such as GO [189]. Consistent with previous analysis, KEGG pathway enrichment in the gene clusters 2 and 12 revealed strong overrepresentation of lipid and vitamin A metabolism associated pathways (Figure 85), like "PPAR signaling pathway" (p = 7.21E-06), "fatty acid degradation" (p = 5.43E-09) and "retinol metabolism" (p = 9.23E-06). Moreover, metabolism-associated terms were detected in down-regulated gene cluster 1, including "metabolic pathways" (p = 8.38E-06).

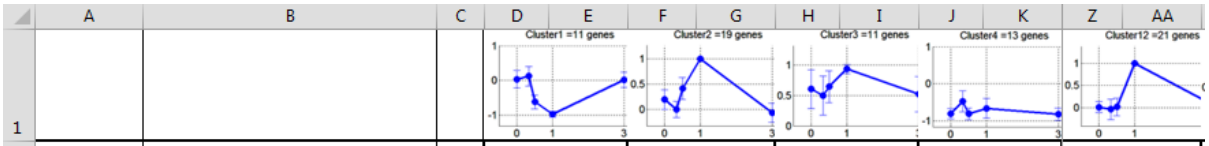

				Cluster-1		Cluster-2		Cluster-3		Cluster-4		Cluster-12	
	GO-ID	Description	Size	Count	pValue	Count	pValue	Count	pValue	Count	pValue	Count	pValue
4	KEGG:03320	PPAR signaling pathway	82			3	7,21E-06					5	4,23E-10
5	KEGG:00071	Fatty acid degradation	49			4	5,43E-09					3	2,17E-06
6	KEGG:00000	KEGG pathways	7577	7	6,86E-04	14	1,78E-08			4	1,68E-01	14	3,71E-07
7	KEGG:01212	Fatty acid metabolism	51			1	3,55E-02					3	2,45E-06
8	KEGG:01100	Metabolic pathways	1281	5	8,38E-06	6	9,41E-06	2	4,13E-02			5	3,16E-04
9	KEGG:00830	Retinol metabolism	89			3	9,23E-06					1	6,33E-02
10	KEGG:00062	Fatty acid elongation	26			2	8,05E-05						
11	KEGG:01040	Biosynthesis of unsaturated fatty acids	27			2	8,69E-05					1	1,95E-02
12	KEGG:00140	Steroid hormone biosynthesis	87	1	3,06E-02							1	6,19E-02
13	KEGG:01230	Biosynthesis of amino acids	79	2	2,25E-04								
14	KEGG:04146	Peroxisome	83			2	8,32E-04					1	5,91E-02
15	KEGG:00590	Arachidonic acid metabolism	88			2	9,35E-04					1	6,26E-02
16	KEGG:04014	Ras signaling pathway	228										
17	KEGG:00524	Butirosin and neomycin biosynthesis	5	1	1,77E-03								
18	KEGG:04750	Inflammatory mediator regulation of TRP channels	127			2	1,94E-03					1	8,96E-02
19	KEGG:04270	Vascular smooth muscle contraction	128			2	1,97E-03					1	9,03E-02
20	KEGG:04142	Lysosome	124									2	2,23E-03
21	KEGG:00400	Phenylalanine, tyrosine and tryptophan biosynthesis	7	1	2,48E-03								
22	KEGG:00072	Synthesis and degradation of ketone bodies	11					1	3,40E-03				
23	KEGG:00120	Primary bile acid biosynthesis	16	1	5,67E-03								
24	KEGG:00340	Histidine metabolism	26										
25	KEGG:00360	Phenylalanine metabolism	22	1	7,79E-03								

Figure 85: Analysis of KEGG pathways overrepresentation in time-dependent gene clusters. This figure shows a snapshot of the results obtain for overrepresentation of KEGG pathways. Strongest overrepresentations of KEGG pathways were observed in clusters, which contain down-regulated genes (cluster 1) and up-regulated genes (clusters 2 and 12). Cluster 1 revealed a high enrichment of metabolic pathways, whereas clusters 2 and 12 were highly associated to fatty acid metabolism, gray colored boxes indicate p-value<10^{-5}, data are attached in the supplement 3.

Taken together, GO and KEGG analyses revealed strong down-regulation of metabolism associated genes upon early time points of liver injury. Interestingly, the results showed strong up-regulation of lipid metabolism associated genes and pathways in WISP1 knockout mice compared to wild type mice, which has never before been described. Hence, the results led to the hypothesis that the absence of WISP1 in the knockout mice altered lipid metabolism, potentially influencing the susceptibility to hepatotoxic substances.

3.16.3 Absence of WISP1 leads to altered expression of metabolism-associated genes

Since GO and KEGG analyses revealed alterations regarding metabolism, various genes were chosen to be confirmed by qRT-PCR. First, Cyp4a14 (cytochrome P450, family 4, subfamily a, polypeptide 14) and Cyp4a10 (cytochrome P450, family 4, subfamily a,

polypeptide 10) were investigated, since their upregulation was higher in the WISP1 knockout mice compared to wild type mice (Figure 86). These cytochrome P450 enzymes are known to be involved in ω-hydroxylation of saturated and unsaturated fatty acids [190]. Furthermore, Fuzzy C-Mean clustering revealed a down-regulation of Serpina12 and Serpina1d already in the control condition and after CCl_4 administration at all time points in the WISP1 knockout mice. These serine protease inhibitors are known to be involved in obesity and inflammation [191]. Finally, CIDEC was chosen as the gene array analysis revealed an up-regulation on D1, where enhanced susceptibility was detected in WISP1 knockout mice upon induction of acute liver damage. Recently, CIDEC was reported to promote the formation of fat droplets and to be involved in the development of alcoholic steatohepatitis in mice and humans [192].

Cluster	Memberchip Degree	ProbeSet	Symbol	Description	KO vs WT	KO vs WT (8h)	KO vs WT (12h)	KO vs WT (1d)	KO vs WT (3d)
2	0,893	13119	Cyp4a14	cytochrome P450, family 4, subfamily a, polypeptide 14	1,19	-1,34	2,38	9,07	1,25
12	0,542	13117	Cyp4a10	cytochrome P450, family 4, subfamily a, polypeptide 10	-1,4	1,15	1,74	8,66	-1,29
4	0,956	68054	Serpina12	serine (or cysteine) peptidase inhibitor, clade A (alpha-1 antiproteinase, antitrypsin), member 12	-2,29	-1,29	-2,19	-2,42	-1,99
4	0,845	20703	Serpina1d	serine (or cysteine) peptidase inhibitor, clade A, member 1D	-18,96	-2,32	-5,07	-5,1	-11,53
2	0,83	14311	Cidec	cell death-inducing DFFA-like effector c	1,19	1,12	1,39	3,75	-1,44

Figure 86: Analysis of Fuzzy C-Means clustering of WISP1 knockout mice versus wild type mice. Analysis revealed up-regulation (red color) of Cyp4a14, Cyp4a10 and CIDEC at 12h and D1 in the WISP1 knockout mice compared to wild type mice. Down-regulation (green color) was detected for Serpina12 and Serpina1d at all time points. Red color = fold change is greater two and pValue < 0.05, light red = fold change is greater two and pValue > 0.05, green = fold change is less minus two and pValue < 0.05, light green = fold change is less minus two and pValue > 0.05. Date are attached in the supplement 2.

Quantitative RT-PCR was performed using RNA from liver homogenates of wild type and WISP1 knockout mice after administration of 460 mg/kg CCl_4 for 30min, 2h, 8h, 12h, 18h and D1. The results confirmed gene array data, showing a stronger induction of Cyp4A14 and Cyp4a10 in the WISP1 knockout mice at 18h and D1 compared to wild type mice (Figure 87).

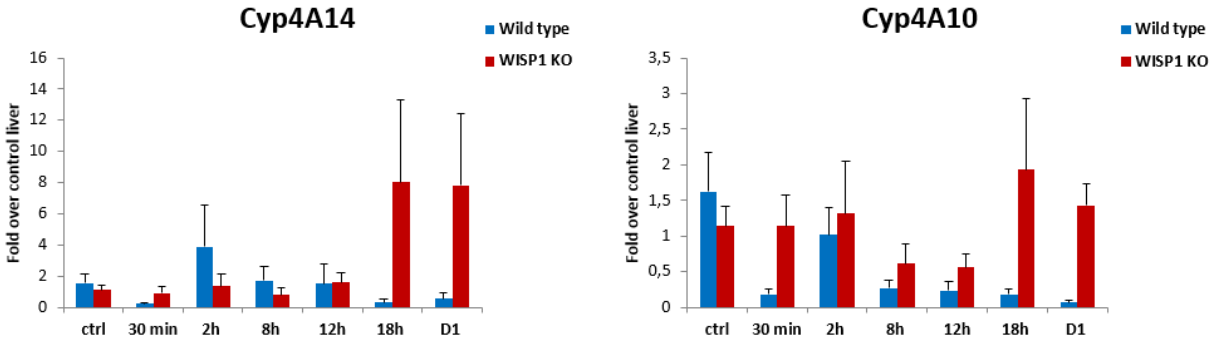

Figure 87: Time-dependent quantitative RT-PCR of Cyp4A14 and Cyp4A10 expression in wild type and WISP1 knockout mice after administration of CCl_4. Results revealed enhanced Cyp4A14 expression at 18h and D1 after CCl_4 administration. Cyp4A10 expression was stronger induced at 30 min, 18 h and D1 after CCl_4 administration. Data represent mean of six independent biological replicates ± S.E.

Quantification of Serpina1d expression detected just a small decrease in control conditions and at 2h in WISP1 knockout mice, which did not completely reflect the data obtained from gene array (Figure 88). However, Serpina12 was strongly down-regulated at all time points in the WISP1 knockout mice compared to wild type mice. Finally, qRT-PCR analysis of CIDEC showed that its expression was upregulated in wild type and WISP1 knockout mice after administration of CCl_4, however on D1, the induction was higher in WISP1 knockout mice compared to wild type mice.

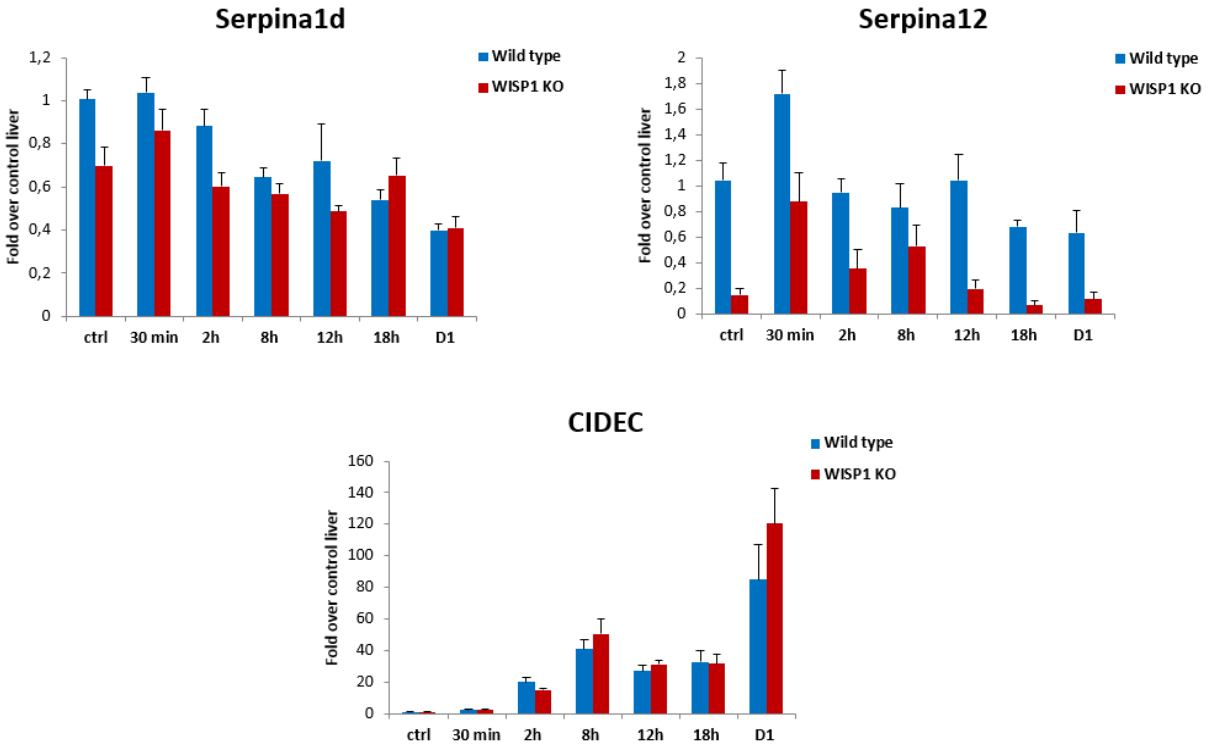

Figure 88: Time-dependent quantitative RT-PCR of Serpina1d, Serpina12 and CIDEC expression in wild type and WISP1 knockout mice after administration of CCl_4. Results showed a slight decrease in Serpina1d expression in WISP1 knockout mice under control conditions. However, up to D1 expression levels were comparable. Furthermore, analysis revealed a downregulation of Serpina12 at all time points in the WISP1 knockout mice compared to wild type mice. CIDEC was induced upon CCl_4 administration in both the wild type and WISP1 knockout mice. Enhanced expression levels were detected in the WISP1 knockout mice on D1 compared to wild type mice. Data represent mean of six independent biological replicates ± S.E.

Taken together, quantitative RT-PCR confirmed the gene array data, showing an up-regulation of Cyp4a14, Cyp4a10 and CIDEC at late time points after CCl_4 administration. Moreover, down-regulation of Serpina12 in WISP1 knockout mice was also confirmed; however, there was only a slight decrease in Serpina1d as detected with qRT-PCR.

4 DISCUSSION

In the past, hepatotoxic effects were mainly associated with altered metabolism or redox state. However, nowadays it is well known that hepatotoxic effects are triggered by various cellular and molecular mechanisms, such as induction of ER stress [99] or inflammation [55]. Previous gene array studies by our group revealed activation of MAPK signaling and ER stress, induction of inflammation, down-regulation of metabolism and finally regeneration [171] leading to a detailed description of fundamental biological features occurring upon drug-induced liver injury. In this study, WISP1 was identified as highest up-regulated gene among its protein family. In order to study the influence of WISP1 upon drug-induced liver injury, a knockout mouse model was established. Two well-known and robust models to investigate hepatocellular injury and regeneration were chosen: CCl_4 and APAP. Surprisingly, genetic deletion of WISP1 led to enhanced susceptibility to CCl_4 administration as well as to APAP. CCl_4-induced liver injury was associated with increased immune cell infiltration and increased expression of pro-inflammatory cytokines. Moreover, stress-associated signal transduction and inflammation-associated signaling pathways were stronger activated in WISP1 knockout mice compared to wild type mice upon CCl_4 administration. Interestingly, liver regeneration was not impaired by the absence of WISP1. Gene array analysis of WISP1 knockout and wild type mice revealed alterations regarding lipid metabolism, including strong up-regulation of cytochrome p450 enzymes in the WISP1 knockout mice as well as up-regulation of CIDEC, which was reported to be involved in the development of alcoholic steatohepatitis. Taken together these results suggested that genetic deletion of WISP1 may alter the inflammatory response upon acute liver injury and potentially also lipid metabolism in the liver, which might influence the susceptibility to hepatotoxic-induced liver damage.

Upon previous gene array analysis, Wnt-induced secreted protein-1 (WISP1) was detected as one of the most up-regulated genes among the CCN family members. During my study I was able to validate WISP1 expression upon CCl_4 administration by qRT-PCR in a time-dependent manner, confirming a strong induction of WISP1 within the early injury phase (2h up to D1) in C57Bl/6N mice. CCN proteins were reported to be dynamically expressed upon various mitogenic signals as well as environmental alterations, such as inflammatory cytokines [130, 132]. Therefore, an up-regulation of WISP1 upon liver injury, whereby various cytokines and growth factors play an important role, is to be expected. Nonetheless, this is the first time that expression of WISP1 is considered to be connected with acute liver injury. While performing qRT-PCR analysis of different cell populations from liver tissue, it was observed that NPCs showed the highest WISP1 expression in control condition, whereas upon CCl_4 administration, the induction of WISP1 was strongest in hepatocytes. To determine the overall contribution of WISP1 expression derived from NPCs compared to whole liver, it is important to consider that NPCs just make about 20 % of the liver cell mass compared to 80 % of hepatocytes. Furthermore, hepatocytes express up to four times more RNA mass than NPCs (Agata Widera´s dissertation [193]). Preliminary experiments from our

laboratory suggest that hepatocytes do not secrete WISP1 very effectively as shown by adeno-associated virus-derived overexpression of WISP1 (Daniela González´s dissertation, unpublished). Therefore, further experiments are necessary to determine the cell sources of WISP1 in liver tissue. Another difficulty in assessing the cell source of WISP1 in liver tissue is that histological analysis of WISP1 expression was not successful. This also makes it difficult to determine if there is a zonal localization and expression of WISP1. As reviewed in [132], CCN proteins were reported to be expressed upon various types of diseases such as cancer, liver fibrosis or osteoarthritis. While investigating WISP1 expression in a human liver disease cohort, containing patients suffering from fibrosis, cirrhosis or hepatocellular carcinoma, WISP1 expression was increased in cirrhosis and hepatocellular carcinoma patients' samples. In line with this, CCN2 protein levels are known to be elevated in human patients suffering from liver fibrosis and correlate with the severity of systemic fibrosis [132]. Moreover, expression of CCN1 was found to be significantly higher in nodular HCC than the expression in solitary and small HCC, suggesting that CCN1 correlates with the recurrence and metastasis of HCC [134]. Taken together, these findings also highlight the importance and possible influence of WISP1 also in human liver diseases.

The implementation of a WISP1 knockout mice was an essential tool in my thesis. PCR and qRT-PCR analyses revealed successful validation of the absence of WISP1 in the knockout mice. Interestingly, WISP1 expression was determined in several tissues of which the strongest expression was detected in the lung, spleen and brain of wild type mice and lower expression was observed in the liver, intestine and muscles, which correlates with previous publications [128, 134]. Moreover, Königshoff et al reported that WISP1 is up-regulated in patients suffering from idiopathic pulmonary fibrosis as well as in the mouse model of bleomycin-induced lung fibrosis. Depletion of WISP1 by a neutralizing antibody led to reduced bleomycin-induced lung fibrosis in mice [194]. This indicates that WISP1 might not only be important for the liver but also for the lung. However, the functions of WISP1 can be diverse and seem to be highly organ- and cell type dependent.

However, contrary to other family members such as CCN1, CCN2 and CCN5, genetic deletion of WISP1 did not lead to embryonic or perinatal lethality, thus suggesting that WISP1 may not play an important role during development. Recently, another WISP1 knockout mouse was reported to show defects in bone integrity, confirming no embryonic lethality of mice lacking WISP1 [195]. Analysis of bone tissue in our WISP1 knockout mice also showed similar bone defects (Ingo Seiler bachelor thesis, University Tübingen). Additionally, analyses of wild type and WISP1 knockout mouse livers did not reveal any difference regarding physiological or histological parameters. Further analyses regarding the redox state and metabolism associated gene Cyp2e1, which is important for drug metabolization [30], did not reveal any difference in WISP1 knockout mice compared to wild type mice in terms of control conditions. Therefore, WISP1 knockout mice were used to further study the role of WISP1 in acute liver injury.

A central result of my study was that genetic deletion of WISP1 led to enhanced susceptibility to hepatotoxic substances including CCl_4 and APAP. When regarding

histological analyses of WISP1 knockout mouse livers after administration of CCl_4, I was able to show that the dead cell areas were doubled in size compared to wild type mice. Furthermore, the first hepatic injury was observed after 12h of CCl_4 administration and full dead cell area was detected after 18h in WISP1 knockout mice. However, wild type mice showed first dead cell area at 18h after CCl_4 administration and full dead cell area was achieved on D1. This suggested that the genetic deletion of WISP1 did not only lead to enhanced susceptibility to hepatotoxic compounds, but also to a time-shift in developing liver damage. WISP1 was reported to promote cell survival via activation of Akt signaling [106] as well as upon TNFα mediated cardiomyocyte death [155]. Therefore, Akt signaling in wild type and WISP1 knockout mice was examined, leading to the conclusion that Akt signaling is not the main pathway involved as there was even a slightly stronger activation in the WISP1 knockout mice. However, during my study I was able to show for the first time that WISP1 may act as a pro-survival factor upon acute liver injury *in vivo,* induced by both CCl_4 and APAP. This suggests that the protective role may not be an unique mechanism induced by a special hepatotoxic compound but rather a general key mediator in response to hepatocellular stress.

In the past, hepatotoxicity was associated with an altered redox state [45] as well as alterations in metabolism [46, 47]. To test the hypothesis, that deletion of WISP1 may alter the redox state or metabolism in hepatocytes upon CCl_4 administration, glutathione content as well as cytochrome p450 enzyme (Cyp2E1) were investigated. Interestingly, the absence of WISP did not alter the redox state or expression of Cyp2E1, suggesting that WISP1 influences neither the redox state nor the metabolism of hepatotoxic compounds, which could be a cause for enhanced susceptibility to hepatotoxic compounds.

In the current study, increased WISP1 expression was detected upon a maximal dose of CCl_4 in C57Bl/6N mice. Using a lower dose of CCl_4 in wild type mice confirmed the up-regulation of WISP1 expression. However, the expression of WISP1 in wild type mice was shown to be more strongly induced and maximal induction was detected earlier. These effects could be due to the fact that wild type mice have a different genetic background (129S5/SvEvBrd * C57BL/6J) compared to C57Bl/6N, which were used for initial experiments. Moreover, dose-dependent effects could also be an explanation for the detected differences. Interestingly, WISP1 protein levels were detected at high concentrations in the plasma of wild type mice. This is consistent with the fact that CCN proteins are secreted extracellular matrix proteins [132]. However, liver tissue homogenates revealed only low levels of WISP1 protein compared to plasma samples. Interestingly, WISP1 protein concentrations showed a biphasic behavior in liver tissue upon exposure to CCl_4, with peaks at early time points (30min) and D1 after CCl_4 administration. This could be due to the fact, that CCN proteins are known to be dynamically expressed upon various mitogenic signals and environmental disorders [130, 132]. Furthermore, Sedlaczek et al also showed a biphasic increase at 6h and 72h of CCN2 upon CCl_4 administration in rat livers [196]. Jun et al investigated the role of CCN1 upon wound healing, thereby showing similar biphasic pattern of mRNA expression and protein levels, suggesting a distinct function during inflammation

and maturation phase of wound healing [197]. Moreover, the expression of CCN proteins is known to be down-regulated during adulthood [132], which could explain the low levels of WISP1 upon control conditions.

CCN proteins were reported to be dynamically expressed upon mitogenic signals as well as environmental stress [130, 132]. Therefore, the first increase of WISP1 protein secretion could be due to cellular stress and the second increase could be induced through cytokine production leading to the initiation of liver regeneration to restore tissue homeostasis. CCl_4 administration was reported to induce cellular stress, as shown by the induction of stress-associated pathways at early time points such as JNK [198]. Moreover, at D1 sterile inflammation, which is initiated by DAMPs released during CCl_4-induced liver damage, caused secretion of cytokines and growth factors leading to the activation of a regeneration program [8, 116, 199]. Therefore, the conditions for two types of regulatory mechanisms of WISP1 secretion upon CCl_4 intoxication are consistent with the molecular events observed in this investigation, namely early stress signaling and subsequent regenerative responses. Nonetheless, it remains unclear, if high basal levels of WISP1 are enough to exert a protective phenotype or if the induction of WISP1 expression is needed to generate this effect.

Liver regeneration, which is perhaps the best studied aspect of liver injury [14], includes the secretion of cytokines and growth factors such as TGFβ, IL-6 or HGF [8, 116, 199] followed by the expression of proliferation markers, such as PCNA, and cyclins, such as cyclin D, E or A [200]. The current study revealed no difference in the ability to recover from drug-induced liver injury in wild type mice compared to WISP1 knockout mice, since the regeneration process was comparable in both sets of mice. However, WISP1 knockout mice displayed an enhanced and prolonged activation of proliferation, which could be due to the fact that the enhanced dead cell area in WISP1 knockout mice needed longer to be fully recovered. Taken together, the absence of WISP1 seemed to have no influence on liver regeneration. A similar effect was observed upon investigation of TGFβ signaling with regard to the control of liver regeneration. Oe et al showed that mice containing a conditional disruption of TGFβ type II receptor exhibited an enhanced proliferative response in the liver, however, the termination of liver regeneration was not altered. The authors suggested that increased signaling by activin A may act as a compensatory mechanism to regulate liver regeneration when TGFβ signaling is blocked [201]. Therefore, it remains to be determined whether similar compensatory effects may influence liver regeneration in mice lacking WISP1.

A central aspect of this study was to investigate signal transduction pathways, such as mitogen-activated protein kinase (MAPK) signaling after CCl_4 administration. Especially stress-activated protein kinases, such as JNK, were shown to play an important role during drug-induced liver injury [7, 48, 49, 85]. For example, Gunawan et al reported that usage of JNK inhibitor reduced liver damage upon APAP administration. Moreover, knockout mice for JNK1 and JNK2 were also protected upon APAP-induced liver injury [84]. Furthermore, Nakagawa et al showed that the genetic deletion of ASK1, which is an activating kinase for

JNK, led to attenuated liver injury upon APAP administration [202]. Interestingly, the JNK inhibitor SP600125 was not effective against CCl_4-induced liver injury [84]. Investigating signal transduction in the current study, revealed an enhanced activation of stress-associated signaling (JNK) in WISP1 knockout mice upon the administration of CCl_4. Also, the second peak of ERK activation (on day 1) was not observed in mice lacking WISP1. Additional signaling pathways, or their downstream targets, showed no significant differences in wild type and WISP1 knockout mice, including p38, c-myc or ATF3 expression. Furthermore, ER stress, which is associated with the induction of cell death via CHOP [101, 102], was shown to be non-differentially activated in the wild type mice compared to WISP1 knockout mice. Moreover, studying RIP3 activation, which has recently been described as an early mediator of APAP toxicity [51], did not show any difference in wild type mice compared to WISP1 knockout mice. Taken together, one hint which could explain the advenced liver damage is the enhanced JNK activation. Since GADD45β was reported to inhibit JNK phosphorylation leading to reduced APAP toxicity in mice [110, 180], the hypothesis was that attenuated JNK phosphorylation is connected to increased GADD45β expression. Surprisingly, GADD45β expression was even higher in WISP1 knockout mice, leading to the conclusion that GADD45β is not the cause for reduced JNK activity in wild type mice. For this reason, further investigations are needed to examine whether JNK is really the cause or just a consequence of increased cellular stress upon genetic deletion of WISP1. Therefore, the usage of JNK inhibitors *in vivo*, such as SP600125, or *in vitro* approaches using siRNA to knockdown JNK activity in hepatocytes should lead to a reduced hepatotoxicity in the WISP1 knockout mice, provided that JNK caused enhanced susceptibility in mice lacking WISP1.

The investigation of expression of CCN family members upon CCl_4 administration revealed increased expression of the family members upon genetic deletion of WISP1. Since CCN family members were reported to have overlapping functions because of their structure similarities [132, 195], it can be speculated that expression of other CCN family members could be induced to compensate for the lack of WISP1. CCN proteins, including CCN1 and CCN2, were reported to induce ROS production in fibroblasts [112]. However, despite their similar structure, they can mediate opposing functions, for example CCN1 was reported to reduce liver fibrosis [143], whereas CCN2 was shown to promote fibrosis [147]. Moreover, CCN1 was shown to act in synergistically with TNFα and FasL, leading to the production of ROS as well as to a robust activation of JNK, further leading to TNFα-induced apoptosis [112, 146]. Thus, one potential mechanism is that increased CCN1 expression in the WISP1 knockout mice lead to an enhanced JNK activation and further contributing to enhanced cell death. To examine this hypothesis *in vivo* studies using an antibody against CCN1 or siRNA to knockdown CCN1 expression could be helpful. Beyond that, the treatment of wild type mice using CCN1 in combination with CCl_4 should lead to enhanced liver damage compared to wild type mice treated only with CCl_4.

The current study revealed not only enhanced susceptibility to CCl_4-induced liver damage, but also to APAP-induced hepatotoxicity. Signal transduction upon CCl_4-induced liver injury revealed alterations in JNK, ERK1/2 and STAT3 signaling. Therefore, the

investigation of these pathways after APAP administration was another central approach in my study. However, none of these pathways showed any significant difference in activation comparing wild type mice to WISP1 knockout mice. As reported by Gunawan et al, JNK signaling was involved in APAP-induced toxicity validated by the usage of the JNK inhibitor SP600125, yet the JNK inhibitor was not effective with regard to CCl_4-induced liver damage nor upon Concanavalin A hepatotoxicity [84]. Moreover, regarding ER stress, Uzi et al confirmed a reduction in liver damage when using CHOP knockout mice upon APAP administration [103]. On the contrary, Campos et al detected no difference in the protection against CCl_4-induced liver damage by using similar CHOP knockout and wild type mice [99]. Taken together, this suggests that signaling and molecular mechanisms can be different concerning various models. Therefore, enhanced susceptibility may be mediated through different pathways upon APAP administration in the WISP1 knockout mice.

Investigating the Wnt/β-catenin pathway could be useful since WISP1 is a target of the Wnt/β-catenin pathway. It is an important pathway controlling the liver zonation [30, 128, 154], which is relevant for drug metabolism. In the past, most studies investigated CCN1-3 proteins, focusing on their receptors and binding partners. Just recently, Stephens et al investigated interactions of WISP1 with integrin receptors by using truncated versions of WISP1 [203]. They found that WISP1 mediated adhesion of epithelial cells, as well as CXCL3 secretion and activation of β-catenin, mainly through the C-terminal domain of the protein. However, the results did not reflect an all or nothing situation, suggesting that WISP1 may act through various domains. Moreover, the interaction of WISP1 was reported to depend on different receptors with regard to two different cell lines [203]. Therefore, it would be interesting to study the interaction of truncated versions of WISP1 with various receptors on hepatocytes and NPCs *in vitro*. This might be further beneficial with regard to the identification of potential mechanisms of WISP1 in these cells. Furthermore, it might also help to gain more information regarding the mechanism of WISP1 *in vivo*.

Sterile inflammation is a well-known aspect during drug-induced liver injury [25, 54]. Upon hepatotoxic compound exposure, DAMPs are release and cause production of pro-inflammatory cytokines and chemokines by binding to TLRs on macrophages leading to further recruitment of neutrophils and circulating monocytes [53, 64]. The role of leukocytes in hepatotoxic liver injury is not fully understood. Accumulation of neutrophils can cause further cell death by the release of ROS and proteases. However, both neutrophils and macrophages can also contribute to wound healing by phagocytosis of cell debris [61, 65, 66]. Although sterile inflammation is well-described feature of DILI, its contribution to the progress of liver injury is still controversial. Liu et al reported that the depletion of neutrophils using anti-Gr-1 antibody led to reduced liver injury upon APAP administration [67]. Contrary to the proposed pro-damaging role of inflammation, deleption of Kupffer cells by clodronate liposomes led to enhanced hepatic injury [73]. Moreover, genetic deletion of STAT3 in myeloid cells attenuated liver damage, accompanied by enhanced inflammation which was detected by an increased number of infiltrating immune cells as well as increased cytokine production [55]. During my study I was able to show that the genetic deletion of

WISP1 was associated with enhanced liver damage and a stronger inflammatory response. The enhanced inflammatory response was characterized by stronger activation of hepatoprotective STAT3 signaling, as well as an increased expression of pro-inflammatory cytokines. Furthermore, an increased number of infiltrating immune cells was detected upon CCl_4 administration in WISP1 knockout mice. However, it remains unclear whether increased inflammatory response is a cause or a consequence of the enhanced hepatic injury, since enhanced inflammation was observed at same time that the first hepatotoxic events were observed in WISP1 knockout mice. The implementation of additional *in vivo* models focusing on liver inflammation (hepatitis), such as Concanavalin A or D-galactosamine in combination with LPS or TNFα, could be useful for further investigations in the future.

The implementation of *in vitro* studies using primary mouse hepatocytes compromised various advantages and disadvantages. For example, isolated and cultivated hepatocytes represent a rather inflammatory liver than a healthy or control liver, as reported by Godoy et al [204]. This is due to alterations in the gene expression patterns and the transcriptional regulatory networks in hepatocytes, which can also influence the expression and mode of action of WISP1. However, since *in vivo* studies include complex mechanisms and interactions of various cell types in the liver as well as infiltrating immune cells [64], it is rather difficult to examine the role of WISP1 on hepatocytes alone. Furthermore, hepatocytes make up about 80% of the liver mass [8] and WISP1 expression was mainly derived by hepatocytes upon CCl_4 administration as shown in my study. *In vivo* experiments also revealed an enhanced inflammation in WISP1 knockout mice, which was consistent with an advanced liver damage and an increased WISP1 expression upon CCl_4 administration. To examine whether hepatocytes themselves are more susceptible to cytokine or APAP stimulation, *in vitro* studies using WISP1 knockout hepatocytes and wild type hepatocytes were implemented. Primary hepatocytes are the most relevant *in vitro* tool to determine liver functions including drug toxicity, metabolism or transport [205-207]. Stimulation of hepatocytes using TNFα or TGFβ in combination with actinomycin D, revealed an enhanced susceptibility of WISP1 knockout hepatocytes, which was associated with an enhanced caspase 3 activation. This suggests that the genetic deletion of WISP1 in hepatocytes makes them more susceptible to cell death, which was also confirmed by stimulation using APAP. So it is likely that WISP1 in hepatocytes is needed to develop the protective phenotype *in vitro* as well as *in vivo*. In fact, further investigations regarding the effect on NPCs are needed, since high expression of WISP1 was found in the NPCs upon control conditions. Moreover, deeper insights on the molecular events leading to enhanced susceptibility in hepatocytes are needed. Therefore, stimulation of knockout hepatocytes *in vitro* using WISP1 protein or adenoviruses to restore WISP1 expression, could be useful to test whether the hepatocytes could be rescued. Furthermore, the usage of truncated versions of WISP1 could be beneficial to get a deeper insight in the mechanism of the protective effect.

A central aspect of the current study was the usage of gene array analysis combined with qRT-PCR analyses in the wild type and WISP1 knockout mice upon CCl_4 administration.

The analyses revealed a strong up-regulation of cytochrome P450 enzymes and a down-regulation of serine protease inhibitors, which were associated to inflammation and obesity [191], at all time points. Cytochrome P450 gene 4 family (CYP4) is known to metabolize medium (C_{10}-C_{16}) saturated, unsaturated and branched chain fatty acids by ω-oxidation, which becomes important during increased influx of fatty acids or in cases where the mitochondrial oxidation system is insufficient for metabolizing fatty acids. Therefore, strong up-regulation of CYP4A genes should prevent from excessive increase of fatty acids, which can cause lipid toxicity and initiates fatty liver inflammation (steatohepatitis) [190, 208, 209]. Moreover, analysis of KEGG pathways revealed up-regulation of fatty acid degradation and PPAR signaling, which is involved in the induction of CYP4A enzymes and regulation of lipid and glucose homeostasis [210, 211]. Furthermore, Murahovschi et al reported that WISP1 might link obesity to inflammation and insulin resistance [162]. Taken together, the results of my study suggest that genetic deletion of WISP1 may alter lipid metabolism in hepatocytes which could be a mediator for enhanced toxicity, since there is a connection between obesity and an increased risk of hepatotoxicity [212, 213]. Moreover, the accumulation of fatty acids can cause lipid toxicity in the liver [208]. Further investigations regarding altered pathways,, such as PPAR signaling, need to be addressed to explain and clarify potential effects of WISP1 during lipid metabolism. For example, *in vitro* stimulation of wild type and WISP1 knockout hepatocytes using oleic acid could reveal alterations in the uptake and metabolism of free fatty acids, as well as alterations in the signal transduction.

Finally, cell death-inducing DFF45-like effector C (CIDEC), which is reported to be localized in the cytoplasm and to be involved in promoting the formation of fat droplets [214], is up-regulated in WISP1 knockout mice on D1. CIDEC was shown to participate in the development of metabolic disorders as well as in the regulation of cell apoptosis [214-217]. Recently, Xu et al suggested that CIDEC promotes the development of alcoholic steatohepatitis in mice and humans, by acting synergistically with ethanol to induce ROS production leading to hepatocellular death [192]. Therefore, it is likely that CIDEC may contribute to the development of liver injury in the WISP1 knockout mice. However, further investigations are needed to clarify this hypothesis.

Taken together, the present study revealed a yet unknown role of WISP1 as a protective mediator upon acute liver injury. The genetic deletion of WISP1 led to an enhanced stress-associated and pro-inflammatory signaling. Enhanced inflammation was confirmed by an increased expression of pro-inflammatory cytokines as well as enhanced immune cell infiltration. However, it still remains unclear whether inflammation is the consequence of enhanced liver damage, or if inflammation might cause hepatotoxic effects. Finally, gene array analysis revealed an altered lipid metabolism in the WISP1 knockout mice, which could also contribute to the development of liver injury. Further investigations are needed to clarify the potential mechanism of WISP1 upon lipid metabolism and toxicity. Although potential binding partners and receptors need to be investigated along with the precise mechanism through which WISP1 is mediating its pro-survival role, it seems as if in future WISP1 might be a promising target for therapeutical interventions, since also the

human liver disease patients' samples revealed an increased WISP1 expression. Lastly, this study highlighted the importance of the transcriptional network and uncovered a yet unknown important mediator upon the development of acute liver damage. This might further help to acquire a deeper insight in the mechanisms and the progress of hepatotoxicity. Further studies regarding the role of WISP1 in chronic diseases, such as fibrosis or cancer could unveil even further important influences of WISP1.

LIST OF FIGURES

LIST OF TABLES

SUPPLEMENT

All tables are available in digital from on the attached CD.

Supplement 1: Groups of similar regulated genes CCl_4-WISP1

Supplement 2: Fuzzy Cluster KO vs WT CCl_4 WISP1_FC15_pVal05

Supplement 3: Functional Profiling Fuzzy KO-WT_pV05

REFERENCES

1. Blachier, M., et al., *The burden of liver disease in Europe: a review of available epidemiological data.* J Hepatol, 2013. **58**(3): p. 593-608.
2. Blachier, M., et al., *The burden of liver disease. A review of available epidemiological data.* http://www.easl.eu/medias/EASLimg/Discover/EU/54ae845caec619f_file.pdf, 2013: p. 1-64.
3. Pellicoro, A., et al., *Liver fibrosis and repair: immune regulation of wound healing in a solid organ.* Nat Rev Immunol, 2014. **14**(3): p. 181-94.
4. Tsochatzis, E.A., J. Bosch, and A.K. Burroughs, *Liver cirrhosis.* Lancet, 2014. **383**(9930): p. 1749-61.
5. Jaeschke, H., et al., *Mechanisms of hepatotoxicity.* Toxicol Sci, 2002. **65**(2): p. 166-76.
6. Yuan, L. and N. Kaplowitz, *Mechanisms of drug-induced liver injury.* Clin Liver Dis, 2013. **17**(4): p. 507-18, vii.
7. Han, D., et al., *Regulation of drug-induced liver injury by signal transduction pathways: critical role of mitochondria.* Trends Pharmacol Sci, 2013. **34**(4): p. 243-53.
8. Taub, R., *Liver regeneration: from myth to mechanism.* Nat Rev Mol Cell Biol, 2004. **5**(10): p. 836-47.
9. Bandara, L.R. and S. Kennedy, *Toxicoproteomics -- a new preclinical tool.* Drug Discov Today, 2002. **7**(7): p. 411-8.
10. Crispe, I.N., *Liver antigen-presenting cells.* J Hepatol, 2011. **54**(2): p. 357-65.
11. Jungermann, K. and T. Kietzmann, *Zonation of parenchymal and nonparenchymal metabolism in liver.* Annu Rev Nutr, 1996. **16**: p. 179-203.
12. Jenne, C.N. and P. Kubes, *Immune surveillance by the liver.* Nat Immunol, 2013. **14**(10): p. 996-1006.
13. Vollmar, B. and M.D. Menger, *The hepatic microcirculation: mechanistic contributions and therapeutic targets in liver injury and repair.* Physiol Rev, 2009. **89**(4): p. 1269-339.
14. Hoehme, S., et al., *Prediction and validation of cell alignment along microvessels as order principle to restore tissue architecture in liver regeneration.* Proc Natl Acad Sci U S A, 2010. **107**(23): p. 10371-6.
15. LeCluyse, E.L., et al., *Organotypic liver culture models: meeting current challenges in toxicity testing.* Crit Rev Toxicol, 2012. **42**(6): p. 501-48.
16. Oinonen, T. and K.O. Lindros, *Zonation of hepatic cytochrome P-450 expression and regulation.* Biochem J, 1998. **329 (Pt 1)**: p. 17-35.
17. Braeuning, A., et al., *Differential gene expression in periportal and perivenous mouse hepatocytes.* FEBS J, 2006. **273**(22): p. 5051-61.
18. Wisse, E., et al., *Structure and function of sinusoidal lining cells in the liver.* Toxicol Pathol, 1996. **24**(1): p. 100-11.
19. Blouin, A., R.P. Bolender, and E.R. Weibel, *Distribution of organelles and membranes between hepatocytes and nonhepatocytes in the rat liver parenchyma. A stereological study.* J Cell Biol, 1977. **72**(2): p. 441-55.
20. Bataller, R. and D.A. Brenner, *Liver fibrosis.* J Clin Invest, 2005. **115**(2): p. 209-18.
21. Dufour, J.-F. and P.-A. Clavien, *Signaling pathways in liver diseases.* Springer-Verlag, 2005.
22. Weibel, E.R., et al., *Correlated morphometric and biochemical studies on the liver cell. I. Morphometric model, stereologic methods, and normal morphometric data for rat liver.* J Cell Biol, 1969. **42**(1): p. 68-91.
23. Gebhardt, R., *Metabolic zonation of the liver: regulation and implications for liver function.* Pharmacol Ther, 1992. **53**(3): p. 275-354.
24. Godoy, P., et al., *Recent advances in 2D and 3D in vitro systems using primary hepatocytes, alternative hepatocyte sources and non-parenchymal liver cells and their use in investigating mechanisms of hepatotoxicity, cell signaling and ADME.* Arch Toxicol, 2013. **87**(8): p. 1315-530.

25. Ramadori, G., et al., *Physiology and pathophysiology of liver inflammation, damage and repair.* J Physiol Pharmacol, 2008. **59 Suppl 1**: p. 107-17.
26. Ishibashi, H., et al., *Liver architecture, cell function, and disease.* Semin Immunopathol, 2009. **31**(3): p. 399-409.
27. Williams, J.A., et al., *Reaction phenotyping in drug discovery: moving forward with confidence?* Curr Drug Metab, 2003. **4**(6): p. 527-34.
28. Guengerich, F.P., *Cytochrome P450s and other enzymes in drug metabolism and toxicity.* AAPS J, 2006. **8**(1): p. E101-11.
29. Anzenbacher, P. and E. Anzenbacherova, *Cytochromes P450 and metabolism of xenobiotics.* Cell Mol Life Sci, 2001. **58**(5-6): p. 737-47.
30. Colnot, S. and C. Perret, *Liver zonation.* Molecular pathology of liver diseases. S.P.S. Monga (ed.), 2011. **5**: p. 7-16.
31. Cederbaum, A.I., *Role of CYP2E1 in ethanol-induced oxidant stress, fatty liver and hepatotoxicity.* Dig Dis, 2010. **28**(6): p. 802-11.
32. Torre, C., C. Perret, and S. Colnot, *Transcription dynamics in a physiological process: beta-catenin signaling directs liver metabolic zonation.* Int J Biochem Cell Biol, 2011. **43**(2): p. 271-8.
33. Park, B.K., et al., *The role of metabolic activation in drug-induced hepatotoxicity.* Annu Rev Pharmacol Toxicol, 2005. **45**: p. 177-202.
34. McCarver, D.G. and R.N. Hines, *The ontogeny of human drug-metabolizing enzymes: phase II conjugation enzymes and regulatory mechanisms.* J Pharmacol Exp Ther, 2002. **300**(2): p. 361-6.
35. Maes, M., M. Vinken, and H. Jaeschke, *Experimental models of hepatotoxicity related to acute liver failure.* Toxicol Appl Pharmacol, 2016. **290**: p. 86-97.
36. Jaeschke, H., et al., *Models of drug-induced liver injury for evaluation of phytotherapeutics and other natural products.* Food Chem Toxicol, 2013. **55**: p. 279-89.
37. Hubner, G., *[Ultrastructural liver damage caused by direct action of carbon tetrachloride in vivo and in vitro].* Virchows Arch Pathol Anat Physiol Klin Med, 1965. **339**(3): p. 187-97.
38. Smith, D.H., *Carbon tetrachloride toxicity.* Br Med J, 1965. **2**(5475): p. 1434.
39. Ingawale, D.K., S.K. Mandlik, and S.R. Naik, *Models of hepatotoxicity and the underlying cellular, biochemical and immunological mechanism(s): a critical discussion.* Environ Toxicol Pharmacol, 2014. **37**(1): p. 118-33.
40. Brautbar, N. and J. Williams, 2nd, *Industrial solvents and liver toxicity: risk assessment, risk factors and mechanisms.* Int J Hyg Environ Health, 2002. **205**(6): p. 479-91.
41. Weber, L.W., M. Boll, and A. Stampfl, *Hepatotoxicity and mechanism of action of haloalkanes: carbon tetrachloride as a toxicological model.* Crit Rev Toxicol, 2003. **33**(2): p. 105-36.
42. Raucy, J.L., J.C. Kraner, and J.M. Lasker, *Bioactivation of halogenated hydrocarbons by cytochrome P4502E1.* Crit Rev Toxicol, 1993. **23**(1): p. 1-20.
43. Hinson, J.A., D.W. Roberts, and L.P. James, *Mechanisms of acetaminophen-induced liver necrosis.* Handb Exp Pharmacol, 2010(196): p. 369-405.
44. Xie, Y., et al., *Mechanisms of acetaminophen-induced cell death in primary human hepatocytes.* Toxicol Appl Pharmacol, 2014. **279**(3): p. 266-74.
45. Mitchell, J.R., et al., *Acetaminophen-induced hepatic necrosis. IV. Protective role of glutathione.* J Pharmacol Exp Ther, 1973. **187**(1): p. 211-7.
46. Tonge, R.P., et al., *Role of CYP1A2 in the hepatotoxicity of acetaminophen: investigations using Cyp1a2 null mice.* Toxicol Appl Pharmacol, 1998. **153**(1): p. 102-8.
47. Zaher, H., et al., *Protection against acetaminophen toxicity in CYP1A2 and CYP2E1 double-null mice.* Toxicol Appl Pharmacol, 1998. **152**(1): p. 193-9.
48. Du, K., et al., *Pathophysiological significance of c-jun N-terminal kinase in acetaminophen hepatotoxicity.* Expert Opin Drug Metab Toxicol, 2015. **11**(11): p. 1769-79.

49. Hanawa, N., et al., *Role of JNK translocation to mitochondria leading to inhibition of mitochondria bioenergetics in acetaminophen-induced liver injury.* J Biol Chem, 2008. **283**(20): p. 13565-77.
50. Gujral, J.S., et al., *Mode of cell death after acetaminophen overdose in mice: apoptosis or oncotic necrosis?* Toxicol Sci, 2002. **67**(2): p. 322-8.
51. Ramachandran, A., et al., *Receptor interacting protein kinase 3 is a critical early mediator of acetaminophen-induced hepatocyte necrosis in mice.* Hepatology, 2013. **58**(6): p. 2099-108.
52. McDonald, B. and P. Kubes, *Innate Immune Cell Trafficking and Function During Sterile Inflammation of the Liver.* Gastroenterology, 2016. **151**(6): p. 1087-1095.
53. Kubes, P. and W.Z. Mehal, *Sterile inflammation in the liver.* Gastroenterology, 2012. **143**(5): p. 1158-72.
54. Jaeschke, H., et al., *Acetaminophen hepatotoxicity and repair: the role of sterile inflammation and innate immunity.* Liver Int, 2012. **32**(1): p. 8-20.
55. Horiguchi, N., et al., *Dissociation between liver inflammation and hepatocellular damage induced by carbon tetrachloride in myeloid cell-specific signal transducer and activator of transcription 3 gene knockout mice.* Hepatology, 2010. **51**(5): p. 1724-34.
56. Imaeda, A.B., et al., *Acetaminophen-induced hepatotoxicity in mice is dependent on Tlr9 and the Nalp3 inflammasome.* J Clin Invest, 2009. **119**(2): p. 305-14.
57. Brenner, C., et al., *Decoding cell death signals in liver inflammation.* J Hepatol, 2013. **59**(3): p. 583-94.
58. Huang, H., et al., *Damage-associated molecular pattern-activated neutrophil extracellular trap exacerbates sterile inflammatory liver injury.* Hepatology, 2015. **62**(2): p. 600-14.
59. Chen, C.J., et al., *Identification of a key pathway required for the sterile inflammatory response triggered by dying cells.* Nat Med, 2007. **13**(7): p. 851-6.
60. Heymann, F. and F. Tacke, *Immunology in the liver--from homeostasis to disease.* Nat Rev Gastroenterol Hepatol, 2016. **13**(2): p. 88-110.
61. Zimmermann, H.W., C. Trautwein, and F. Tacke, *Functional role of monocytes and macrophages for the inflammatory response in acute liver injury.* Front Physiol, 2012. **3**: p. 56.
62. Nikolaou, K., M. Sarris, and I. Talianidis, *Molecular pathways: the complex roles of inflammation pathways in the development and treatment of liver cancer.* Clin Cancer Res, 2013. **19**(11): p. 2810-6.
63. Gardner, C.R., et al., *Exaggerated hepatotoxicity of acetaminophen in mice lacking tumor necrosis factor receptor-1. Potential role of inflammatory mediators.* Toxicol Appl Pharmacol, 2003. **192**(2): p. 119-30.
64. Adams, D.H., et al., *Mechanisms of immune-mediated liver injury.* Toxicol Sci, 2010. **115**(2): p. 307-21.
65. Nathan, C., *Neutrophils and immunity: challenges and opportunities.* Nat Rev Immunol, 2006. **6**(3): p. 173-82.
66. Kono, H. and K.L. Rock, *How dying cells alert the immune system to danger.* Nat Rev Immunol, 2008. **8**(4): p. 279-89.
67. Liu, Z.X., et al., *Neutrophil depletion protects against murine acetaminophen hepatotoxicity.* Hepatology, 2006. **43**(6): p. 1220-30.
68. Jaeschke, H. and J. Liu, *Neutrophil depletion protects against murine acetaminophen hepatotoxicity: another perspective.* Hepatology, 2007. **45**(6): p. 1588-9; author reply 1589.
69. Liu, J., et al., *Metallothionein-I/II knockout mice are sensitive to acetaminophen-induced hepatotoxicity.* J Pharmacol Exp Ther, 1999. **289**(1): p. 580-6.
70. Klune, J.R. and A. Tsung, *Molecular biology of liver ischemia/reperfusion injury: established mechanisms and recent advancements.* Surg Clin North Am, 2010. **90**(4): p. 665-77.
71. van Golen, R.F., et al., *Sterile inflammation in hepatic ischemia/reperfusion injury: present concepts and potential therapeutics.* J Gastroenterol Hepatol, 2013. **28**(3): p. 394-400.
72. Ishida, Y., et al., *A pivotal involvement of IFN-gamma in the pathogenesis of acetaminophen-induced acute liver injury.* FASEB J, 2002. **16**(10): p. 1227-36.

73. Sato, A., et al., *Involvement of the TNF and FasL produced by CD11b Kupffer cells/macrophages in CCl4-induced acute hepatic injury.* PLoS One, 2014. **9**(3): p. e92515.
74. Karlmark, K.R., et al., *Hepatic recruitment of the inflammatory Gr1+ monocyte subset upon liver injury promotes hepatic fibrosis.* Hepatology, 2009. **50**(1): p. 261-74.
75. Sekine, S., et al., *Liver-specific loss of beta-catenin blocks glutamine synthesis pathway activity and cytochrome p450 expression in mice.* Hepatology, 2006. **43**(4): p. 817-25.
76. Zeng, G., et al., *Wnt'er in liver: expression of Wnt and frizzled genes in mouse.* Hepatology, 2007. **45**(1): p. 195-204.
77. Yu, J. and D.M. Virshup, *Updating the Wnt pathways.* Biosci Rep, 2014. **34**(5).
78. van den Bosch, M.H., et al., *Wnts talking with the TGF-beta superfamily: WISPers about modulation of osteoarthritis.* Rheumatology (Oxford), 2016. **55**(9): p. 1536-47.
79. Staal, F.J. and H.C. Clevers, *WNT signalling and haematopoiesis: a WNT-WNT situation.* Nat Rev Immunol, 2005. **5**(1): p. 21-30.
80. Vlad, A., et al., *The first five years of the Wnt targetome.* Cell Signal, 2008. **20**(5): p. 795-802.
81. Fujiyoshi, M. and M. Ozaki, *Molecular mechanisms of liver regeneration and protection for treatment of liver dysfunction and diseases.* J Hepatobiliary Pancreat Sci, 2011. **18**(1): p. 13-22.
82. Fausto, N., J.S. Campbell, and K.J. Riehle, *Liver regeneration.* Hepatology, 2006. **43**(2 Suppl 1): p. S45-53.
83. Shuai, K. and B. Liu, *Regulation of JAK-STAT signalling in the immune system.* Nat Rev Immunol, 2003. **3**(11): p. 900-11.
84. Gunawan, B.K., et al., *c-Jun N-terminal kinase plays a major role in murine acetaminophen hepatotoxicity.* Gastroenterology, 2006. **131**(1): p. 165-78.
85. Cubero, F.J., et al., *Combined Activities of JNK1 and JNK2 in Hepatocytes Protect Against Toxic Liver Injury.* Gastroenterology, 2016. **150**(4): p. 968-81.
86. Bhushan, B., et al., *Pro-regenerative signaling after acetaminophen-induced acute liver injury in mice identified using a novel incremental dose model.* Am J Pathol, 2014. **184**(11): p. 3013-25.
87. Sweeney, S.E. and G.S. Firestein, *Primer: signal transduction in rheumatic disease--a clinician's guide.* Nat Clin Pract Rheumatol, 2007. **3**(11): p. 651-60.
88. Kyriakis, J.M. and J. Avruch, *Mammalian MAPK signal transduction pathways activated by stress and inflammation: a 10-year update.* Physiol Rev, 2012. **92**(2): p. 689-737.
89. Saklatvala, J., *The p38 MAP kinase pathway as a therapeutic target in inflammatory disease.* Curr Opin Pharmacol, 2004. **4**(4): p. 372-7.
90. Fremin, C. and S. Meloche, *From basic research to clinical development of MEK1/2 inhibitors for cancer therapy.* J Hematol Oncol, 2010. **3**: p. 8.
91. Xia, Z., et al., *Opposing effects of ERK and JNK-p38 MAP kinases on apoptosis.* Science, 1995. **270**(5240): p. 1326-31.
92. Mizukami, Y., et al., *A novel mechanism of JNK1 activation. Nuclear translocation and activation of JNK1 during ischemia and reperfusion.* J Biol Chem, 1997. **272**(26): p. 16657-62.
93. Lewis, T.S., P.S. Shapiro, and N.G. Ahn, *Signal transduction through MAP kinase cascades.* Adv Cancer Res, 1998. **74**: p. 49-139.
94. Costa, R.H., et al., *Transcription factors in liver development, differentiation, and regeneration.* Hepatology, 2003. **38**(6): p. 1331-47.
95. Sanders, J.A., et al., *Postnatal liver growth and regeneration are independent of c-myc in a mouse model of conditional hepatic c-myc deletion.* BMC Physiol, 2012. **12**: p. 1.
96. Dang, C.V., *c-Myc target genes involved in cell growth, apoptosis, and metabolism.* Mol Cell Biol, 1999. **19**(1): p. 1-11.
97. Nevzorova, Y.A., et al., *Overexpression of c-myc in hepatocytes promotes activation of hepatic stellate cells and facilitates the onset of liver fibrosis.* Biochim Biophys Acta, 2013. **1832**(10): p. 1765-75.
98. Zeeshan, H.M., et al., *Endoplasmic Reticulum Stress and Associated ROS.* Int J Mol Sci, 2016. **17**(3): p. 327.

99. Campos, G., et al., *The transcription factor CHOP, a central component of the transcriptional regulatory network induced upon CCl4 intoxication in mouse liver, is not a critical mediator of hepatotoxicity.* Arch Toxicol, 2014. **88**(6): p. 1267-80.
100. Grootjans, J., et al., *The unfolded protein response in immunity and inflammation.* Nat Rev Immunol, 2016. **16**(8): p. 469-84.
101. Malhi, H. and R.J. Kaufman, *Endoplasmic reticulum stress in liver disease.* J Hepatol, 2011. **54**(4): p. 795-809.
102. Hetz, C., *The unfolded protein response: controlling cell fate decisions under ER stress and beyond.* Nat Rev Mol Cell Biol, 2012. **13**(2): p. 89-102.
103. Uzi, D., et al., *CHOP is a critical regulator of acetaminophen-induced hepatotoxicity.* J Hepatol, 2013. **59**(3): p. 495-503.
104. Tabas, I. and D. Ron, *Integrating the mechanisms of apoptosis induced by endoplasmic reticulum stress.* Nat Cell Biol, 2011. **13**(3): p. 184-90.
105. Martelli, A.M., et al., *The phosphatidylinositol 3-kinase/Akt/mTOR signaling network as a therapeutic target in acute myelogenous leukemia patients.* Oncotarget, 2010. **1**(2): p. 89-103.
106. Su, F., et al., *WISP-1 attenuates p53-mediated apoptosis in response to DNA damage through activation of the Akt kinase.* Genes Dev, 2002. **16**(1): p. 46-57.
107. Porta, C., C. Paglino, and A. Mosca, *Targeting PI3K/Akt/mTOR Signaling in Cancer.* Front Oncol, 2014. **4**: p. 64.
108. Shuh, M., et al., *Tumor Necrosis Factor-alpha: Life and Death of Hepatocytes During Liver Ischemia/Reperfusion Injury.* Ochsner J, 2013. **13**(1): p. 119-30.
109. Liedtke, C. and C. Trautwein, *The role of TNF and Fas dependent signaling in animal models of inflammatory liver injury and liver cancer.* Eur J Cell Biol, 2012. **91**(6-7): p. 582-9.
110. Papa, S., et al., *Mechanisms of liver disease: cross-talk between the NF-kappaB and JNK pathways.* Biol Chem, 2009. **390**(10): p. 965-76.
111. Malhi, H., M.E. Guicciardi, and G.J. Gores, *Hepatocyte death: a clear and present danger.* Physiol Rev, 2010. **90**(3): p. 1165-94.
112. Chen, C.C. and L.F. Lau, *Deadly liaisons: fatal attraction between CCN matricellular proteins and the tumor necrosis factor family of cytokines.* J Cell Commun Signal, 2010. **4**(1): p. 63-9.
113. Guicciardi, M.E. and G.J. Gores, *Life and death by death receptors.* FASEB J, 2009. **23**(6): p. 1625-37.
114. Schuster, N. and K. Krieglstein, *Mechanisms of TGF-beta-mediated apoptosis.* Cell Tissue Res, 2002. **307**(1): p. 1-14.
115. Pinzani, M. and F. Marra, *Cytokine receptors and signaling in hepatic stellate cells.* Semin Liver Dis, 2001. **21**(3): p. 397-416.
116. Fausto, N., *Liver regeneration.* J Hepatol, 2000. **32**(1 Suppl): p. 19-31.
117. Yamamura, Y., et al., *Critical role of Smads and AP-1 complex in transforming growth factor-beta -dependent apoptosis.* J Biol Chem, 2000. **275**(46): p. 36295-302.
118. Yoo, J., et al., *Transforming growth factor-beta-induced apoptosis is mediated by Smad-dependent expression of GADD45b through p38 activation.* J Biol Chem, 2003. **278**(44): p. 43001-7.
119. Godoy, P., et al., *Extracellular matrix modulates sensitivity of hepatocytes to fibroblastoid dedifferentiation and transforming growth factor beta-induced apoptosis.* Hepatology, 2009. **49**(6): p. 2031-43.
120. Perlman, R., et al., *TGF-beta-induced apoptosis is mediated by the adapter protein Daxx that facilitates JNK activation.* Nat Cell Biol, 2001. **3**(8): p. 708-14.
121. Sanderson, N., et al., *Hepatic expression of mature transforming growth factor beta 1 in transgenic mice results in multiple tissue lesions.* Proc Natl Acad Sci U S A, 1995. **92**(7): p. 2572-6.
122. Liao, J.H., et al., *The involvement of p38 MAPK in transforming growth factor beta1-induced apoptosis in murine hepatocytes.* Cell Res, 2001. **11**(2): p. 89-94.

123. Park, H.J., et al., *Role of MAP kinases and their cross-talk in TGF-beta1-induced apoptosis in FaO rat hepatoma cell line.* Hepatology, 2002. **35**(6): p. 1360-71.
124. Joliot, V., et al., *Proviral rearrangements and overexpression of a new cellular gene (nov) in myeloblastosis-associated virus type 1-induced nephroblastomas.* Mol Cell Biol, 1992. **12**(1): p. 10-21.
125. O'Brien, T.P., et al., *Expression of cyr61, a growth factor-inducible immediate-early gene.* Mol Cell Biol, 1990. **10**(7): p. 3569-77.
126. Bradham, D.M., et al., *Connective tissue growth factor: a cysteine-rich mitogen secreted by human vascular endothelial cells is related to the SRC-induced immediate early gene product CEF-10.* J Cell Biol, 1991. **114**(6): p. 1285-94.
127. Brigstock, D.R., et al., *Proposal for a unified CCN nomenclature.* Mol Pathol, 2003. **56**(2): p. 127-8.
128. Pennica, D., et al., *WISP genes are members of the connective tissue growth factor family that are up-regulated in wnt-1-transformed cells and aberrantly expressed in human colon tumors.* Proc Natl Acad Sci U S A, 1998. **95**(25): p. 14717-22.
129. Leask, A. and D.J. Abraham, *All in the CCN family: essential matricellular signaling modulators emerge from the bunker.* J Cell Sci, 2006. **119**(Pt 23): p. 4803-10.
130. Holbourn, K.P., K.R. Acharya, and B. Perbal, *The CCN family of proteins: structure-function relationships.* Trends Biochem Sci, 2008. **33**(10): p. 461-73.
131. Chen, C.C. and L.F. Lau, *Functions and mechanisms of action of CCN matricellular proteins.* Int J Biochem Cell Biol, 2009. **41**(4): p. 771-83.
132. Jun, J.I. and L.F. Lau, *Taking aim at the extracellular matrix: CCN proteins as emerging therapeutic targets.* Nat Rev Drug Discov, 2011. **10**(12): p. 945-63.
133. Bork, P., *The modular architecture of a new family of growth regulators related to connective tissue growth factor.* FEBS Lett, 1993. **327**(2): p. 125-30.
134. Weiskirchen, R., *CCN proteins in normal and injured liver.* Front Biosci (Landmark Ed), 2011. **16**: p. 1939-61.
135. Bornstein, P. and E.H. Sage, *Matricellular proteins: extracellular modulators of cell function.* Curr Opin Cell Biol, 2002. **14**(5): p. 608-16.
136. Mo, F.E., et al., *CYR61 (CCN1) is essential for placental development and vascular integrity.* Mol Cell Biol, 2002. **22**(24): p. 8709-20.
137. Mo, F.E. and L.F. Lau, *The matricellular protein CCN1 is essential for cardiac development.* Circ Res, 2006. **99**(9): p. 961-9.
138. Ivkovic, S., et al., *Connective tissue growth factor coordinates chondrogenesis and angiogenesis during skeletal development.* Development, 2003. **130**(12): p. 2779-91.
139. Baguma-Nibasheka, M. and B. Kablar, *Pulmonary hypoplasia in the connective tissue growth factor (Ctgf) null mouse.* Dev Dyn, 2008. **237**(2): p. 485-93.
140. Crawford, L.A., et al., *Connective tissue growth factor (CTGF) inactivation leads to defects in islet cell lineage allocation and beta-cell proliferation during embryogenesis.* Mol Endocrinol, 2009. **23**(3): p. 324-36.
141. Russo, J.W. and J.J. Castellot, *CCN5: biology and pathophysiology.* J Cell Commun Signal, 2010. **4**(3): p. 119-30.
142. Lau, L.F., *Cell surface receptors for CCN proteins.* J Cell Commun Signal, 2016. **10**(2): p. 121-7.
143. Kim, K.H., et al., *Matricellular protein CCN1 promotes regression of liver fibrosis through induction of cellular senescence in hepatic myofibroblasts.* Mol Cell Biol, 2013. **33**(10): p. 2078-90.
144. Jun, J.I. and L.F. Lau, *The matricellular protein CCN1 induces fibroblast senescence and restricts fibrosis in cutaneous wound healing.* Nat Cell Biol, 2010. **12**(7): p. 676-85.
145. Lau, L.F., *CCN1/CYR61: the very model of a modern matricellular protein.* Cell Mol Life Sci, 2011. **68**(19): p. 3149-63.
146. Chen, C.C., et al., *Cytotoxicity of TNFalpha is regulated by integrin-mediated matrix signaling.* EMBO J, 2007. **26**(5): p. 1257-67.

147. Brigstock, D.R., *Connective tissue growth factor (CCN2, CTGF) and organ fibrosis: lessons from transgenic animals.* J Cell Commun Signal, 2010. **4**(1): p. 1-4.
148. Uchio, K., et al., *Down-regulation of connective tissue growth factor and type I collagen mRNA expression by connective tissue growth factor antisense oligonucleotide during experimental liver fibrosis.* Wound Repair Regen, 2004. **12**(1): p. 60-6.
149. Li, G., et al., *Inhibition of connective tissue growth factor by siRNA prevents liver fibrosis in rats.* J Gene Med, 2006. **8**(7): p. 889-900.
150. Perbal, A. and B. Perbal, *The CCN family of proteins: a 25th anniversary picture.* J Cell Commun Signal, 2016. **10**(3): p. 177-190.
151. Raghu, G., et al., *FG-3019 anti-connective tissue growth factor monoclonal antibody: results of an open-label clinical trial in idiopathic pulmonary fibrosis.* Eur Respir J, 2016. **47**(5): p. 1481-91.
152. Wang, Q., et al., *Cooperative interaction of CTGF and TGF-beta in animal models of fibrotic disease.* Fibrogenesis Tissue Repair, 2011. **4**(1): p. 4.
153. Adler, S.G., et al., *Phase 1 study of anti-CTGF monoclonal antibody in patients with diabetes and microalbuminuria.* Clin J Am Soc Nephrol, 2010. **5**(8): p. 1420-8.
154. Xu, L., et al., *WISP-1 is a Wnt-1- and beta-catenin-responsive oncogene.* Genes Dev, 2000. **14**(5): p. 585-95.
155. Venkatachalam, K., et al., *WISP1, a pro-mitogenic, pro-survival factor, mediates tumor necrosis factor-alpha (TNF-alpha)-stimulated cardiac fibroblast proliferation but inhibits TNF-alpha-induced cardiomyocyte death.* J Biol Chem, 2009. **284**(21): p. 14414-27.
156. Lu, S., et al., *WISP1 overexpression promotes proliferation and migration of human vascular smooth muscle cells via AKT signaling pathway.* Eur J Pharmacol, 2016. **788**: p. 90-7.
157. Tong, Y., et al., *WISP1 mediates hepatic warm ischemia reperfusion injury via TLR4 signaling in mice.* Sci Rep, 2016. **6**: p. 20141.
158. Colston, J.T., et al., *Wnt-induced secreted protein-1 is a prohypertrophic and profibrotic growth factor.* Am J Physiol Heart Circ Physiol, 2007. **293**(3): p. H1839-46.
159. Dooley, S., et al., *Hepatocyte-specific Smad7 expression attenuates TGF-beta-mediated fibrogenesis and protects against liver damage.* Gastroenterology, 2008. **135**(2): p. 642-59.
160. Parisi, M.S., et al., *Expression and regulation of CCN genes in murine osteoblasts.* Bone, 2006. **38**(5): p. 671-7.
161. Klee, S., et al., *WISP1 mediates IL-6-dependent proliferation in primary human lung fibroblasts.* Sci Rep, 2016. **6**: p. 20547.
162. Murahovschi, V., et al., *WISP1 is a novel adipokine linked to inflammation in obesity.* Diabetes, 2015. **64**(3): p. 856-66.
163. New, L.S. and E.C. Chan, *Evaluation of BEH C18, BEH HILIC, and HSS T3 (C18) column chemistries for the UPLC-MS-MS analysis of glutathione, glutathione disulfide, and ophthalmic acid in mouse liver and human plasma.* J Chromatogr Sci, 2008. **46**(3): p. 209-14.
164. Livak, K.J. and T.D. Schmittgen, *Analysis of relative gene expression data using real-time quantitative PCR and the 2(-Delta Delta C(T)) Method.* Methods, 2001. **25**(4): p. 402-8.
165. Bolstad, B.M., *Low level analysis of High-density OligonucleotideArray Data: Background, Normalization and Summarization.* Berkeley: University of California, 2004.
166. Gentleman, R.C., et al., *Bioconductor: open software development for computational biology and bioinformatics.* Genome Biol, 2004. **5**(10): p. R80.
167. Smyth, G.K. and R.C. Gentleman, *Limma linear models for microarray data.* Bioinformatics and Computational Biology using R and Bioconductor, Springer: New York, 2005: p. 397-420.
168. Benjamini, Y. and Y. Hochberg, *Controlling the false discovery rate: a practical and powerful approach to multiple testing.* J. R. Stat. Soc. Ser. B, 1995. **57**(1): p. 289-300.
169. Dai, M., et al., *Evolving gene/transcript definitions significantly alter the interpretation of GeneChip data.* Nucleic Acids Res, 2005. **33**(20): p. e175.
170. Bezdek, J.C. and R.J. Hathaway, *Numerical convergence and interpretation of the fuzzy c-shells clustering algorithm.* IEEE Trans Neural Netw, 1992. **3**(5): p. 787-93.
171. Campos, G., *Genome-wide response patterns in stressed hepatocytes.* Dissertation, 2013.

172. Raucci, A., R. Palumbo, and M.E. Bianchi, *HMGB1: a signal of necrosis.* Autoimmunity, 2007. **40**(4): p. 285-9.
173. Zhou, R.R., et al., *HMGB1 cytoplasmic translocation in patients with acute liver failure.* BMC Gastroenterol, 2011. **11**: p. 21.
174. Assy, N., et al., *Use of proliferating cell nuclear antigen as a marker of liver regeneration after partial hepatectomy in rats.* J Lab Clin Med, 1998. **131**(3): p. 251-6.
175. Kurki, P., et al., *Expression of proliferating cell nuclear antigen (PCNA)/cyclin during the cell cycle.* Exp Cell Res, 1986. **166**(1): p. 209-19.
176. Martinez-Gac, L., et al., *Control of cyclin G2 mRNA expression by forkhead transcription factors: novel mechanism for cell cycle control by phosphoinositide 3-kinase and forkhead.* Mol Cell Biol, 2004. **24**(5): p. 2181-9.
177. Ehrenfried, J.A., et al., *Cell cycle-mediated regulation of hepatic regeneration.* Surgery, 1997. **122**(5): p. 927-35.
178. Van Sweringen, H.L., et al., *CXC chemokine signaling in the liver: impact on repair and regeneration.* Hepatology, 2011. **54**(4): p. 1445-53.
179. Jarpe, M.B., et al., *Anti-apoptotic versus pro-apoptotic signal transduction: checkpoints and stop signs along the road to death.* Oncogene, 1998. **17**(11 Reviews): p. 1475-82.
180. Kim, Y.H., et al., *Metformin ameliorates acetaminophen hepatotoxicity via Gadd45beta-dependent regulation of JNK signaling in mice.* J Hepatol, 2015. **63**(1): p. 75-82.
181. Lu, D., C.D. Wolfgang, and T. Hai, *Activating transcription factor 3, a stress-inducible gene, suppresses Ras-stimulated tumorigenesis.* J Biol Chem, 2006. **281**(15): p. 10473-81.
182. Allan, A.L., et al., *Activating transcription factor 3 induces DNA synthesis and expression of cyclin D1 in hepatocytes.* J Biol Chem, 2001. **276**(29): p. 27272-80.
183. Allen-Jennings, A.E., et al., *The roles of ATF3 in liver dysfunction and the regulation of phosphoenolpyruvate carboxykinase gene expression.* J Biol Chem, 2002. **277**(22): p. 20020-5.
184. Woolbright, B.L. and H. Jaeschke, *Sterile inflammation in acute liver injury: myth or mystery?* Expert Rev Gastroenterol Hepatol, 2015. **9**(8): p. 1027-9.
185. Campion, S.N., et al., *Hepatic Mrp4 induction following acetaminophen exposure is dependent on Kupffer cell function.* Am J Physiol Gastrointest Liver Physiol, 2008. **295**(2): p. G294-304.
186. Wang, S.Y., et al., *Spermine attenuates the action of the DNA intercalator, actinomycin D, on DNA binding and the inhibition of transcription and DNA replication.* PLoS One, 2012. **7**(11): p. e47101.
187. Werner, T., *Bioinformatics applications for pathway analysis of microarray data.* Curr Opin Biotechnol, 2008. **19**(1): p. 50-4.
188. Groves, J.T., *Models and mechanisms of cytochrome P450 action* in *Cytochrome P450: Structure, Mechanism and Biochemistry*, P.R.O.d. Montellano, Editor. 2005, Kluwer Academic/ Plenum Publishers: New York.
189. Kanehisa, M., et al., *The KEGG resource for deciphering the genome.* Nucleic Acids Res, 2004. **32**(Database issue): p. D277-80.
190. Hardwick, J.P., *Cytochrome P450 omega hydroxylase (CYP4) function in fatty acid metabolism and metabolic diseases.* Biochem Pharmacol, 2008. **75**(12): p. 2263-75.
191. Heiker, J.T., *Vaspin (serpinA12) in obesity, insulin resistance, and inflammation.* J Pept Sci, 2014. **20**(5): p. 299-306.
192. Xu, M.J., et al., *Fat-Specific Protein 27/CIDEC Promotes Development of Alcoholic Steatohepatitis in Mice and Humans.* Gastroenterology, 2015. **149**(4): p. 1030-41 e6.
193. Widera, A., *Stress in the liver: stereotypic genomic responses in vitro and in vivo involve inflammation and loss of metabolic functions.* Dissertation, 2014.
194. Konigshoff, M., et al., *WNT1-inducible signaling protein-1 mediates pulmonary fibrosis in mice and is upregulated in humans with idiopathic pulmonary fibrosis.* J Clin Invest, 2009. **119**(4): p. 772-87.
195. Maeda, A., et al., *WNT1-induced Secreted Protein-1 (WISP1), a Novel Regulator of Bone Turnover and Wnt Signaling.* J Biol Chem, 2015. **290**(22): p. 14004-18.

196. Sedlaczek, N., et al., *Proliferating bile duct epithelial cells are a major source of connective tissue growth factor in rat biliary fibrosis.* Am J Pathol, 2001. **158**(4): p. 1239-44.
197. Jun, J.I., K.H. Kim, and L.F. Lau, *The matricellular protein CCN1 mediates neutrophil efferocytosis in cutaneous wound healing.* Nat Commun, 2015. **6**: p. 7386.
198. Meng, Z., et al., *FXR regulates liver repair after CCl4-induced toxic injury.* Mol Endocrinol, 2010. **24**(5): p. 886-97.
199. Michalopoulos, G.K., *Liver regeneration.* J Cell Physiol, 2007. **213**(2): p. 286-300.
200. Kwon, Y.H., et al., *The Cdk inhibitor p21 is required for necrosis, but it inhibits apoptosis following toxin-induced liver injury.* J Biol Chem, 2003. **278**(32): p. 30348-55.
201. Oe, S., et al., *Intact signaling by transforming growth factor beta is not required for termination of liver regeneration in mice.* Hepatology, 2004. **40**(5): p. 1098-105.
202. Nakagawa, H., et al., *Deletion of apoptosis signal-regulating kinase 1 attenuates acetaminophen-induced liver injury by inhibiting c-Jun N-terminal kinase activation.* Gastroenterology, 2008. **135**(4): p. 1311-21.
203. Stephens, S., et al., *A functional analysis of Wnt inducible signalling pathway protein -1 (WISP-1/CCN4).* J Cell Commun Signal, 2015. **9**(1): p. 63-72.
204. Godoy, P., et al., *Gene network activity in cultivated primary hepatocytes is highly similar to diseased mammalian liver tissue.* Arch Toxicol, 2016. **90**(10): p. 2513-29.
205. Swift, B., N.D. Pfeifer, and K.L. Brouwer, *Sandwich-cultured hepatocytes: an in vitro model to evaluate hepatobiliary transporter-based drug interactions and hepatotoxicity.* Drug Metab Rev, 2010. **42**(3): p. 446-71.
206. Lake, B.G., et al., *In vitro assays for induction of drug metabolism.* Methods Mol Biol, 2009. **481**: p. 47-58.
207. Grinberg, M., et al., *Toxicogenomics directory of chemically exposed human hepatocytes.* Arch Toxicol, 2014. **88**(12): p. 2261-87.
208. Hardwick, J.P., et al., *PPAR/RXR Regulation of Fatty Acid Metabolism and Fatty Acid omega-Hydroxylase (CYP4) Isozymes: Implications for Prevention of Lipotoxicity in Fatty Liver Disease.* PPAR Res, 2009. **2009**: p. 952734.
209. Hoek-van den Hil, E.F., et al., *Quercetin induces hepatic lipid omega-oxidation and lowers serum lipid levels in mice.* PLoS One, 2013. **8**(1): p. e51588.
210. Wanders, R.J., J. Komen, and S. Kemp, *Fatty acid omega-oxidation as a rescue pathway for fatty acid oxidation disorders in humans.* FEBS J, 2011. **278**(2): p. 182-94.
211. Kersten, S., B. Desvergne, and W. Wahli, *Roles of PPARs in health and disease.* Nature, 2000. **405**(6785): p. 421-4.
212. Michaut, A., et al., *Acetaminophen-induced liver injury in obesity and nonalcoholic fatty liver disease.* Liver Int, 2014. **34**(7): p. e171-9.
213. Fromenty, B., *Drug-induced liver injury in obesity.* J Hepatol, 2013. **58**(4): p. 824-6.
214. Xu, L., L. Zhou, and P. Li, *CIDE proteins and lipid metabolism.* Arterioscler Thromb Vasc Biol, 2012. **32**(5): p. 1094-8.
215. Matsusue, K., et al., *Hepatic steatosis in leptin-deficient mice is promoted by the PPARgamma target gene Fsp27.* Cell Metab, 2008. **7**(4): p. 302-11.
216. Yonezawa, T., et al., *Which CIDE are you on? Apoptosis and energy metabolism.* Mol Biosyst, 2011. **7**(1): p. 91-100.
217. Gong, J., Z. Sun, and P. Li, *CIDE proteins and metabolic disorders.* Curr Opin Lipidol, 2009. **20**(2): p. 121-6.

ACKNOWLEDGEMENT

The completion of my PhD degree would never have been possible without the support and guidance of numerous people. I am deeply grateful to everyone who contributed to this work and supported me throughout the whole time, only some of whom it is possible to give particular mention here.

First of all, I would like to express my sincere gratitude to my supervisor **Prof. Dr. med. Jan G. Hengstler** for giving me the chance to work in his laboratory at the Leibniz Research Center for Working Environment and Human Factors (IfADo) in Dortmund, Germany. His guidance, support and encouragement have contributed to my growth and development as a scientist.

Moreover, I am deeply grateful to my co-supervisor and mentor **Dr. Patricio Godoy** for supporting me throughout my whole time as a PhD student. Without his encouragement, constant help and tremendous knowledge, this dissertation would not have been possible. Thank you!

In addition, my special thanks go to a number of people, who directly contributed to this work and from whom I was allowed to learn a lot: **Katharina Rochlitz, Dr. Gisela Campos, Dr. Agata Widera** and **Dr. Regina Stöber**. It has been a pleasure for me to work with Katharina Rochlitz, who supported me all the time not only with her technical excellence, but also with listening throughout hard times. Dr. Gisela Campos, for her kindness and patience during all discussions and in the lab. Furthermore, Dr. Agata Widera, who introduced me a long time ago in the lab and supported me all the time with her great experience as well as with her “coolness”. Finally my special thanks go to Dr. Regina Stöber, my office mate and always friendly colleague. Thank you for the constant “emotional support”, all the fun we had in the office and the scientific advice during my PhD time. Furthermore, I would like to thank the students Saskia Leserer, Alexandra Schäfer and David Feuerborn for their excellent and kind assistance in the lab and contribution to this work.

My special thanks go to Elmar Kriek, our animal attendant, who did an excellent job! His calm and always positive attitude was not only beneficial when working with the mice, but also for the whole working atmosphere. Thank you very much for your perfect support!

My sincere thanks go to Dr. Rosemarie Marchan, for helping me with the English corrections and her everlasting lovely smile.

Thanks to all my colleagues and friends from IfADo, who always offered their help and support. I really enjoyed the nice working atmosphere! Thank you all!

Dr. Vanessa Hausherr	Kathrin Gianmoena	Sara Schlüter
Dr. Ramona Lehmann	Dr. Meinolf Blaszkewicz	Reham Hassan Reyad Khalil Alkashef

Daniela González Leiva	Iris Glaeser	Kirsten Liesenhoff-Henze
Dr. Ahmed Ghallab	Georgia Günther	Marion Page
Dr. Julia Liebing	Dr. Bettina Büttner	Dr. Seddik El Kariem Hammad
Brigitte Begher-Tibbe	Dr. Cristina Cadenas	Dr. Sonja Vosbeck
Dr. Rosemarie Marchan	Dr. Raymond Reif	Dr. Alshaimaa Adawy
Dr. Nachiket Vartak	Amruta Vartak Damle	

Finally, I want thank all my friends and my family for their constant help and sympathy. This work would not have been possible without your support!

Schließlich geht noch einen ganz besonderer Dank an meine Mutter und an meine große Liebe Dennis. Ihr habt stets an mich geglaubt und mich unterstützt, besonders in den schweren Momenten! Danke, dass ich mit eurer Hilfe diesen Weg gehen durfte! Mein Vater, der all dies nicht mehr erleben durfte, wäre jetzt sicherlich sehr stolz. Du bist immer in meinem Herzen!